UNIVERSITY OF SOUTHAMPTON

Numerical modelling of sprayed concrete lined (SCL) tunnels

Alun Howell Thomas BA CEng MICE

Doctor of Philosophy

Department of Civil & Environmental Engineering

June 2003

UNIVERSITY OF SOUTHAMPTON

ABSTRACT

FACULTY OF ENGINEERING & APPLIED SCIENCE
DEPARTMENT OF CIVIL & ENVIRONMENTAL ENGINEERING

Doctor of Philosophy

NUMERICAL MODELLING OF SPRAYED CONCRETE LINED (SCL) TUNNELS

by Alun Howell Thomas

While considerable effort has been spent investigating the behaviour of the ground during tunnelling, comparatively little work has been done on sprayed concrete tunnel linings. Discrepancies have often been noted between field data of stresses and strains in sprayed concrete linings and design predictions using "closed-form" analytical or numerical methods. Experimental data suggests that sprayed concrete behaves in a more complex way than is normally assumed in design. These discrepancies can lead to uneconomic or unsafe designs because the factor of safety in the lining cannot be determined with the normal certainty. The goal of this research was to examine the effect of the constitutive model for sprayed concrete in numerical analyses of tunnel linings.

An extensive literature search has been undertaken to examine the state of knowledge of sprayed concrete behaviour. There is considerable experience of SCL tunnelling throughout the world but much of this information is slow to reach countries where SCL tunnelling is relatively new. Problems of increasing complexity have been analysed using the FLAC finite difference program, starting with uniaxial laboratory tests performed on a sample of sprayed concrete, then the large-scale load tests performed on sprayed concrete rings as part of an earlier research project and culminating with the 3D analysis of a single tunnel face as it advances. The results of these analyses have been compared with the results from the original experiments and field data from the Heathrow Express project.

This research has found that the constitutive modelling of sprayed concrete can have a large influence on design predictions of SCL tunnel behaviour. Variations in the construction sequence for the tunnel can also have a significant influence on the loads in the lining.

to err is human ....

to really #@*! things up you need a computer

Table of contents

List of tables

List of figures

List of appendices

ACKNOWLEDGEMENTS

Firstly, this research has been supported by an Industrial Fellowship from the Royal Commission for the 1851 Exhibition with funding from Mott MacDonald, an EPSRC research grant (GR/N22830) and a scholarship from the Mott MacDonald Charitable Trust. Without this support this research would not have been possible and I am extremely grateful to all concerned.

Secondly, throughout this work, I have benefited greatly from the advice and guidance of my supervisors – Chris Clayton and Dave Powell. Special thanks are owed to Dave for initiating the whole project and to Chris for keeping me on the right track.

A great debt is owed to other researchers in this field, especially those who performed laboratory testing on sprayed concrete and fieldwork, for providing the fundamental knowledge, which anchored this research to reality. Particular thanks are extended to Pierre van der Berg, Yining Ding and Wolfgang Kusterle.

In addition I must also thank numerous colleagues at Mott MacDonald – especially all in the Tunnels Division for teaching me everything I know about tunnels and also Chris Pound and Yu Sheng Hsu for all their help with FLAC. Thanks go to my colleagues at the University of Southampton and especially to Richard Harkness for his boundless enthusiasm and computing expertise.

Finally, to everyone else who has had a hand in helping me along – Thank you!

This is dedicated to my grandfather and others who spent the best years of their lives underground.

p.s. Hvala, moja lijepa pametna Andrea za sve!

List of symbols and abbreviations

α	utilization factor = stress / strength or r / yield strength
acc.	according to
agg.	aggregate
ACI	American Concrete Institute
B	relaxation time in Kelvin creep model – see 4.3.5.2
BEM	Boundary Element Method
BM	bending moment
BTS	British Tunnelling Society
bwc	by weight of cement and microsilica
c/c	centre to centre
CCM	Convergence Confinement Method
C/D	cover (depth from ground surface to tunnel axis)/ tunnel diameter
CTA	Central Terminal Area (Heathrow Airport)
Cu	undrained shear strength
Cv	coefficient of consolidation
δ_v	vertical deformation
ε	strain
ε_{dev}	deviatoric strain
E	Young's modulus of elasticity
Ea / R	activation energy = 4000 K – see 2.3.3.8
E_{max}	maximum value of the elastic modulus
E_0	initial tangent modulus
E_{tan}	tangent elastic modulus
e_{ij}	deviatoric strain
$\dot{e}_{ij} = \sqrt{2..\dot{J}'_2}$	deviatoric strain rate
est.	estimated
fc	strength – fcu or fcyl
fcu	uniaxial compressive cube strength

fcyl	uniaxial compressive strength (from tests on cylinders)
FDM	Finite Difference Method
FEM	Finite Element Method
FLAC	FLAC3D & FLAC (2D) finite difference program by Itasca
FOB	full overburden pressure
G	elastic shear modulus
G_{vh}	independent shear modulus
GGBS	Granulated Ground Blast Furnace Slag
γ_f	partial factor of safety for loads (see BS8110)
γ_m	partial factor of safety for materials (see BS8110)
HEX	Heathrow Express project
HME	Hypothetical Modulus of Elasticity
HSE	Health & Safety Executive
I_{10}	SFRS toughness index
ICE	Institution of Civil Engineers
ITA	International Tunnelling Association
JLE	Jubilee Line Extension project
J_2	second deviatoric invariant of principal stresses $J_2 = 1/6 \, . \, ((\sigma_1-\sigma_2)^2+(\sigma_2-\sigma_3)^2+(\sigma_3-\sigma_1)^2)$
k	permeability
K	elastic bulk modulus
K_0	ratio of horizontal effective stress to vertical effective stress
long.	longitudinal
λ	stress relaxation factor – see 2.3.1.2
max.	maximum
NATM	New Austrian Tunnelling Method
OCR	overconsolidation ratio
OPC	ordinary Portland cement
p	mean total stress
p'	mean effective stress

PFA	Pulverised Fly Ash
pts	points
r	deviatoric stress = $2.(J_2)^{0.5}$
R	tunnel radius
R	universal constant for ideal gas – see Ea/R above
RH	Relative Humidity
σ	stress (compression is taken to be negative)
σ_v	vertical stress
$\sigma_1, \sigma_2, \sigma_3$	principal stresses
SBP	Self Boring Pressuremeter
SCL	Sprayed Concrete Lined / Lining
SFRS	Steel Fibre Reinforced Shotcrete
θ	Lode angle (or angle of similarity) where $\cos\theta = \frac{2\sigma_1 - \sigma_2 - \sigma_3}{2\sqrt{3J_2}}$; $\theta = 0°$ corresponds to the tensile meridian and $\theta = 60°$ corresponds to the compressive meridian
t	time or age
T4	Terminal 4 (Heathrow Airport)
υ	Poisson's ratio
w/c	water/cement ratio
w.r.t.	with respect to
z	depth / distance in the z direction
2D	two dimensional
3D	three dimensional

Subscripts

A_h	in the horizontal plane / direction
A_{hh}	in the horizontal plane / direction
A_o	initial value (e.g.: value of modulus at strain is zero)
A_t	time-dependent value
A_{tan}	tangential (e.g.: tangential elastic modulus)
A_u	undrained (in context of geotechnical parameters)
A_v	in the vertical plane / direction
A_{xx}	in the direction of x-axis
A_{yy}	in the direction of y-axis
A_{zz}	in the direction of z-axis
A_{28}	value at an age of 28 days

1 INTRODUCTION

1.1 Background

Sprayed concrete lined (SCL) tunnels are becoming increasingly common world-wide. While sprayed concrete was first developed for use in rock tunnelling, the advantages of its flexibility of geometric form and its low mobilisation costs have been exploited in all types of ground conditions. Indeed it has come close to supplanting traditional tunnelling methods, using segmental linings, as the first choice for constructing complex arrangements of short tunnels and shafts in soft ground. However, recent high profile tunnel collapses (e.g.: at Heathrow, London in 1994) have exposed the vulnerability of SCL tunnelling to poor construction practices and a discomforting level of uncertainty in the design of SCL tunnels. For these reasons in the UK there is a tendency to regard sprayed concrete linings as a high risk option. Hence, in the first instance, the context for this research is that of shallow SCL tunnels in soft ground in urban areas. It is recognised that this represents only one facet of SCL tunnelling but it is an important sector for the UK tunnelling industry both at home and abroad.

Recent improvements in construction and risk management have addressed the problems associated with SCL tunnelling during construction (ICE 1996, Powell *et al.* 1997, Audsley *et al.* 1999). Yet despite advances in instrumentation and methods of interpreting monitoring data, there is still a discrepancy between the observed behaviour of SCL tunnels and the predictions made during design (Golser *et al.* 1989, Clayton *et al.* 2000). Not only does this uncertainty raise concerns over the safety and cost-effectiveness of the linings in the short-term but also in the long-term. Because the exact loading of the lining at an early age is unknown, clients and designers are reluctant to accept sprayed concrete as part of the permanent lining, in case it has been damaged by high loading. Concerns over the durability have also discouraged the use of permanent sprayed concrete.

This research has focused on the design of SCL tunnels. Having described SCL tunnels and their design in a little more detail, the structure of this thesis and its goal will be outlined.

1.2 SCL tunnels and their design

1.2.1 The history of SCL tunnelling

Figures 1.1 and 1.2 show a typical excavation sequence and cross section for a large diameter tunnel in soft ground at a shallow depth (i.e. the cover from crown to ground surface is between 2 and 4 times the diameter). The arrangement of the excavation sequence is influenced by the geometry of the tunnel, the stability of the ground and the construction plant. In shallow tunnels it is important to close the invert as close to the face as possible, in order to limit ground deformations. However, the designer has a fair degree of freedom in choosing the exact arrangement. Figures 1.3 to 1.5 show 3 different arrangements for similar tunnels. After each stage of the excavation sequence has been mucked out, sprayed concrete is sprayed on the exposed ground surface. The lining is often built up in several layers with mesh reinforcement inserted between the layers (see Figure 1.6). Alternatively short fibres can be added to the mix to provide some tensile capacity. Steel arches or lattice girders may be included. In soft ground they may be required for forepoling or simply to ensure that the lining is constructed to the correct shape. Once that section of lining is complete, the next stage is excavated and so the process progresses and a closed tunnel lining is formed. Normally, the sprayed concrete lining does not form part of the permanent works and another lining is installed at a later date (see Figure 1.1). More details on the construction of SCL tunnels can be found in the ICE guide (ICE 1996)[1].

To understand the origin and merits of sprayed concrete tunnel linings, one must first appreciate some fundamental tunnelling principles.

1. Tunnelling involves soil-structure interaction.

[1] On a point of nomenclature, in this thesis, all tunnels with a sprayed concrete lining will be referred to as 'SCL' or 'sprayed concrete lined' tunnels. The terms merely describe the physical constituents of the lining and do not make any claims on how it was designed. The term NATM will not be used as an abbreviated label for sprayed concrete lined tunnels. The NATM (New Austrian Tunnelling Method) is a design philosophy, not a construction method (Brown 1981). SCL tunnels are often designed in accordance with the NATM but this is not always the case (see also BTS 2004).

2. The load to be carried by the composite structure of the ground and lining arises from the insitu stresses and groundwater pressure.
3. Deformation of the ground is inevitable and it must be controlled to permit a new state of equilibrium to be reached safely.
4. Often the strength of the ground depends on how much it is deformed.
5. The load on the lining will depend on how much deformation is permitted and how much stress redistribution within the ground is possible.
6. The art of tunnelling is to maintain as far as possible what inherent strength the ground has so that the amount of load carried by the structure is minimised.

These basic principles have been understood implicitly or explicitly by experienced tunnellers since tunnels were first constructed. However, they were brought to the forefront of attention by the pioneering work of engineers, such as Ladislaus von Rabcewicz, who developed the tunnelling philosophy that is now marketed as the New Austrian Tunnelling Method (NATM). In his early work in rock tunnels, Rabcewicz (1969) recognised that sprayed concrete was a material well suited to tunnelling for the reasons below.

- Sprayed concrete is a structural material that can be used as a permanent lining.
- The material behaviour of sprayed concrete (which is initially soft and creeps under load but can withstand large strains at an early age) is compatible with the goal of a lining which permits ground deformation (and therefore stress redistribution in the ground).
- The material behaviour (specifically the increase in stiffness and strength with age) is also compatible with the need to control this deformation so that strain softening in the ground does not lead to failure.
- Sprayed concrete linings can be formed as and when required and in whatever shape is required. Hence the geometry of the tunnel and timing of placement of the lining

can be tailored to suit a wide range of ground conditions. Sprayed concrete can also be combined with other forms of support such as rock bolts and steel arches [2].

Sprayed concrete was first used as temporary (and permanent) support in rock tunnels in the 1950's. However, the principles above apply equally to soft rocks and soils. In the 1970's shallow SCL tunnels were successfully constructed in soft ground as part of metro projects in cities such as Frankfurt and Munich. Figure 1.7 charts the rise of SCL tunnelling in the UK. SCL tunnelling is relatively new to the UK and has only become widely used within the last 15 years. Following the collapse of a series of SCL tunnels in 1994, this construction method came under intense scrutiny. Vociferous sceptics have asserted and some still do that SCL tunnelling can not and should not be used in soft ground at shallow depths (e.g.: Kovari (1994)).

Reports by the Health & Safety Executive (1996) and the Institution of Civil Engineers (ICE 1996) have established that SCL tunnels can be constructed safely in such conditions and the reports provided guidance on how to ensure this during design and construction. The reports drew attention to weaknesses of this method:

- The person spraying the concrete (the nozzleman) has a considerable influence over the quality of the lining so the method is vulnerable to poor workmanship. This is particularly true for certain geometries of linings[3].
- The performance of the linings and ground must be monitored during construction to verify that both are behaving as envisaged in the design. The data from this monitoring must be reviewed regularly in a robust process of construction

[2] One may also note: the lower mobilisation times and costs for major plant items; the same equipment can be used for shaft construction as well as tunnelling; the method is compatible with the Observational Method which permits optimisation of support (and therefore costs) during construction; the freedom of form permits tunnels of varying cross-sections and sizes and junctions to be built more quickly and cost-effectively than if traditional methods are used.

[3] ie. where the geometry makes it difficult to spray the lining or to form clean joints.

management that ensures that abnormal behaviour is identified and adequate countermeasures are taken.

- It is difficult to install instrumentation in sprayed concrete linings and to interpret the results (Golser *et al.* 1989, Mair 1998, Clayton *et al.* 2000).
- It is difficult to predict the behaviour of SCL tunnels in advance (see 1.2.3).

The specific disadvantages of this method, as applied to soft ground, are [4]:

- It is of critical importance to minimise deformations. Otherwise strain-softening and plastic yielding in the ground can lead rapidly to collapse. Complex excavation sequences can lead to a delay in closing the invert of the tunnel (and forming a closed ring). This delay can permit excessive deformations to occur.
- In shallow tunnels the time between the onset of failure and total collapse of a tunnel can be very short, so much tighter control is required during construction.

Following the HSE and ICE reports, a considerable amount of guidance has been produced on such subjects as certification of nozzlemen (see Austin *et al.* (2000) for the latest guidance), instrumentation and monitoring (HSE 1996) and risk management. The UK tunnelling industry has incorporated much of this into its standard practices. Since the collapse at Heathrow, more than 200,000 m^3 of shallow SCL tunnels have successfully constructed in a variety of soft ground conditions. Major projects such as the Heathrow Baggage Transfer Tunnel (Grose & Eddie 1996) and the CTRL North Downs Tunnel (Watson *et al.* 1999) have demonstrated the great benefits to be gained from this method, not least in terms of time and cost savings compared to conventional construction methods. Nonetheless SCL tunnels are still perceived to be difficult to design because of the complex behaviour of sprayed concrete.

---

[4] One may also note: that advance rates are slower than for shield-driven tunnels so SCL tunnels are not economic for long tunnels (i.e. greater than about 500 m) with a constant circular cross-section; a higher level of testing is required for quality control during construction, compared to segmental tunnel construction - This includes mix design tests before the works actually commence; the surface finish of a sprayed concrete lining is quite rough and will contain protruding steel fibres, if they have been used, so it is unsuitable for public areas.

1.2.2 Permanent sprayed concrete linings

Considerable cost savings are possible if the concrete, sprayed as the initial ground support, can be included in the permanent lining (the so-called "single shell" or "monocoque" approach) (Golser & Kienberger 1997). Permanent sprayed concrete linings may be formed in several ways and in actual fact the "single shell" may consist of several layers of sprayed concrete, placed at different times. Projects often specify a design life in excess of 100 years and there are concerns over the durability of permanent sprayed concrete linings. Specifically they centre on the stability of the components of hydration, the susceptibility of steel reinforcement to corrosion and damage to the structure of the concrete due to early loading.

Table 1.1: Typical design requirements for permanent sprayed concrete linings

Parameter	Value	Source / comments
Max. water/binder ratio	0.45	-
Min. cement content	380 kg/m^3	Good to add 5 - 10% of micro-silica (bwc)
Min. compressive strength	Depends on lining loads – typically 30 to 40 MPa	No reduction with time after 28 days
Max. accelerator dosage	Keep as low as possible	-
Water permeability	>= 10^{-12} m/s	Darby & Leggett 1997
Water penetration	=< 50 mm	Lukas *et al.* 1998
Max. crack width	0.4 mm	ÖBV 1990
Curing period	7 days	By spraying with water
Bond between layers of concrete	1 MPa	EFNARC 1996

Sprayed concrete can be produced with acceptable durability characteristics (equal to that of insitu concrete, as indicated by its permeability and porosity values (Neville 1995, Palermo & Helene 1998, Norris 1999)), although this increases the unit cost of the material. Reliable predictions of the stress distribution in the lining at an early age would help to quantify the problem of early age loading.

Sprayed concrete is still not widely used as part of the permanent works (at least in public tunnels) (Golser & Kienberger 1997, Watson *et al.* 1999) and no clear performance specification has been established. Table 1.1 summarises typical requirements. Accounts of pioneering projects in the field of permanent sprayed concrete linings can be found in Kusterle (1992), Arnold & Neumann (1995), Darby & Leggett (1997), Zangerle (1998) and Palermo & Helene (1998).

1.2.3 Design methods

Broadly speaking there are three categories of design methods – empirical, (closed-form) analytical and numerical. Of the empirical methods in current use, such as the Q-system (Barton *et al.* 1975) or RMR (Bieniawski 1973), most have been developed for rock tunnels. Analytical and numerical methods are generally used for the design of SCL tunnels. Analytical methods include continuum "closed-form solution" models (e.g.: Muir Wood 1975 & Curtis 1976) and the Convergence-Confinement Method (CCM) (Panet & Guenot 1982). Bedded Beam Models are used less often these days, because of their limited ability to model the soil-structure interaction. To a degree they have been superseded by 2D numerical modelling.

In the course of designing any given tunnel, a range of design tools will be used. As the project evolves the tools tend to increase in complexity from simple empirical approaches to complex numerical modelling. One must recognise that all design methods are merely approximations of the real case. Therefore the use of several different design tools is extremely important since they serve as independent checks on each other.

The continuum analytical (closed form) methods are relatively simple to implement and provide information on stresses in the lining and its deformation. Some of them may be extended to include features such as plasticity in the ground or the timing of lining placement. However, they share several fundamental limitations: they assume plane strain or axisymmetry and the solutions are almost invariably developed only for circular tunnels, constructed in full-face excavation in homogeneous ground. The modelling of soil-structure

interaction is limited, yet this is fundamental to all tunnels. More specifically, the closed form solutions in their basic forms make no allowance for stress redistribution ahead of the face. The CCM assumes that K_0 equals 1.0 and that the stress in the lining independently increases as a function of the ground's convergence until the resistance provided by the lining equals the radial stress in the ground.

To overcome these limitations, one must turn to numerical methods. In contrast to the design tools already outlined, numerical methods offer a broad capability to model explicitly complex geometries, including adjacent structures and geological strata, complex constitutive behaviour, the details of the construction processes and transient and dynamic effects. Hence they are increasingly popular and are even used on site during construction (e.g.: Golser 1999). Commercially available programs for numerical analysis offer a wide range constitutive models and elements. This leads to the impression than one can model almost anything.

However, one should not treat computer programs as black boxes, which receive input at one end and produce "the answer" at the other end. Within the accuracy of the solution algorithm, a computer program will produce an output that is correct according to the input data. The output from numerical analyses is still only an estimate of how the ground and tunnel would behave in reality. Empirically-based correction factors or simplifications are often used in numerical modelling (e.g.: corrections for 3D effects in 2D analyses or the Hoek & Brown failure criterion). Table 1.2 lists the main sources of errors in modelling (after Woods & Clayton 1993). For this reason and because of the additional complexities involved in numerical modelling and in analysing tunnels, it is often recommended that numerical analyses are considered as a tool to investigate which are the important mechanisms, rather than a means of obtaining precise predictions of a tunnel's behaviour (Coetzee *et al.* 1998). Despite the significant improvements in computers over recent years, many of the simplifications in numerical analyses are driven by the limitations in computing power.

Table 1.2: Sources of errors in modelling

Aspect of the model	Example
Geometry	2D analyses instead of 3D
Construction method	"Wished in place" analyses
Constitutive modelling & parameter selection	Assuming linear elasticity for the lining
Theoretical basis of the solution	Modelling discontinuous ground as a continuum
Interpretation	Application of factors of safety
Human error	Errors in input data

Soft ground is normally considered as a continuum. Therefore the **finite element method** (FEM) or **finite difference method** (FDM) is normally used. Hybrid models can also be used – namely, FEM and FDM or FEM and the boundary element method (BEM) - but this is normally done just as a means of reducing the mesh size (e.g.: Kropik 1994 – see also Schweiger & Beer 1996 for an overview of numerical methods).

The process of building a FEM or FDM model is essentially the same and end-products are often very similar (Watson 1997, Coetzee *et al.* 1998)[5]. The object to be analysed is represented by a mesh of many elements or zones – in a process called *discretization*. The material properties, material behaviour, boundary conditions and loads are assigned to the model and the problem is solved. Usually in FEM a stiffness matrix is assembled for the whole mesh, in order to relate the displacements to the stresses. These vary in a prescribed manner within each element. The matrix is then solved using standard matrix reduction techniques, in a so-called "implicit" solution technique. In FDM, the 'dynamic relaxation' solution technique is used. Newton's law of motion is expressed as a difference equation and it is used to relate explicitly the unbalanced forces at each calculation point (grid point) in the mesh to the acceleration of the mass associated with each grid point. For a very small time-

[5] It is worth bearing in mind that 2 FE programs may well produce different answers when analysing nominally the same problem (Chan *et al.* 2000)

step[6], the incremental displacements can be calculated. These are used to calculate a new set of unbalanced forces (from the constitutive relationships) – see Figure 1.8. This calculation step is repeated many times for each grid point in the mesh, in a "time-marching" method until the out-of-balance force has reduced to a negligible value – i.e. equilibrium has been reached for a statical problem. This requires a very large number of calculation steps, although each one is quick to perform. A finer mesh is required in a FDM model than an FEM one because FDM uses constant strain zones.

Usually the FEM (using implicit solution techniques) can solve linear and moderately non-linear problems faster than the FDM (using explicit solution techniques). However, for heavily non-linear problems the FEM (using implicit solution techniques) may be slower if it uses an iterative solution technique with the load subdivided into a number of increments. The accuracy of solutions then depends heavily the number of increments and the solution algorithms (Potts & Zdravkovic 1999). The explicit, time-marching solution method by default approaches solutions slowly and so removes the problems associated with the size of load increments. Both material and geometric nonlinearity (e.g.: creep or large strain behaviour) can be modelled easily in FDM (Hoek *et al.* 1998). Physical instability can be also easier to model and detect using the FDM.

1.3 Structure of the thesis

The research presented here seeks to determine the extent of the influence of the material model for sprayed concrete in design analyses. The hypothesis is that, just as the use of more realistic constitutive models for the ground has improved the predictions of ground movements around tunnels (Gunn 1993, Addenbrooke 1996), more realistic models of the sprayed concrete will help to produce more realistic predictions of behaviour. Because of the complexity of the geometry, construction sequence and material behaviour involved in SCL tunnelling, it is necessary to use numerical models to analyse this problem. The structure of this thesis is as follows:

[6] In static mechanical problems this time-step is fictitious – ie. it is not related to real time.

Chapter 2 contains the literature review. This chapter seeks to explain which aspects of the behaviour of sprayed concrete are believed to be important in determining the stress and strain distribution within the tunnel lining, how they may be modelled and why the current modelling of sprayed concrete lined tunnels is inadequate.

Chapter 3 presents the several case studies that will be examined using numerical modelling later. The results from the modelling will be compared with this data from small and large laboratory experiments and from the Heathrow Express (HEX) project in London.

The numerical modelling of sprayed concrete is discussed in more depth in Chapter 4. Various constitutive models are proposed for sprayed concrete and the derivation of their parameters is explained. The performance of these models both in theory and as implemented in the FLAC finite difference program is compared with experimental data. The reasons behind the choice of FLAC for this study are explained.

Chapter 5 contains the results from the numerical modelling of the large-scale laboratory test on a ring of sprayed concrete. The results are compared with the test data.

In Chapter 6 results are presented from a 3D numerical model of the construction of an SCL tunnel in London Clay. This case study is based on the construction of the large diameter tunnels at the Terminal 4 station for the Heathrow Express project. In addition to using different constitutive models for the sprayed concrete lining, the geometry of the tunnel, the advance length and the constitutive model for the ground have been varied. The results are compared with field data from the HEX project.

In Chapter 7 the results from the numerical modelling and their implications for the design of SCL tunnels are discussed.

Conclusions and recommendations for further research are presented in Chapter 8.

Figure 1.1 Typical long-section through SCL tunnel

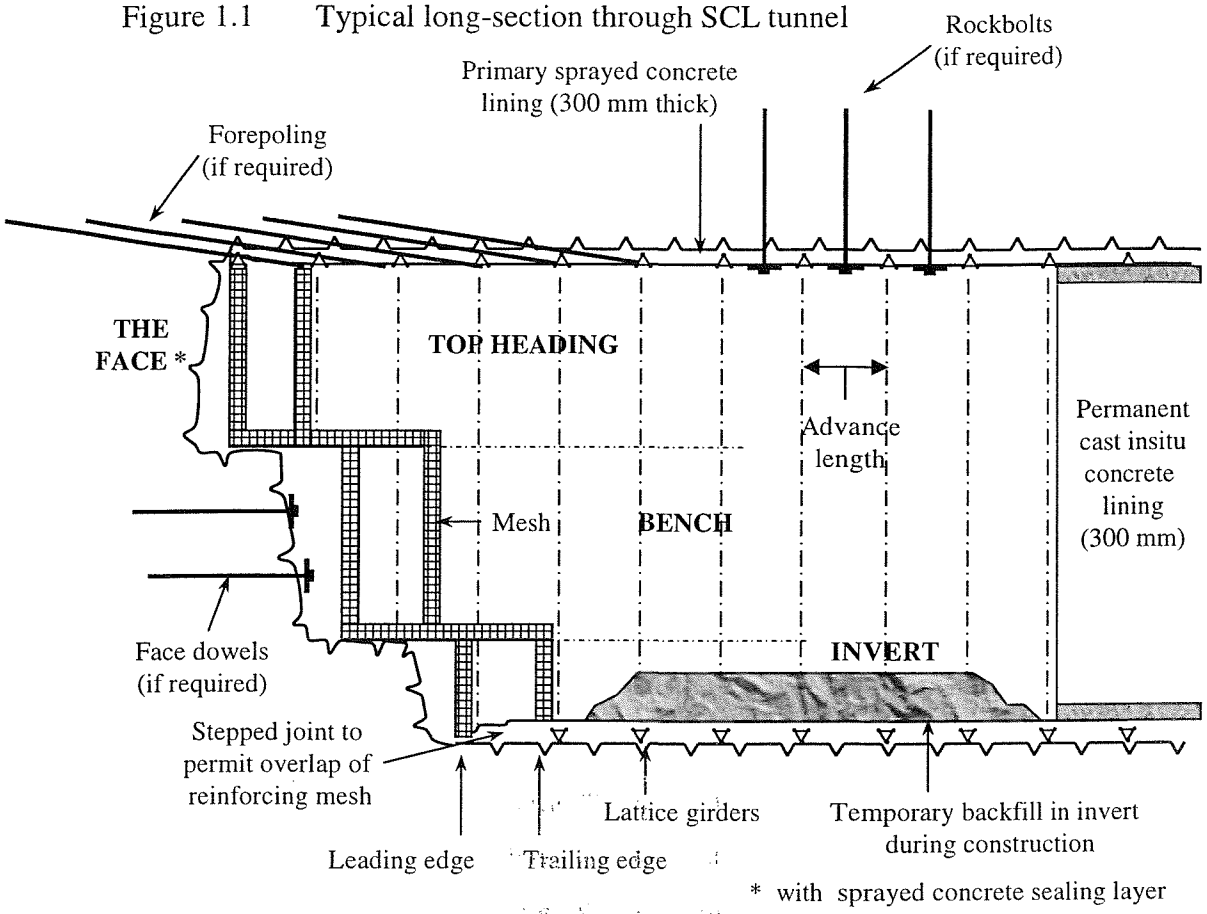

Figure 1.2 Typical cross-section from SCL tunnel

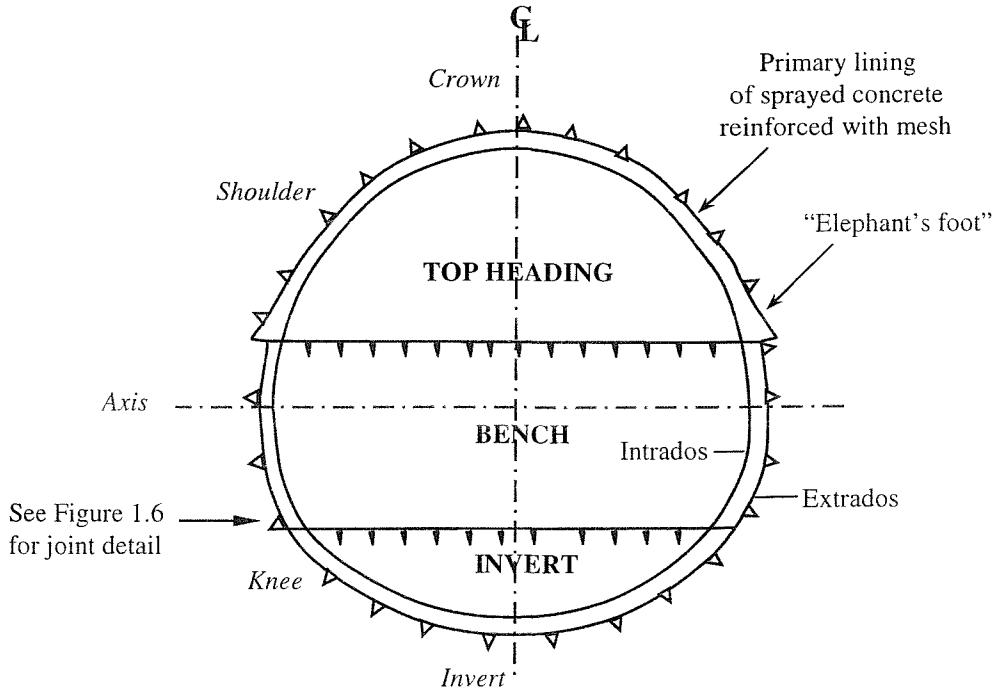

Figure 1.3 Top Heading, Bench & Invert construction sequence

Figure 1.4 Side gallery & enlargement construction sequence

Figure 1.5 Pilot & enlargement construction sequence

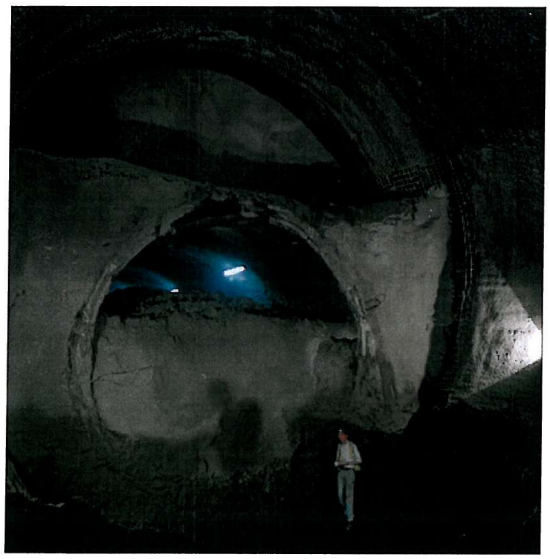

Figure 1.6 Typical detail of sprayed concrete lining

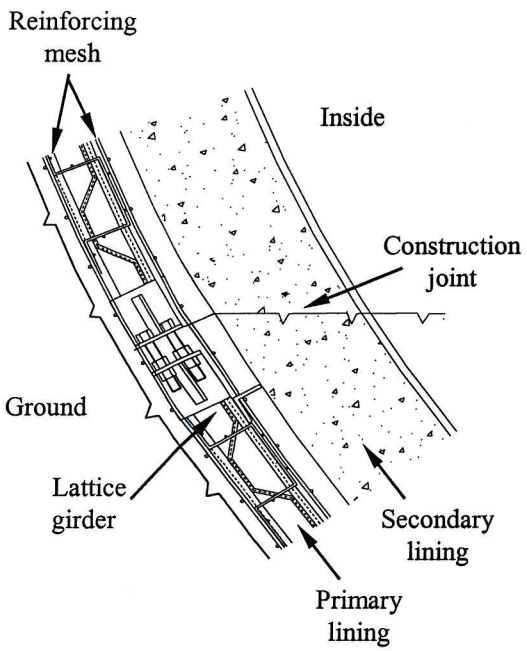

Figure 1.7 Development of SCL tunnelling in the UK

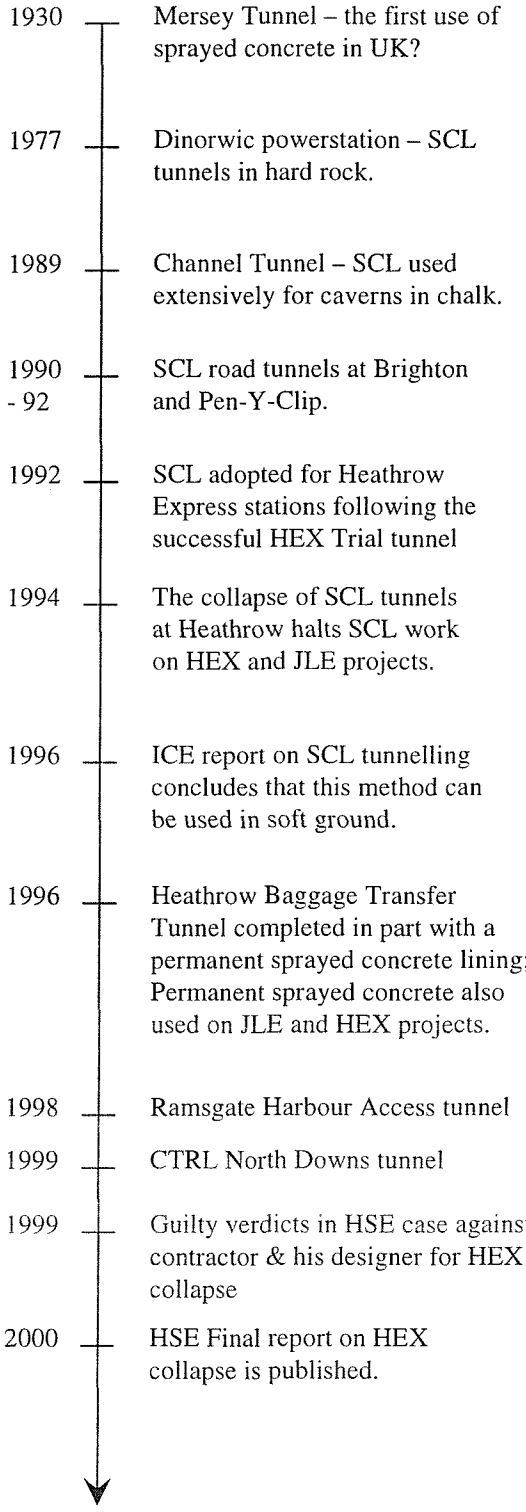

Figure 1.8 FLAC calculation loop

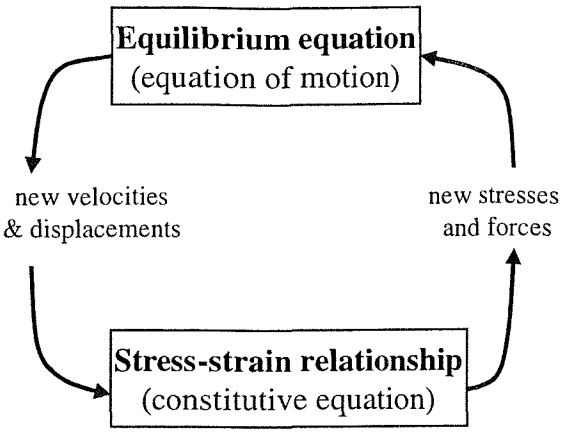

2 LITERATURE REVIEW

2.1 Sprayed concrete – the material

2.1.1 The origins of sprayed concrete

The invention of sprayed concrete is generally attributed to Carl Ethan Akeley in 1907, who used a dry-mix sprayed mortar to apply a durable coating to dinosaur bones. However, in Germany, August Wolfsholz had been developing equipment for spraying cementitious mortar in tunnels for rock support from as early as 1892 (Strubreiter 1998), and Carl Weber patented a method for spraying concrete in 1919 (Atzwanger 1999). While sprayed concrete was used on a few engineering projects to repair concrete structures or for rock support in the first half of this century, this material and method first attracted serious attention after its use on a series of pioneering projects in Venezuela and Austria by Rabcewicz in the 1950's (Rabcewicz 1969).

The early sprayed concrete was not a high quality product. Large quantities of accelerating additives were required to get the sprayed concrete to adhere to the ground and so that reasonably thick layers could be sprayed. The environment during spraying was very unhealthy due to the large quantities of dust and the caustic nature of the accelerators. Despite the accelerators, a large quantity of the sprayed concrete failed to adhere and fell as waste material onto the tunnel floor – so-called "rebound". The material was very sensitive to the influence of the nozzleman, since he controlled how the material was sprayed (which determines the compaction) and the water content. Because of this and the accelerators, long-term strengths of sprayed concrete were much lower than conventionally cast concrete and the material was more variable in quality.

Hence, research and development since the 1970's has focused primarily on accelerators and admixtures (to achieve higher early strengths with lower dosages of these expensive and often hazardous additives, without compromising long-term strength, and to reduce dust and rebound) and spraying equipment (to improve the quality, spraying quantity and automation).

Research into the durability and mechanical properties other than strength and stiffness followed later as the early challenges were overcome and design approaches and usage developed.

2.1.2 The composition of sprayed concrete

"Sprayed concrete is concrete which is conveyed under pressure through a pneumatic hose or pipe and projected into place at high velocity, with simultaneous compaction" (DIN 18551 1992). It behaves in the same general manner as concrete but the methods of construction of SCL tunnels and of placement of sprayed concrete require a different composition of the concrete and impart different characteristics to the material, compared to conventionally placed concrete. Sprayed concrete consists of water, cement and aggregate, together with various additives[7].

The composition of the concrete is tailored so that: it can be conveyed to the nozzle and sprayed with a minimum of effort; it will adhere to the excavated surface, support its own weight and the ground loading as it develops; it attains the strength and durability requirements for its purpose in the medium to long-term. Table 2.1 contains a comparison of the constituents of a high quality sprayed concrete and an equivalent strength cast insitu concrete [8]. Considering each component in turn, one may note that:

- the water cement ratio in sprayed concrete is higher in order that the mix can be pumped & sprayed;
- ordinary Portland Cement is normally used, in conjunction with cement replacements such as pulverised fly ash (PFA), though special cements are sometimes used;
- the mix is "over-sanded" to improve pumpability (Norris 1999), (see Figure 2.1 for grading curve);
- the maximum aggregate size is usually limited to 10 or 12 mm;

[7] On a point of nomenclature, sprayed concrete is also known as "shotcrete", while "gunite" normally refers to sprayed mortar, ie. a mix with fine aggregates only.

[8] Unless otherwise stated the data quoted here for sprayed concrete refer to the wet mix permanent sprayed concrete used on the Heathrow Express Project (Darby & Leggett 1997).

- additives are used to accelerate the hydration reaction (see Figure 2.2 for the effect of increasing accelerator dosage on strength gain);
- plasticisers and stabilisers are added to improve workability as in conventional concrete;
- other components may include micro-silica, which is added to improve immediate adhesion (which allows the accelerator dosage to be reduced) and to improve long-term density (which improves strength and durability) or steel fibres, which are added for structural reinforcement or crack control.

Table 2.1: Typical mix design

	High quality wet-mix shotcrete	Cast insitu concrete (Neville 1995)
Grade	C40	C40
Water/cement ratio	0.43	0.40
Cement inc. PFA, etc	430 kg/m^3	375 kg/m^3
Accelerator	4 %	-
Plasticiser	1.6 % bwc[9]	1.5 %
Stabiliser	0.7 % bwc	-
Micro-silica	60 kg/m^3	-
Max. aggregate size	10 mm	30 mm
Aggregate < 0.6 mm	30 - 55 %	32 %

Each component represents a large subject in itself and more information on most of them can be found in standard textbooks on concrete technology (e.g.: Neville 1995). Where relevant their influence on the mechanical properties of sprayed concrete will be briefly discussed in section 2.2. More details on the constituents of sprayed concrete can be found in the International Tunnelling Association's state of the art review (Malmberg 1993) and other

[9] Bwc = by weight of cement and microsilica

texts (e.g.: ACI 506R 1990, Melbye 1994, Austin & Robins 1995, Brite Euram [10] 1998 and Brooks 1999,).

2.1.3 Dry mix vs wet mix

Sprayed concrete is produced either by the dry-mix process or the wet-mix process. In the dry-mix process, a mixture of naturally moist or oven-dried aggregate, cement and additives is conveyed by compressed air to the nozzle, where the mixing water (and accelerator, if liquid) is added (see Figure 2.3). In the wet-mix process, ready-mixed (wet) concrete is conveyed by compressed air or pumped to the nozzle, where the liquid accelerator is added (see Figure 2.4).

In the past the dry mix has been preferred, because it could produce sprayed concrete with higher early strengths, and some countries, notably Austria, retain a preference for the dry-mix process. However, there is a global trend towards using the wet-mix process, which is perceived to permit greater control over quality, to be more suited to automation and to be safer (since dust levels are lower). It has been estimated that world-wide about 60% of sprayed concrete is produced by the wet-mix method (Brooks 1999). Each method has its strengths and weakness and the reasons for choosing both methods have been summarised below:

Dry-mix sprayed concrete

- Higher early age strengths (see Table 2.2)
- Lower plant costs
- Small space requirements on site, especially if pre-bagged mixes are used (this is particularly advantageous in urban sites)

[10] The 4 ½ year long Brite Euram project – BRE CT92 0231 - "New materials, design and construction techniques for underground structures in soft rock and clay media", was part funded by the Commission of European Communities and led by Mott MacDonald with Taywood Engineering, Imperial College (London), the Institute of Mechanics, Materials and Geostructures (Greece), Dragados y Construcciones and Sprayed Concrete Ltd.

- More flexibility during operation (sprayed concrete can be effectively available "on tap", less cleaning required)

Wet-mix sprayed concrete

- Greater quality control (the mix is batched at a plant and the accelerator dosage cannot be altered by the nozzleman)
- Robotic spraying is required because of the weight of the nozzle and hose but this leads to higher outputs than dry-mix (up to 18-20 m^3 per hour) and reduces variability due to the human factor. The additional plant cost is partially offset by the reduction in labour costs
- Lower rebound (typically 16%, compared to 21 to 37% for dry mixes (Lukas *et al.* 1998))
- Less dust (with dust levels within acceptable limits – see Figure 2.5)
- The use of ready-mix batches and robotic spraying permits records of the exact mix and quantities sprayed to be kept more easily (Davik & Markey 1997)

Table 2.2: Compressive strengths of modern mixes (after Lukas *et al.* 1998)

Age	Dry mix spray cement (Oven dry agg.)	Dry mix spray cement (Moist aggregate)	Wet mix 6 % alkali free acc.[11]	Dry mix 6 % alkali free acc.
6 minutes	0.95	0.5	0.5	-
1 hour	1.3	1.0	1.0	-
1 day	23.0	21.0	15.0	17.0
56 days	41.0	39.0	61.0	39.0

Broadly speaking, dry-mix sprayed concrete is best suited to projects that require small and intermittent volumes of sprayed concrete and where there are space constraints on site or long journey times from the point of batching to the face. Wet-mix sprayed concrete is best suited

[11] NB: higher equivalent cement content in this mix; refer to original report for the full mix details

to projects that require regular and large volumes of sprayed concrete and where a batching plant can be located close to the point of use. The cost difference between modern high quality dry and wet-mix sprayed concrete has reduced to the extent that, if one includes all relevant factors (such as rebound, labour costs and cycle time), there is little to choose between the two methods - see Table 2.3.

Table 2.3: Normalised cost comparisons between dry and wet mix sprayed concrete

Source & notes	Dry mix	Wet mix
Lukas *et al.* (1998) – all costs exc. rebound	0.72	1.00
Röthlisberger (1996) – all costs	1.12	1.00
Strubreiter (1998) – whole costs over 1000 m tunnel	0.91	1.00

2.1.4 New trends in sprayed concrete

The development of new techniques and additives for sprayed concrete continue to improve its performance. The main disadvantages of the dry-mix method are the high levels of dust and the variability of the product due to the influence of the nozzleman. To counteract this, pre-wetting nozzles (to reduce dust) and special spray cements, which require no additional accelerator, have been developed (Testor 1997). The main disadvantages of wet mix sprayed concrete are the higher plant costs, lower strengths and limited pot life of the sprayed concrete once mixed. However, the extra plant cost is partially offset by the benefits of automation. Health and safety considerations and the need for higher production rates are leading to increasing levels of automation.

2.2 Sprayed concrete - its behaviour

This section will consider the mechanical behaviour of sprayed concrete from the perspective of the design engineer, who is concerned primarily with structural integrity of the tunnel lining during construction and what constitutive model he should use in design analyses.

Table 2.4 contains the properties of a sprayed concrete and an equivalent strength concrete mix described in Table 2.1. Although the properties of this sprayed concrete are at the higher

end of the typical values for sprayed concrete, there is a trend towards using such higher quality sprayed concrete as the norm on major construction projects (Brooks 1999).

Table 2.4: Typical properties of sprayed and cast concrete

Property	High quality sprayed concrete	Cast insitu concrete
Compressive strength @ 1 day in MPa	20	6 (est.)
Compressive strength @ 28 days in MPa	59	44
Elastic modulus @ 28 days in GPa	34	31 (est.)
Poisson's ratio,ν, @ 28 days	0.48 - 0.18 [12]	0.15 - 0.22
Tensile strength @ 28 days in MPa	> 2 (est.) [12]	3.8 (est.)
Initial setting time (start - end) in mins	1 - 3 [13]	45 – 145 (est.)
Shrinkage after 100 days in %	0.1 – 0.12	0.03 – 0.08
Specific creep after 160 days in % /MPa	0.01 - 0.06	0.008
Density kg/m^3	2140 – 2235	2200 – 2600
Total porosity in %	15 – 20 [14]	15 – 19
Permeability in m/s	2.0 x 10^{-12} to 10^{-14}	10^{-11} to 10^{-12}
Microcracking @ 28 days in cracks/m	1300	-
Coefficient of thermal expansion in -/K	8.25 – 15 x 10^{-6} [15]	10 x 10^{-6} [16]
Slump in mm	50 - 80 [17]	50

One could start by asking a series of basic questions.

- How strong is sprayed concrete?
- Is it brittle or ductile?

[12] Kuwajima 1999

[13] Melbye 1994

[14] Blasen 1998 & Lukas *et al.* 1998

[15] Kuwajima 1999 & Pöttler 1990

[16] DIN 1045 1988

[17] Brite Euram 1998

- Do its properties or behaviour change with time?
- Do its properties change with pressure, temperature or other environmental conditions?

2.2.1 Strength in compression

Theories and mechanisms

Strength is often the first parameter that an engineer examines when considering a new material. As with all materials, the strength of concrete is governed as much by the flaws and imperfections within the material, as by the intrinsic strengths of the main components and their interaction. In the case of concrete the main components are the hydrated cement paste and the aggregate. Typical compressive strengths of the hydrated cement paste (in the form of very dense cement paste compacts) can be up to 300 to 500 MPa, while the compressive strength of rocks commonly used for aggregate lies between 130 and 280 MPa (Neville 1995). The imperfections are voids or pores, microcracks and macrocracks (both due to shrinkage and loading). The total porosity of concrete typically ranges between 15 and 20 % of the volume (see Table 2.5). It comprises gel pores (between the individual crystals and particles of gel) and capillary pores, which remain after hydration and are partially occupied by excess water, and air pores, which may be either intentional (entrained air pores) or accidental (due to poor compaction) – see Figure 2.6. The porosity of sprayed concrete tends to lie at the higher end of the range for concretes (Kusterle 1992, Lukas *et al.* 1998, Blasen 1998, Oberdörfer 1996) - see Table 2.5 - with the highest porosities generally in wet mix sprayed concrete. Considering a wet mix sprayed concrete, a dry mix sprayed concrete (spray cement with moist aggregate) and a normal cast concrete, all with the same water/cement ratio of 0.55, Blasen (1998) found that porosity of the wet mix was 16 % greater than the cast concrete, while the porosity of the dry mix was only 8.7 % higher. Consequently, wet mix sprayed concretes generally achieve lower strengths than comparable dry mixes.

Failure of concrete in compression is governed by cracking under uniaxial or biaxial compression and by crushing under multi-axial stress (Neville 1995, Chen 1982). Existing microcracks due to hydration and drying shrinkage start to grow when the load exceeds about 30 % of the maximum compressive strength of mature concrete (Feenstra & de Borst 1993). These microcracks are mainly located at the interface between the aggregate and hardened

cement paste. As the size of the microcracks increases, the effective area resisting the applied load decreases and so the stress rises locally faster than the nominal load stress (Neville 1995). This leads to strain hardening and the curved shape of the stress-strain graph for concrete in compression (see Figure 2.7) - i.e. the tangent modulus decreases with increasing strain. Clearly, the higher the initial level of porosity in the concrete, the higher the initial local stresses will be. Above an applied stress of about 70 % of the maximum compressive strength, cracking occurs within the paste and the microcracks start to join up (Rokahr & Lux 1987). After the maximum compressive strength has been reached, macrocracks form as the microcracks localise in narrow bands and the load that the concrete can sustain decreases (Feenstra & de Borst 1993).

Table 2.5: Composition of porosity

Pore type	Pore diameter	Mix type	% of total volume
Gel	< 0.1 μm	Dry & Wet	3 - 4 % est. [11]
Capillary	0.1 – 10 μm	-	15 - 19 % [18]
		Wet	13 - 17 % [19]
		Dry & Wet	17.5 % [20]
Entrained air pores	> 10μm &	Wet	0.9 - 4.5 % [11]
& accidental voids	0.001 to 0.1 m	Dry & Wet	3.7 % [12]
			Wet 17 - 22 % [11]
	Total porosity		Dry 18 - 20 % [11]
			Dry & Wet - 21.1 % [12]

Under triaxial compressive stresses, the cracking may be suppressed by the lateral stresses and, if the confinement is high, the mode of failure is crushing. Hence, the maximum compressive stress under triaxial compressive loading is much higher than the uniaxial or biaxial strength (Chen 1982, Neville 1995). However, in the case of a tunnel lining, the stress

[18] Kusterle 1992

[19] Cornejo-Malm 1995

[20] Blasen 1998 (average values from 337 samples)

state is largely biaxial since the radial stresses in the lining are much lower than the tangential and longitudinal stresses (Meschke 1996). In compression, the biaxial strength is only 16 % greater than the uniaxial strength, when $\sigma_2 / \sigma_1 = 1.0$, and 25 % greater, when $\sigma_2 / \sigma_1 = 0.5$ (Chen 1982) – see Figure 2.8. In intermediate states of stress between pure compression and pure tension, the presence of a tensile stress reduces the maximum compressive stress attainable (Chen 1982). In the biaxial stress case, it is often assumed that the maximum compressive stress reduces linearly from the uniaxial value (when the tensile stress is zero) to zero (when the tensile stress equals the maximum uniaxial tensile stress) – see Figure 2.8.

To summarise, the strength of concrete depends on one hand on the strength of the main components – the hardened cement paste and aggregate – and on the other hand on the density of the sample. Strength rises with age since the quantity of hardened cement paste increases with age as the hydration process continues and the quantity of voids decreases, rather than any actual change in the mechanical properties of the microscopic constituents (Ulm & Coussy 1995). On a microscopic level, the local stress depends on the effective area of solid material sustaining the stress (if one ignores any contribution of pore water pressure) and the growth of cracks then depends of the strength of the hardened cement paste – aggregate bond compared to these local stresses. From this simplified theory of how concrete behaves under compressive loading, one would conclude that, to improve the strength of a concrete, one should improve the density of the material, by maximising hydration and minimising the porosity, and one should also improve the hardened cement paste – aggregate interaction.

Influences on behaviour

Modern specifications typically require compressive strengths of 20 MPa (for temporary sprayed concrete) to 40 MPa or higher (for permanent sprayed concrete) at 28 days (Brooks 1999). However, the sprayed concrete must also possess sufficient adhesion to adhere to the ground and to support load, from the ground as well as other sources, such as blasting, soon after it has been sprayed. Hence, in contrast with conventional concrete, the sprayed concrete mix must be designed to attain a relatively high early compressive strength (see Figure 2.2) as

well as meeting the long-term criteria. Furthermore, the mix must meet more stringent workability and pumpability criteria than conventional concrete. Of these competing criteria, traditionally the early age strength (which determines the thickness of layers that can be formed and the safety of the tunnel heading) and the pumpability requirements have dominated, at the expense of longer term strength (Kusterle 1992, Leggett & Darby 1997).

Accelerators - Accelerating the hydration reaction will increase the strength of the sprayed concrete at early ages (see Figure 2.2). Traditionally, high early strengths have been achieved by adding accelerators to the mix in the spraying nozzle. This has several disadvantages. Firstly, accelerating the hydration reaction causes more, smaller hydrated calcium-silicate crystals to grow. A slower reaction permits larger crystals to grow, resulting in higher strengths in the long-term (Fischnaller 1992, Atzwanger 1999)[21]. Secondly, many of the early accelerators were very alkaline and hazardous to the health of workers in the tunnel. Some accelerators, such as waterglass (sodium silicate), not only led to low strengths at 28 days but even caused the strength to decrease with age (Kusterle 1992). The concerns over low long-term strengths and health and safety have forced the introduction of new accelerators – modified sodium silicates, so-called "alkali-free" or "low-alkali" accelerators (Brooks 1999). With these new products and other new additives, the compressive strength gain of sprayed concrete can be controlled with a fair degree of accuracy and tailored to suit the particular requirements of the project. Together with new cements and additives such as microsilica, the competing demands of high early strength and long-term strength can be met more satisfactorily (see Table 2.2).

Cement – To reduce the need for accelerators, new types of cement have been introduced. The so-called "spray cements" have been developed for use with the dry mix process (Testor 1997, Lukas *et al.* 1998). If gypsum (hydrated calcium sulphate) is removed from cement, the speed of the hydration reaction increases dramatically. Normally the gypsum reacts to form a film of calcium sulfoaluminate (ettringite) on the surface of the tricalcium aluminate in

[21] A more detailed discussion of the hydration of cement and its chemistry can be found in Neville (1995)

cement particles. Otherwise, the tricalcium aluminate is free to react immediately and form hydrated calcium aluminate directly (Neville 1995, Atzwanger 1999). The reaction is so rapid that most of these new cements can only be used with oven-dried aggregate, otherwise hydration may occur in the delivery hoses. No accelerator is required. The latest "spray cements" can also be used with naturally moist aggregates. While costs are reduced by not having to use accelerators, extra costs are incurred in the preparation and storage of the cement and aggregate. For wet mix sprayed concrete, Ordinary Portland Cement is normally used.

Cement replacement – Pulervised fly ash and ground granulated blast furnace slag are added to the sprayed concrete mix as cement replacements in the normal manner, though ground granulated blast furnace slag (GGBS) cannot be used in the same quantities as in conventional concrete. Because of its particles' angular shape GGBS can only be used to replace up to 35 % of the cement (Brite Euram 1998). Above this level there are problems pumping the mix. Since these materials react more slowly than cement, their beneficial contributions to durability characteristics, density and strength are only seen over the longer term (i.e. at ages greater than 28 days).

Water / cement ratio – The lower the water/cement ratio, the higher the strength because fewer voids are left after hydration. Complete hydration requires a water/cement ratio of approximately 0.23. However, pumpability requirements dictate that higher water/cement ratios are used for wet mix sprayed concrete than for cast concrete. In the dry mix process, the water / cement ratio is controlled by the nozzleman. Typically average values are 0.3 to 0.55; the ratio for wet mixes lies in the range of 0.4 to 0.65 (Malmberg 1993).

Grading curve & aggregate - The maximum aggregate diameter is usually limited to about 10 to 12 mm, compared to 20 mm for cast concrete. Strength increases with increasing maximum diameter of aggregate but the larger the pieces of aggregate the more of them are lost in rebound (Kusterle 1992, Brite Euram 1998, Austin *et al.* 1999). As a whole the grading curve for sprayed concrete is biased towards the finer end (see Figure 2.1) for ease of

pumping (Norris 1999). Both crushed and round gravel can be used as aggregate. Some experimental evidence suggests that the type of gravel causes little difference in the quality of the sprayed concrete (Springenschmid *et al.* 1998). However, anecdotal evidence from various sites suggests that the grading curve and sometimes the type of aggregate too may have a great influence on the sprayed concrete. Aggregate that has a smooth grading curve should be used and angular particles should be avoided since they are more difficult to pump. If necessary, either the sand or the aggregate may be angular but one of the two should be rounded.

Microsilica - The addition of microsilica has two main advantages. Firstly, it improves the adhesion of the sprayed concrete, permitting accelerator dosages to be reduced or thicker layers of sprayed concrete to be placed. The higher adhesion reduces dust and rebound (Brite Euram 1998). Secondly, acting as a very reactive pozzolanic pore-filler, microsilica improves the long-term density, which is beneficial for strength and durability. In general microsilica improves the quality of the sprayed concrete, improving durability as well as mechanical properties (Kusterle 1992, Norris 1999). The main disadvantage is its high water demand, which requires more plasticiser or water or both (Norris 1999, Brooks 1999). However, it has been suggested that, in the case of dry mix sprayed concrete, this additional water may be partially responsible for the reduction in dust and rebound (Austin *et al.* 1999).

Fibres – Contradictory evidence exists as to whether the addition of steel fibres alters the compressive strength of sprayed concrete. Vandewalle (1996) suggests that they have little beneficial effect, while Brite Euram (1998) suggests that steel fibres increase the compressive strength by 10 to 35 %. Polypropylene fibres were also found to enhance strength but they also increase the water demand so that there is little overall benefit (Brite Euram 1998).

Other additives & admixtures - Individually plasticisers, stabilisers and other additives may not have a detrimental impact on the mechanical properties of sprayed concrete but one must always be aware that combinations of accelerators and additives may produce unfavourable

results, such as significantly reduced strengths (Brite Euram 1998). Compatibility testing before work begins on site is used to identify such unfavourable combinations.

Anisotropy – Concrete is not naturally anisotropic and the anisotropy seen in sprayed concrete is a consequence of the way in which it is produced (see section 2.3.7). Compressive strengths have been found to be 10 - 25% higher in the plane perpendicular to the direction of spraying (Cornejo-Malm 1995, Huber 1991, Fischnaller 1992). However, others have reported no variation in strength with direction of testing (Purrer 1990, Brite Euram 1998). At first sight, higher strengths perpendicular to the direction of spraying may seem paradoxical since spraying is the sole means of compaction for sprayed concrete. This "softer response" may be due to compaction at the less dense interfaces between layers of sprayed concrete (Aldrian 1991). The strength is normally tested in the direction of spraying, since the samples are usually cored from sprayed test panels or the lining itself, whereas the major compressive stresses are in the plane perpendicular to this (Golser & Kienberger 1997, Probst 1999). Hence the use of strength values from cores is conservative.[22] Steel fibre-reinforced sprayed concrete exhibits pronounced anisotropy in its behaviour under both compression and tension (see 2.2.2). Normally anisotropy of the sprayed concrete (and indeed the stiffening effect of the layers of mesh or fibres) is ignored.

In conclusion, if properly implemented, sprayed concrete can achieve high early strengths and long-term strengths (see Table 2.2). The exact shape of the strength gain curve will depend on the sprayed concrete mix and additives. Because of the interest in early age strength gain, several authors have proposed equations that can be used relate the compressive strength to age (Aldrian 1991, Chang 1994, Alkhiami 1995 & Yin 1996 (after Weber 1979), Pöttler

[22] It should be noted that the compressive strengths of sprayed concrete are normally determined from cylindrical cored samples. The values depend on the dimensions of the samples (Neville 1995), though as a guide, the Norwegian Concrete Association suggested that the compressive strength of a drilled core (height to diameter ratio of 2.0) will be 0.64 times the strength of a cast cube specimen (NCA 1993). This conversion consists of 2 factors: 0.8 for the cube/cylinder correction & 0.8 for insitu sampling.

1990, Meschke 1996) – see Figure 2.9 and Appendix A. Other more complex approaches have been developed to include ageing in numerical analyses (see section 2.3).

2.2.2 Strength in tension

Theories and mechanisms

Even more so than in the case of compression, when under tension, cracking governs the behaviour. Up to 60 % or more of the maximum uniaxial tensile stress few new microcracks are created and so the behaviour is linearly elastic (Chen 1982). The period of stable crack propagation under tension is shorter than compression. At about 75 % of the maximum uniaxial tensile stress unstable crack propagation begins and a few cracks grow rapidly until failure occurs. The actual failure strength is much lower than theoretical predictions based on molecular cohesion in a flawless material would suggest. The exact cause of tensile rupture is unknown but it is believed to originate in flaws in the hardened cement paste itself and at the paste / aggregate interface, rather than in the voids and pores, although these features contribute to the formation of stress concentrations (Neville 1995).

Normally the tensile strength of concrete is ignored in design because it is low – typically about one tenth of the compressive strength – and because of the brittle nature of the failure once the maximum is reached. To counteract this, tensile reinforcement is added to the concrete. Reinforcement in sprayed concrete tunnel linings is normally steel mesh or steel fibres, although experiments have been performed with other materials, such as polypropylene fibres (Brite Euram 1998). When reinforced concrete is loaded with a tensile stress, cracking occurs in the concrete as before. However, the bond between the uncracked concrete and the steel bars permits a gradual transfer of the tensile load from the cracking concrete to the steel as the load increases (see Figure 2.10). The reinforced concrete continues to act as a composite and hence it has a stiffer response to loading than the reinforcement or concrete alone. This phenomenon is known as "tension stiffening" (Feenstra & de Borst 1993).

Fibre reinforcement has a similar effect but the interaction between the fibres and the matrix is more complex. The fibres bridge the opening cracks, thereby continuing to carry tensile

forces across the cracks. The fibres are usually deformed in some manner to improve their resistance to being pulled out of the concrete as a crack opens. High grade steel is used for the fibres (typically yield strengths around 1000 MPa) so that failure occurs by means of a "ductile" process in which individual fibres are pulled out of the concrete. If lower strengths are used, the individual fibres would snap and the overall failure process would be a brittle one. The typical dosage for steel fibres ranges from 20 to 60 kg/m^3.

Influences on behaviour

The tensile strength of sprayed concrete is subject to the same influences and can be improved in the same ways as the compressive strength (see section 2.2.1). A spin-off of this is that the tensile strength of concrete can be reliably estimated from the compressive strength. Various empirical formulae have been proposed (see Appendix C). It is generally assumed that the tensile strength increases with age at the same rate as compressive strength.

Sprayed concrete tunnel linings are formed by spraying several layers of concrete. Mesh or bar reinforcement is placed on the surface of the last layer sprayed and encased in concrete by the next layer (see Figure 1.6). Because the sprayed concrete must be sprayed through the mesh, complete encasement is difficult to achieve (Podjadtke 1998). Sprayed concrete rebounds off the bars and "shadows" are left behind the individual bars (see Figure 2.11). Not only does this reduce the bonded length of the mesh but it also provides an ideal location for corrosion of the steel to occur, if water permeates through the lining.

Steel fibre reinforced shotcrete (SFRS) has many advantages (Brite Euram D1 1997, Vanderwalle *et al.* 1998): fibres are more effective in controlling shrinkage cracking than typical mesh or bar reinforcement; they can be included in the sprayed mix, reducing the cycle time and improving safety, since there is no mesh to be fixed at the face; SFRS can behave in an almost elastic-perfectly plastic manner (Norris & Powell 1999), withstanding very large post-yield strains; corrosion of the fibres is not generally thought to be a significant problem (Nordstrom 2001) and there are no problems of shadowing. These qualities are especially desirable in rock tunnels, where large deformations are expected and SFRS can be

used in conjunction with rock bolts or in permanent sprayed concrete linings, which are acting mainly in compression (Annett *et al.* 1997, Rose 1999).

Although the fibres orientate themselves mainly in the plane perpendicular to the direction of spraying (e.g.: Cornejo-Malm 1995, Norris & Powell 1999), the moment capacity of SFRS is quite small, at typical fibre dosages. If a large moment capacity is required, then bars or mesh reinforcement are needed. This is usually assumed to be the case in soft ground tunnels, especially at junctions. Hence, SFRS alone is rarely used in soft ground tunnelling. If one could be certain that the tensile stresses due to bending were well below the yield strength for SFRS, this material could be used more widely, with potentially large cost savings (Norris 1999). The German Concrete Society's guidelines on SFRS include a design method in which the strength from flexural tests can be converted into a permissible tensile strength (DBV 1992).

Because the fibres orientate themselves in the plane perpendicular to the direction of spraying, when tested in compression in this plane, SFRS exhibits a stiffer response pre-peak, higher peak stresses and a softer post-peak response, compared to tests performed in the same direction as spraying (Brite Euram 1998). The axial and lateral strains at ultimate stress are lower for the same reason.

2.2.3 Strength in other modes of loading

The input parameters for concrete models, such as Drucker-Prager or Mohr-Coulomb plasticity models, are generally derived from the compressive and tensile strengths. Unlike soils, the shear strength of sprayed concrete is not normally tested directly. However, the shear strength may be critical to the performance of the sprayed concrete lining (Barrett & McCreath 1995, Kusterle 1992), particularly if the lining thickness is very small (NCA 1993). Information on the shear strength of sprayed concrete bonded to various rocks is contained in Figure 2.12 (see also NCA (1993)) for information on bond strengths to rock).

Similarly, the bond strength of sprayed concrete (both to the substrate and between successive layers of sprayed concrete) is important to the performance of sprayed concrete. In rock

tunnels, when considering the lining, acted upon by a single wedge, the failure of sprayed concrete linings has been found to occur in two stages - usually by debonding, followed by failure in flexure (Barrett & McCreath 1995, NCA 1993). Table 2.6 contains typical values for the peak strengths of sprayed concrete in other loading modes. The bond strength between layers of sprayed concrete has been examined in the context of permanent sprayed concrete linings, in which the final layer may be added months after the first (Kusterle 1992, Brite Euram 1998). Typical values of bond strength between layers of sprayed concrete range between 0.8 and 2.6 MPa (Brite Euram 1998). In soft ground the tunnel lining is subjected to a more even loading than in rock tunnels so the bond strength may not be an important parameter for soft ground tunnels.

Table 2.6: Strength in other modes of loading (after Barrett & McCreath 1995)[23]

Age	"Poor" bond strength MPa	"Good" bond strength MPa	Direct shear strength MPa	Flexural strength MPa	Diagonal tensile strength MPa	Uniaxial compressive strength MPa
8 hours	-	-	1.0	-	0.75	5.0
1 day	-	-	2.0	-	1.0	10.0
7 days	-	-	6.0	4.0	1.75	30.0
28 days	0.5	1.0	8.0	6.0	2.0	40.0

2.2.4 Stress – strain relationship in compression

Behaviour and influences

The mechanisms behind the stress-strain behaviour of concrete in compression have been described already in section 2.2.1. A stress-strain curve for an uniaxial test typically shows a linear elastic response up to the limit of proportionality, followed by what becomes an increasingly softer response as the maximum compressive strength is approached (see Figure 2.7). After reaching a peak value, the stress that can be sustained falls with increasing strain

[23] All sprayed concrete strengths are for an unreinforced mix with silica fume added.

until the ultimate compressive strain is reached and the sample fails completely. In fact the onset of failure may occur before the peak stress, since the maximum volumetric strain is reached at a stress of between 0.85 and 0.95 of the peak and after this point dilation starts (Brite Euram C2 1997). The observed shape of the post-peak descending branch of the stress/strain curve depends heavily on the confinement and the boundary conditions imposed by the experimental equipment, due to the localisation of cracking (Choi *et al.* 1996, Swoboda *et al.* 1995). For that reason, one could describe concrete as being a "near-brittle" material and ignore the post peak region, concentrating rather on the pre-peak region, for which generalised mathematical relationships have been developed (e.g.: BS 8110 Part 2 1985), that agree well with a large range of uniaxial, biaxial and triaxial data, including tests on sprayed concrete (Brite Euram C2 1997).

The stress-strain behaviour of concrete under multi-axial stress states is very complex. While the increase in compressive strength has been clearly established, it is more difficult to form a definitive picture of the strain behaviour since it depends heavily on the boundary conditions in the experiments (Chen 1982), although increasing the confining pressure appears to lead to more ductile behaviour (Michelis 1987, Aydan *et al.* 1992a) - see Figure 2.7. Triaxial behaviour will not be discussed further since this stress state in a tunnel lining is basically biaxial. The effect of tension in mixed biaxial loading is to reduce the peak (and failure) principal compressive and tensile strains (Chen 1982). The maximum strength envelope under biaxial loading can be considered to be independent of the stress path (Chen 1982).

Furthermore the stress level in a tunnel lining is relatively low. Considering a typical tunnel, where the principal stresses in the lining might be 5.0, 5.0 and 0.5 MPa and the 28 day strength is 25 MPa, the normalised octahedral mean stress (σ_{oct}/f_{cyl}) is only 0.14. Hence one can ignore those effects, which occur at moderate to high stress levels, such as the curved nature of the yield surface meridians (see Figure 2.13).

Particular points of interest to the designer are the initial elastic modulus, the limit of proportionality (i.e. limit of elastic range), the peak stress and strain. The behaviour post peak

and at high stress/strength ratios (e.g.: > 0.85) will not be discussed further here on the grounds that structures are not normally designed to operate in this region.

2.2.4.1 Elastic region

Elastic limit - The behaviour of sprayed concrete at early age, in compression tests, has been characterised as viscous (from 0 to 1 or 2 hours old), visco-elastic (1 to 11 hours) and elasto-plastic (from 11 hours onwards) (Brite Euram 1998). This behaviour may vary depending on the level of loading. Figure 2.14 shows how the ratio of yield stress to peak stress for sprayed concrete (estimated visually from stress-strain curves or from published data from (Aydan *et al.* 1992a)) varies with age. Some data suggest that the yield point is relatively high – 0.70 to 0.85 of the peak stress (Aydan *et al.* 1992a). Other data suggest much lower ratios, tending towards the generally accepted yield ratio for mature concrete of 0.3 to 0.4 (Chen 1982, Feenstra & de Borst 1993). If one examines tests that included unloading/reloading cycles (e.g.: Moussa 1993, Probst 1999), one can see that all the strain is not be recovered upon unloading even at low stresses. This supports the view that the elastic limit is low.

Elastic modulus - Considerable data exists for the elastic modulus (calculated from uniaxial compression tests) and how it varies with age (eg: Chang 1994, Kuwajima 1999). The modulus grows rapidly with age in a similar way to compressive strength, although it may grow at a faster rate (Chang 1993). Various formulae have been proposed to relate the elastic modulus to age (see Figure 2.15 and Appendix A). Other more complex approaches have been developed to include ageing in numerical analyses (see section 2.3.3.8). Sprayed concrete may exhibit anisotropy, with the elastic modulus in the plane perpendicular to the direction of spraying being higher than in the plane parallel to direction of spraying. Celestino (1999) reports that it is 40% higher while Cornejo-Malm recorded an increase of 10% (see also section 2.2.1).

Poisson's ratio - Within the elastic range and up to 80 % of the maximum stress, Poisson's ratio remains constant for mature concrete, ranging between 0.15 and 0.22 and with an average of about 0.2 (Chen 1982). The actual value of the Poisson's ratio depends mainly on

the type of aggregate, with lower values in concrete with lightweight aggregate (Neville 1995). Mature sprayed concrete exhibits the same behaviour but there is some evidence that the Poisson's ratio varies with age. Kuwajima (1999) measured the dynamic Poisson's ration using ultrasound and found that it decreased with age from close to 0.5 to about 0.28 (see Figure 2.16). Dynamic Poisson's ratio values are usually higher than static ones (Neville 1995). Aydan *et al.* (1992a) and Aydan *et al.* (1992b) report a similar variation with age. They measured values of Poisson's ratio close to 0.45 initially falling to about 0.2 at 12 hours but they do not state how these values were obtained (see Appendix A for equation relating Poisson's ratio to age). Plane strain compression tests from the Brite Euram project (Brite Euram 1998) suggest that the Poisson's ratio at early ages (3 to 16 hours) is closer to the mature values.

2.2.4.2 Plastic region up to peak stress

The strain at peak stress decreases with increasing age (see Figure 2.17), from as high as 5.0 % at 1 hour old to a relatively constant value of 1.0 %, from 100 hours onwards. The peak strain of mature concrete is normally assumed to be about 0.3% in uniaxial and biaxial loading (Chen 1982, BS 8110 Part 1 1997). The ultimate strain (at failure) decreases with age (see Figure 2.18) and the behaviour becomes more brittle (see Figure 2.7) (Swoboda et al 1995). Swoboda & Moussa (1992) observed a similar trend, although they plotted a graph of maximum strain against the logarithm of the compressive strength of the sprayed concrete rather than its age. It is believed that the deformation behaviour of mature sprayed concrete is not affected much by changes in mix constituents (Brite Euram 1998), e.g.: the normalised stress at maximum volumetric strain does not change with variation in accelerator dosage and the strain at peak stress is also independent of accelerator dosage (Swoboda & Moussa 1992).

The addition of steel fibres appears to make the sprayed concrete more ductile, with a strain at peak stress of about 0.42% (28 days), compared to 0.20% for plain sprayed concrete (Brite Euram 1998).

2.2.4.3 Unloading

In uniaxial compression tests, the unloading (and reloading) modulus is stiffer than the initial loading modulus (Michelis 1987, Probst 1999, see Figure 2.19). Probst (1999) suggests multiplying the current value of (initial) modulus by a factor of 1.1 to 1.5, to account for this, while the average of results from Aldrian (1991) was 1.27. For loads up to 70 % of the peak stress, Moussa (1993) found that, when reloaded after unloading, the stress-strain path would rejoin the original curve at the point where it had departed on unloading and continue as if the unloading had not occurred (as one would expect for concrete (Chen 1982)). Using a new testing rig, which does not require demoulding and therefore minimises disturbance of the samples, Probst (1999) observed the same behaviour as Moussa in uniaxial tests, even up to 80 % of peak stress (see Figure 2.19).

2.2.4.4 Damage due to loading and temperature

As mentioned earlier, the question of whether or not early loading damages the concrete is of great importance in the debate over the use of permanent sprayed concrete linings. Little research has been done on this aspect of sprayed concrete. Moussa (1993) concluded from experimental work that stresses below a utilization factor, α, of 70% of the current peak stress had no detrimental effect on the later peak stress. He proposed a linear relationship between the reduction factor and the stress above this level:

$$R_{dfc} = 2.532\ (\sigma/f_{c\,t1} - 0.69) \qquad 2.1$$

which ranges from 0 at α=0.69 to 0.78 at α=1.0, where $\alpha = \sigma/f_{c\,t1}$ and σ = the stress applied and $f_{c\,t1}$ = the uniaxial strength at the age of loading, t1. However, the experimental data were quite scattered (Swoboda *et al.* 1995). By comparing the strength of samples from creep tests with samples from parallel shrinkage tests, Huber (1991) found that the strength of loaded samples was 80 % of the unloaded ones. The utilization factors in the creep tests ranged from 20 to 70 %.

Similarly, Cervera *et al.* (1999a) proposed a reduction factor for the ultimate peak stress, to account for the effects of (constant) elevated ambient temperatures during curing. The reduction factor is $k^{iso} = [(100-T^{iso})/(100-20)]^{nT}$, where nT = 0.25 to 0.4 and T^{iso} is the

(constant) temperature during hydration. This gives comparable reductions to those found experimentally by Seith (1995), e.g.: 25% reduction in strength for curing at 60 °C compared to curing at 16 °C. Although the temperature in linings rises to more than 40 °C during hydration, this rise is short-lived. This is less onerous than prolonged curing at elevated temperatures in the study by Seith. Therefore thermal damage in real tunnels is probably negligible.

2.2.5 Stress – strain relationship in tension

The mechanisms behind the stress-strain behaviour of unreinforced concrete in tension have been described already in section 2.2.2. Experimental data on conventional concrete in tension are scarce, especially for concrete at early ages. A stress-strain curve for a uniaxial test on mature concrete typically shows a linear elastic response up to 60 % of the maximum stress (Chen 1982). As increasingly more microcracking occurs, the response becomes softer until the maximum stress is reached. After the peak stress, the stress quickly drops to zero for unreinforced concrete, though the precise nature of the descending branch of the stress-strain curve depends heavily on the arrangement of the testing rig (Hannant *et al.* 1999, Chen 1982). Reinforcement enables tensile forces to be carried even though the concrete has cracked, as discussed earlier (see section 2.2.2 and Figure 2.10). The utilization factor in areas of tensile stress is likely to be much higher than in areas of compressive stress because the tensile strength is much lower.

At very early ages (i.e. less than 4 hours old), cast concrete appears to behave plastically and can be strained by up to 0.5 % or more (Hannant *et al.* 1999). However, this ultimate strain reduces sharply with increasing age and is about 0.05% at 5 hours.

Sprayed concrete exhibits the same behaviour (see Figure 2.20). In uniaxial tensile tests, plain sprayed concrete and fibre-reinforced sprayed concrete (SFRS) behave similarly (Brite Euram 1998) and, as for plain concrete, the ultimate strain reduces sharply in the first few hours. The effect of the steel fibres can be seen in Figure 2.20 as converting an otherwise brittle failure into a more ductile one, in which the stress-strain curve descends slowly from the peak. A similar effect is observed in flexural tests on SFRS beams. Taking the toughness index, I_{10},

values of 4 and 6 as indicative of "fair" and good" performance, SFRS typically falls into the "good" category while polypropylene fibre-reinforced sprayed concrete falls into the "fair" category (Brite Euram 1998)[24]. However, new High Performance Polymers are being developed which may provide comparable performance to SFRS (Tatnall & Brooks 2001).

Poisson's ratio is the same in tension as in compression in the elastic region. The elastic modulus under tension is also assumed to be equal to that under compression for unreinforced concrete.

The variation in the material properties of sprayed concrete with age has already been discussed. The variation with material properties with time is covered under durability in section 2.3.10. In the following sections, the variation of sprayed concrete's behaviour with time will be considered. This can be subdivided into two categories: - stress-independent changes (due to shrinkage and temperature effects - section 2.2.6) and stress-dependent changes (due to creep – section 2.2.7).

2.2.6 Shrinkage and temperature effects

The following sections will cover the subject of shrinkage (plastic, autogeneous, drying and carbonation shrinkage) and expansion due to temperature effects, both of which induce strains in concrete.

2.2.6.1 Theories and mechanisms

Plastic shrinkage is the contraction caused by the loss of water from the fresh concrete's surface due to evaporation or suction, by adjacent dry soil or existing concrete, while the concrete is still plastic (Neville 1995). If the water lost exceeds the volume brought to the surface by bleeding, surface cracks may appear. Plastic shrinkage increases with increasing evaporation, cement content and water/cement ratio and increases with a decreasing tendency for bleeding. A typical value for (linear) shrinkage after 24 hours is 0.2 % (for 400kg/m^3 cement, air temp = 20 °C, relative humidity = 50 %, air velocity of 1.0 m/s - Neville 1995).

[24] For explanations of the term I_{10} see the ITA report (Malmberg 1993) or Vandewalle (1996)

Plastic settlement also occurs in the first hours after casting and is sometimes confused with plastic shrinkage. Plastic settlement is caused by differential settlement of the concrete over obstructions such as large aggregate or reinforcement (Neville 1995). Two key factors influencing this are the degree of compaction and the rate of build-up of concrete. In the case of sprayed concrete, in the crown of the tunnel the sprayed concrete is loaded by its own self-weight from the moment it is sprayed. This represents some of the most extreme conditions for sprayed concrete: the degree of compaction is least and rebound is greatest in the crown due to vertical spraying; the bond to the substrate depends heavily on the preparation of that surface and the early age strength gain of the sprayed concrete, which also controls the adhesion between subsequent layers of sprayed concrete. If one of these properties is inadequate or too thick a layer of sprayed concrete is sprayed, lumps of sprayed concrete will simply fall out of the lining. The presence of reinforcement will help to prevent this but this would imply that the sprayed concrete is hanging off the reinforcement - potentially leading to plastic settlement cracking.

Autogeneous shrinkage occurs when there is no movement of water to or from the concrete. During hydration water is drawn from the capillary pores. This "self-desiccation" causes the cement matrix to contract. Typical values of autogeneous shrinkage are 0.004 %, i.e. an order of magnitude smaller than plastic shrinkage (Neville 1995). The magnitude of autogeneous shrinkage is likely to be greater in sprayed concrete due to the faster rate of hydration and high cement content.

Drying shrinkage occurs in the hardened cement paste as water is lost to the air[25]. First the water from the larger voids and capillary pores is lost and this causes no shrinkage. However, when the absorbed water in the hardened cement paste is removed, shrinkage occurs. The constituents of sprayed concrete and its curing mean that sprayed concrete is likely to shrink more than a similar strength cast insitu concrete

[25] Plastic shrinkage (see above) is the early part of drying shrinkage while the concrete is still plastic.

Considering the constituents, drying shrinkage increases primarily with increasing cement content, decreasing quantity of aggregate and decreasing stiffness of the aggregate (Neville 1995). The reasons lie in the increased quantity of hardened cement paste and the restraining effect of aggregate respectively. Most natural aggregate itself does not shrink but shrinkage does vary considerably depending on what aggregates are used. The actual grading curve has little influence other than indirectly by altering the relative proportions of cement and aggregate (Powers 1959). Water/cement ratio has no direct influence but increasing the ratio reduces the proportion of aggregate. Cement type generally has little influence on shrinkage, though cements, which have low gypsum contents, tend to shrink more than normal. More accurately, for each cement there is an optimum gypsum content, which minimises shrinkage (Powers 1959). Low gypsum contents also mean a fast reaction, which produces a different gel structure and porosity. This would suggest that the fast reacting sprayed concrete mixes and especially those made with dry-mix "spray cements" will produce sprayed concrete that exhibits high shrinkage and shrinkage cracking. The fineness of the cement also influences shrinkage, because increasing fineness reduces the number of larger particles, which restrain shrinkage (Powers 1959). Silica fume, fly ash and ground granulated blast furnace slag are known to increase shrinkage and are all commonly used in sprayed concrete. The use of plasticisers and other water reducing admixtures implies a higher cement content in the mix and hence higher shrinkage, although the admixtures themselves are not believed to cause additional shrinkage.

Considering curing and the tunnel environment, one would expect that any measure that reduces moisture loss from the concrete would reduce drying shrinkage. In the extreme, concrete stored underwater actually swells rather than shrinking. Drying shrinkage increases considerably with decreasing relative humidity. Shrinkage at a relative humidity of 40 % can be 3 times greater than at a relative humidity of 80 %. However, concrete is subject to a series of competing influences. For example, prolonged moist curing reduces drying but also reduces the quantity of unhydrated cement available to restrain shrinkage (Neville 1995). Well-cured concrete shrinks faster and, since it is more mature, the capacity for creep is much

reduced. This reduces the ability to reduce the stresses due shrinkage. On the other hand, the more mature concrete is stronger.

The effect of ventilation depends on the rate at which moisture can move within the concrete. During the early stages, increased ventilation may increase shrinkage (Kuwajima 1999). At later ages, the rate of evaporation is much greater than the rate of movement of water in the concrete and so increased ventilation has no effect. In the case of tunnels the movement of air stems from tunnel ventilation and may be highly localised in nature, since the forced ventilation is provided by means of ventilation ducts. Typically, relative humidity in a tunnel is around 50 % (though it may be higher) and the temperature is fairly constant within the range from 12 to 24 °C, depending on the time of year. The flow of air from ventilation ducts will dry out the sprayed concrete adjacent to them. Concrete with a temperature of 25°C (in air at 20°C and 50% RH), being dried by a current of air at 10 km/hr (which is 2.8 m/s), would lose around 0.5 kg of water per m^2 per hour (see Figure 2.21). If there were no flow of air, it would lose around 0.15 kg per m^2 per hour. Considering Figure 2.21, one can see that given the high local air velocities at the end of a vent duct (around 20 km/hr), the high temperature of the sprayed concrete during initial hydration (typically 30 to 45°C) and the large surface area, considerable volumes of water could be lost (adjacent to the vent duct) in the early stages of hydration (Oberdörfer 1996). However, experimental results on sprayed concrete are contradictory. Increased ventilation has been found to increase the rate of shrinkage but to reduce the total magnitude (Cornejo-Malm 1995). The magnitude of the shrinkage will depend on the origin of the water that is being removed, i.e. "free" water in capillary pores or "absorbed" water in gel pores, which in turn depends on the original water/cement ratio, the degree of hydration and the porosity of the aggregate (Powers 1959).

Curing – the prevention of water loss - is recognised to be important for proper hydration of concrete. While moist curing is normally specified for a period of between 4 to 7 days after construction, it is difficult to achieve in tunnels. Spraying with water or covering with impermeable sheets or wet matting are usually deemed impractical in a tunnel during construction. Curing compounds can be applied to external faces or internally as special

additives. Externally applied compounds have to be removed before additional layers of concrete are cast or sprayed to ensure that the bond is not impaired.

Drying shrinkage continues to take place over years, albeit at a much reduced rate. Typically only 20 to 50 % of the total shrinkage will have occurred within the first month and about 80 % of the total within the first year (Neville 1995).

Carbonation shrinkage occurs in the surface layers of concrete. Carbon dioxide from the air forms carbonic acid, which reacts with various hydrates in the hardened cement paste, notably calcium hydroxide. Hence, this shrinkage is irreversible. The rate of carbonation slows as the depth of carbonation increases, because the carbon dioxide has further to permeate and because the products of carbonation reduce the porosity of the concrete (Blasen 1998). Carbonation is greatest at moderate levels of relative humidity – i.e. 50 - 75 % - since both the lack of water and saturation slow the process. Although the levels of carbon dioxide may be higher than normal in a tunnel due to construction traffic, the fact that carbonation occurs at the same time as drying is liable to reduce the overall contribution of carbonation to shrinkage, because the carbonation will be occurring while the relative humidity is quite high. Typical values for the depth of carbonation are 2 to 3 mm after 6 months (Oberdörfer 1996).

Expansion and contraction due to temperature changes occur in tunnel linings during the first few days. The thermal coefficient of expansion for sprayed concrete is generally assumed to be the same as cast insitu concrete. This is largely determined by the coefficients of expansion for the cement and aggregate and their proportions in the mix. Typical values range from 4 to 14 x 10^{-6} per °C (Neville 1995, ACI 209R 1992) and codes often assume an average value of 10 x 10^{-6} per °C (DIN 1045 1988, ACI 209R 1992). Similar values have been suggested for sprayed concrete (see Table 2.4).

Typical profiles of temperature in sprayed concrete linings can be found in Kusterle (1992), Fischnaller (1992), Hellmich & Mang (1999) – e.g. see Figure 2.22. As one would expect the maximum rise in temperature depends heavily on the thickness of the sprayed concrete layer

(see Table 2.7), the initial temperature of the mix and the rate of hydration. The peak rise in temperature occurs about 7 to 10 hours after spraying for dry mix sprayed concrete and at 10 to 15 hours for wet mix sprayed concrete (Cornejo-Malm (1995)). Typically the maximum temperature lies between the centre of the lining and the extrados and ranges between 28 to 45 °C (i.e.10 to 25 °C above the ambient temperature). Fischnaller (1992) suggests that wet mix sprayed concrete produces higher temperature rises while Cornejo-Malm (1995), quoting lower figures, suggested that wet and dry mix produce similar temperature rises. Typically after 48 hours the maximum temperature rise (above ambient temperature) has fallen to less than 20 to 30 % of the peak temperature rise (Kusterle 1992).

Table 2.7: Maximum temperature rises in sprayed concrete linings (Kusterle 1992)

Thickness of lining in mm	Max. temperature rise in °C
50 - 100	6 – 9
100 - 150	10 – 15
300	25

Assuming a thermal coefficient of $10x10^{-6}$ per °C and a rise of 20 °C, the heat of hydration would induce a maximum compressive strain of 0.02 % for a perfectly confined sample of concrete. As the concrete cools, it will contract by 0.02 % over the following 48 hours. The initial tendency to expand tends not to induce much compressive stress (because the elastic modulus is still small and creep rates are high) whereas the contraction could induce significant tensile stresses in lightly loaded linings. Although shrinkage of a uniform ring would not induce tensile stresses, sprayed concrete linings are made up of a series of panels of different ages. Therefore there is the potential for differential shrinkage and partial restraint. That said, since the concrete in a lining is not fully restrained so the influence of shrinkage may be small.

2.2.6.2 Cracking due to shrinkage

The very early ages at which cracking is most likely to occur, the variation in conditions within the tunnel (e.g.: ventilation duct in the crown, invert covered with excavated material)

and the possibility of water transfer from the ground all complicate the prediction of cracking due to shrinkage. Indeed it has been reported that water from the ground can actually lead to swelling in the invert and generally a reduction in shrinkage (Kuwajima 1999). Golser *et al.* (1989) report that the shrinkage of the tunnel lining is greatest in the crown, 50% smaller at axis level and negligible in the invert. Creep of tensile stresses (due to shrinkage or bending moments) may lead to additional cracking (Negro *et al.* 1998), although the case study cited may not be representative of general conditions in tunnels. Although the temperature in the thin shell of a tunnel lining peaks and falls much more quickly than, for example, a base slab, which might take several weeks to return to ambient temperature (Eierle & Schikora 1999), the stiffness of the sprayed concrete rises much faster than normal concrete and so there is just as much risk of the stress induced by the contraction exceeding the tensile strength of the concrete. It has been suggested that the stiffness of concrete rises faster than strength (Eierle & Schikora 1999, Chang 1994). Typical values for shrinkage are 0.10 to 0.12 % for wet mixes after 100 days and 0.06 to 0.08 % for dry mixes after 180 days (Cornejo-Malm 1995). Given that the concrete is not fully restrained in a tunnel lining, it is the non-uniform nature of the volume change, rather than merely the magnitude of the shrinkage, which causes cracking.

According to some experimental evidence, the general restraint of shrinkage by reinforcement is quite small. The uniaxial shrinkage strain for fibre reinforced sprayed concrete (both polypropylene and steel fibres at low to moderate dosages) was only 8 % less than that of ordinary sprayed concrete after 300 hours while 0.39 % (by area) steel bar reinforcement reduced the shrinkage strain by 16 % (Ding 1998). The addition of fibres may increase porosity (Chang 1994, Ding 1998, Brite Euram 1998), leading to higher shrinkage and creep at higher dosages (60 kg/m^3 or more) (Ding 1998).

2.2.7 Creep

2.2.7.1 Theories and mechanisms

Creep is defined as the increase in strain with time under a sustained stress and relaxation is the decrease in stress with time in a sample under constant strain (Neville *et al.* 1983)[26]. Relaxation is also sometimes referred to as creep and here the comments on creep can be taken to apply equally to relaxation unless otherwise stated. In discussions on creep, the term "specific (or unit) creep" is often used. Specific creep is the creep strain per unit stress (typically in units of 10^{-6} -/MPa).

Creep can be divided into two components, depending on moisture movement. "Basic creep" is the creep that occurs under conditions of no moisture movement to or from the sample (i.e. conditions of hygral equilibrium). "Drying creep" is the additional creep, which occurs during drying of the sample. The total creep is the sum of these two components. Furthermore, creep components can be divided into reversible and irreversible parts (see Figure 2.23 and England & Illston 1965). On unloading, along with the instantaneous elastic recovery, there will be a gradual recovery of a portion of the creep. While this is relevant for conditions of varying stress, it can be ignored if unloading does not occur. In any case, experimental evidence for sprayed concrete suggests that reversible creep forms a very small percentage of the total strain (typically less than 10 %) in samples that are loaded for a prolonged period, i.e. more than 7 days - see Figure 2.24 (Huber 1991, Abler 1992, Fischnaller 1992, Ding 1998, Probst 1999).

The mechanisms behind creep are not fully understood, although it is recognised that its origin lies within the cement paste and not the aggregate. Shrinkage and creep are normally assumed to be independent and a simple superposition of strains is often used. In reality they probably are not independent since both are related to movement of water within and from the concrete (Neville *et al.* 1983). In the case of drying creep, obviously the movement of

[26] A more detailed discussion of creep in concrete can be found in Neville *et al.* (1983) or in a shorter form in Neville (1995)

water from the concrete plays a role and in practice it may be difficult to distinguish this from drying shrinkage [27]. In the case of basic creep, movement of water from the absorbed layers on the cement paste to internal voids may be a cause of the creep. The fact that creep increases with increasing porosity tends to support this theory (Neville 1995). However, the largely irreversible nature of creep would suggest that the viscous movement of gel particles and to a lesser extent (at higher stresses) microcracking also play a significant role. Like shrinkage, creep occurs over a prolonged period and for conventional concrete 60 to 70 % of the final magnitude of creep strain occurs within the first year (Neville 1995). Creep strains after one year are typically 2 to 3 times the magnitude of the elastic strain[28].

It appears that creep of concrete under uniaxial tension may be 20 - 30 % higher than in compression, but relatively little work exists on this subject and some of it is contradictory (Neville *et al.* 1983). No specific work on creep in tension of sprayed concrete has been found in the course of this review. Creep in tension reduces the risk of cracking due to uneven shrinkage. Creep in compression will reduce the compressive stresses induced by thermal expansion during hydration and therefore increase the risk of tensile stresses forming on cooling.

Lateral creep has the effect of increasing the apparent Poisson's ratio (creep Poisson's ratio) in uniaxial tests, as creep strain occurs in the direction of the lateral expansion, unless the stress is lower than half the strength (Neville 1995). At lower stresses the Poisson's ratio is the same as normal (i.e. about 0.20). However, experimental results from uniaxial tests vary considerably - υ = 0.11 to 0.5 (Golser & Kienberger 1997, Rathmair 1997). Even so one can at least say that the effect of creep is an overall decrease in volume. Under multi-axial stress, the apparent Poisson's ratio is normally lower – 0.09 to 0.17 and considerable creep will occur even under hydrostatic compression (Neville 1995). The simple superposition of the

[27] Creep is time-dependent strain due to applied load; shrinkage is time-dependent strain independent of the applied load.

[28] As estimated from Figure 7.1, BS 8110 Part 2 (1985), assuming RH = 50 %, age at loading = 1 day and an effective section depth of 300 mm.

creep strains due to the stress in a given direction and the Poisson's ratio effect of the creep strains in the two other normal directions is unlikely to be valid (Neville 1995, Mosser 1993) but any errors may be smaller in the case of tunnel linings due to the predominately biaxial stress conditions.

2.2.7.2 Influences on behaviour

Creep of concrete and sprayed concrete alike increases with decreasing **relative humidity** (i.e. increasing drying), increasing **cement content**, increasing **stress** and decreasing **strength** (Fischnaller 1992, Huber 1991, Neville *et al.* 1983). The latter two explain why under a constant stress, applied at an early age, creep is greater for more slowly hydrating concretes (since the stress/strength ratio will be higher). However, if one considers concretes loaded with the same stress/strength ratio, the creep is lower for more slowly hydrating concretes (since the magnitude of the stress applied is lower). In the case of uniaxial compression creep is proportional to the applied stress at low stresses (up to 0.4 of the uniaxial strength (Pöttler 1990, Huber 1991, Aldrian 1991)). Above this level it is believed to increase at an increasing rate. At very high stresses (> 0.8 of f_{cu} (Abler 1992)), creep will lead to failure (so-called "tertiary" creep - Jaeger & Cook 1979).

Creep and creep rates are significantly higher at an **early age** of loading since the strength is lower and this is of importance for SCL tunnels, since the lining is loaded from the moment it is formed. On the other hand, sprayed concrete exhibits a rapid development in strength so, after 24 or 48 hours, the creep behaviour is relatively close to that at greater ages (Kuwajima 1999). Nevertheless, a sample loaded at an age of 8 days may creep by 25 % more than a similar sample loaded at 28 days (Huber 1991).

Creep is also influenced by the **aggregate** in the mix, which restrains the creep. Increasing the proportion of aggregate reduces the magnitude of creep but the effect is small for the ranges of proportion of aggregate in normal mixes. Creep decreases with increasing modulus of the aggregate.

Other mix parameters (such as water/cement ratio and cement type) appear to influence creep only insofar as they influence strength and its growth with time (Neville *et al.* 1983). Hence the types of cement or cement replacements used do not themselves appear to affect (basic) creep behaviour, but their affect on the rate of strength gain will influence creep. Cement replacements, which reduce the porosity (such as microsilica), may well reduce drying creep, since they will restrict water movement.

Considering other influences, the creep of concrete increases with temperature (ACI 209R 1992) but for the case of most tunnel linings, since the increase in temperature due to hydration is relatively small and short-lived, this effect can probably be ignored. This may not be the case in deep tunnels where the ambient temperature of the rock is relatively high. Creep decreases with increasing size of the specimen since this affects drying (ACI 209R 1992, Huber 1991). Some experimental evidence has shown that reinforcement (both bars and fibres) reduces creep (see Figure 2.25 and Ding 1998). Typically, 20 kg/m^3 of steel fibres (0.21 % steel by volume) and 0.39 % bar reinforcement reduce the magnitude of creep by the same amount, roughly 25 % after 180 hours compared to plain concrete. Due to their distributed nature, the fibres have more effect than bar reinforcement.

2.2.8 Variation in properties with environmental conditions

The effects of relative humidity in tunnels on shrinkage and creep, and of temperature on strength gain and creep have already been discussed. This leaves air pressure, production influences (including curing and spraying) and the loading on the lining (including exceptional events such as fires) as the main environmental influences on material behaviour.

Due to several recent high profile tunnel fires (Bolton 1999, Bolton & Jones 1999), the **fire resistance** of tunnel linings has come under scrutiny. Sprayed concrete has in the past been used as fire protection in tunnels (Kompen 1997). However, the fire loading in a tunnel tends to be quite severe (Varley & Both 1999). Explosive spalling due to the build-up of moisture within the concrete would be likely in most conventional sprayed concrete or segmental tunnel linings. Although less dense than the concrete used for segmental linings, sprayed concrete may have a higher coefficient of thermal expansion and so is unlikely to perform any

better than conventional concrete. In the worst case the entire lining thickness can be destroyed. One countermeasure may be the addition of polypropylene fibres to the concrete mix. During a fire, the polypropylene fibres melt and the resulting capillaries provide an escape path for moisture in the concrete, thus avoiding spalling. Although early research has shown promising results, little work has been done so far in this field (Varley & Both 1999).

Dynamic behaviour is rarely a concern, although the subject of seismic design of tunnels is of growing concern. Since sprayed concrete tunnel linings are not generally subject to cyclic loading, fatigue is not of concern, though one may note that steel fibre reinforced concrete performs significantly better under cyclic loads than plain concrete (Vandewalle *et al.* 1998). Cyclic loading could be applied to a sprayed concrete lining, in a railway tunnel, where it forms the permanent lining and is in intimate contact with the trackbed.

Sprayed concrete is rarely used in compressed air tunnelling. Some evidence exists to suggest that considerable quantities of air are lost through the sprayed concrete lining (Strobl 1991). Research has focused on measuring the air permeability of sprayed concrete linings, so that air losses and supply requirements, as well as surface settlements, can be estimated more accurately (Kammerer & Semprich 1999) and the numerical modelling of construction under compressed air (Hofstetter *et al.* 1999).

2.2.9 Durability and construction defects

As mentioned in section 2.2.3, concerns over **durability** of sprayed concrete tunnel lining are preventing the more widespread use of the material in the permanent lining of tunnels (see 1.2.2 & Table 1.1). Durability can be assessed by examining the permeability of the sprayed concrete (which, typically, must be less than 1×10^{-12} m/s (Watson *et al.* 1999)), oxygen and chloride diffusion, freeze-thaw resistance, resistance to sulphate attack and the progress of carbonation. Water permeability may also be assessed by means of a penetration test, according to the German standard DIN 1048. Penetration depths of less than 50 mm indicate good quality, "impermeable" concrete.

Results from the extensive Brite Euram project suggest that average water permeabilities range from 0.5 to 4.5 x 10^{-12} m/s, oxygen diffusion coefficients range from 1.79 to 14.2 x 10^{-9} m/s and chloride diffusion coefficients range from 1.57 to 9.21 x 10^{-12} m/s. The overall assessment was that sprayed concrete could be produced with as good durability characteristics as a similar conventionally cast concrete (Brite Euram 1998, Norris 1999) – see Figure 2.26. Water penetration depths are typically 14 to 25 mm (i.e. well within the 50 mm limit) (Röthlisberger 1996). Some experimental work has demonstrated the detrimental impact of non-alkali accelerators on the sulphate resistance of sprayed concrete but, nonetheless, the levels of absorbed SO_3 at 100 days, which ranged from 0.69 to 2.10 %, were well below the recommended limit of 3.00 % (Lukas *et al.* 1998, Atzwanger 1999). Similarly, depths of carbonation have been found to be satisfactory – typically, 2 to 3 mm after 6 months (Oberdörfer 1996).

However, one may note that the test samples are often stored and cured in more favourable conditions than are present in tunnels. Curing measures are rarely implemented on site, because they would slow the advance of the tunnel. Consequently it is believed that the quality of the sprayed concrete suffers. Experimental evidence suggests that the detrimental impacts on the sprayed concrete of less favourable curing conditions and drying are limited (Hefti 1988, Cornejo-Malm 1995, Oberdörfer 1996, Bernard & Clements 2001). Therefore, the benefits of improving curing may not justify the additional cost and disruption. The addition of additives, such as microsilica, may offer a more cost-effective means of improving durability characteristics.

On a more general note, while the latest additives and accelerators are not believed to have detrimental effects on the sprayed concrete over the long term, as far as the author is aware no detailed evidence has been produced to support this, either from petrographic examinations or accelerated ageing tests.

As already mentioned sprayed concrete and in particular dry-mix sprayed concrete is susceptible to poor workmanship. Common problems include the failure to clean the

substrate, the inclusion of rebound [29], voids, shadowing behind bars and an intermittent flow of shotcrete (leading to a film of pure accelerator being sprayed on the substrate). The manner in which it is sprayed as well as the quantities of accelerator and water added at the nozzle has a strong influence over the quality of the sprayed concrete. Sprayed concrete is therefore inherently more variable as a material than conventionally cast, ready-mixed concrete. Typically, the standard deviation in 28 day compressive strengths might be 5 MPa for a 35 MPa mix (Brite Euram 1998 – from field trials, Bonapace 1997). This would give a rating of Fair to Poor according to ACI 214-77 (Neville 1995). A similar cast insitu concrete typically might have a standard deviation of about 3.5 MPa, which rates as Very Good to Good (Neville 1995). There is evidence that the quality can be worse where the lining is more difficult to form such as at joints (HSE 2000).

2.3 Numerical modelling of SCL tunnels

2.3.1 Introduction

With the growth in use of numerical modelling in design, concerns have been raised about validation, the risk of inexperienced users operating modelling programs improperly and inadequate checking of work (Bond & MacLeod 2001). The question of validation can be addressed firstly by running verification examples (eg: provided by the software supplier) and secondly by checking the results of modelling against closed-form analytical solutions and existing data (from the field or the laboratory). The other concerns can be overcome by applying the normal procedures and methodology that one would expect during design or research. Guidance on the management of numerical modelling in design can be found in the NAFEMS Quality System Supplement to ISO 9001 (NAFEMS 1993).

General overviews of numerical modelling of tunnels can be found in Schweiger & Beer (1996) and Mair (1998). Clearly different modelling techniques are required depending on the type of ground (e.g.: discrete element method for rock; FEM for soft ground) and the

[29] Rebound is loose material – usually predominately the larger pieces of aggregate and fibres – which fails to adher during spraying and falls down.

construction method (e.g.: the gap parameters to model the unfilled annulus around a segmental tunnel lining). The constitutive model for the lining is only one part of the numerical model (see Table 1.2). Different aspects of the model may assume more or less importance depending on what is the main focus of interest. For example, the model of the tunnel lining may have little influence on the prediction of surface settlements. One should also bear in that, in principle at least, the same outcome could be obtained from a complex model by using (widely) different parameters and / or 'sub-models'[30] for the various elements. The following discussion will focus on the modelling of SCL tunnels in soft ground.

2.3.1.1 Numerical modelling of tunnels in general

Guidance on general topics, such as the construction of the mesh or boundary conditions and their locations, may be found in texts such as Potts & Zdravkovic (1999). The boundaries of the mesh should be far enough away from the area of primary interest that they do not influence the deformations and stresses there. To achieve this for surface settlement the mesh would have to be very big – about 20 tunnel diameters wide (van der Berg 1999). Table 2.8 contains typical recommendations for the size of meshes where the tunnel face is the main area of concern. Similarly there is a trade-off between using a very large number of well-shaped elements to model the geometry of the problem in fine detail and the significant increase in runtime that follows from this. At the boundaries, the far field conditions can be modelled either by fixing the displacements or by applying a constant stress. Since the boundaries are not far enough for the tunnel to have no effect on them, the former is likely to underestimate the loads on the tunnel and the later will overestimate the loads. However, if the recommendations in Table 2.8 are followed the discrepancy between the two boundary conditions should be acceptably small.

[30] Here the term 'sub-model' refers to constitutive models and other idealizations within the numerical model of a particular problem.

Table 2.8: Recommendations for mesh sizes (see Figure 2.27)

Dimension	Van der Berg 1999	MM [31]	Gunn 1993
X	13 R	13 R	3 times depth to axis
Y ahead of face	10 R	12 R	-
Y behind face	4 R	12 R	-
Z	13 R	10 R	3 times depth to axis

2.3.1.2 2D vs 3D

The stress redistribution caused by tunnelling is three-dimensional in nature. The error that is introduced by ignoring this (e.g.: by simply assuming plane strain conditions) depends on the ground conditions. However, as an indication, it is a reasonable assumption that 50% of the total deformation and load redistribution occurs in London Clay before the tunnel face arrives at the point in question (Muir Wood 1975 & Thomas *et al.* 1998). From the study by Soliman *et al.* (1993), for a typical large diameter tunnel in clay, ignoring the three-dimensional effects (and assuming 100% stress relief) might lead to an overestimate of deformations, hoop forces and hoop bending moments by factors of about 2.0, 1.2 and 2.5 respectively. One can attempt to allow for the three-dimensional stress relaxation in 2D analyses by means of:

- the "Stress-reduction" technique
- the "Stiffness-reduction" method
- Numerical shrinkage (Chan *et al.* 2000)
- the Gap Parameter method (e.g.: Rowe & Lee (1992))
- the Hypothetical Modulus of Elasticity (HME) – see section 2.3.3.2
- a combination of the above

The first four function in a similar manner. The goal is to generate movement in the ground towards the tunnel and thereby a re-orientation of the stresses around the tunnel. In the first method, the zones of the tunnel are removed and the initial stresses acting outwards on the

[31] Typical values used by Mott MacDonald (Pound 1999)

tunnel boundary, which were in equilibrium with the initial ground stresses acting inwards, are progressively reduced. Therefore the cavity converges. In the second method, the stiffness of the area represented by the tunnel is reduced, causing inward movement. Similarly causing the zones in the tunnel to shrink generates ground movement into the tunnel. In the case of the gap parameter method, the zones in the tunnel area are removed but the lining elements are installed at a predetermined distance from the edge of the excavated area. Thus the ground can converge by a certain amount before coming into contact with the lining and applying load to it.

The first two are the most commonly used, while the HME is used for SCL tunnels only and the gap parameter for TBM tunnels. Numerical shrinkage is rarely used. All of these techniques require a considerable amount of judgement on the part of the modeller in their application (Hafez 1995, Schweiger & Beer 1996). The different techniques do not necessarily give the same results (Oettl *et al.* 1998). The parameters for these methods may be chosen to produce a predetermined volume loss for the tunnel[32]. The volume loss is chosen either on the basis of prior experience or estimated using empirical relationships (e.g. Macklin 1999). In the stress-reduction technique, a relaxation factor, λ, must be chosen. This, like the parameters in the other methods, depends not only on the distance from the face at which the lining is installed (Panet & Guenot 1982) but also on the relative stiffness of the ground compared with that of the lining and the behaviour of the ground more generally (Cosciotti *et al.* 2001). Where there is no prior knowledge of the ground to guide engineers in the choice of λ, it has been suggested that it can be obtained from the results of 3D modelling (Cosciotti *et al.* 2001).

This seems to imply that, if time and resources permit, one might just as well use 3D for all analyses.

[32] Volume loss is the volume of the surface settlement trough minus the excavated volume of the tunnel expressed as a percentage of the excavated volume – see 3.2.3.

For shallow tunnels (i.e. C/D ~ 2), axisymmetry is not a valid assumption (Rowe & Lee (1992)). Similarly, a longitudinal plane strain model of a tunnel is not valid because this represents an infinitely wide slot, cut through the ground.

The value of using 3D models and avoiding such correction factors has been increasingly recognised (Haugeneder *et al.* 1990, Hafez 1995, Yin 1996, Burd *et al.* 2000), not least because the situation becomes increasingly difficult as more complex models are analysed (such as cross-sections with multiple headings or coupled consolidations analyses (e.g. Abu-Krisha 1998)).

2.3.1.3 Construction sequence

For segmentally lined tunnels it can be reasonably assumed that the lining is constructed in one action, albeit at a given distance from the actual face. In SCL tunnels the excavation and construction sequence is much more complex and is rarely replicated fully in modelling. The way in which the sequence is simplified can have a great impact on the results. For example, modelling the excavation as full face rather than according to the exact sequence can lead to a more even pattern of lining loads (Guilloux *et al.* 1998) and less unloading in the ground (Minh 1999).

Experience and common sense suggest that increasing the advance length or rate may result in higher loading of the lining (Pöttler 1990). Convergence can increase by as much as 50% if the advance rate is increased from 2 m to 8 m per day, while the hoop load in the lining could fall by 15 %, for a tunnel in soft ground (Cosciotti *et al.* 2001). The difference reduces as the stiffness of the ground increases. The load decreases because the sprayed concrete is more heavily loaded at a young age and deforms more. This permits more stress redistribution in the ground and therefore a lower load in the final case. However, there is the risk that the lining is damaged through overstressing. Kropik (1994) reports a 20% increase in crown deformations when the advance length is increased from 1m to 2m in a soft ground tunnel. Hellmich *et al.* (1999c) noted the importance of when the lining acts as effective support in determining the final loads, despite the simplifications of the construction sequence in their numerical model. It was also noted that the sooner the lining can carry load (i.e. the sooner

the percolation threshold is passed in the thermochemomechanical constitutive model – see 2.3.3.8), the higher the loads in the lining. This applies for both axial forces and bending moments[33]. The concept of delaying the installation of the completed lining in highly stressed rock tunnels, in order to reduce the load in the final lining, is a basic tenet of the NATM.

Similarly, and in line with experience on site (e.g.: Thomas *et al.* 1998), Kropik (1994) noted that closing the invert early (i.e. close to the face) led to a reduction in deformation of the lining.

In the past "unlined" analyses have often been used in 2D and 3D simulations (e.g.: Gunn 1993, Krenn 1999, Minh 1999, Burd *et al.* 2000). Researchers have often reported that they obtained a good correlation between the results of such analyses and field data. Obviously such simulations are completely unrealistic and any apparent good match probably stems from peculiarities of the analyses (e.g.: the use of a prescribed volume loss or a simple ground model) which prevent the failure that would occur in the real case. Dasari (1996) notes that in his work there was little difference between 2D analyses of lined and unlined tunnels but that the introduction of the lining greatly reduced the settlements in the 3D analyses of the same tunnel.

The load from the ground is generally assumed to increase with time monotonically (e.g.: Grose & Eddie 1996). While this may be true for segmentally lined tunnels (e.g.: Barratt *et al.* 1994), given the complex excavation sequences and geometries in SCL tunnels, the mode of action of the lining may well change and the loading may vary. For example, one could consider the lining in the Top Heading as cantilevering off the completed rings behind it

[33] Hellmich et al (1992c) found that varying the stiffness of the lining, which was modelled with a constant linear elastic model, made little difference to the hoop forces but influenced the hoop bending moments greatly. From this they concluded that the hoop force does not depend on the material properties of the lining. However, this is only true for the most simple cases in their study. When there is true interaction between the lining and the ground, the early age stiffness, and particularly the point at which it becomes effective, had a great influence on the stresses in the lining.

initially, resulting in bending in the longitudinal direction (see Figure 1.1). When the ring is completed, the lining acts mainly in compression and the main bending moments act in the hoop direction.

2.3.2 Constitutive modelling of the ground

In the case of segmentally lined tunnels, the properties of the tunnel lining are well-defined and easy to model. Sprayed concrete linings were seen (at least from a UK perspective) as a very specialised field. It is perhaps for this reason that in the past more effort has been expended on developing the modelling of the ground than sprayed concrete. Although engineers are still far from attaining the "Holy Grail" of a model that can replicate all aspects of the behaviour of the ground, including its inherent variability, the modelling of soft ground is now quite sophisticated. Taking London Clay as an example, the following paragraphs will deal with the different facets of its behaviour in turn.

2.3.2.1 Undrained vs drained behaviour

Water is present in London Clay, normally at hydrostatic pressures. The first question that one might ask is whether or not the material behaves in a drained or undrained manner. The general assumption is that London Clay, which has a permeability of between 10^{-9} and 10^{-11} m/s (Addenbrooke 1996 – see also Figure 2.28), can be assumed to behave as an undrained material in the short term (i.e. within 1-2 months) [34]. Typically Addenbrooke (1996) found in his numerical simulations that it took 10 to 15 years for the consolidation process to be substantially complete.

The results of coupled consolidation analyses depend on the initial and ultimate pore pressure distributions (which are governed by boundary conditions), the permeability of the ground and the tunnel, the depth of the tunnel and its diameter and the pore pressure changes due to

[34] Based on a c_v of 3 m^2/year for London Clay and field observations of pore pressure changes (Kambo 1997, Mott MacDonald 1998)

tunnelling[35] (Addenbrooke 1996). The initial stress state also influences the changes in pore pressures (Addenbrooke 1996 & Abu Krisha 1998).

Opinion is divided about whether tunnels in London Clay act as drains or are impermeable (Mair 1998). Certainly it is very difficult to construct a tunnel that is perfectly dry. However, the water ingress observed in shallow tunnel systems such as the London Underground often may be due to local events (e.g.: leaking water pipes) rather than a more general draining of the ground. Some field data has shown little reduction in pore pressures around tunnels (Gourvenec *et al.* 1999), which would suggest they are effectively impermeable.

A large increase in settlement over a time period of years after construction has been observed (Bowers *et al.* 1996, Addenbrooke 1996). Mair (1998) suggests that tunnelling in a stiff clay like London Clay should only induce negative pore pressure changes (due to unloading). Therefore the dissipation of the changes in pore pressure should result in swelling rather than consolidation. If this is so, consolidation could only occur if water is being drained from the ground by another mechanism; for example, if the tunnel is not impermeable and is draining water from the surrounding ground. However, stress redistribution also results in loading (due to ground arching) and positive pore pressures which will dissipate over time, leading to some consolidation. Ground movements may also occur due to the opening of fissures in the clay.

Undrained numerical analyses are normally sufficient to obtain the short-term loads on tunnel linings in London Clay. This study has therefore restricted itself to the short-term case.

2.3.2.2 Insitu stress state

This is governed by the pore pressures, self-weight of the ground and the ratio of the horizontal effective stress to the vertical effective stress. The first two are relatively well defined. The vertical total stress can be taken as approximately:

$$\sigma_v = 20z \qquad 2.2$$

[35] This is influenced by the construction sequence (Minh 1999).

where σ_v is the vertical total stress and z is the depth in m. In contrast the horizontal stress is very difficult to measure and there is considerable debate about its values in London Clay (e.g.: Gourvenec *et al.* 1999, van der Berg 1999). The term K_0 (which is the ratio of horizontal effective stress to vertical effective stress) is commonly used in discussions about tunnel design.

In the course of its history the London Clay has been overlain by the upper levels of the clay and other geological strata, some of which will have since been removed by erosion. Hence it is overconsolidated. The horizontal stress is higher than the vertical stress. Other mechanical and physicohemical mechanisms (such as underdrainage [36]) may have contributed to the preconsolidation. Depending on the stress history at a site (i.e. the amount of overburden removed, surcharge applied and drainage conditions), the K_0 distribution will vary. In contrast it has been suggested that the σ'_h profile is much less sensitive to the stress history (Burland *et al.* 1979). A typical value for the overconsolidation ratio (OCR) at a depth of 18 m is about 7.8 [37]. Overconsolidation due to a uniform load from overlying strata leads to a profile of OCR that decreases with depth. Mayne & Kulhawy (1982) have suggested an empirical relationship that predicts a profile, which increases with depth initially and then decreases. Figure 2.29 shows this tends to be lower than the field data but this has been used often for design analyses (Powell *et al.* 1997 and Pound & Beveridge 2001).

Segmental tunnels constructed in London Clay generally tend to squat initially (i.e. the vertical convergence is greater than the horizontal convergence (Ward & Thomas 1965)). The same pattern of movement is seen in the adjacent ground (Mair & Taylor 1993) while pressure cell data has shown that the horizontal load may be about 70% of the vertical load (Barratt *et al.* 1994, Bowers & Redgers 1996). SCL tunnels too show more movement in the vertical direction than the horizontal (Kambo 1997, van der Berg 1999).

[36] The London Clay in central London has been affected by underdrainage but this is not believed to be important at Heathrow (van der Berg 1999).

[37] Based on an original overburden pressure of 1700 kPa acting at the current ground surface and a current surface surcharge of 60 kPa (Mott MacDonald 2001).

The choice of K_0 value has a considerable influence of the results of both 2D and 3D numerical models (Huang 1991, Addenbrooke 1996, Guilloux *et al.* 1998, Krenn 1999, van der Berg 1999). If K_0 is assumed to be greater than 1.0, the horizontal movements tend to be overestimated and the surface settlement troughs are wider in comparison to field data. Surface settlements are reduced. More "realistic" predictions are obtained by using a K_0 less than 1.0 throughout the model or in a zone beside the tunnel (Addenbrooke 1996, van der Berg 1999, Lee & Ng 2002). This suggests that some aspect of the behaviour of the clay is not being modelled correctly in the numerical simulations – for example, the way that stress is relieved ahead of the face in the horizontal plane. Axial loads are increased especially in the crown compared to a model with $K_0 = 1.0$ but bending moments are reduced (Guilloux *et al.* 1998).

Normally design analyses assume a constant value for K_0 but profiles which vary with depth are sometimes used.

2.3.2.3 Elastic behaviour

Stiffness

Figure 2.30 shows the variation in undrained Young's modulus (at 0.1% strain) with depth for London Clay. Different relationships have been proposed for this (see van der Berg 1999 for a review) but, in the later modelling, the variation of maximum stiffness has been assumed to be as follows:

$$E_{max} = 1500*Cu \qquad \text{in kPa} \qquad 2.3$$

where E_{max} is the maximum value of the undrained elastic modulus at small strains (i.e. $\varepsilon < 0.001\%$) and Cu is the undrained shear strength (see later). For an undrained analysis, the Poisson's ratio, ν, should be 0.5 but this can cause numerical problems. Therefore a value of 0.48 is often used or the bulk modulus is set to 100 times the shear modulus.

The stiffer the ground is (in comparison to the lining) the lower the lining deformations and loads tend to be (Guilloux *et al.* 1998).

Nonlinear stress-strain behaviour

Numerical models that assume linear elastic behaviour for the ground tend to predict settlement troughs that are wider than field data would suggest (Lee & Rowe 1989, Gunn 1993, Leca 1996, Burd *et al.* 2000, Tang *et al.* 2000). This suggests that the stiffness is too low at low strains and too high at high strains. High quality laboratory tests and back-analysis of constructions have revealed that the behaviour of many geomaterials is nonlinear and that they exhibit a high stiffness at low strains (Atkinson 2000). Hence the 'small strain stiffness' behaviour has been incorporated into analyses of tunnels, with a consequent improvement in the predictions of settlement troughs (Gunn 1993, Addenbrooke 1996, Krenn 1999, Pound & Beveridge 2001).

Several relationships have been proposed for the nonlinear stress-strain behaviour of London Clay. Firstly, there is the curve-fitted formula proposed by Jardine *et al.* (1986)

$$\frac{E_{u.\tan}}{Cu} = A + B.\cos(\alpha I^{\gamma}) - \left(\frac{B.\alpha.\gamma.I^{\gamma-1}}{2.303}\right).\sin(\alpha I^{\gamma}) \qquad 2.5$$

where $I = \log_{10}(\varepsilon_a/C)$, ε_a is the axial strain and A, B, C, α and γ are empirical constants determined from experimental data (see original paper for full details).

Secondly, there is the logarithmic stress-strain function of Puzrin & Burland (1996) – see Appendix D for a full definition.

$$\frac{E_{\tan}}{E_{\max}} = 1 - \alpha.[\ln(1+x)]^{R} - \frac{\alpha.Rx}{(1+x))}[\ln(1+x))]^{R-1} \qquad 2.6$$

Thirdly there is a power law in which the tangent moduli depend on the hydrostatic stress, the overconsolidation ratio and the deviatoric strain (Dasari 1996), e.g.:

$$G_{\tan} = 0.667.\ B.p'^{\,n2}.OCR^{m2}.\varepsilon_q^{\,b2} \qquad 2.7$$

Addenbrooke (1996) recommended the Puzrin & Burland model in preference to the relationship proposed by Jardine *et al.* (1986) because the former could model unloading.

When combined with a yield surface, the resulting nonlinear elastoplastic model exhibits less yielding than a plain linear elastoplastic model (Krenn 1999). Simply incorporating plasticity makes the settlement trough narrower and deeper, but not as much as adding in elastic nonlinearity (see Table 2.10 & Dasari 1996). Figure 2.34 shows each of the models in comparison with test data.

Table 2.9: Surface settlement trough widths (Krenn 1999)

Model	Linear elastic	Linear elastic perfectly plastic	Nonlinear elastic (Puzrin & Burland (1996))
Normalised Trough Width	1.00	0.31	0.19

Anisotropy

From experimental data London Clay is known to exhibit (cross-) anisotropy, with a higher stiffness in the plane of bedding than perpendicular to it. Table 2.9 contains typical parameters that are assumed for London Clay.

Table 2.10: Typical anisotropic parameters for London Clay (Lee & Rowe (1989) and Van der Berg (1999))

Parameter	Value
E_h	$1.6\ E_v$
G_{hh}	$E_h/2.4$
G_{vh}	$0.433*E_v$ [38]
ν_{hh}	$(1-0.5*(E_h/E_v))$
ν_{vh}	0.49

Since the changes in shear strain induced by tunnelling are larger than the changes in volumetric strain, Lee & Rowe (1989) concluded that G_{vh}, the independent shear modulus

[38] Addenbrooke (1996) proposes 0.444. He also used 0.2 which resulted in a narrow and deep settlement trough but did not produce realistic stress distributions in the ground.

may be the most important anisotropic parameter in tunnelling analyses and recommended low values (e.g.: around $0.25*E_v$). In 2D analyses, Addenbrooke (1996) found little difference between the settlement troughs produced by isotropic and anisotropic nonlinear models of London Clay whereas Lee & Ng (2002) found that an anisotropic model predicted more realistic settlement trough in 3D analyses.

The ratio of horizontal to vertical undrained shear strength has been estimated at 1.40 (Harrison 1995).

2.3.2.4 Non-elastic behaviour

Plasticity

The subject of yielding in geomaterials is a complex one. Non-elastic strains may occur well before the material fails. Various multiple yield surfaces models have been proposed in an attempt to replicate this (see Van der Berg 1999 for an overview). More simple plastic models are generally used in the numerical modelling of tunnels – e.g.: simple yield functions such as Mohr-Coulomb and Drucker-Prager with an associated flow rule - and therefore the discussion below is restricted to these models.

The inclusion of plasticity of the ground results in more deformation around a tunnel. In simplified 2D analyses with a linear elastic lining, the geotechnical model has been found to have a significant influence on the loads in the lining (Yin 1996 and Oettl *et al.* 1998). Bending moments were less affected than hoop forces. Incorporating plasticity resulted in an increase in load of approximately 25 to 50 %, depending on the model. This is entirely understandable since, where the changes in stress due to the formation of the tunnel exceed the strength of the ground, the lining must help to carry the excess load (see also 2.3.2.6).

The amount of yielding depends on the choice of yield surface. For example, a Drucker-Prager yield criterion results in less deformation than a Mohr-Coulomb criterion if the strengths are matched on the compressive meridians and vice versa if the strength is matched on the tensile meridians (see Figure 2.32) (Oettl *et al.* 1998). If a "cap" strain-hardening model is used, the yielding is no longer localised to the area around the tunnel and there is

more deformation throughout the model, compared to the simpler plasticity models (Oettl *et al.* 1998). The Modified Cam Clay model is not recommended for the undrained behaviour of heavily overconsolidated clays since it overpredicts the strength of the soil on the dry side of the critical state line (Dasari 1996).

The nonlinear behaviour of a geomaterial can be modelled by means of a strain-softening plasticity model as an alternative to a nonlinear elastic model (see 2.3.2.3). One example of this is a curve-fitted relationship for a strain-softening elastoplastic model by Pound (1999).

$$cohesion = Cu.\left(1 - \frac{\tau_{mob}}{\left(1+\left(190\varepsilon_{pl}\right)^2+\left(145\varepsilon_{pl}\right)^{0.56}\right)}\right) \qquad 2.8$$

where τ_{mob} = 0.99.((1-Cu'/Cu) and Cu' = the mobilised shear strength = 0.5.($\sigma_{xx} - \sigma_{zz}$), due to the initial insitu stresses (see Figure 2.33). In this particular model for undrained clay, the cohesion of a Mohr-Coulomb plasticity model increases with increasing plastic strain, ε_{pl}, commencing at shear stresses greater than 1% of the undrained shear strength, Cu (see also 6.3.3).

Strength

Considering London Clay as a simple elastoplastic material, a key parameter is its undrained strength for the short-term design case. Figure 2.31 shows the undrained shear strength versus depth. The following relationship has been used for tunnel designs at Heathrow in London,

$$Cu = 0.67*(50+8z) \qquad \text{in kPa} \qquad 2.9$$

where Cu is the undrained shear strength, z is the depth in m below ground surface and 0.67 is a correction factor to account for the difference in the strength of small samples and the insitu material (Pound 1999).

2.3.2.5 Spatial variation of properties

As mentioned in previous paragraphs, the properties of soft ground such as London Clay tend to vary with depth and this should be included in any numerical model. However, since this is a natural material, the properties of the ground also vary about the mean values. Stochastic

methods (Hoek *et al.* 1998) offer one means of incorporating this additional variability but they are rarely used in engineering.

2.3.2.6 Stress-paths

Figure 2.35 shows the stress paths around a tunnel (after Lee & Rowe (1989)). As the tunnel is excavated, radial unloading occurs at the edge of the excavation while there are increases in the tangential stress around the tunnel. The principal stresses rotate until the major principal stress is in the tangential direction. This process of stress redistribution is sometimes referred to as "arching" and it is a three-dimensional phenomenon. This is intuitively obvious and the magnitudes of the stress changes can be estimated for simple cases using elasto-plastic closed-form solutions (e.g. Mair & Taylor 1993). Lee & Rowe (1989) suggest that (for a circular tunnel excavated in full-face mode in ground with a K_0 of 0.7) above the crown and below the invert the ground experiences triaxial extension, whereas at the axis, the situation lies between triaxial extension and compression. Similarly, Tang *et al.* (2000) found that in the case of $K_0 = 1.5$, the soil at the crown and invert underwent triaxial extension while at the axis the ground experienced triaxial compression. Ahead of the face the vertical stress increases due to "arching" in the longitudinal direction, so initially the soil experiences triaxial compression followed by a reduction in confinement as the face approaches.

If the state of deviatoric stress changes from loading to unloading, it has been proposed that the tangent shear modulus varies depending on the strain decrement from that change, i.e. the maximum deviatoric strain minus current deviatoric strain, in accordance with Masing's rules (Dasari 1996). Lee and Rowe (1989) noted that the ratio of loading to unloading modulus can be as low as 0.5. Similarly, after a change from unloading to reloading, the calculation uses the strain increment from the smallest deviatoric strain in that unload-reload loop. Figure 2.33 shows the resulting stress strain response. Unloading in the plasticity models is assumed to be elastic. Figure 2.36 shows the variation of the tangent Young's modulus with deviatoric strain.

Changes in the direction of the stress path may also result in different responses – i.e. the material response depends on its recent stress history (Stallebrass *et al.* 1994). This effect can be modelled using a multi-surface kinematic hardening constitutive model. In addition to a yield surface and bounding surface, a history surface is added to give the material a memory of its stress history. While some evidence exists to support the use of this model, by the authors' own admission, the reported variation in surface settlement predictions may owe as much to the variation in K_0 as they do to the use of the new model (Stallebrass *et al.* 1994). Heave over the centreline of the tunnel gradually disappeared and the trough deepened as the K_0 decreased from 1.4 towards 1.0. In the context of a tunnel, Dasari (1996) notes that beside the axis there is a 180° change in the direction of the stress path. This should result in a much stiffer response by the ground than above the crown, where unloading continues along the same stress path (see Figure 2.37). Subsequent work has cast some doubt on the original experimental work, which was used as the basis for the kinematic hardening model. It has been suggested that the apparent stress history effects are in fact creep effects in the clay during the experiments (Clayton & Heyman 2001).

2.3.2.7 Time-dependent behaviour

Factors such as creep and ageing in geomaterials (see Van der Berg 1999 for an overview) are rarely considered although there is evidence that they may be important factors as noted above. This subject will not be discussed further.

2.3.3 Constitutive modelling of sprayed concrete

In contrast to the geotechnical model, relatively crude models are normally used for sprayed concrete (e.g.: Bolton *et al.* 1996, Watson *et al.* 1999 & Sharma *et al.* 2000). Therefore, it is perhaps unsurprising that there is often a significant discrepancy between the behaviour predicted by numerical analyses and that observed on site (e.g.: Addenbrooke 1996, van der Berg 1999). Consideration of the behaviour of sprayed concrete observed in laboratory experiments would suggest that a comprehensive model would incorporate age-dependent parameters, the non-linear stress-strain curve, creep and possibly shrinkage. Improving the modelling of the sprayed concrete could make the prediction of behaviour more reliable.

2.3.3.1 Linear elastic models

The most commonly used model is a linear elastic one, because of its simplicity and computational efficiency. Typically, elastic models predict axial forces and bending moments in linings that are unrealistically high compared with field data from strain gauges and pressure cells (Golser *et al.* 1989, Pöttler 1990, Yin 1996, Rokahr & Zachow 1997). This is no surprise since sprayed concrete only behaves in a linear elastic manner up to about 30% of its uniaxial compressive strength (Feenstra & de Borst 1993, Hafez 1995).

A logical improvement on a simple elastic analysis is to incorporate the increase in magnitude of the stiffness with age (see Figure 2.15 & Appendix A). In numerical models, this is often implemented as a "stepped" approximation of the curve, since the excavation sequence is modelled as a series of steps. Figure 2.38 shows typical values in such an analysis. The increase in stiffness with age will lead to irrecoverable strains on unloading at later times (Meschke 1996).

In a limited study [39] Bolton *et al.* (1996) reported that once the modulus had reached 5 GPa (i.e. after 6 hours), and was 100 times the elastic modulus of the ground, further increases in magnitude with time had little effect on the magnitude of surface settlement. Since this value is reached quite quickly, it was concluded that the early age development of elastic modulus was unimportant in the prediction of surface settlement.

In a 3D numerical model, Berwanger (1986) also found that the ultimate stiffness of the sprayed concrete had a limited influence on surface settlement but it did have a large influence on the stresses in certain parts of the lining, notably the footing of the Top Heading. Similarly, in 2D numerical models, Pöttler (1990), Huang (1991), Hirschbock (1997) and Cosciotti *et al.* (2001) found that increasing the stiffness of the lining increased the stresses in it. Considering a tunnel constructed in one stage, in a 2D analysis, Hellmich *et al.* (1999c)

[39] The age-dependent model was used in 2D analyses. Dasari (1996) himself notes that the introduction of the lining had little effect on the results for those 2D analyses but did have a marked influence on the results of his 3D FE analyses.

found that the stiffness of the lining affected only the hoop bending moments and not the hoop forces. However, by extrapolating their finding that the stresses in the lining are influenced by how long it takes for the lining to start to carry meaningful loads, one could postulate that in a multi-stage construction sequence the rate of growth of stiffness will be an important factor[40].

Several authors have suggested that the relative stiffness of the lining compared with that of the ground would affect the amount of influence of a time-varying modulus (Hellmich *et al.* 1999c, Cosciotti *et al.* 2001). In weaker ground the rate of stiffening of the lining is less important. In a detailed study using 3D numerical models, Soliman *et al.* (1994) reported that a variable elastic modulus led to significantly larger lining deformations (20 - 30 % more) and lower bending moments (reduced by up to 50%) compared to a constant elastic modulus. The thrust loads were slightly lower - reduced by about 20% - and hence the stresses in the ground were not increased by much. This may well explain why surface settlements seem to be independent of the constitutive model of the lining (see also Moussa 1993).

In conclusion, in a multi-stage construction sequence, using an age-dependent elastic modulus for the lining will result in lower stresses in the lining. The bending moments are reduced more than the hoop forces. The reduction appears to be due more to the lower stiffnesses during early loading (i.e. ages less than 48 hours), compared to a (high) constant stiffness model, than how the stiffness develops beyond that period.[41]

2.3.3.2 Hypothetical Modulus of Elasticity (HME)

An initial and very successful attempt to improve numerical modelling came in the form of the Hypothetical Modulus of Elasticity (HME) method (Pöttler 1985). Several reduced values

[40] For example, if an age-dependent elastic model is used, the invert of the tunnel will be relatively soft when the ring is first closed and will permit much more deformation than if a high stiffness was assigned to that section as soon as it is built.

[41] If the load is applied over a period that is much longer than that for hydration, numerical analyses give virtually the same results as one obtains by using a constant stiffness model with the 28 day stiffness, since most of the load is applied when the stiffness of the lining is close to this value (Hellmich *et al.* 1999c).

of elastic modulus are used in an analysis. Typical values are shown in Table 2.11. The "softer" lining leads to more realistic results - larger lining deformations and lower stresses - without excessive computation time. Though the concept of an Effective Modulus is not new to creep analysis (e.g.: BS 8110 Part 2 1985)[42], the HME is intended to account for shrinkage and advance rate as well as creep.

$$E_{HME} = E_T.f_v.f_{s,k}.f_{vv} \qquad 2.10$$

where E_T = the stiffness at the time in question, f_v = correction factor for the age-dependent stiffness during the loading up to the time in question, $f_{s,k}$ = correction factor for creep and shrinkage, f_{vv} = the crown deformation occurring before lining placement as a fraction of total deformation of ground at the crown – i.e. the effects of 3D & timing of placement.

Table 2.11: Values of Hypothetical Modulus of Elasticity

Project	HME	Application
CTRL North Downs	7.5 GPa	Age < 10 days; Strength limited to 5 MPa
(Watson *et al.* 1999)	15.0 GPa	Age > 10 days; Strength limited to 16.75 MPa (= 0.67 fcu)
Heathrow Express	0.75 GPa	Initial value
(Powell *et al.* 1997)	2.0 GPa	Value after adjacent section is constructed & until lining is complete
	25.0 GPa	Mature SCL

The correction factors in equation 2.8 require knowledge of how the lining and ground will deform as well as how creep will alter the stresses in the lining. While the first can be estimated using various analytical tools, the second cannot. So the basis of the values of HME is usually empirical.

[42] Also, the Trost-Bazant creep model uses an age-dependent effective modulus (Neville *et al.* 1983).

Clearly, given the low stiffnesses at early ages, one would expect that using the HME approach would result in significantly lower predictions of stresses than using a (high) constant stiffness model.

2.3.3.3 Nonlinear elastic models

As noted earlier, the stress-strain curve for concrete is non-linear (see Figure 2.7). Models, such as the Cauchy, Hyperelastic and Hypoelastic models, attempt to replicate the non-linear stress-strain behaviour of concrete. This non-linear behaviour begins at relatively low stresses[43] and is due to microcracking at the interface between the aggregate and cement paste, which themselves are still responding elastically (Neville 1995). Since this plastic deformation lies behind the non-linearity, plasticity models are required if unloading occurs. However, if unloading can be neglected, non-linear elastic models represent an economic means of modelling the non-linear response of concrete to loading and a significant improvement on linear elastic models (Chen 1982). Consequently they have been widely used in the analysis of concrete structures, although they have been rarely used in the analysis of sprayed concrete tunnels.

Specific non-linear elastic models used for the analysis of SCL tunnels include: Saenz's equation (see Chen 1982) which Kuwajima (1999) found fitted experimental data for stress-strain curves well; the Rate of Flow method (see section 2.3.3.6) and the parabolic equation below (Moussa 1993) [44].

$$\sigma_c = f_c \cdot \left(\frac{\varepsilon_c}{\varepsilon_1}\right) \cdot \left(2 - \frac{\varepsilon_c}{\varepsilon_1}\right) \qquad 2.11$$

[43] At early ages, due to the more ductile response, the ratio of yield strength to ultimate strength is higher – between 0.5 and 1.0 (Aydan et al 1992a , Moussa 1993). Rokahr & Lux 1987 report a linear response up to 0.8 at 24 hours (see also section 2.3.4.2 & Figure 2.15).

[44] Although Moussa (1993) did also propose a 7th order polynomial function to describe the uniaxial compressive stress-strain curve more precisely.

where f_c is the peak stress, ε_1 is the strain at peak stress and σ_c and ε_c are the equivalent uniaxial stress and strain respectively.

In these models, the behaviour of concrete is treated as an equivalent uniaxial stress-strain relationship. Biaxial effects may be accounted for in the tangent moduli. This is a reasonable approximation up to a utilization factor of about 0.8.

The Kostovos-Newman model (Kostovos & Newman 1976, Brite Euram C2 1997) is formulated in terms of octahedral stresses and unlike the others is designed for generalised states of stress. Although quite lengthy in its formulation, one advantage of this model is the fact that all the parameters can be determined from the uniaxial compressive strength of a cylindrical sample.

Considering it in more detail, its key advantages are that:

- The model includes the effects of deviatoric stress on hydrostatic strains;
- The model has been shown to agree well with existing test data for concrete and sprayed concrete (Brite Euram C2 1997, Eberhardsteiner *et al.* 1987) – see Figure 2.13 – and hence it has been recommended for use in modelling mature sprayed concrete (Brite Euram 1998);
- The increase in strength with increasing hydrostatic stress is accounted for.

However, it should be noted that, as with nonlinear elastic models, it is only valid up to the point of onset of ultimate failure, which is at about 85% of the ultimate strength.

Moussa (1993) found that incorporating nonlinearity into the elastic model resulted in a reduction in hoop forces of about 20% and a reduction of up to 50% for bending moments. The surface settlements were virtually unchanged and there was only slightly more plastic deformation in the ground adjacent to the tunnel.

2.3.3.4 Elastoplastic models

A general elastic perfectly plastic constitutive model requires an explicit stress/strain relationship within the elastic region, a yield surface (failure criterion) defining when plastic strains begin and a flow-rule (governing the plastic strains). In the following sections, the 3 components of a plasticity model will be discussed, firstly for the compressive region, secondly for the tensile region and finally for intermediate regions, before outlining the impact of elastoplasticity on the results of tunnel analyses. Appendix C contains details of plasticity models already used for analysing sprayed concrete tunnel linings.

Elastic behaviour

Isotropic linear elasticity is generally assumed. Several researchers have incorporated the time-dependency of the stiffness or non-linearity into their models (Meschke 1994, Moussa 1993).

Yield criteria

Since the first one parameter yield criteria were proposed by Rankine, Tresca and von Mises, many others have been formulated (Owen & Hinton 1980). More and more complex criteria have been proposed to match experimental data more accurately over a wider range of stresses. In the case of concrete, the 2 parameter Mohr-Coulomb[45] and Drucker-Prager yield criteria have been used often in the past. New yield criteria have been developed which can replicate the curved nature of the yield surface meridians (see Figure 2.13) and also the shape of the surface in the deviatoric stress plane, which is initially almost triangular (see Figure 2.39) but tends to an almost circular shape at high hydrostatic stresses (Hafez 1993, Chen 1982). Curved yield surfaces are also advantageous since the corners and edges are difficult to handle in numerical analysis (Hafez 1993). Hence, for the purposes of analysis of sprayed concrete tunnel linings, the Drucker-Prager criterion is the widely used (see Appendix C).

Considering a moderately heavily loaded tunnel, where the principal stresses in the lining might be 8, 3 and 0.5 MPa and the 28 day strength equals 25 MPa, the normalised octahedral stress, σ_{oct}/f_{cu}, is only 0.15 which is quite low. So the assumption of straight meridians in the Drucker-Prager criterion is reasonable. The Drucker-Prager criterion can also be amended to reflect the increase in yield stress in biaxial states of stress (see Figure 2.8 & Hafez 1993, Meschke 1996). However, the shape of the Mohr-Coulomb criterion in the deviatoric plane agrees better with the almost triangular yield surface suggested by test data in the deviatoric plane at low hydrostatic stress.

Post-yield stress/strain relationships

Various theories have been proposed for post yield behaviour: perfect plasticity, isotropic work hardening (or softening), kinematic work hardening or a combination of isotropic and kinematic hardening. Kinematic hardening is only really needed for cyclic loading in concrete (Chen 1982). Most of the models (see Appendix C) assume isotropic hardening up to a peak stress and perfect plasticity thereafter. However, in experiments it has been observed that stress decreases with increasing strain after a peak value (see Figure 2.7). The shape of this descending branch of the stress/strain curve depends heavily on the confinement and the boundary conditions imposed by the experimental equipment (see section 2.3.4). It is usually assumed that the hardening behaviour does not vary with age.

In classical plasticity models the plastic strains vectors are obtained from the plastic potential and a flow rule, which can be either associated or non-associated. Associated flow rules assume that the plastic potential coincides with the yield function. Hence the vectors of plastic strain are normal to the yield surface. In the absence of experimental evidence to support a particular non-associated flow rule, the assumption of an associated flow rule is a common simplification (Chen 1982; Hellmich *et al.*, 1999b).

[45] There is a preference in geotechnical engineering for the name Coulomb and in applied mechanics for the name Mohr, hence the name Mohr-Coulomb is used here (Chen 1982).

Tension

In the plasticity models used in tunnel analyses, the Rankine criterion is generally used for yield in tension (see Appendix C) According to this brittle fracture occurs when the maximum principal stress reaches a value equal to the tensile strength (Chen 1982). Post-failure behaviour in tension will be discussed later in section 2.4.3.5.

Compression and tension

For states in which one of more of the principal stresses is compressive and the others are tensile, an assumption must be made about the nature of the yield surface. It is usually assumed that the presence of tension reduces the compressive strength linearly (see Figure 2.8, Chen 1982). However, there is some doubt about the exact effect (Feenstra & de Borst 1993). In multisurface plasticity models (e.g.: Meschke 1996, Lackner 1995), a check is performed in each principal stress direction to see which of the yield surfaces is active and the relevant yield criteria is then applied.

Influence on the predictions of numerical models

Typically strain-hardening plasticity models predict an increase of 15 - 30 % in the magnitude of deformations and a reduction of 10 - 25 % in the magnitude of bending moments in the concrete shell, compared to an age-dependent elastic model (Hafez 1995, Hellmich *et al.* 1999c). However, the influence of plasticity obviously depends on how heavily the lining is loaded and the ability of the ground to sustain the stress, which is redistributed back into it. If the ground is close to failure, the stress redistribution due to plastic deformation in the lining may exacerbate the situation (Hafez 1995).

2.3.3.5 Tensile behaviour

Plain concrete

Since the tensile strength of concrete is much lower than the compressive strength, in many normal load cases, failure in tension (ie. cracking) may well occur while the compressive stresses are well below failure levels (Chen 1982). While some insitu investigations have revealed tensile stresses in sprayed concrete tunnel linings (Hughes 1996, Negro et al 1998) and cracking is of major concern, when considering permanent sprayed concrete linings, the

simplest tensile models have usually been used. Namely, the concrete behaves in a linear elastic manner up to a tensile cut-off at the uniaxial tensile strength. This approach may simply have been adopted due to limits on computing power.
The maximum principal stress failure criterion is the most commonly used. According to it, once the tensile stress acting on a plane exceeds the strength, a crack is formed and the stress carried across the crack falls to zero. In reality, if the width of the crack is not too great, 40 to 60 % of the shear forces can still be carried due to aggregate interlocking (Chen 1982). Therefore the behaviour of concrete after cracking is highly non-linear and orthotropic (Kullaa 1997). Alternatively one can assume a maximum principal strain criterion, where cracks form once a limiting strain value is exceeded (Chen 1982).

A more sophisticated approach is to assume that the tensile stress of plain concrete decreases linearly, bilinearly or exponentially with increasing strain (Lackner 1995). The difficulty in determining the softening curve has led to the use of fracture energy to calculate the parameters for use in these models (Feenstra & de Borst 1993). The fracture energy is the area under a stress-deformation curve and a correction is required to account for the size of the mesh elements. This approach can also be used for the post peak softening behaviour in compression (Feenstra & de Borst 1993). Meschke (1996) and Kropik (1994) used a (Rankine) maximum stress failure criterion followed by linear tension softening. The gradient of the descending stress-strain line is assumed to be E/100 – one hundredth of the initial elastic modulus. While this would seem to model correctly the pre-crack and post-crack behaviour of plain concrete, the composite material of reinforced concrete actually exhibits tension hardening (see Figure 2.10).

The cracks can be modelled either discretely or smeared over the elements in question. The concept of the smeared crack can be further sub-divided into non-linear elastic, plastic or damage theory models (Lackner 1995). Smeared cracks can be either fixed (once they have formed) or rotate their orientation as the direction of the tensile stresses changes. To avoid re-meshing, the smeared crack approach is usually adopted (Kullaa 1997).

Reinforced concrete

Like cracks, bar reinforcement can be modelled discretely (Kullaa 1997, Eierle & Schikora 1999). However, for both features, this can be a laborious process even in a simple 2D mesh and is too complex an approach at this time for the 3D analysis of tunnels. Reinforcement and the tensile behaviour of reinforced concrete are rarely considered, either explicitly (e.g.: Haugeneder *et al.* 1990) or implicitly.

In the case of a smeared crack model, the reinforcing effects of steel and fibres may be incorporated by modifying the post-crack (tension softening) properties of the concrete elements. For example, it can be assumed that a fraction of the tensile stress across the crack can still be sustained. In the case of steel fibre reinforced shotcrete, a value of 0.3 has been proposed for this (Brite Euram C2 1997). Obviously, a single fixed value does not take account of the variation in behaviour with crack width or the anisotropic distribution of the fibres. Moussa (1993) chose to multiply the value of the ultimate tensile strain by a factor of 10 to account for the presence of reinforcement.

Influence on the predictions of numerical models

Given the dearth of information on this subject, it is not possible to comment in detail on the influence of the model of tensile behaviour. In general one may note that the assumption of an infinite tensile capacity (e.g.: in an elastic model) obviously overestimates the capacity of the lining, while a brittle tensile cut-off would underestimate the capacity and result in an overestimate of stress redistribution. A pragmatic approach, which could be adopted, is to use a simple tension model and to compare the predictions of tensile stresses with the tensile capacity. More complex analyses can then be undertaken if required.

2.3.3.6 Creep models

General comments

Rheology is the study of flow. Hence the term "rheological" is often used to cover empirically based creep models, such as those that have been idealised as an arrangement of simple units, each with rigidly defined behaviour. In the following sections other creep

models – such as power law models – will also be discussed, with some comments on the effect of incorporating creep into the numerical model.

Rheological models

Typically these models consist of Hookeian springs, Newtonian dashpots and St Venant plastic elements, arranged in series or parallel (Jaeger & Cook 1979, Neville *et al.* 1983), although more exotic units have been devised (e.g.: springs in dashpots or Power's sorption elements). Figure 2.40 (a, b & c) shows the 3 most commonly used rheological models, in the analysis of sprayed concrete – namely, the generalised Kelvin (Voigt) model, the Maxwell model and the Burgers model, which consists of a Maxwell model in series with a Kelvin model.

The 3 models listed above are visco-elastic models and so the principle of superposition remains valid. The spring stiffnesses and dashpot viscosities can be either linear or non-linear. From Figure 2.40 (a), it can be seen that the Kelvin model produces a complete recovery on unloading and so it is often used for fully recoverable transient creep. The Maxwell model produces no recovery and is used for steady-state creep, as well as stress relaxation, unlike the Kelvin model[46]. Combined in a Burgers model, one could say that they cover the whole of concrete's creep behaviour, with the Kelvin model replicating young concrete's behaviour and the Maxwell model the mature concrete behaviour. However, it would be unreasonable to expect that such a simple model could cover such complex behaviour and more elaborate rheological models (e.g.: Freudenthal-Roll model with one Maxwell and 3 Kelvin elements in series) have been proposed (see Neville *et al.* 1983, Chapter 14 for an overview).

Appendix B contains a list of rheological models used in analyses of sprayed concrete linings, together with their parameters. In addition to the generalised Kelvin model and Burgers model, a modified Burgers model (with 2 Kelvin elements) and a Bingham model have been

[46] Strictly speaking creep refers only to increasing strain with time, under a constant load. Relaxation refers to the reduction in stress over time observed in samples held under a constant strain.

proposed. All of the rheological models appear to be formulated for deviatoric stresses only, although there is some experimental evidence to suggest that considerable creep may occur under hydrostatic loading too (Neville 1995). The models are almost exclusively based on the results of uniaxial creep tests. In addition to creep in the direction of loading, lateral creep occurs (see section 2.2.8).

Generalised Kelvin model

Research in the mid 1980's by Rokahr and Lux made a significant contribution to the understanding of creep effects in early age sprayed concrete. Based on the results of creep experiments on samples, they proposed a generalised Kelvin model, valid for ages from 8 hours to 10 days. They were able to model numerically what Rabcewicz (1969) had intuitively deduced - namely, that creep in the sprayed concrete reduces the stresses in the lining (Rokahr & Lux 1987) (see Figure 2.41). While the utilization factor (stress-strength ratio) may be high at early ages, as the stress reduces due to creep and the strength increases, the utilization factor falls and the factor of safety increases. Some subsequent fieldwork has supported this (e.g.: Schubert 1988). Although a simple model, both the spring and dashpot parameters are stress dependent and the viscosity increases with age.

Others too (Swoboda & Wagner 1993, Kuwajima 1999, Sercombe *et al.* 2000) have adopted a generalised Kelvin model, most notably Kuwajima, who investigated how the parameters vary with age over the first 100 hours. However, for the purposes of back-analysing the creep tests, he chose average values, which leads to overestimates of strains. It was suggested that calculations could be simplified further, by assuming that the entire visco-elastic strain occurs instantaneously, without affecting the predictions adversely.

Burgers model

Based on a Burgers model (see Figure 2.40 (c)), but formulated as a time-hardening model, Petersen's model was valid for low levels of stress only (Yin 1996). Pöttler (1990) corrected this and expressed it in polynomial form. However, doubts remain over the validity of the parameters. The original data came from tests performed at ages greater than 30 hours. The

creep rate calculated with Pöttler's formulae initially decreases with time but then rises after 1.5 days, in contrast to the observed behaviour. Yin attempted to correct this by re-formulating the model (as a power law creep model) and estimating the parameters, based on the assumption that they increase with age in the same manner as strength and elastic modulus, as proposed by Weber (see Appendix A and Figures 2.9 & 2.15).

Zheng (referred to in Yin 1996) and Huang (1991) utilised an expanded Burgers model, though, in contrast to Neville *et al.* (1983), they viewed the Maxwell element as representative of the behaviour of young concrete and the Kelvin elements of mature concrete. While the irreversible viscous flow of a dashpot may make sense for very young sprayed concrete (or concrete in the case of Zheng, who was examining an extruded concrete lining), creep at mature ages is not fully reversible, as the Kelvin element implies.

Viscoplastic model

In the course of the Brite Euram project (1997) on sprayed concrete, a Bingham model for shear stresses was proposed for very young sprayed concrete – i.e. between 2 and 7 hours old (see Figure 2.40 (d)). Four of the five parameters in this visco-plastic model vary with age, although this was not incorporated into the formulae. The fifth, Poisson's ratio, may also vary with age during the first 12 hours (see Figure 2.16). The resistance of the frictional element (St Venant element) increases with increasing hydrostatic stress.

Rate of flow model

A model has been proposed for sprayed concrete, based on the Rate of Flow Method (England & Illston 1965, Schubert 1988, Golser *et al.* 1989) with a view to back-calculating stresses from strain histories (Schropfer 1995). Strain histories are broken down into 4 main components as below (see also Figure 2.23):

(a) instantaneous recoverable strain - elastic strain
(b) recoverable creep - delayed elastic strain
(c) irreversible ("yielding") strain - irreversible creep strain
(d) shrinkage (and thermal strain)

Thermal strains are regarded as negligible (Golser *et al.* 1989). Based on extensive test results, equations have been written to describe each component (Golser *et al.* 1989) and subsequently refined to obtain better agreement at early ages and make the elastic modulus dependent on stress intensity (Aldrian 1991) - see Appendix B and section 2.4.6.

Aldrian (1991) proposed a relative deformation modulus, V*, which is a reduction factor for the elastic modulus to account for the effect of the utilization factor, α, - the stress/ strength ratio - as well as the age of the sprayed concrete (Appendix B). It is unclear what this actually means, since pre-loading, even to high utilization factors, does not appear to reduce the initial slope of the stress-strain curve on reloading (Moussa 1993, Probst 1999). In contrast, the reloading modulus is usually higher. The factor, V*, ranges from 1.0 at $\alpha = 0.0$ to 0.13 at $\alpha = 1.0$, at 28 days. It seems that this factor was intended for use in the incremental form of the equations to convert the initial elastic modulus into a tangent modulus and so account for the non-linear nature of the stress-strain curve.

Many numerical analyses have been performed at the Montanuniversitat Leoben, in Austria, using the modified Rate of Flow Method, most recently to investigate the transfer of loads between primary and secondary linings (and the ground) due to creep (Aldrian 1991, Rathmair 1994, Pichler 1994, Schiesser 1997). Golser & Kienberger (1997) contains an overview of this work. However, it has not been possible to implement this method in 3D finite element analyses (Rathmair 1994) and in 2D analyses it has been noted that agreement becomes poorer with increasing numbers of load steps. The Rate of Flow Method has also been criticised because it relies on the principle of superposition and therefore there is no allowance for plastic strains.

Other creep models

Other existing creep models include power laws (e.g.: Andrade's 1/3 power law (Jaeger & Cook 1979)) and creep coefficients, as well as some methods which have been mentioned already in passing – namely, the Effective Modulus (or HME) and Rate of Flow methods.

These models are generally not suitable for sprayed concrete either because, like the standard expressions for elastic modulus and strength gain, derived for older (normal) concrete (e.g.: CEB-FIP, ACI), they cannot replicate the early-age behaviour of sprayed concrete (Han 1995, Kuwajima 1999) or because of the simplifications in the models themselves.

Power laws (Jaeger & Cook 1979) are empirical in nature and were first used to fit curves to data on creep in metals. Of the three stages of creep - transient, secondary and tertiary - only the first is of interest in the case of shotcrete linings soon after construction. The general form for a transient creep power law is $\varepsilon = A\ t^{n}$, where ε is the strain, t is time and A and n are constants. Although a few authors have used forms of power laws in the analysis of SCL tunnels (Schubert 1988, Alkhiami 1995, Yin 1996, Rathmair 1997), they are not widely used because of their inferior ability to model the complex creep behaviour (e.g.: the existence of recoverable and irrecoverable portions of creep). Because of their widespread use in general engineering, power law creep models often come as standard in numerical analysis programs (e.g.: ABAQUS, FLAC), but it is not always possible to combine the creep model with more sophisticated elastic or elasto-plastic models in those programs (Rathmair 1997).

Standard methods for calculating the effects of creep in concrete have been published by various bodies, such as CEB-FIP and the American Concrete Institute (Neville *et al.* 1983, Chapters 12 & 13). Both use a creep coefficient, which is a multiple of parameters that account for factors such as water/cement ratio, cement content and size of the structural member. While the strength of these methods lies in their ability to obtain a coefficient for a wide range of concretes and situations, their weakness lies in the fact that the parameters are valid for hardened (normal) concrete, aged 7 days old or more. Furthermore they are not suitable for the variable loads experienced by a tunnel lining.

Influence on results of numerical models

Creep of sprayed concrete has long been postulated as being responsible for easing stress concentrations in linings (Rabcewicz 1969, Rokahr & Lux 1987, Soliman *et al.* 1994). Many numerical studies (albeit in 2D) have been performed which have demonstrated significant

reductions in axial forces and bending moments when a creep model is used for the lining (e.g.: Huang 1991, Schropfer 1995, Yin 1996) but hard evidence from the field in support of this is scarce.

However, since the load-bearing system is a composite consisting of the ground and the lining, movement of the lining should be expected to cause movement of the ground and a change in the load on the lining. Therefore this case is not as simple as the standard laboratory creep test in which a constant load is applied to a sample and the increasing strain over time recorded. Whether the creep of the lining results in a reduction in the lining stresses depends on the strength and material behaviour of the surrounding ground. If the ground is elastoplastic or susceptible to creep itself, the load in the lining might be expected to actually increase following creep (Pöttler 1990, Schiesser 1997, Yin 1996). It is known that the creep capacity of concrete decreases rapidly with age. Several authors have proposed relationships to predict this (e.g.: Golser *et al.* 1989, Rokahr & Lux 1987, Pöttler 1990 Aldrian 1991) but there is little agreement between them on the rate of change of this property (see Figure 2.41 – normalised age-dependency of creep rate or specific creep). Similarly some researchers have included stress-dependency in their creep models (e.g.: Golser *et al.* 1989, Aldrian 1991, Probst 1999).

Some numerical models, that have included creep, have shown unrealistically large reductions in stresses. For example, in analyses performed by Rathmair (1994) the axial force was reduced to 5% of its initial value, although the same author reports a reduction of stress of only 50% in laboratory relaxation tests on sprayed concrete.

2.3.3.7 Shrinkage

Generally it has been assumed that shrinkage is not important for tunnel linings. Typically after 100 days the free shrinkage strain is less than 0.1%. However, Hellmich *et al.* (1999c) and Hellmich *et al.* (2000) report that, in the case of plane strain analyses, shrinkage does have an appreciable impact on the stress distribution in a lining and may reduce the bending moments considerably. The effect is most pronounced in the longitudinal direction because of

the plane strain restraint. It is unclear whether shrinkage would have such a large influence in more complex 3D analyses, although differential shrinkage / thermal expansion could quite conceivably lead to cracking at the joints between sections of a lining.

2.3.3.8 Ageing

General comments

Ageing makes the task of modelling sprayed concrete considerably more complicated than is the case for other materials. While one may assume that in a tunnel the load increment due to an advance is applied as soon as the ground is excavated and choose values of parameters (e.g.: stiffness) that are consistent with the ages of the different parts of the lining at this moment (see Figure 2.38), one must also check that the new parameters are consistent with the constitutive model. All of the properties of sprayed concrete vary with age and Appendix A contains numerous empirical relationships for predicting the most commonly used properties (e.g.: strength) at all ages. The age of the individual parts of the lining can be determined approximately from their distance from the tunnel face for a given advance rate and excavation sequence.

Thermo-chemo-mechanically coupled model

The fundamental reason for ageing is the ongoing hydration of the cement. Hence various authors have sought to quantify how the degree of hydration (ξ) varies with time and then relate all the material properties to this. An overview of the theory can be found in Ulm and Coussy (1995, 1996). The thermo-chemo-mechanically coupled model aims to account for:

- the chemo-mechanical coupling between hydration and the evolution of properties such as strength, stiffness and autogeneous shrinkage
- the thermo-mechanical couplings such as dilation due to the exothermic hydration reaction (Hellmich & Mang 1999) or damage criteria (Cervera *et al.* 1999b)
- the thermo-chemical couplings such as the reduction in final strengths and stiffnesses due to increased curing temperatures (Cervera *et al.*, 1999b)
- the thermodynamically activated nature of hydration itself

An underlying intrinsic material function - the chemical affinity or driving force of hydration ($A_{(t)}$ or $A_{(\xi)}$) - can be determined experimentally (see Figure 2.43). Being intrinsic it is independent of field variables and boundary effects (Hellmich 1999a & Hellmich *et al.* 2001). Strength can then be related to the progress of this function with time, t, as below.

$$\frac{d\xi}{dt} = (1-\xi_0)\cdot\left[\frac{df_c/dt}{f_{c,\infty}}\right] = A_{(\xi)}.e^{-E_A/RT_i} \qquad 2.12$$

$$A_{(\xi)} = a_A \cdot \left[\frac{1-e^{-b_A.\xi}}{1+c_A.\xi^{d_A}}\right] \qquad 2.13$$

The exponential term in equation 2.10 accounts for the thermodynamically activated nature of hydration. T is temperature in K. ξ_0 is the "percolation threshold", below which the concrete cannot sustain any deviatoric stress and f_c is the compressive strength. a_A, b_A, c_A and d_A are all constants (see Appendix A). Similarly, other relationships have been proposed between properties such as tensile strength, autogeneous shrinkage and stiffness and the degree of hydration (ξ) (see Figure 2.44 a & b) – see also Appendix A and Eierle & Schikora (1999). Sercombe *et al.* (2000) contains tentative relationships [47] for the development of short and long-term creep with the degree of hydration. In common with the empirical formulae, it is assumed that the hydration kinetics are independent of the loading history.

Alternatively, the effect of temperature on hydration can be accounted for by the simpler method of equivalent age (Cervera *et al.* (1999a) and D'Aloia & Clement (1999)). An elevated temperature speeds up hydration. The value at a given age can be read from a graph of the parameter's growth at a reference temperature, using an age, which has been corrected for the more advanced degree of hydration. Cervera *et al.* (1999a) note that normally all of the cement does not hydrate and the final degree of hydration can be found from:

[47] The relationships are based on one creep test on a sprayed concrete sample at an age of 28 days.

$$\xi_\infty = 1.031\ w/c\ /[0.194 + w/c] \sim 0.71 \text{ for } w/c = 0.43 \qquad 2.14$$

$A_{(\xi)}$ profiles have only been developed for a few concretes and different researchers have proposed widely differing values for some of the key parameters, e.g.: the profile itself or the percolation threshold. A standard means of determining $A_{(\xi)}$ is to work back from data on the development of strength with time. However, if one already knows this, other parameters (e.g.: stiffness and tensile strength) can be determined directly. The benefit of the thermo-chemo-mechanical approach is that it links the properties to the fundamental process behind them - namely, hydration. This provides some further insight into the behaviour of concrete at early ages and makes the inclusion of temperate effects straightforward where this is relevant. While temperature effects are important for massive structures (e.g.: Aggoun & Torrenti (1996) and Hrstka *et al.* (1999)), most tunnel linings are quite slim (i.e. less than 400 mm thick) and the elevated temperatures due to the heat of hydration are short-lived. Figure 2.45 shows that the effect of elevated temperature on hydration is limited for the temperatures experienced in SCL tunnels.

2.3.3.9 Stress distribution

Even in the simple case of a single advancing tunnel, the stress distribution can be complex. Therefore one must take care to consider both the general picture as well as the values of parameters at specific points in the lining (or ground). The stress state may be characterised as biaxial (since the component in the radial direction is typically an order of magnitude lower) (Meschke 1994, Kropik 1994). The hoop stress (i.e. the stress in the circumferential direction) is the largest compressive stress, although the vectors of principal stresses are not necessarily aligned perfectly with the hoop, longitudinal and radial directions (Kropik 1994). This latter point is particularly true at the face of the tunnel where the major stress appears to arch around corners (see Figure 2.46).

In the few cases where this has been shown, the longitudinal stresses (predicted by numerical models) are usually tensile (Meschke 1994, Kropik 1994, Hafez 1995) [48]. Ahead of the face the vectors of ground displacement are directed towards the (unsupported) face. As one moves towards and behind the face, these vectors rotate so that a plane strain condition is attained (Steindorfer 1997), typically 2 tunnel diameters after the closure of the ring in soft ground. Hence after the lining has been introduced in the model, there is a net longitudinal movement of the adjacent ground elements towards the face. This may be the explanation for the tension in the lining. Kropik (1994) reports that the tensile stresses are greatest on the intrados, which runs counter to what one might expect if the lining initially acts as a cantilever.

Within a given advance length, the hoop stresses are greatest at the leading edge (see Figure 2.46) (Meschke 1994, Kropik 1994, Cosciotti *et al.* 2001). Each advance tends to cause the largest increment in stress in the section of the lining behind the one that has just been built. Meschke (1994) attributes this to the low stiffness and strength of the new section, but this may also be due to arching in the ground, around the unsupported face. In general, in more complex geometries, stress concentrations appear at the locations, such as corners, where one would intuitively expect to see them (e.g.: Soliman *et al.* 1993, Meschke 1994, Hafez 1995). Multiple tunnels and junctions have rarely been modelled in 3D (e.g.: Soliman *et al.* 1993, Kropik 1994, Hafez 1995) and sometimes the simplifications of the models have led to what appear to be erroneous results. For example, Hafez (1995) modelled the lining on its own, under an increasing hydrostatic "ground" pressure. The use of an elastoplastic model for the lining led to higher bending moments and axial forces compared to the elastic model. One might suggest that this is because there was no ground to participate in the stress redistribution during yielding, rather than a true reflection of the consequences of introducing plasticity. However, one should note that the stress distribution may change considerably during construction when there are complex construction sequences (e.g.: the direction of

[48] The exception to this is Yin (1996) who, in a study of very deep tunnels (about 750m cover), reported compressive axial forces which were at times greater than the hoop forces in the lining.

bending moments reversed from the first stage – a non-circular Top Heading with temporary invert – to the next, an almost circular full cross-section (Moussa 1993)).

Because simplified construction sequences have been used in the past to limit computing times, there is little information on how the stresses might vary around the lining. Oettl *et al.* (1998) found that the bending moments and axial forces are highest in the Top Heading of a tunnel, if constructed using a Top Heading, Bench and Invert sequence. In this case, the stresses in the invert were zero because complete stress relief was permitted before the lining was installed in the invert. However, the vector plots of principal stresses from 3D analyses reported by Meschke (1994) tend to support this picture. Similarly Minh (1999) reported that most of the ground deformation and stress redistribution occurred during the excavation of the Top Heading and the excavation of the lining had little effect.

2.3.3.10 Construction defects

Despite the fact that SCL tunnelling is known to be vulnerable to poor workmanship, common construction defects, such as variation in strength and quality, poorly constructed joints and variations in shape and thickness, are not normally considered. In contrast, in the design of segmental linings, it is routine to consider the effects of ovalization (due to ground deformation or poor build quality) and the misalignment of segments (so-called "stepping").

2.4 Summary

In summary, this wide-ranging chapter has provided an introduction to tunnelling using sprayed concrete linings and the material itself. The behaviour of the material has been outlined and finally the state-of-the-art of numerical modelling of SCL tunnels has been discussed. Conclusions on these three subjects will be presented below.

SCL tunnelling – its current usage

SCL tunnels are increasingly popular because of the flexibility that they offer in terms of geometry of the excavation and the ground conditions in which they can be constructed. SCL tunnels are often more cost-effective than traditional tunnelling methods, especially in the

case of short tunnels with complex geometries. The cost-savings of this method could be further enhanced if the primary sprayed concrete lining could be used as part of the permanent works. Sprayed concrete has a complex material behaviour and so simple (closed form) analytical design methods may not provide reliable predictions of SCL tunnels behaviour. Until a higher degree of certainty can be achieved in design, the use of sprayed concrete will be constrained.

The behaviour of sprayed concrete

The constituents of sprayed concrete are basically the same as conventional concrete but include some means of accelerating the hydration process and are placed by spraying. The latter provides the only source of compaction and places additional demands on the mix design.

Sprayed concrete exhibits age-dependency, time-dependency and non-linearity in its material behaviour. The behaviour is summarised below.

- The mechanical properties change rapidly with age during the first week.
- The higher levels of porosity and the effect of the faster hydration reaction on the microscopic structure of sprayed concrete tend to reduce its strength.
- Sprayed concrete can withstand considerable strains at an early age but becomes less ductile with increasing age.
- Sprayed concrete in tunnels exhibits higher levels of creep than concrete in conventional formed structures, mainly because of the earlier loading, the higher cement content and larger surface to volume ratio.
- Sprayed concrete in tunnels exhibits higher levels of shrinkage than concrete in conventional formed structures, mainly because of the higher cement content and larger surface to volume ratio.
- Sprayed concrete can be produced with similar durability characteristics to good quality conventionally placed concrete.

Numerical modelling of SCL tunnels

- It remains difficult to predict the real behaviour of tunnels and the surrounding ground with numerical models.
- There are still few 3D numerical studies of SCL tunnels and even fewer comparative studies, examining the role of the constitutive model of sprayed concrete. There are some exceptions, e.g.: Yin 1996.
- The use of more sophisticated constitutive models for the ground has been shown to improve prediction of some aspects of the behaviour of the ground. Therefore it seems reasonable to postulate that using more sophisticated constitutive models for sprayed concrete will improve the predictions of the behaviour of the lining.
- Phenomena such as plasticity and creep are normally assumed to alleviate stress concentrations in the lining but their effects depend on the response of the ground to the resultant stress redistribution.
- Bending moments are affected more than hoop forces by changes in constitutive model (as one might expect since the application of more sophisticated models tends to modify the stress distribution within the lining more than the loading on the lining).
- Tunnelling is a soil-structure interaction problem in which the modelling of the ground may be the single most important factor. The deformation of the ground far from the tunnel is often influenced little, if at all, by the constitutive model of the lining.
- When modelling tunnel construction in London Clay, the ground model should include the spatial variations in properties and the nonlinear elastoplastic behaviour in order to predict realistic ground movements and stress changes. Anisotropy may be important. The high stiffness of the clay at low strains may not be relevant if one is primarily interested in the situation near the tunnel. An undrained analysis is adequate for the short-term case. The initial stress state is a major influence on the loads on the lining.

Figure 2.1 Typical grading curve for sprayed concrete (EFNARC 1996)

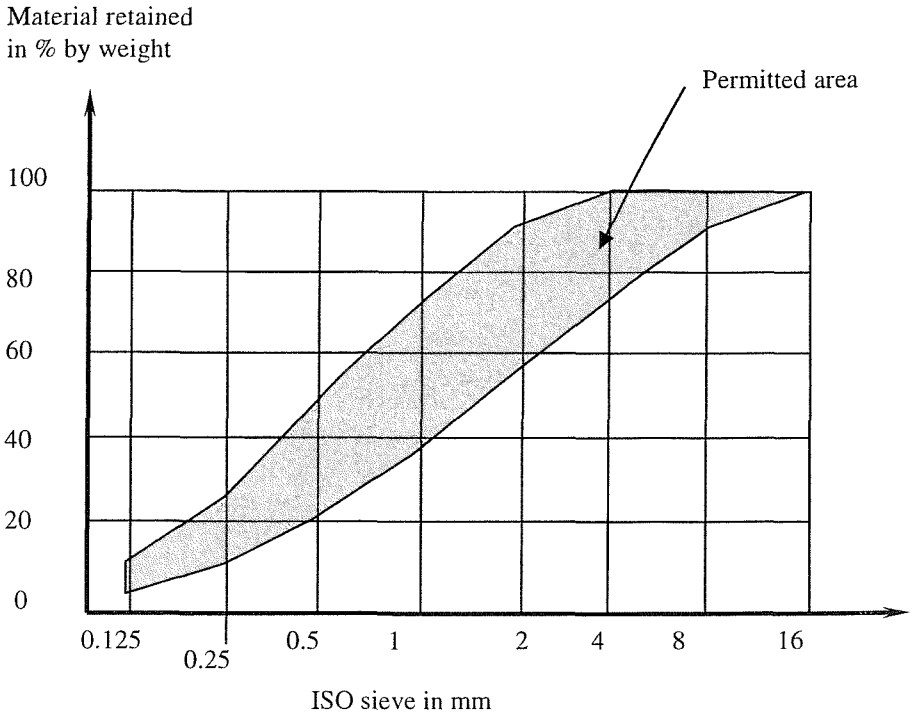

Figure 2.2 Early-age strength gain depending on dosage of accelerator with ÖBV J-curves for minimum strength (after Kusterle 1992)

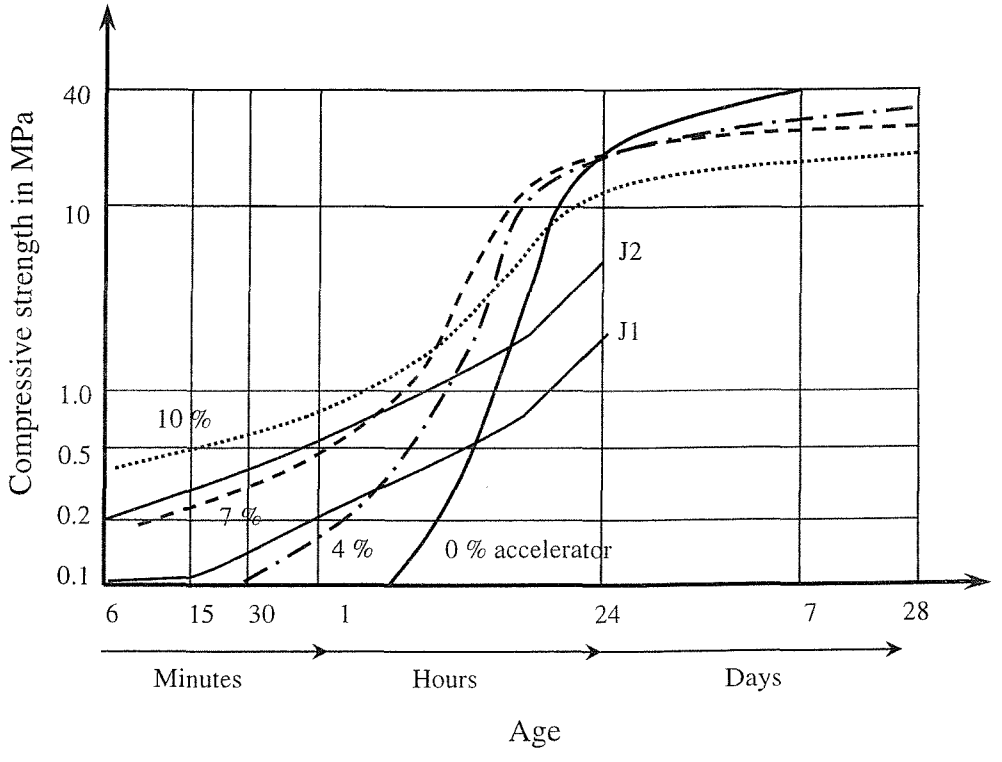

Figure 2.3 Schematic view of dry-mix spraying process

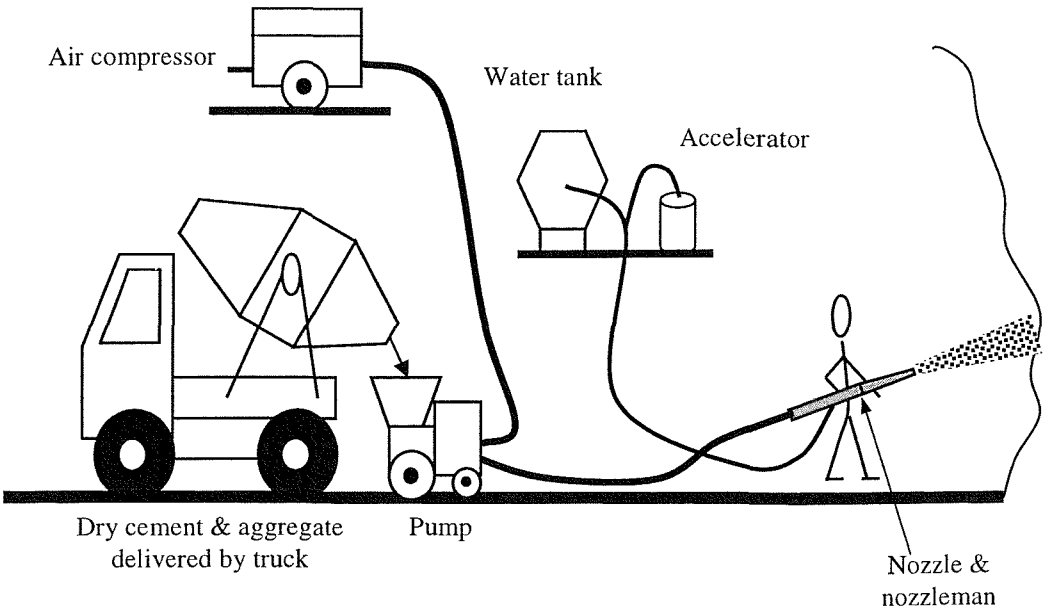

Figure 2.4 Schematic of wet mix (thick stream) spraying process

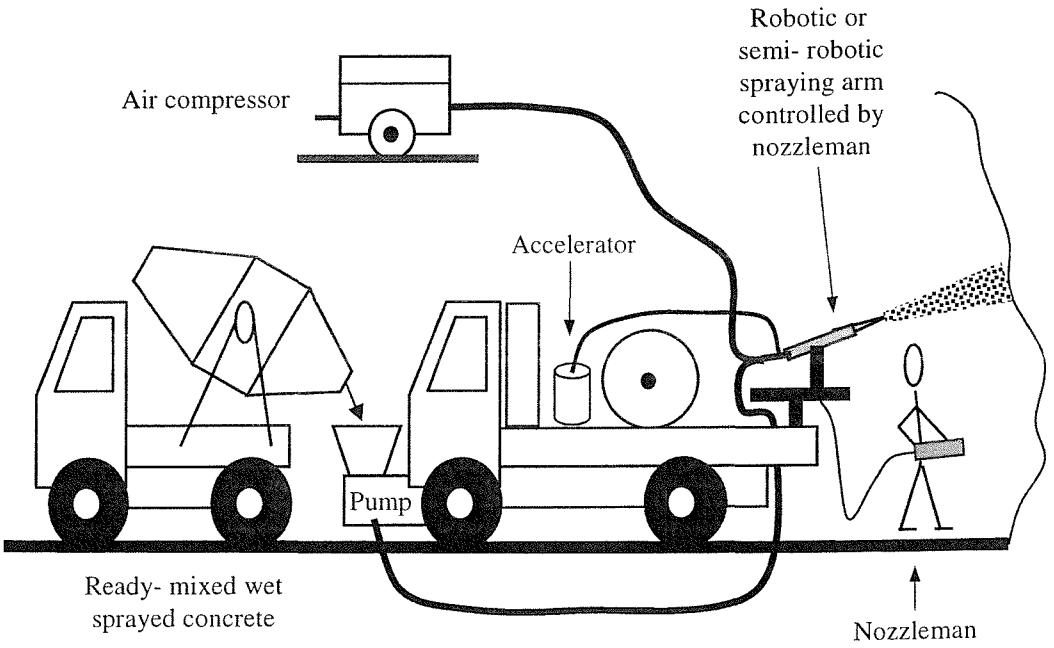

Figure 2.5 Dust levels during spraying (Testor & Pfeuffer 1999)

(Showing the range of readings and the average value according to the German MAK standard for different sprayed concretes)

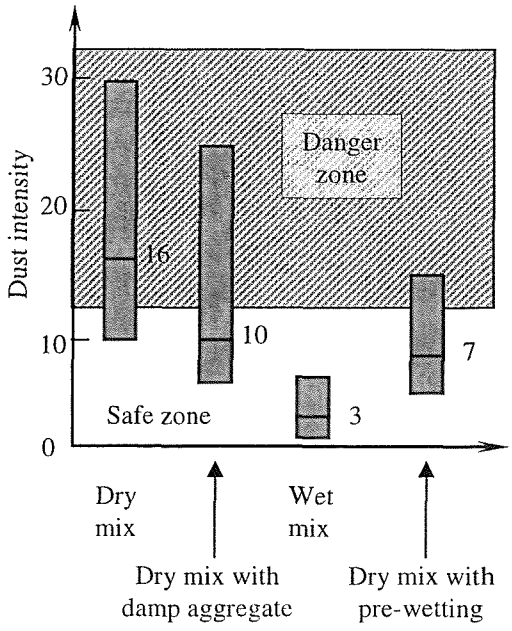

Figure 2.6 Size of the constituents & pores of concrete (after Blasen 1998)

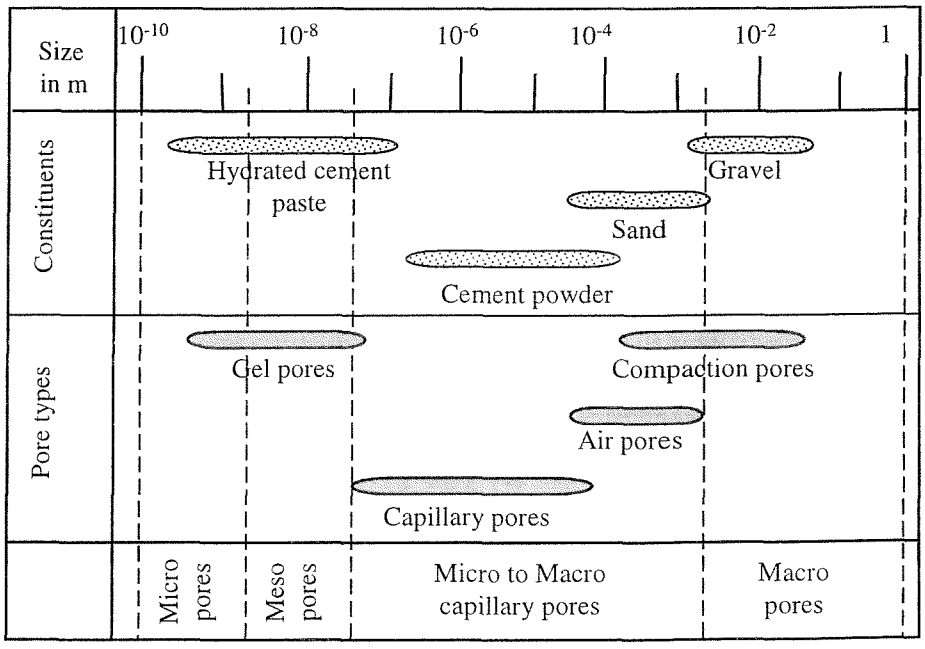

Figure 2.7 Stress-strain curves for sprayed concrete at different ages (after Aydan et al. 1992a)

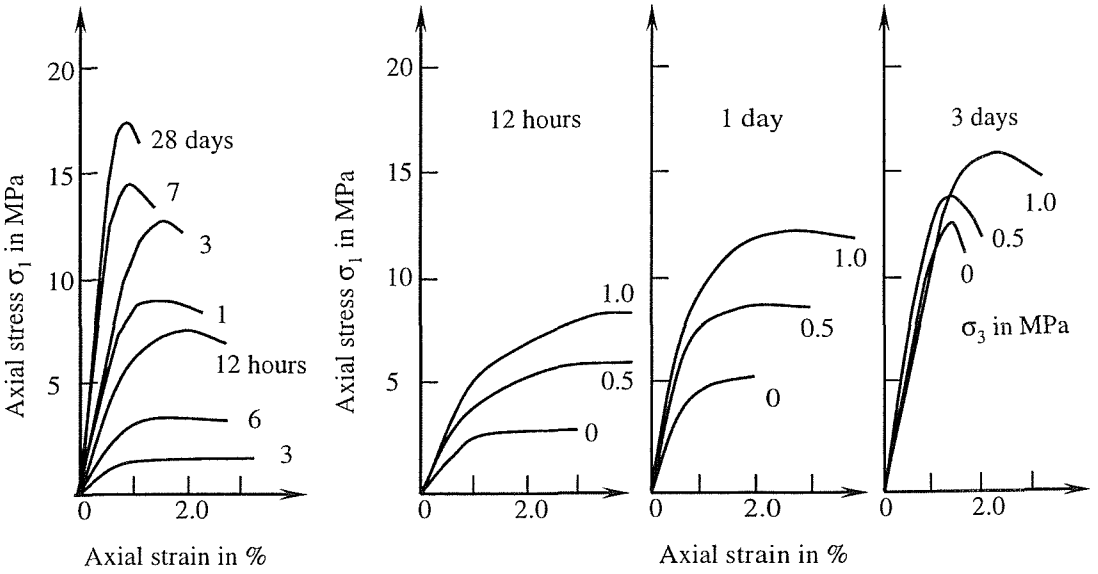

(a) Uniaxial test data

(b) Triaxial test data

Figure 2.8 Normalized biaxial strength envelope for plain concrete from experimental data (after Chen 1982)

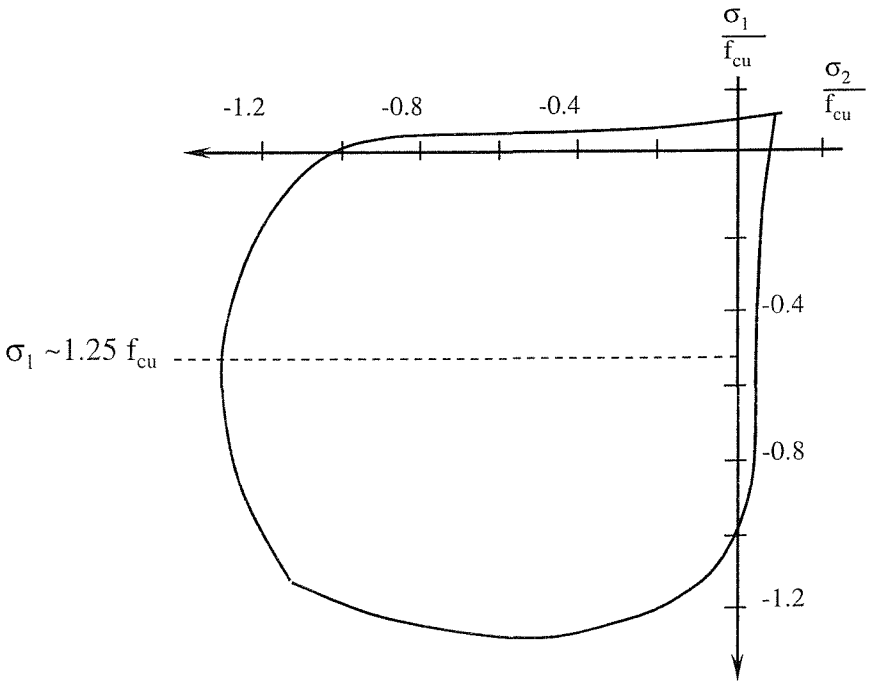

Sign convention = compression is negative

Figure 2.9 Predictions of compressive strength development vs age

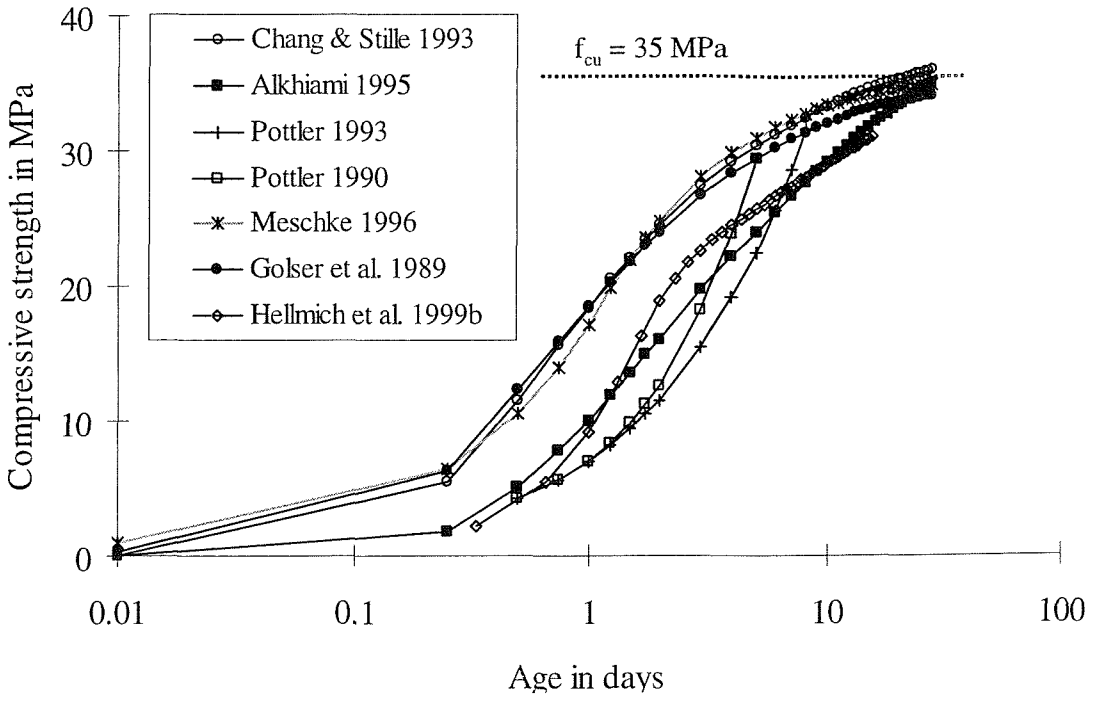

Figure 2.10 Tension stiffening of reinforced concrete (after Feenstra & de Borst 1993)

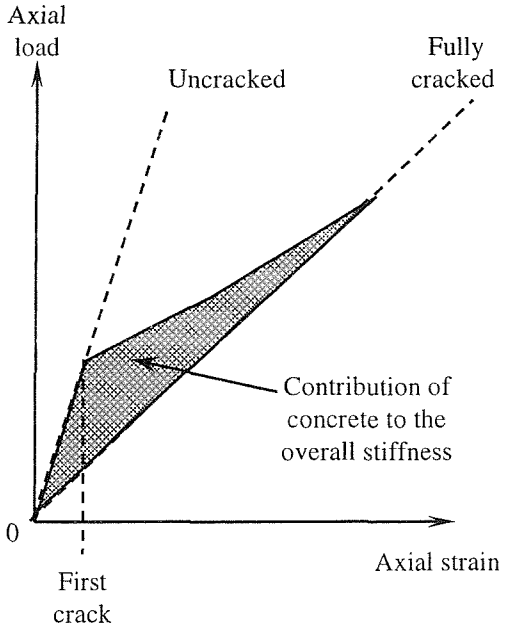

Figure 2.11 "Shadowing" in sprayed concrete behind reinforcement (after Podjadtke 1998)

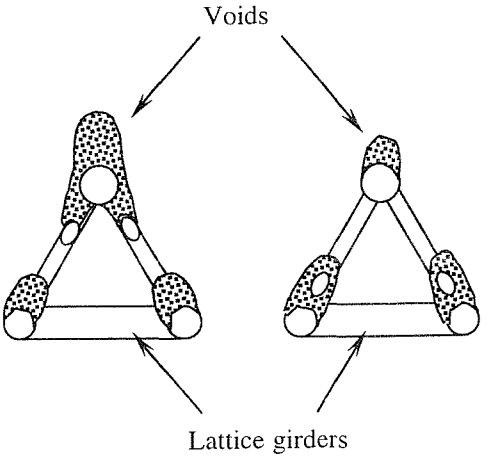

Figure 2.12 Bond strength in shear to various substrates (after Kusterle 1992)

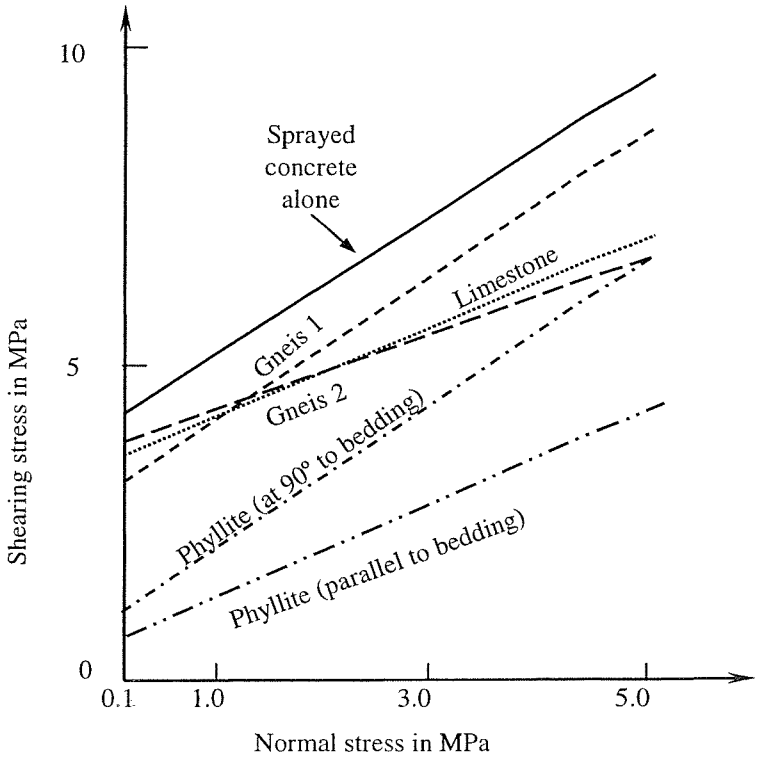

Figure 2.13 Normalized octohedral stress envelope for sprayed concrete (with published data from Aydan *et al.* 1992, Brite Euram 1998 & Probst 1999)

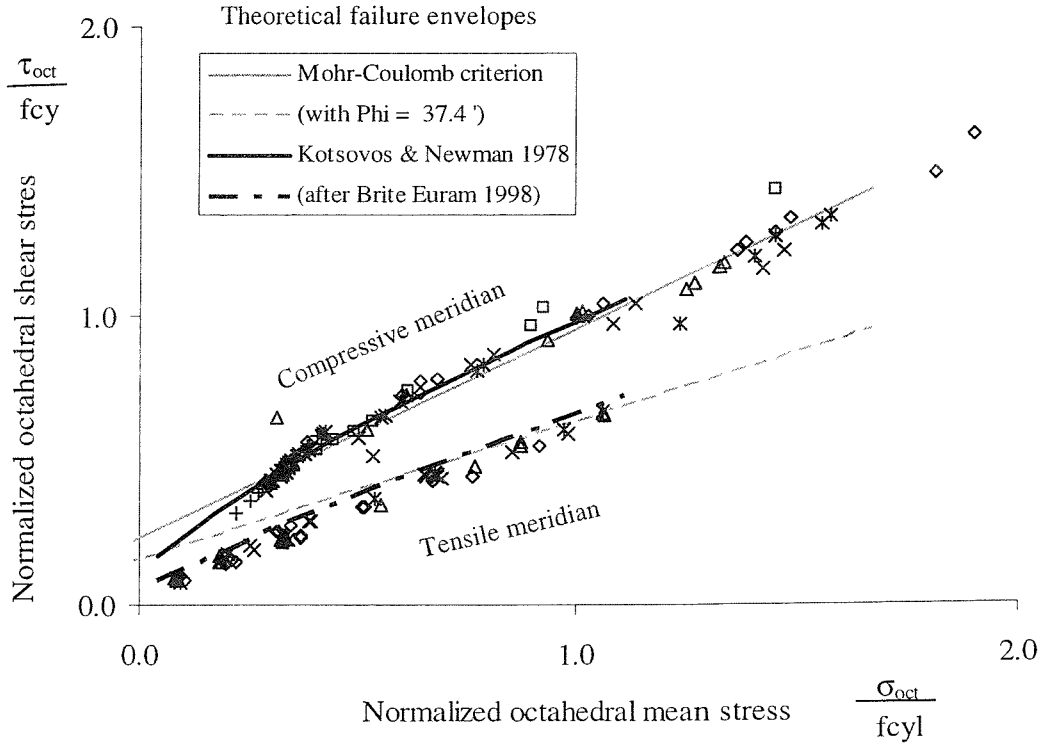

Figure 2.14 Yield stress / peak stress ratio (published data, including data from triaxial tests by Aydan et al. at various confining pressures - sigma 3)

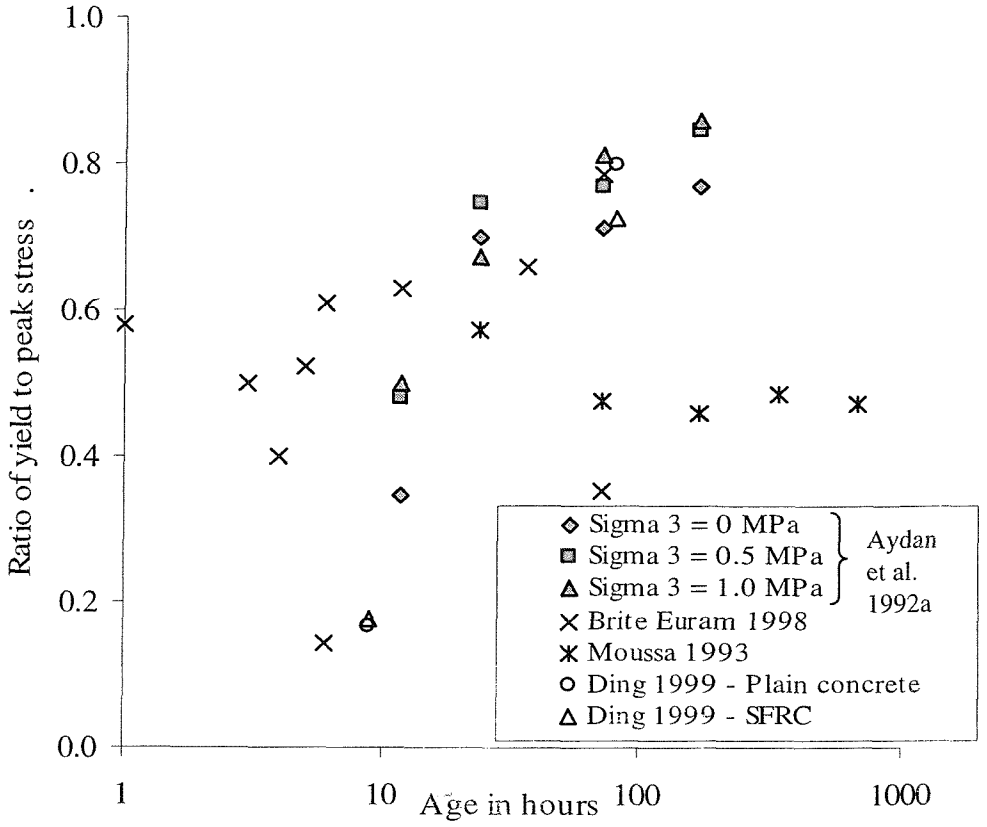

Figure 2.15 Predictions of the development of elastic modulus with age

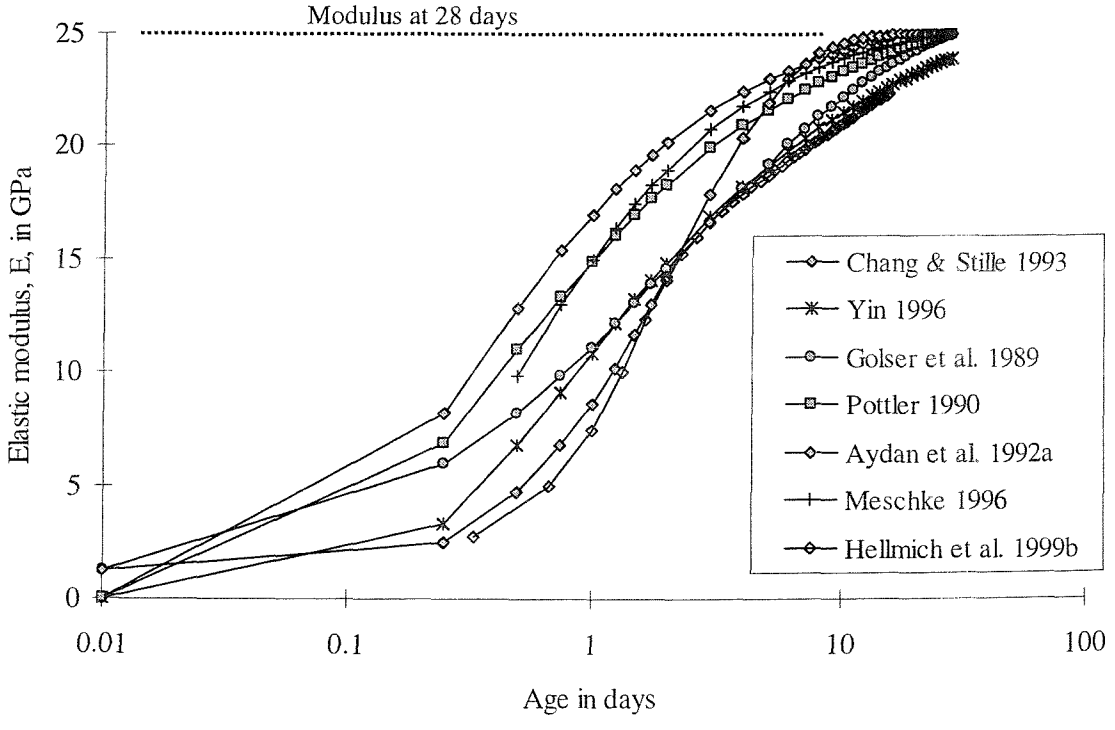

Figure 2.16 Variation of Poisson's ratio with age

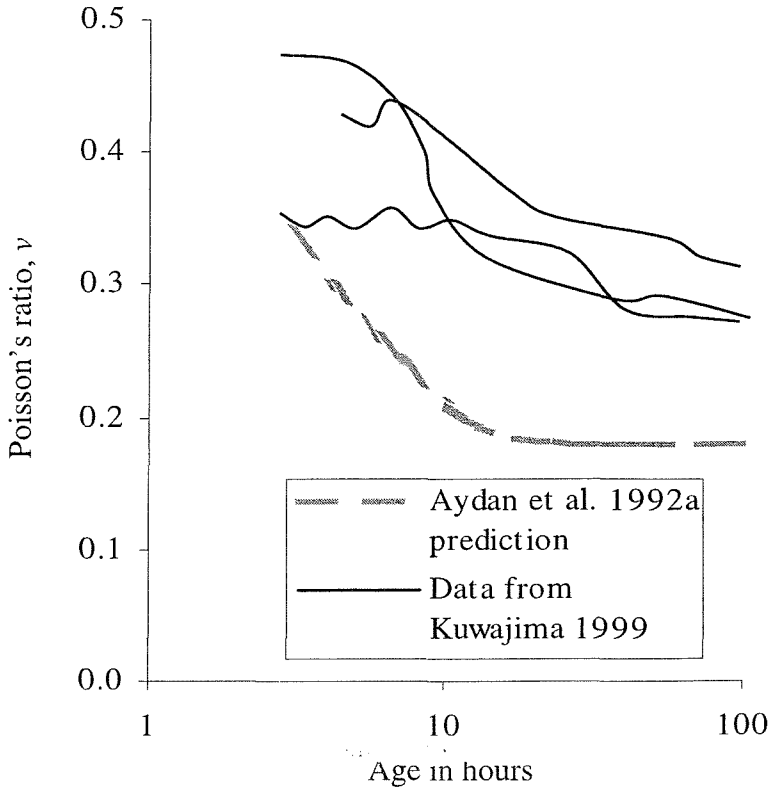

Figure 2.17 Peak compressive strain vs age

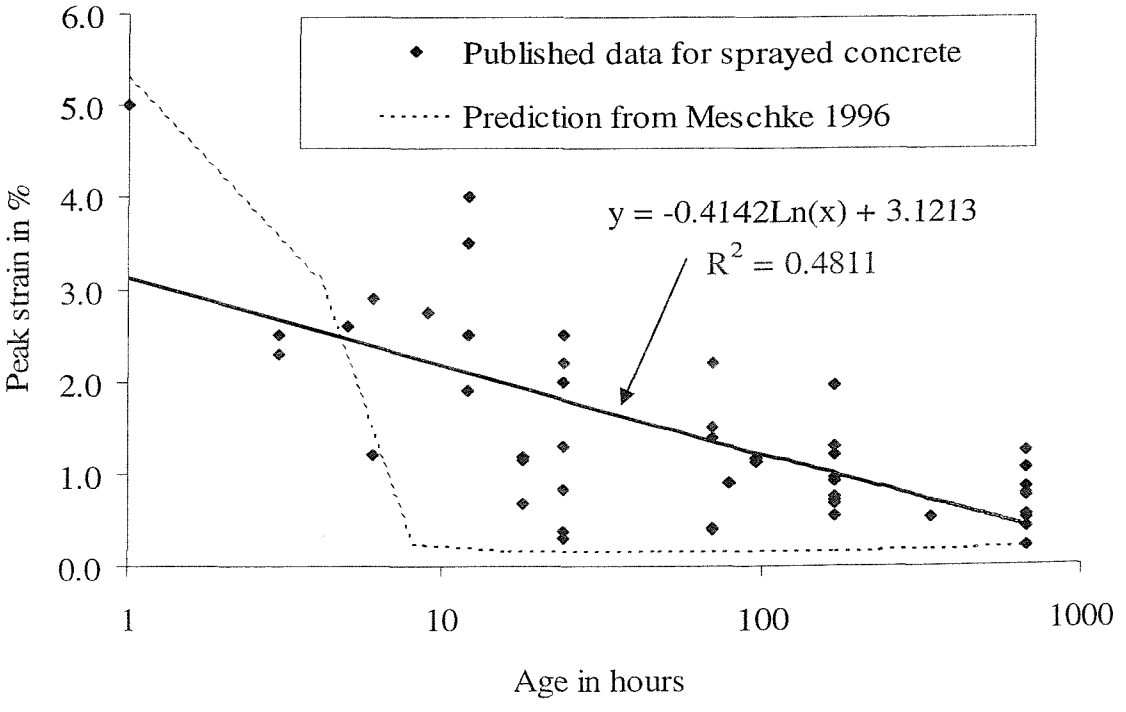

Figure 2.18 Ultimate compressive strain vs age

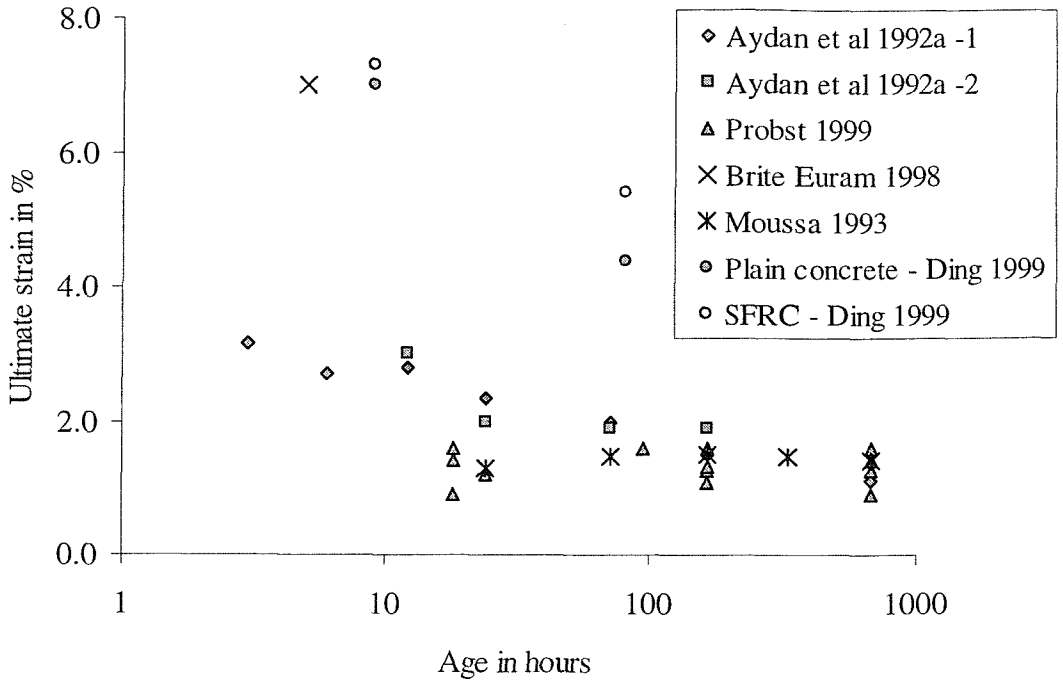

Figure 2.19 Compressive test on sprayed concrete (after Probst 1999)

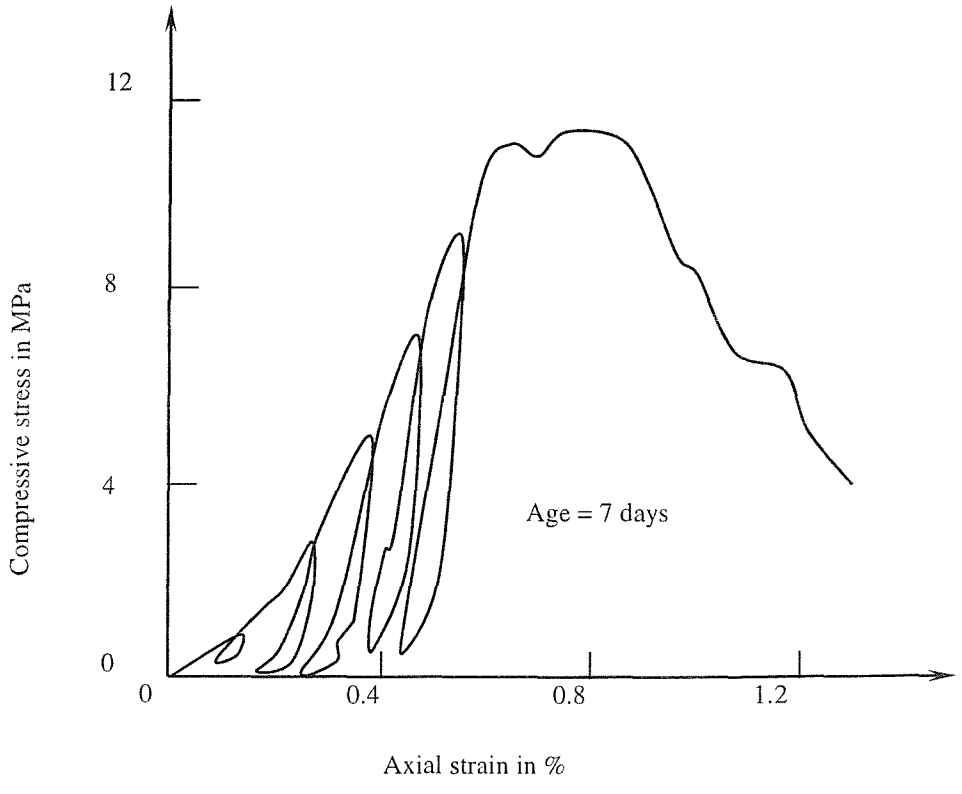

Figure 2.20 Uniaxial tensile tests on samples of mix IK013 at different ages (Brite Euram 1998)

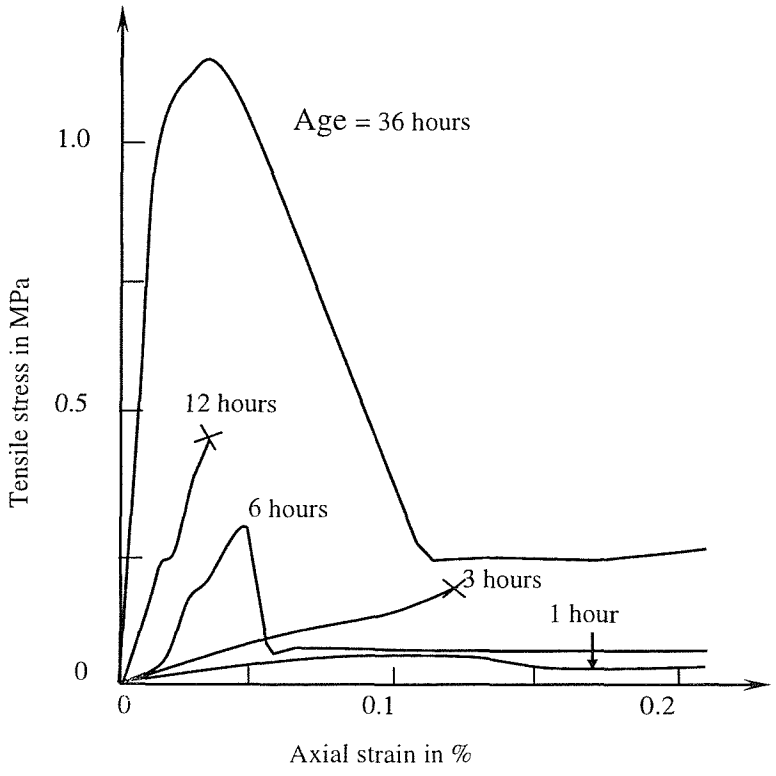

Figure 2.21 Water loss from concrete (after Oberdörfer 1996)

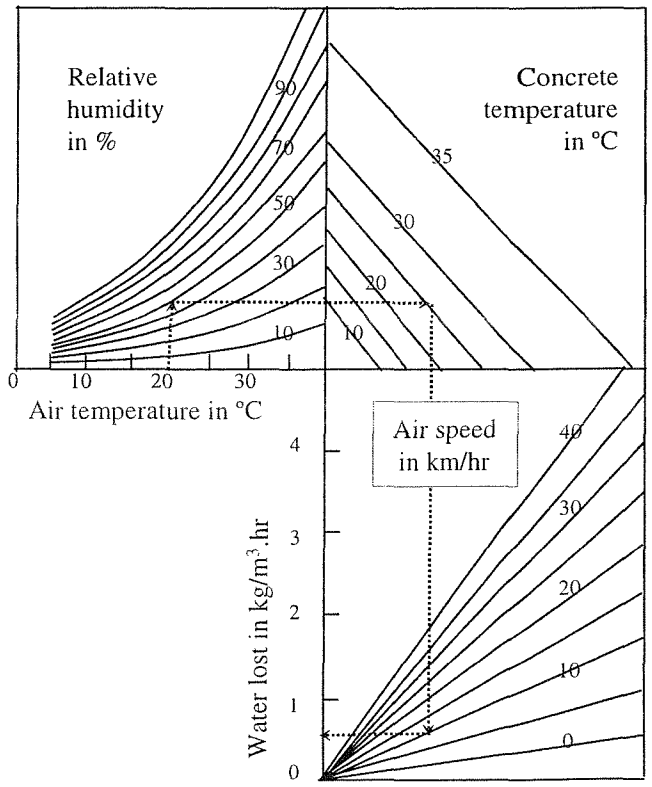

Figure 2.22 Temperature in a sprayed concrete lining (after Kusterle 1992)

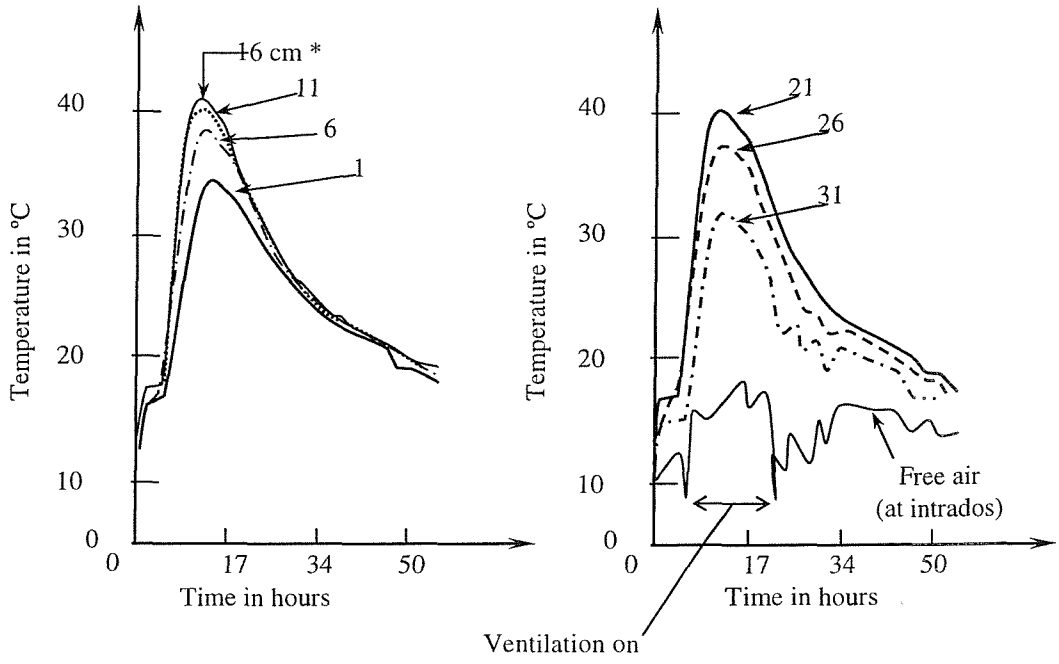

* Distance in cm inwards from extrados of 30 cm thick lining

Figure 2.23 Decomposition of strains according to the Rate of Flow Method (after Golser et al. 1989)

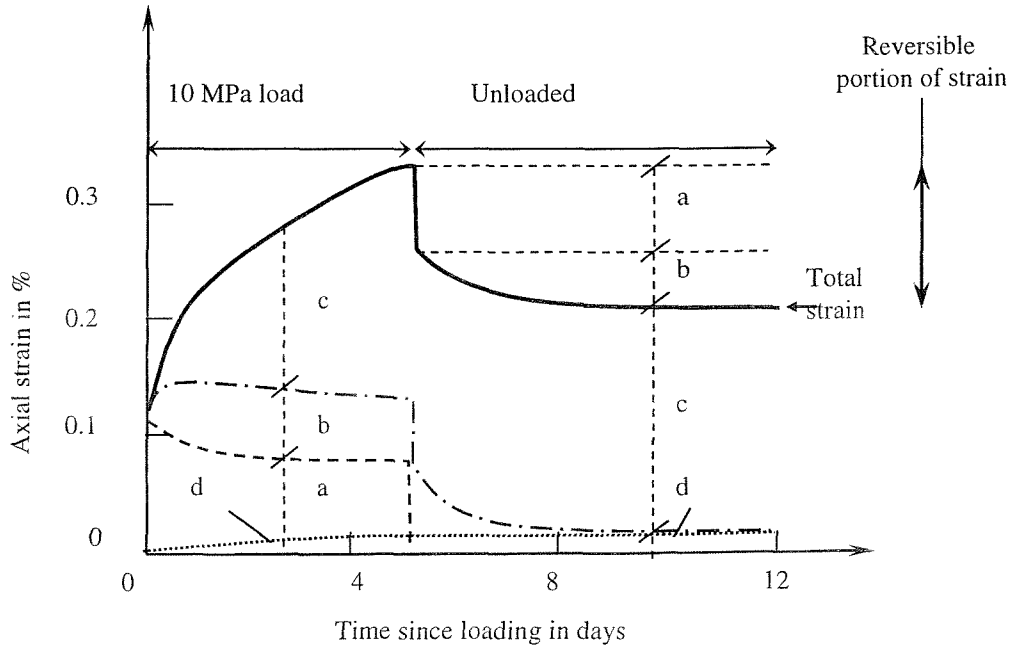

Key:
a Elastic response
b Delayed elastic response
c Irreversible creep
d Shrinkage

Figure 2.24 Composition of strains in a creep test (after Ding 1998)

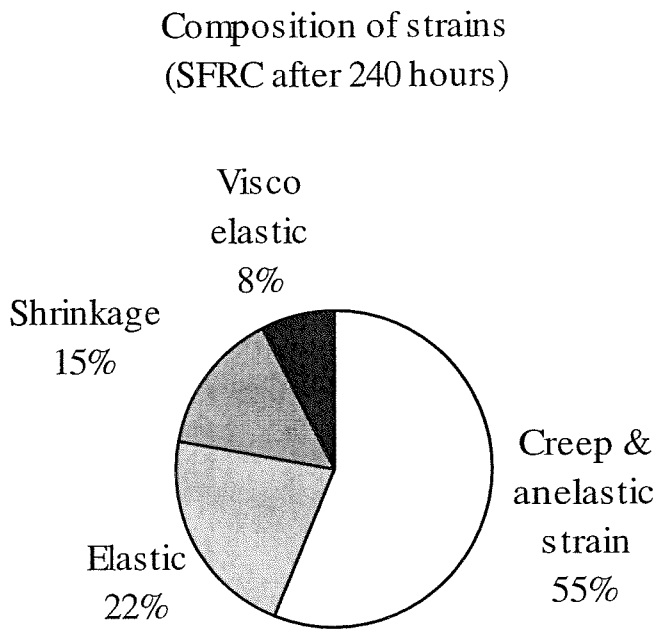

Figure 2.25 Creep test (after Ding 1998)

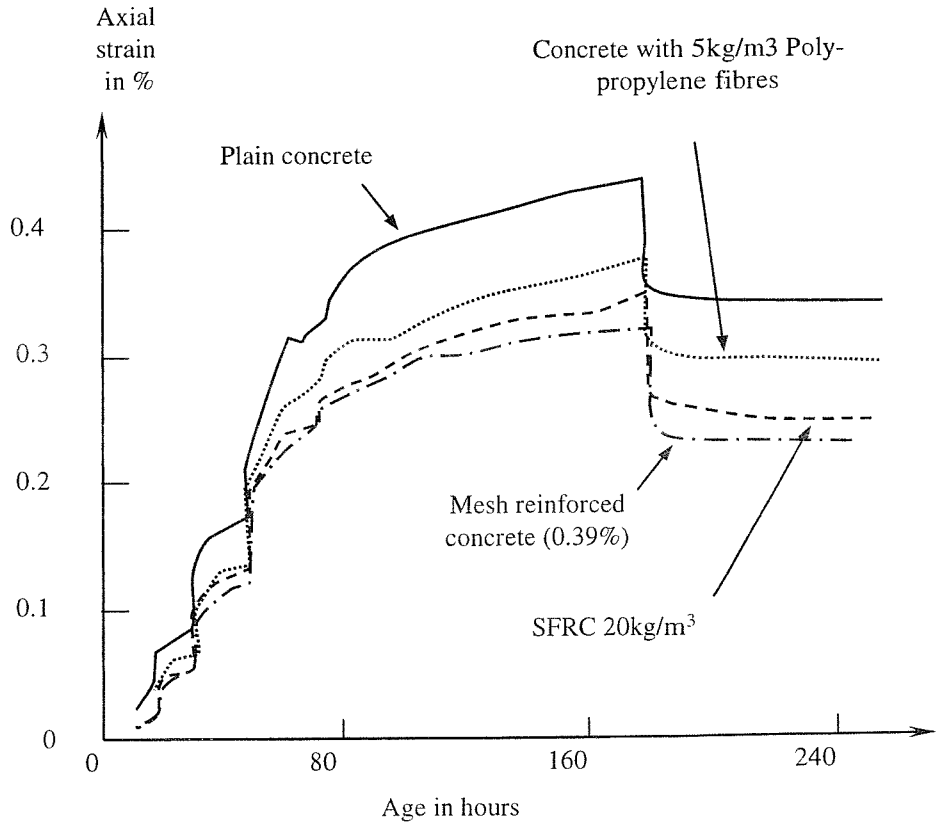

Figure 2.26 Permeabilities of sprayed concrete - categories acc. to Concrete Society Technical Report 31

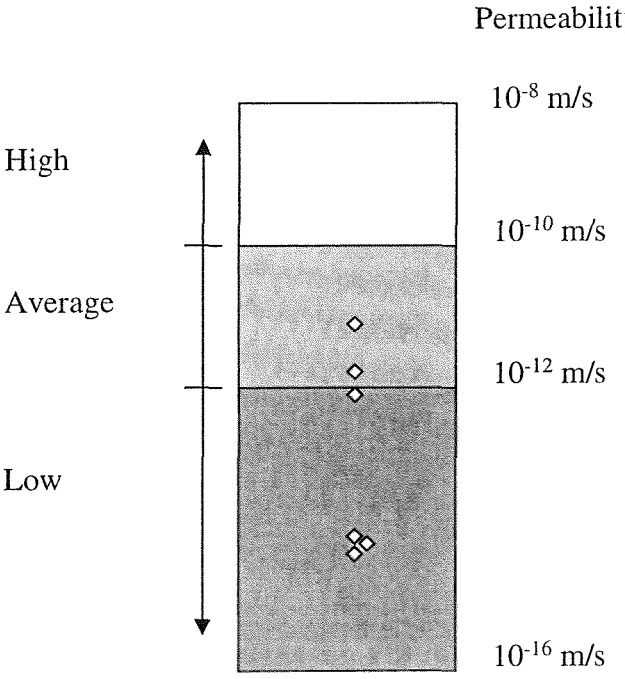

◇ Data from Brite Euram 1998, HEX & JLE projects (unpublished)

Figure 2.27 Typical mesh for a simple numerical model of a tunnel

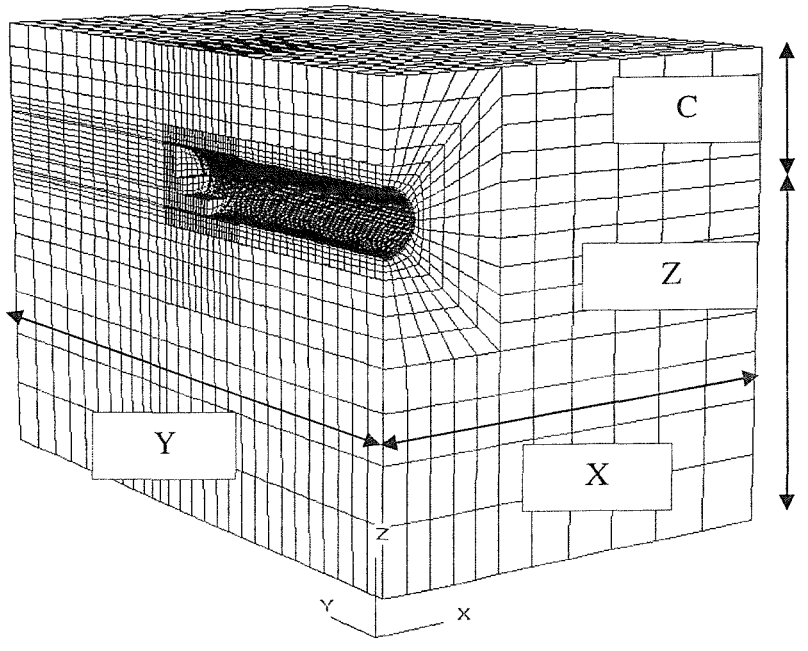

C = cover to axis
X = width of mesh
Y = length of mesh
Z = depth below axis

Figure 2.28 Permeability of London clay (Chandler et al. 1990 from van der Berg 1999)

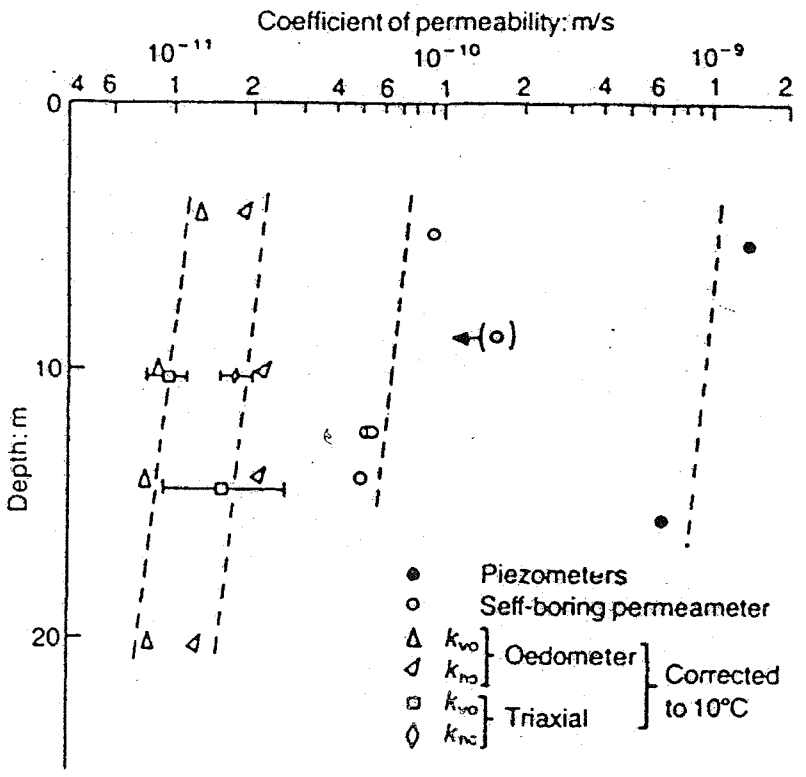

Figure 2.29 K_0 profile for London clay at Heathrow (van der Berg 1999)

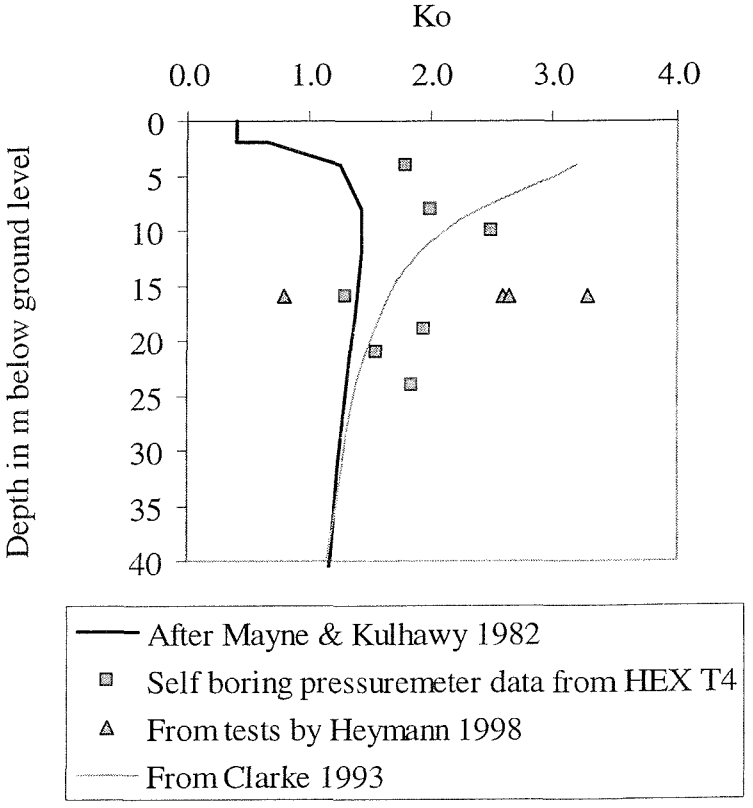

Figure 2.30 Undrained elastic modulus vs depth for London clay (van der Berg 1999)

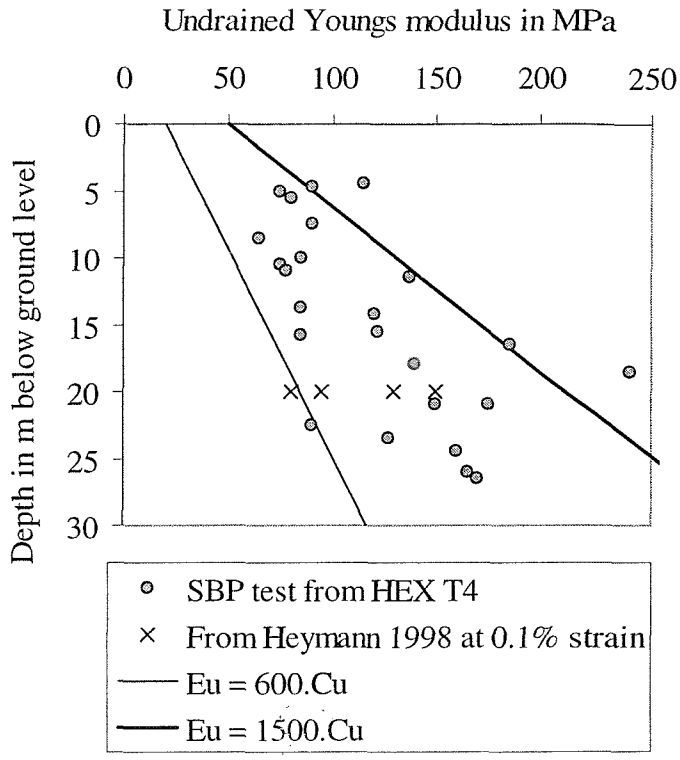

Figure 2.31 Undrained shear strength vs depth for London clay (van der Berg 1999)

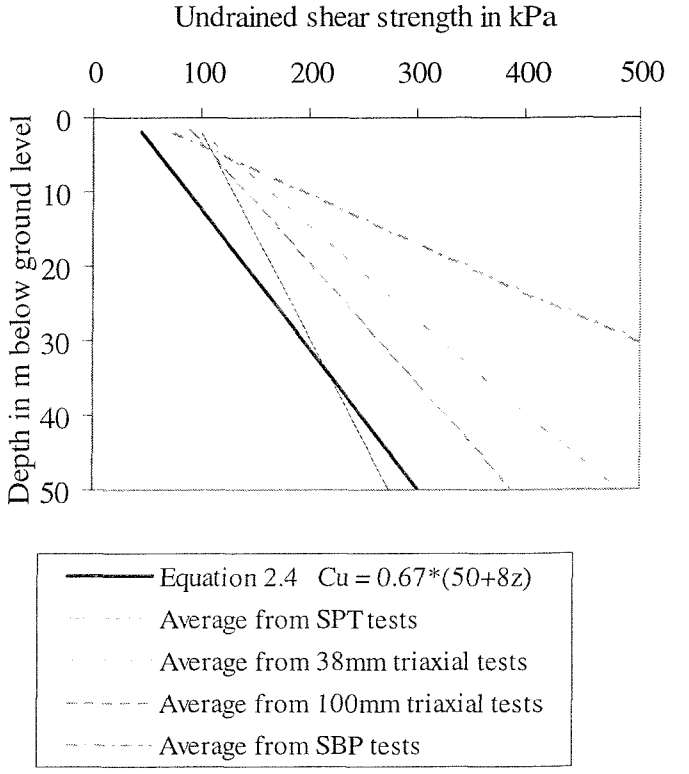

Figure 2.32 Yield surfaces in 3D stress space

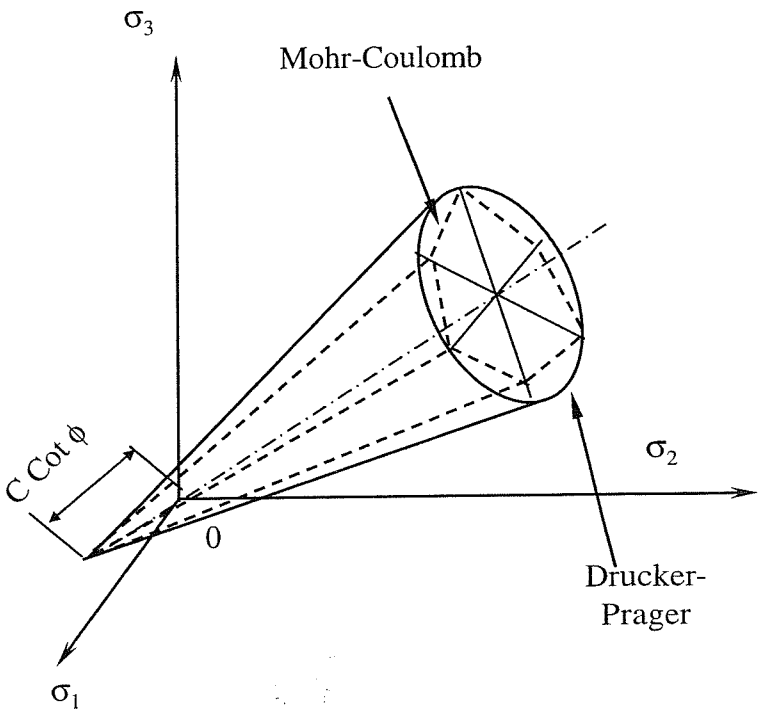

Figure 2.33 Nonlinear stress strain behaviour of London clay

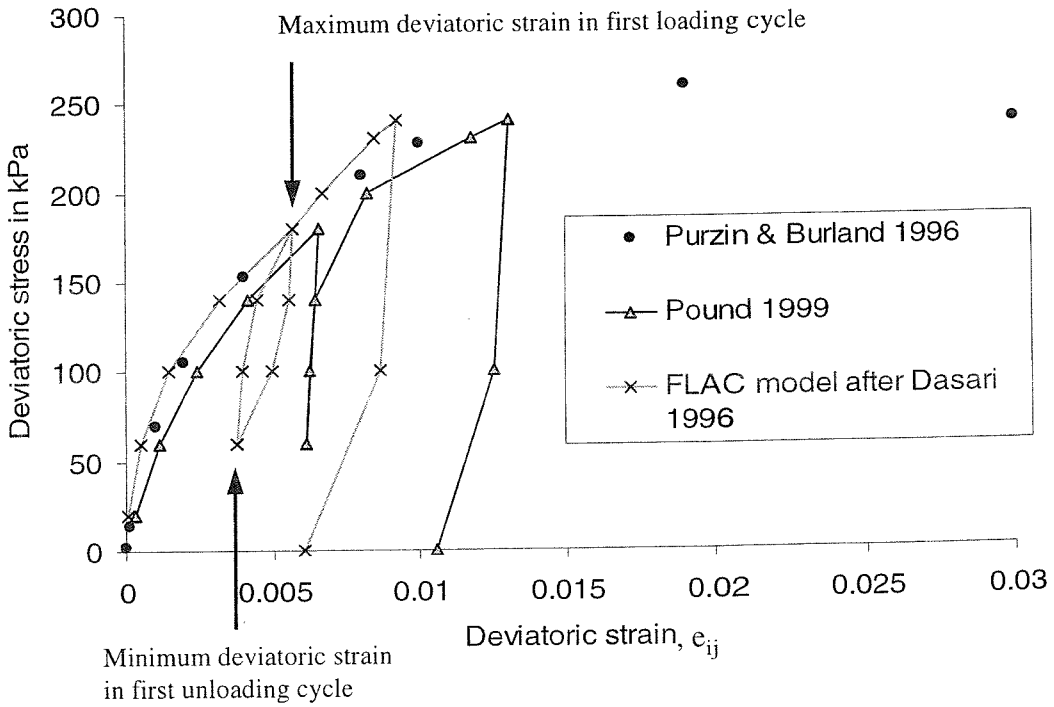

Figure 2.34 Settlement troughs from 2D numerical models (Krenn 1996)

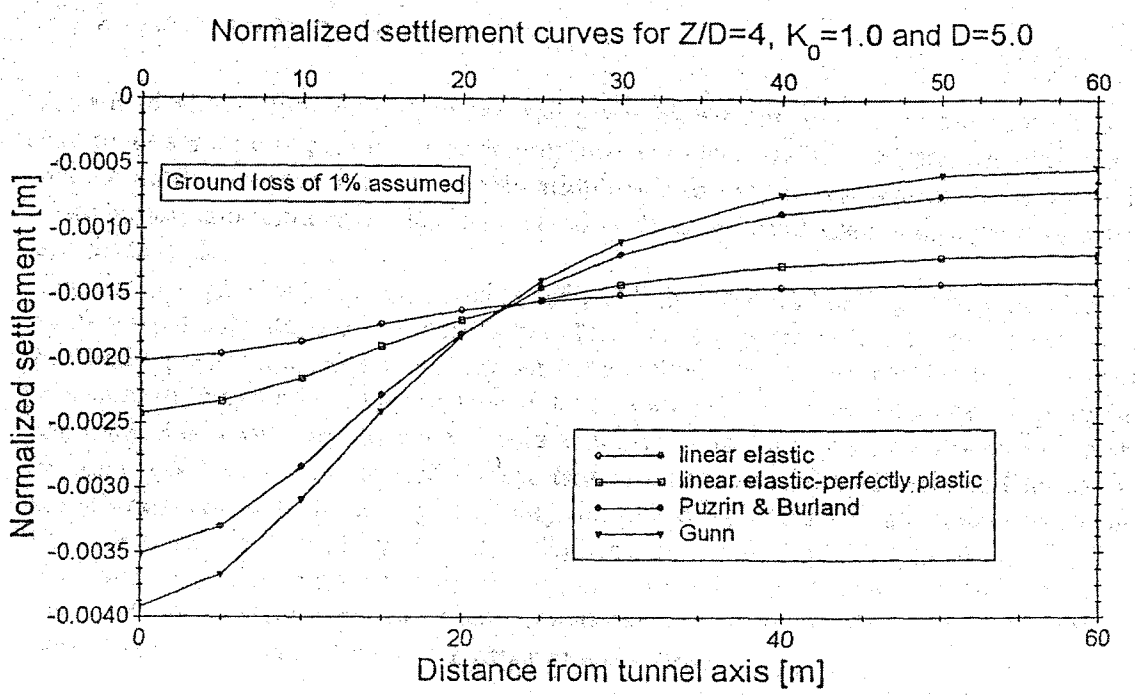

NB: Z = tunnel depth; D = diameter

Figure 2.35 Typical stress paths around an unlined tunnel (Lee & Rowe 1989)

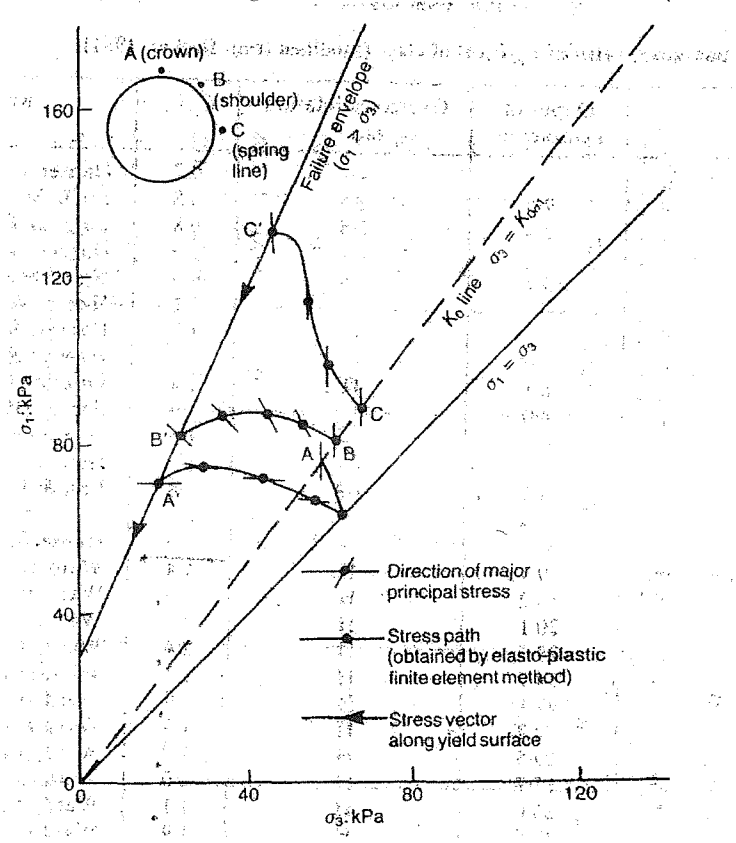

Figure 2.36 Tangent elastic modulus vs axial strain

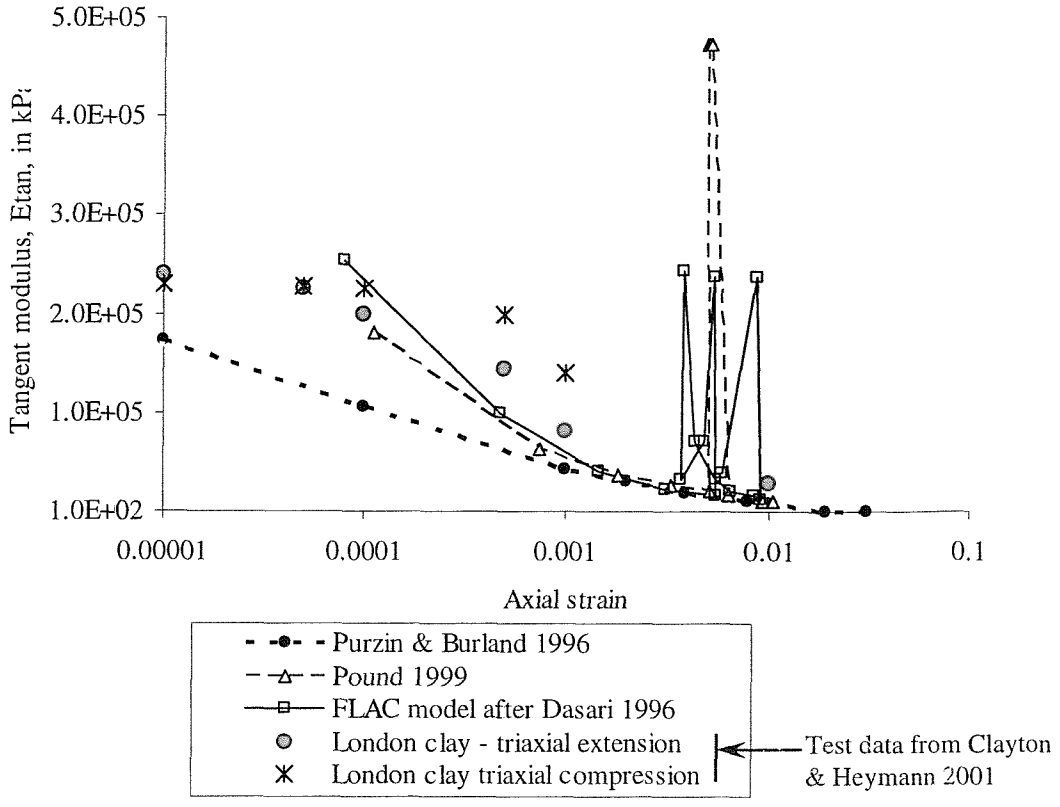

Figure 2.37 The stress paths for various points around a tunnel in over-consolidated clay (Dasari 1996)

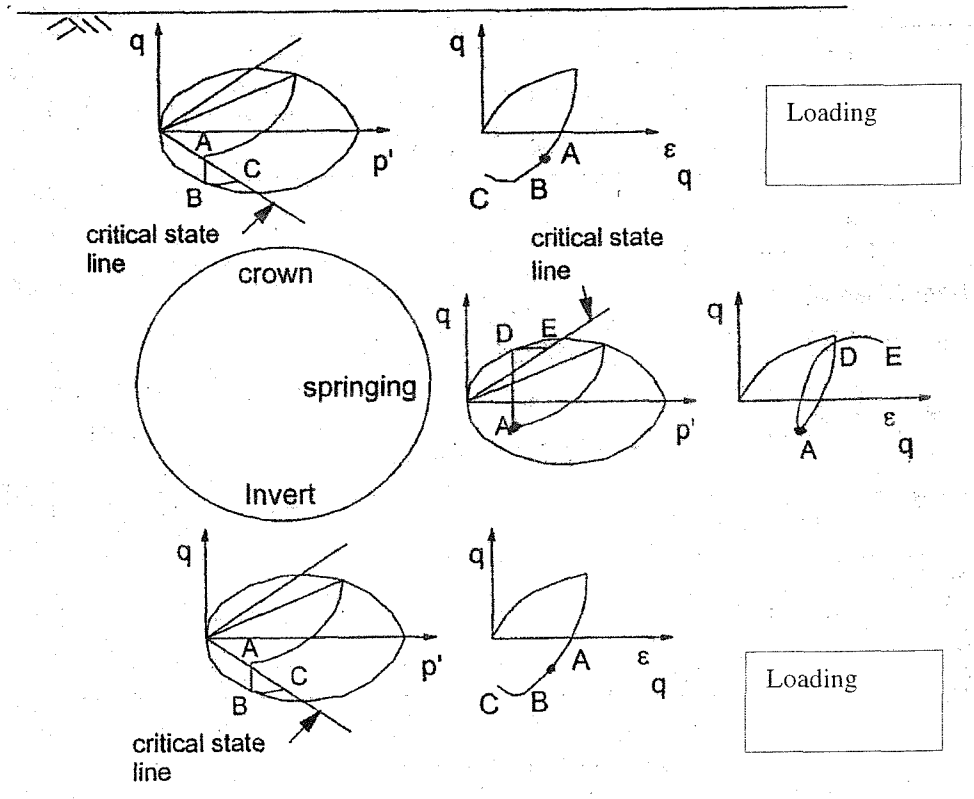

Figure 2.38 Typical approximation of age-dependent stiffness in a numerical model

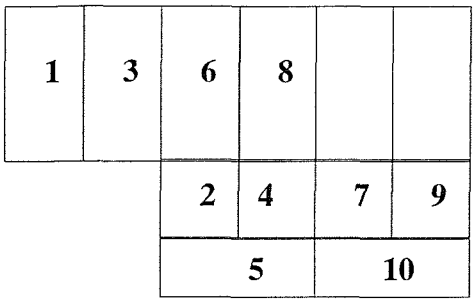

Schematic of the tunnel, showing the stages of the Top Heading, Bench and Invert excavation sequence

Stage	Age at start	E / GPa
1	0	0
2	24	17
3	48	20
4	72	21.6
5	96	22.4
6	120	
7	144	23.4
8	168	
9	192	
10	216	24.1

Notes: 1. All values estimated using Chang 1994 (see Appendix A)
2. Platform tunnels – 9.2m OD, progress rate = 0.8 m / day

Figure 2.39 The failure surface of concrete at low hydrostatic stresses (Chen 1982)

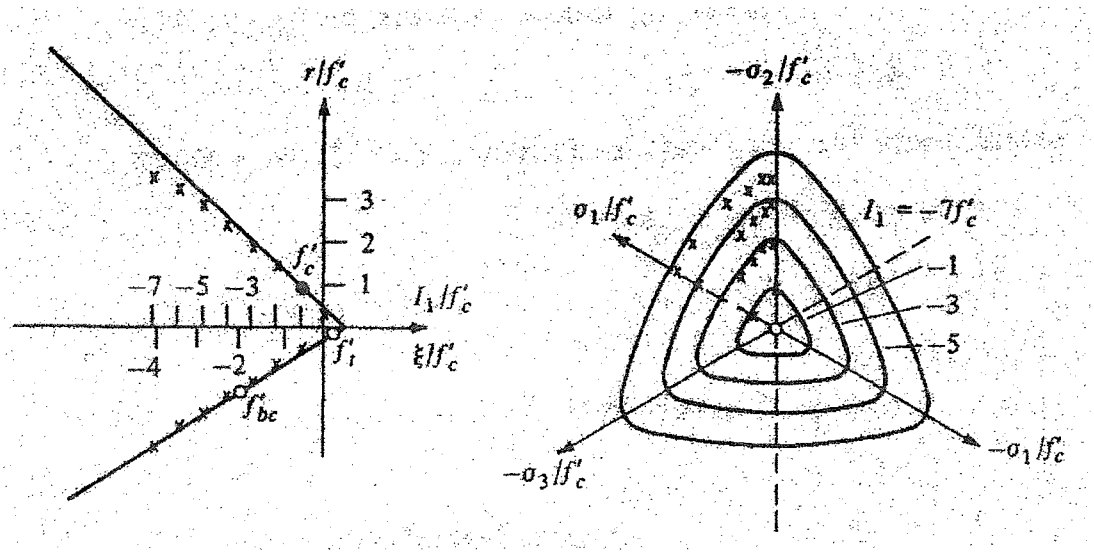

Comparison of William-Warnke criterion with triaxial data (x - from Launay et al. 1972):

(a) hydrostatic section ($\theta = 0°$) $f'_{bc} = 1.8$, $f'_t = 0.15$

(b) deviatoric section

Figure 2.40 Rheological models

(a) Generalized Kelvin model

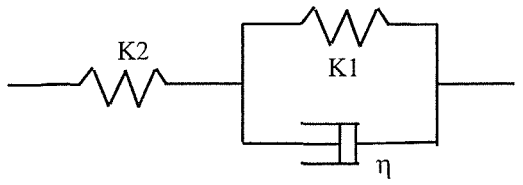

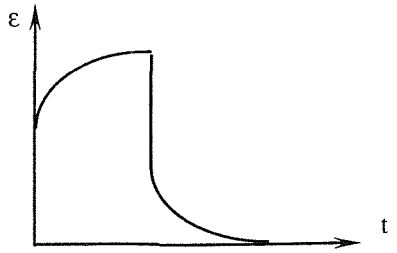

(b) Maxwell model

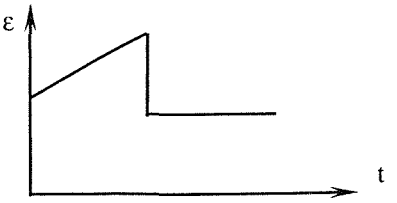

(c) Burgers model

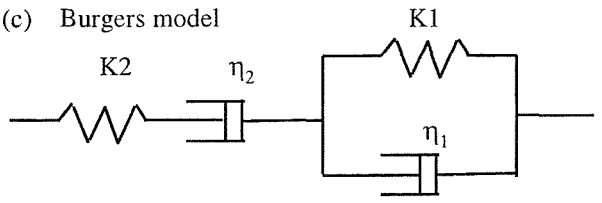

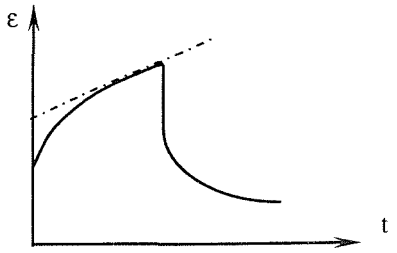

(d) Bingham model

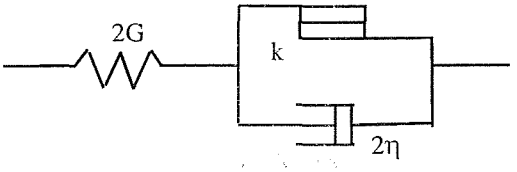

No time-dependent strain until yield strength of fricitional element, k, in Bingham model is exceeded. Thereafter like a Maxwell model

Figure 2.41 Stress reduction due to creep, computed from strain gauge data (Golser et al. 1989)

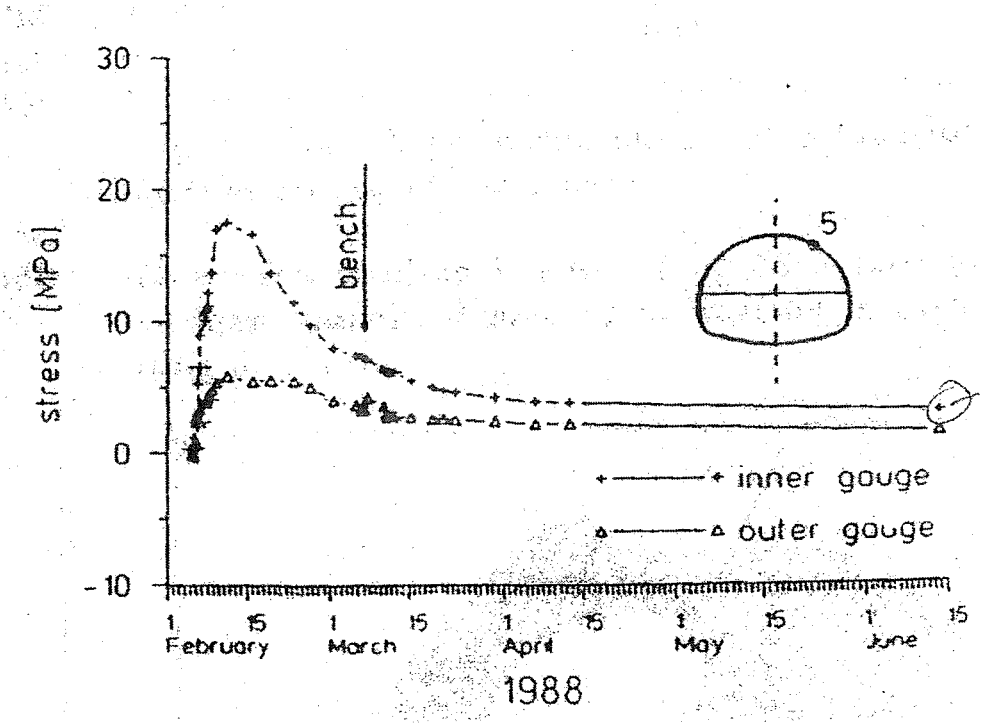

Figure 2.42 Predicted specific creep values

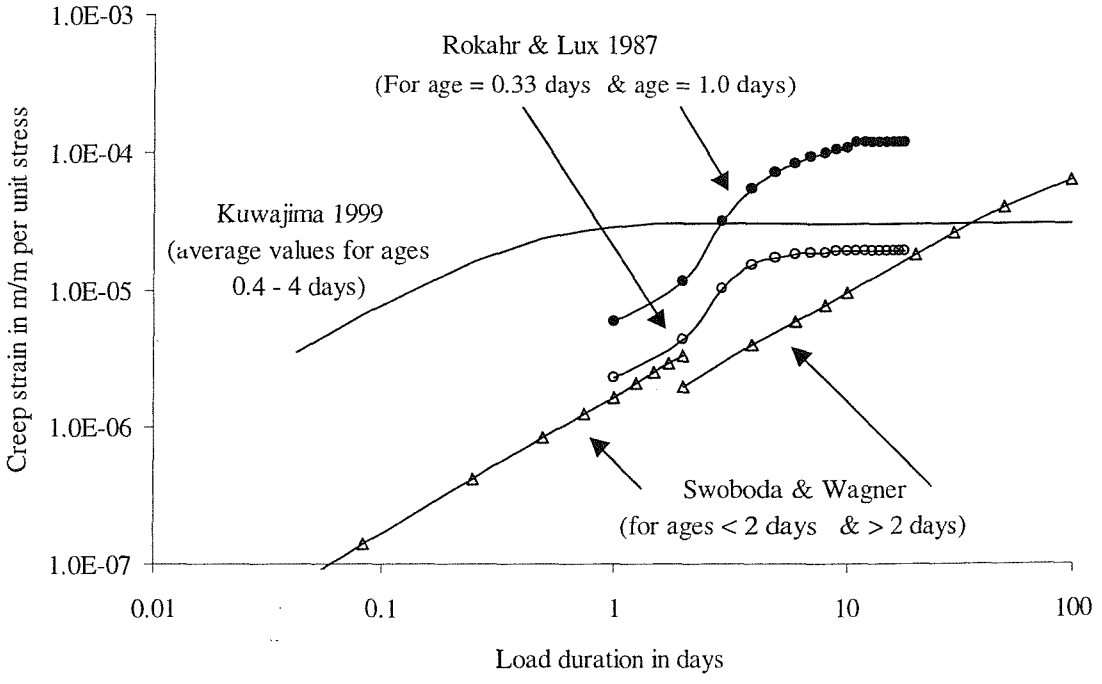

Figure 2.43 Hydration kinetics for shotcrete (Hellmich et al. 1999b)

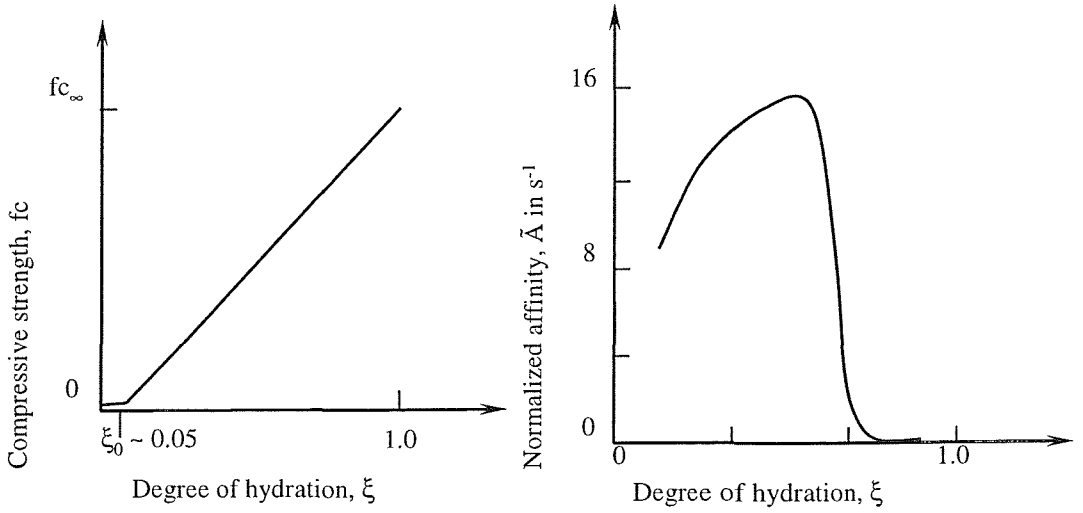

(a) Compressive strength, fc (b) Normalized affinity, Ã

Figure 2.44 Variation of stiffness & shrinkage with the degree of hydration (Hellmich et al. 1999b)

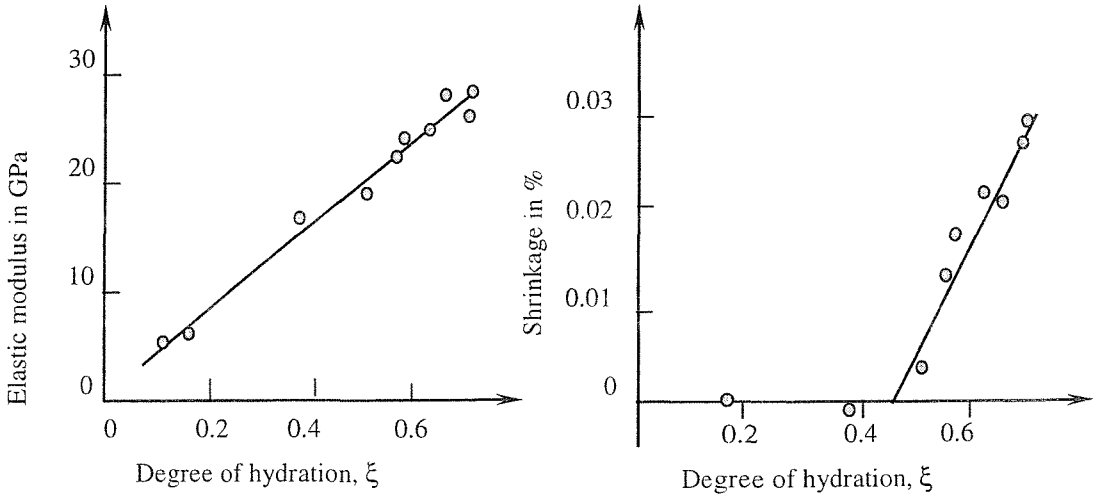

(a) Elastic modulus, E (b) Shrinkage strain

Figure 2.45 Effect of elevated temperature on hydration (based on thermo-chemomechanical model of Hellmich et al. 1999b)

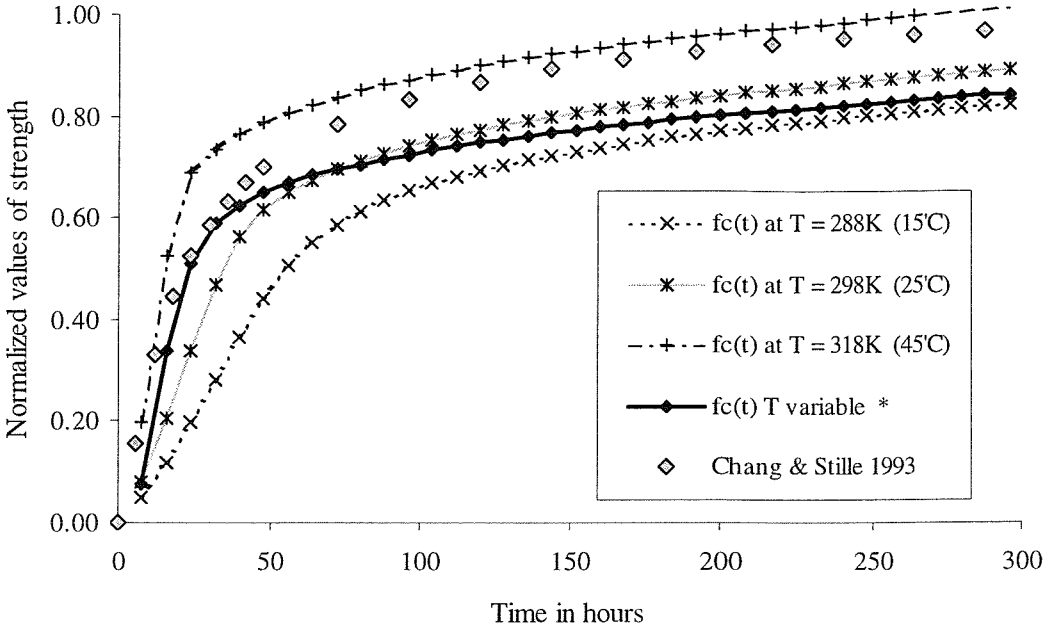

* Temperature profile from Figure 2.22 for a point at 16cm from the extrados of a 30cm thick lining

Figure 2.46 Stress vectors in a tunnel lining (Meschke 1996)

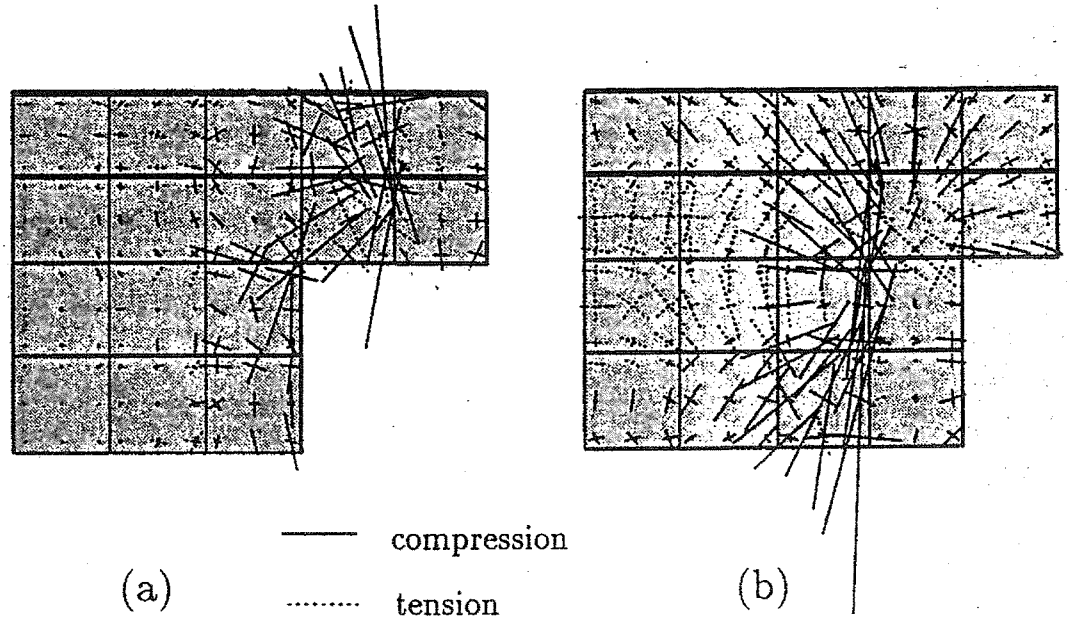

Increments in principal stresses due to excavation of Top Heading

Increments in principal stresses due to excavation of Invert

3 CASE STUDIES

This study proposes to use numerical modelling to investigate the influence of the modelling of the sprayed concrete lining in design analysis. It is important to compare the results of such modelling with experimental evidence or field data in order to assess the accuracy of the modelling and therefore the validity of the conclusions of the investigation. The details of the case studies that will be used for this purpose are contained below.

3.1 Laboratory tests

3.1.1 Uniaxial creep test

A uniaxial creep test on a cylindrical sprayed concrete sample was modelled for the purposes of debugging the FLAC models. The model replicated a test by Huber (1991) – test no. 5 (see Figure 3.1). In the typical manner for creep tests the axial load was applied in increments. The utilization factor (in this case, the axial stress / compressive strength) varied from 30 to 75 %. The shrinkage of an identical sample during the period of the test was recorded along with the development of the elastic modulus and compressive strength with age (Figure 3.2).

Table 3.1: Key properties for Test Series No. 5 (Huber 1991)

Property	Value	Property	Value
Strength at 24 hours	18 MPa	Density	23.77 kN/m^3
Strength at 7 days	26 MPa	Shrinkage after 168 hours	0.027 %
E at 24 hours	24.75 GPa		

The cored samples were 100mm in diameter and 175mm tall. They were stored at 23°C and 50% relative humidity and until loading they were covered in aluminium foil. The loads were applied in the same direction as the concrete was sprayed (although in a tunnel the main load acts at right-angles to this direction). Table 3.1 contains the main properties of the sample. The mix contained 1800 kg of aggregate, 350 kg of cement and had a water/cement ratio of 0.45. The accelerator dosage was 7%.

Because of the low strength of sprayed concrete, tests at early ages are difficult to perform. Small samples are normally obtained by spraying concrete into larger moulds and then cutting prisms or cores from the beams or panels. There is a danger of disturbing the samples and creating fissures when they are extracted at such young ages (ie. 1 to 6 hours). The NCA guide (1993) suggests a reduction factor of 0.8 to allow for such disturbance when considering the strength of cores samples. Similarly the ACI suggests that strengths from cores may be 0.85 times a cast cylinder strength (ACI 506.2 1995). Examining the tests by Huber, the profiles of strength and stiffness seem consistent with other published data. However, the immediate response upon loading in the creep test suggests that the stiffness of the sample in the creep test was lower (see Figure 3.3).

At this point it may also be worth noting that recently in geotechnics there have been a number of developments in the routine stiffness testing. On the one hand improved sampling techniques have reduced the disturbance of samples and on the other the use of "local" instrumentation in triaxial testing has revealed that soil tends to behave much more stiffly at low strains (e.g.: 0.001 to 0.01%) compared to the strains measured in conventional tests (e.g.: 0.1% to 1.0%) (Mair 1998). Bedding effects at the ends of the test specimens and rotation of the specimen can lead to the strains from external measurements exceeding the local strain measurements. The strain in the creep test ranged from 0 to 0.55 %. Experimental error might account for the inconsistency in Huber's data. Given the rapid nature of the short-term creep in sprayed concrete, the rate of loading in the tests might also be a factor. The understanding of young sprayed concrete might be enhanced by a similar improvement in experimental techniques to that seen in geotechnics.

3.1.2 Brite Euram compressive tests

The nonlinear elastic and strain-hardening plasticity models in this study have been compared against uniaxial and triaxial compressive tests, which were performed as part of the Brite Euram project (Brite Euram 1998). The triaxial test was performed at an age of 12 hours on a prismatic sample of steel fibre reinforced concrete (mix IK013 – see Table 3.2) at IMMG, Greece (see Figure 3.4). The uniaxial test was performed at an age of 28 days on a cylindrical

sample of steel fibre reinforced concrete (mix IK013) at Imperial College, London (see Figure 3.5).

Table 3.2: Mix design of IK013

Material / Property		Material / Property	
Water/cement ratio	0.44	f_{cyl} at 1 day	6.3 MPa
Cement (OPC)	450 kg	f_{cyl} at 14 days	16.0 MPa
Accelerator	4 %	f_{cu} at 28 days	35 MPa
Micro-silica	45 kg	Steel fibres (30 mm)	50 kg
Aggregate	1715 kg	Max aggregate size	10 mm

3.1.3 Brite Euram large scale load test

In the final part of the Brite Euram project, 3 large-scale load tests were performed on a 2.5 m internal diameter ring of steel fibre reinforced sprayed concrete (mix IK013). The thickness to diameter ratio was 1:17. The ring was surrounded by a 280mm thick annulus of London Clay and loaded by a circumferential arrangement of jacks (see Figure 3.6). The purpose of the clay was to apply the load evenly to the ring. The loading was intended to replicate a typical ground load at a depth of about 30m, which increased with time and in which the ratio of "vertical" to "horizontal" stresses was 0.85. Typically SCL tunnels in London have thickness to diameter ratios of 1:20 to 1:30 and are situated 15 to 30 m below ground level. The jack loads were applied in 4 increments during the first 260 hours (see Figure 3.7). The ring was then completely unloaded. Further details on the Brite Euram project can be found in Norris & Powell (1999).

The simplifications of the test (such as the construction of the ring in one action) sought to minimise the influence of the other factors present in a real tunnel, leaving the material behaviour of the shotcrete as the major unquantified influence. Despite the fact that this test was conducted under laboratory conditions, there were difficulties in spraying the ring, applying the specified loads and with the clay annulus. The overspray of the ring, of a

nominal thickness of 145 mm, varied from –32.5 to +27.5 mm but generally was about –5.0 mm (i.e. the ring was too thin on average). The recorded jack pressures suggest that the applied load was on average 7 % lower than it should have been.

Figure 3.8 contains the readings from the displacement monitoring system for Test 2. Embedment briquette strain gauges were installed in the rings at the same locations as the displacement transducers (see Figure 3.6). The strain gauge data was only partially consistent with the observed deformation and several gauges malfunctioned (see Figure 3.9). Typically the average strains after load stage 4 are about 500 microstrain which is less than half what one would expect from the measured displacements.

Considering the tests in general, there are doubts about the results. After the early age tests, the rings were loaded to failure. This was only possible with 2 of the rings due to problems with the clay annulus. The failure loads for the 2 (nominally identical) rings differed by 50 %. Generally, one should note that there was a large variation in the properties of nominally identical samples in the course of the Brite Euram project. Typically, the standard deviation of f_{cu} was 5 MPa for a 35 MPa mix (ie. 14 %). One might expect an even larger variation in the properties of sprayed concrete in real tunnels (although Table 3.3 suggests the variation is similar).

For the reasons above, close agreement is not expected between the FLAC model and the test results. Nevertheless, the test data provides a useful check on the general behaviour of the numerical model.

3.2 Field data

3.2.1 Heathrow Express project

The main case study is the construction of the Platform tunnels at the Heathrow Express (HEX) Terminal 4 station, Heathrow Airport, London. The collapse of the SCL tunnels at HEX CTA station in Heathrow prompted a comprehensive re-evaluation of the safety and suitability of constructing shallow SCL tunnels in soft ground in an urban environment and

indeed this research is part of that process. A wide-range of equipment was installed at Heathrow to monitor the behaviour of the ground and tunnels when the tunnelling restarted. This has provided a wealth of information. Comprehensive details of the project, including the design of the SCL tunnels, and the instrumentation that was installed, together with the results from it, can be found in Powell *et al.* (1997) and van der Berg (1999) respectively. In addition to the field data for these tunnels, there is a large amount of information on the behaviour of similar SCL tunnels in London Clay from the rest of the HEX project itself (e.g.: Clayton *et al.* 2000), the HEX trial tunnel (e.g.: Deane & Bassett 1995) and the Jubilee Line Extension Project (e.g.: Bonapace 1997).

Figures 3.10 and 3.11 show the layout of the site. The Platform tunnels were constructed concurrently, before the central Concourse tunnel was built. The Platform tunnels had a face area of 61 m^2, with lattice girders around the whole circumference to help ensure that the correct shape was sprayed. The Concourse tunnel was slightly smaller with a face area of 49 m^2. The shape of the tunnels was basically circular but they were broader than they were tall. The Platform tunnels were 8.3 m high and 9.3 m wide. The advance length was about 1.0 m. The actual average advance rate was 1.2 m per day [49], with a maximum rate of 2.0 m per day (Aldrian & Kattinger 1997). The construction sequence was Top Heading – Bench - Top Heading – Bench - Invert (see Figure 3.12). This "stepped" excavation sequence, which is typical in SCL tunnel construction, meant that the ring was completed within 3 to 6m from the face. On average this took 4.5 days (Thomas *et al.* 1998).

The lining was 300 to 350 mm of sprayed concrete, grade C25, reinforced with 2 layers of steel mesh (8mm bars at 150mm c/c). The construction tolerance for these tunnels was 50 mm with a further allowance of 20 mm for deformation of the linings. The actual average strength of the sprayed concrete at 28 days was 35.0 MPa, with a standard deviation of 5.6 MPa, which equates to a f_{cu} of 25.8 MPa (see Table 3.3). Since routine testing of sprayed concrete is limited to strength development, the choice of all other parameters for the behaviour of sprayed concrete was based mainly on a review of published data.

Table 3.3: HEX primary lining strengths

Age in days	Uniaxial compressive strength in MPa	Standard deviation in MPa
3	23.2	5.3
7	27.1	5.9
28	35.0	5.6
250	46.5	-

As one would expect given their proximity (with a clear separation of 2 tunnel diameters), there was some interaction between the two Platform tunnels. However, to a large degree they behaved independently [50]. The Concourse tunnel represents a much more complex case but the tunnel was more comprehensively instrumented. Hence more emphasis has been placed on the results of monitoring of the Platform tunnels, augmented where possible by information from the Concourse tunnel. One should bear in mind that the results from all monitoring are subject to the influences of the varying soil profile and the soil properties, differences in construction sequences and advance rates, adjacent structures and site-specific construction activities (e.g.: compensation grouting and face dowels). Each instrument has its own precision (and this may be poor in the tough environment of a construction site). The position of instruments may differ from the intended locations. Even with access to all the construction records, it can be very difficult to sift through the competing influences and determine the underlying trends (van der Berg 1999).

3.2.2 Behaviour of the sprayed concrete linings

This section will present data from pressure cells, strain gauges and deformation monitoring of the lining (see Figure 3.10).

[49] The average advance rate for the Concourse tunnel was 2.0m / day.

[50] The average surface settlement on the centreline was 13.7 mm for the Downline Platform tunnel and 14.2 mm for the Upline Platform tunnel.

Stresses in linings – 2 types of cells are routinely installed in SCL tunnels – radial cells which measure the total earth pressure acting on the extrados of the lining and tangential cells which are embedded in the lining itself and measure the stress in the hoop direction. Both cells are discussed here since some comments apply to both and the readings from one can be used to identify anomalous readings from the other.

If the readings from tangential pressure cells in the sprayed concrete lining are to be believed, the final stress in many SCL tunnels in soft ground is quite low - in the range 1 to 5 MPa, which corresponds to about 10 to 30 % of the lining's capacity (Bonapace 1997, Norris & Powell 1999) - and therefore probably lies within the elastic region – see Figure 3.14. However, many authors have questioned the reliability of pressure cells in sprayed concrete (e.g.: Golser et al 1989, Golser & Kienberger 1997, Mair 1998, Kuwajima 1999, Clayton *et al.* 2000), for the following reasons:

- The physical size of the cells (100 mm wide) may lead to shadowing. Incomplete encasement would lead to under-reading of stress.
- During the rapid hydration, the cell may expand and on cooling leave a gap between itself and the concrete, again leading to under-reading (Golser *et al.* 1989).
- The increase in readings due to thermal effects has been calculated as 0.10 MPa/°C for mercury cells and 0.15 MPa/°C for oil-filled cells [51].
- Shrinkage can also induce stresses into the pressure cells (Clayton *et al.* 2000).
- The stiffness of the cell is different from the surrounding lining. If there is no difference the Cell Action Factor is 1.0. The cells at HEX had factors which were close to but lower than 1 (Clayton *et al.* 2000), leading to under-reading.

The results also depend on the measuring system. Pressure cells with a hydraulic measuring system yielded readings that were about 80 kPa higher than vibrating wire cells (Bonapace

[51] The temperature corrections quoted by the manufacturers of pressure cells normally refer to the transducer only and not the whole cell. The peak in recorded pressures often coincides with the peak in the temperature of the concrete (Clayton *et al.* 2000).

1997). Both types of cell were used at Heathrow. Clayton *et al.* (2000) and Aldrian & Kattinger (1997) suggest that tangential cells record changes in stress accurately but should not be assumed to be recording the correct absolute values. Figure 3.15 shows the average tangential cell data for the Platform tunnels (see also Table 3.4). Standard deviation in readings is often almost as large as the average readings themselves. On the Jubilee Line Project (JLE) the tangential stress was on average 2.0 MPa after 3 months (corresponding to about 25% of the full overburden pressure (FOB)) but ranged from 0.0 to 7.0 (Bonapace 1997).

Radial pressure cells are believed to be more reliable because they are easier to install and the cell stiffness and the behaviour of the sprayed concrete have less influence on the readings (Clayton *et al.* 2000). However, like tangential cells, even when the results from a large number of cells are examined, there is usually considerable scatter in the results from radial cells (Bonapace 1997).

In the short-term (i.e. up to 6 months) on average the radial stress for the HEX Platform tunnels was 35% full overburden pressure (FOB). The average of the maximum values was less than 70 % FOB [52]. The average radial stress acting on the Concourse tunnel was 37 %. The pressure builds up rapidly and reaches close to the short-term value within about 10m of the closure of the invert. As Table 3.4 shows the distribution was roughly uniform except in the invert where the pressure was lower. Results from the JLE project are similar (see Table 3.4).

More generally the HEX results are consistent with other field data (e.g.: Mair 1998). The average for JLE readings was about 50% FOB after 3 months, rising to about 70 % after 1 year (though this may include stress increases due to adjacent construction and / or compensation grouting) (Bonapace 1997). At the HEX Trial Tunnel, Bowers *et al.* (1996) recorded little increase in ground stresses over 3 years. Barratt *et al.* (1994) reported 20% FOB acting on a segmentally lined tunnel after 2 years with a long-term radial pressure of

40% (in the crown) to 60% FOB (at the axis) acting on a segmentally lined tunnel after 20 years. The fact that the tangential stresses are higher at the axis runs contrary to what one would expect given K_0 values greater than 1.0 but it is consistent with the known deformation of shallow tunnels in clay.

Table 3.4: Average pressure cell readings for HEX T4 platform tunnels [53]

Location (see Figure 3.17)	HEX σ radial in kPa	σ tangential estimated from HEX σ radial in MPa [54]	HEX σ tangential in MPa	JLE [55] σ radial in kPa	JLE σ tangential in MPa
Crown 1	207	3.1	1.53	150	0.5 to 4.2 [56]
2	-	-	-	-	-
4	192	2.9	1.83	260	2.6
Axis 6	-	-	-	-	-
8	195	2.9	2.41	360	2.6
10	-	-	-	-	-
Invert 12	121	1.8	1.31	100	0.6

Table 3.4 includes estimates of the tangential stresses in the lining from the recorded radial stresses at HEX. These are considerably higher than the recorded tangential stresses. As at HEX, on the JLE project (Harrison 1995, Bonapace 1997) the estimates of loading from radial pressure cells were generally larger than the loads measured by tangential pressure cells

[52] NB: Significant numbers of radial cells at HEX recorded less than 25% FOB.

[53] NB: These values differ from those quoted by van der Berg (1999) and Clayton *et al.* (2000) who have published results from monitoring section MMSVIII for the Concourse tunnel only.

[54] Estimated using the formula for stress in a thin-walled tube, p. $R = \sigma.t$, where $R/t \sim 15$, R = cylinder radius, t = wall thickness, σ = hoop stress & p = external pressure on cylinder.

[55] From personal correspondence with Deane (1997).

[56] The higher value may be due to compensation grouting above the tunnels.

at the same locations, which lends some support to the theory that the tangential cells are under-reading.

Strain gauges - Golser *et al.* (1989) extol the virtues of strain gauges, particularly in comparison to stress cells. However, the back-calculated forces presented by Golser *et al.* (1989) for tunnel linings in soft ground suggest considerable scatter in the strain gauge measurements. The complex material behaviour of the sprayed concrete and the high hydration temperatures make the interpretation of strain gauge readings very difficult. The HEX strain gauges recorded relatively low values – between 0.02 to 0.10 % after 28 days (see Figure 3.16). Shrinkage strains after the same period could be about 0.05 %. Apart from noting that the strains were highest in the Top Heading and lowest in the invert, it is not believed that any further useful information can be obtained from the HEX strain gauge data.

Slot-cutting tests were performed in the lower part of the lining of the Concourse tunnel. The results proved difficult to interpret but they seem to suggest that the first 50 mm at the intrados in this area (ie. from axis to invert) is unstressed or in tension (Hughes 1996). Other investigations using slot-cutting have also found tensile stresses on the intrados of SCL tunnels (Negro *et al.* 1998).

In-tunnel deformation of the linings at HEX was monitoring using 3D surveying of optical targets (see Figure 3.11 for location of the convergence pins). Normally this is used to check that the deformations of the lining remain within predicted limits (see Table 3.6) and stabilise as expected. Some attempts have been made to make more use of this 3D monitoring (e.g.: Rokahr & Zachow (1997) & Steindorfer (1997)). However, there are practical difficulties in interpreting this data. Firstly, the accuracy of the in-tunnel monitoring was about ± 2 to 3 mm (van der Berg 1999). The accuracy of the measurement of vertical movement was found to be better than for horizontal and longitudinal movement (van der Berg 1999). Furthermore, there is a delay before the first measurement is taken and hence the total deformation of the lining is never recorded (Steindorfer 1997). The average delay at HEX was estimated at about 5 hours with the result that an estimated 50 to 60 % of the total

deformation was measured. In general the survival rate of monitoring points is poor as they are at risk of being disturbed by construction equipment. Meaningful results were obtained from about 60% of the points in the Top Heading and Bench and only 12% in the Invert (van der Berg (1999)).

Table 3.5: Trigger & Limit values for in-tunnel deformation (Powell *et al.* 1997) [57]

Warning level	Horizontal movement	Vertical movement
Trigger	9 mm	15 mm
Limit	14 mm	19 mm

The actual movements of the monitoring points in the HEX T4 Platform tunnels are shown in Table 3.6 and Figure 3.17 The movements of the lining are predominately vertical and most movement occurs in the Top Heading. Very little deformation was observed in the invert. Between 60 and 80 % of displacement occurred before the invert was closed and the movements had stabilised by the time the Top Heading face was 10 to 20m away. Van der Berg (1999) reported that, in addition to the vertical movement, the Top Heading appears to ovalise with the crown going upwards (relatively) rather than squatting. The pattern of deformation is likely to depend on the construction sequence and the reports from the JLE project of SCL tunnels squatting (Harrison 1995, Groves & Morgan 1997) may be related to the use of the pilot tunnel and enlargement sequence.

The vertical deformations of the Concourse tunnel were slightly less but the horizontal deformations ranged between 6 and 12 mm. The reasons stated for the good performance of the tunnels (in comparison to the design predictions) included the 40 – 50 mm sealing layer of sprayed concrete which was in addition to the lining thickness, rapid strength development of the sprayed concrete, good workmanship and a conservative design.

Table 3.6: Average total short-term lining deformations in mm [58]

Monitoring position	Vertical movement (+ = upwards)	Horizontal movement (+ = inwards)	Longitudinal movement (+ = forwards)
Crown	-8.4	0.0	+2.8
Shoulder	-9.0	+4.7	-0.5
Knee	-2.0	+1.3	-0.3
Invert	+1.0	0.0	+2.5

3.2.3 Behaviour of the ground

This section contains the results from spade pressure cells, piezometers, surface and sub-surface movement monitoring.

Figure 3.11 contains the typical geotechnical profile for the T4 site. Van der Berg (1999) contains a complete description of the ground conditions at the HEX T4 site. The tunnels were constructed in London Clay, which can be reasonably assumed to behave as a continuum. London Clay is fissured and at shallow depths these fissures tend to be closely spaced. The fissures are either sub-vertically inclined (Groves & Morgan 1997) or randomly orientated (van der Berg 1999). The fissures become more persistent with depth. However, overbreak around the perimeter of the excavations was rare and normally block failure only occurred in the face (Groves & Morgan 1997). Occasional thin lenses of sand and isolated claystones were also found. Based on an assessment of the consistency of the in-tunnel deformation results and observations at the face, it was concluded that the London Clay at Heathrow was homogeneous and variations in behaviour were more likely to be due to adjacent structures.

[57] The Trigger values represented the expected behaviour of the lining while the Limit values represented the behaviour with worst foreseen ground parameters.

[58] From van der Berg (1999), Platform tunnels only; standard deviation of results typically 4 mm.

Radial (earth) **pressure cells** were installed on the extrados of the HEX tunnels (see 3.2.2). Spade pressure cells were installed at the bottom of boreholes near the HEX Trial Tunnel. The initial recorded (total) pressures seem to be higher than one would expect given the initial stress state in the ground. However, the pattern of stress changes is clear and consistent with other information. There is a small rise in stress as the tunnel approaches. The stress then drops sharply and stabilises at a lower level.

Piezometers around the Trial Tunnel and T4 at Heathrow (New & Bowers 1994, Bowers *et al.* 1996, Aldrian & Kattinger 1997) showed that in the crown there was an increase in porewater pressure near the tunnel when the face approached (at about 5 – 6 m from the face, reaching its peak between 2 and 4 m ahead) and then there was a sharp drop as the tunnel passed (see Figure 3.18). The pore pressure may become negative but piezometers cannot normally record negative pore pressure reliably (Clayton *et al.* 2000). Similar significant changes in pressures were observed within half a diameter of the Trial Tunnel. After spraying the Bench, the rate of pore pressure decrease slowed. After ring closure the pore pressure started to increase again. Near the tunnel, approximately 10 to 15m behind ring closure the pore pressures appeared to stabilise at a lower level than the hydrostatic values for more than 18 months, although some cells showed a gradual increase with time (TRL 1992). Aldrian & Kattinger (1997) suggest that this persistently low pore pressure was due to water ingress into the tunnel. Groves & Morgan (1997) reported some small amounts of water ingress, starting within a month after completion of the ring. Further away the pore pressures returned to the original levels after a few months. Measurements near an old tunnel by Gourvenec *et al.* (1999) suggest that in the long-term the pore pressure will return to hydrostatic levels, except close to the tunnel if water is draining into it.

Surface settlement was first recorded when the Top Heading (TH) face was about 2 - 3 diameters from the point in question and the initial settlement stabilised within a similar distance behind the face. On average 50 % of the movement occurred before the face passed beneath the monitoring point, with a further 25 % occurring before the invert was closed (see Figure 3.19). The maximum increment in settlement for a single advance occurred 2 to 3m

behind the face. This is typical behaviour for SCL tunnels in London Clay (Thomas *et al.* 1998, Groves & Morgan 1997). The transverse width of the trough was on average 33 m and the average maximum settlement was 14.0 mm above the centre-line of the Platform tunnels. Sometimes some heave (about 1 mm) was observed ahead of the face (van der Berg 1999). Experience at the HEX and the HEX Trial Tunnel showed that the magnitude of ground movements depends heavily on the time taken to close the invert (New & Bowers 1994, Thomas *et al.* 1998). This appears to be more important than how the tunnel face is subdivided since Trial Tunnel Type 1 and 2 excavation geometries resulted in similar settlement troughs (New & Bowers 1994) – see Table 3.7.

Table 3.7: Volume losses at HEX (Thomas *et al.* 1998)

Tunnel	Volume loss in %	Tunnel	Volume loss in %
Crossover	0.90	T4 Platform tunnels	0.80 - 0.90
Trial tunnel (Type 1 & 2)	1.13 & 1.06	CTA Concourse tunnel [59]	1.20

The construction of the Concourse tunnel appeared to result in more localised movement with a deeper and narrower trough than for the Platform tunnels, but the overall volume loss was apparently lower – about 0.5 %. This may include the effects of some compensation grouting and the true value may be closer to 0.70 %.

In the long-term the settlements increase and the settlement trough tends to become wider. The average increase in maximum settlement above the Trial Tunnel was 42% after 3 years while the overall volume loss increased by 68% (Bowers *et al.* 1996).

Horizontal movements in the transverse direction to the HEX Trial Tunnel show increasing horizontal strain with distance from the centreline until a peak value is reached, followed by a decrease (TRL 1992). In the longitudinal direction, the picture is less clear, which may be due

[59] From Cooper & Chapman 1998.

to the small magnitude of movements (typically less than 2 mm). In general the horizontal deformation appears to be towards the tunnel face initially but after the tunnel has passed the magnitude of longitudinal movement decreases, ie. the relative movement at all times is towards the unsupported face.

Subsurface movements appear to be quite localised. Figure 3.21 contains a summary of the recorded movements at the HEX Platform tunnels. The movements around the Concourse tunnel were found to be very localised in nature though this may well be due to the presence of the adjacent platform tunnels, which were only 5 m away at axis level. It is therefore believed that the results from the Concourse tunnel are under-estimates of the ground movement in comparison to construction such a tunnel on its own (van der Berg 1999).

Table 3.8: Vertical ground movements in mm

Monitoring position	Vertical movement (+ = upwards)
Surface	-14.0 [60]
- 8.0 m	-21.5
-12.5 m	-25.0
-21.5 m	+2.0

Table 3.8 shows the results from the vertical rod extensometers that were installed at HEX from the surface. Similar behaviour was observed at the HEX Trial Tunnel. The precision of the extensometers was about ± 1.0 mm (van der Berg 1999). The extensometer readings support the piezometer data in suggesting that there is an initial compression of ground at between 0.5 to 1.0 diameters ahead of face. Data from the Trial Tunnel showed that vertical movements may be concentrated directly above the tunnel and close to it. Vertical displacements of the ground at the tunnel crown were more than 1.5 times the settlements at the surface (see Table 3.8 & Figure 3.21).

[60] The range was 10 to 19 mm but the some of lower values were due to the use of face dowels (Powell *et al.* 1997).

On the JLE project radial extensometers were installed from inside the tunnels. While some showed localised compression of the ground immediately adjacent to the tunnel axis, the general pattern was unclear (Harrison 1995). Like all instrumentation installed from within a tunnel, the radial extensometers can only record a fraction of the total ground movement.

At Heathrow Terminal 4 station, inclinometers and chain deflectometers were installed in the ground in advance of construction to get a fuller picture of the ground movements (Clayton *et al.* 2000). The chain deflectometers were installed horizontally between the Platform tunnels, ahead of the advancing Concourse tunnel (van der Berg 1999). Movement was first recorded when the Top Heading face was 6 to 12m away for Top Heading and Bench deflectometers and 4.5 m for the Invert deflectometer.

The maximum longitudinal displacement recorded by the inclinometers was 17.5 mm in the centre of the Top Heading (van der Berg 1999), with a precision of about ± 1.0mm. In general the inclinometers recorded slightly higher displacements than the chain deflectometers. By extrapolating the results, the maximum longitudinal displacement into the face of the tunnel has been estimated at between 25 and 30 mm (see Figure 3.22). Inclinometers adjacent to the 5.35 m diameter JLE Trial tunnel recorded a transverse horizontal movement of 17 mm at 1 m from the axis and about 15 mm at 2 m from the axis (Groves & Morgan 1997) while larger movements were recorded at the HEX Trial Tunnel – a maximum transverse movement of 21 mm at 3.5 m from the tunnel axis.

3.2.4 Summary

The movements and stress redistribution at tunnel axis level are quite localised – starting within about 0.5 to 1.0 diameters from the face, extending about 1.0 to 1.5 diameters either side of the tunnel - and the new (short-term) equilibrium condition is established about 2.0 diameters back from the closure of the invert (see Figures 3.15, 3.16 & 3.19). At the surface, movement is first detected earlier – at about 2.0 to 3.0 diameters ahead of the face but it stabilises at a similar distance behind it.

Figure 3.1 Uniaxial creep test – series no. 5 (Huber 1991)

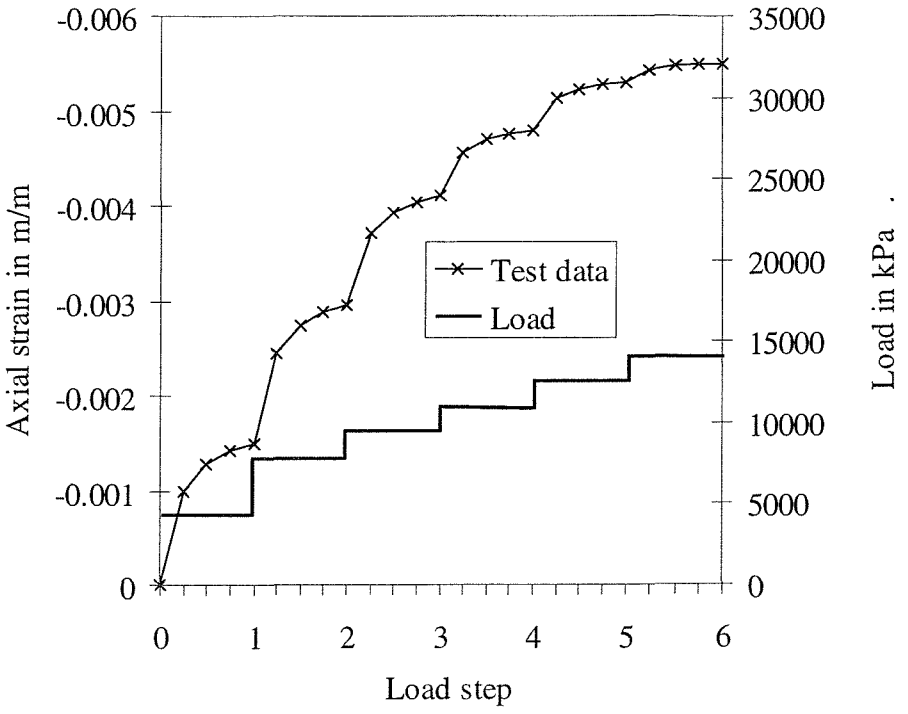

Figure 3.2 Development with age of key properties – series no. 5 (Huber 1991)

(a) Shrinkage (b) Compressive strength & Young's modulus

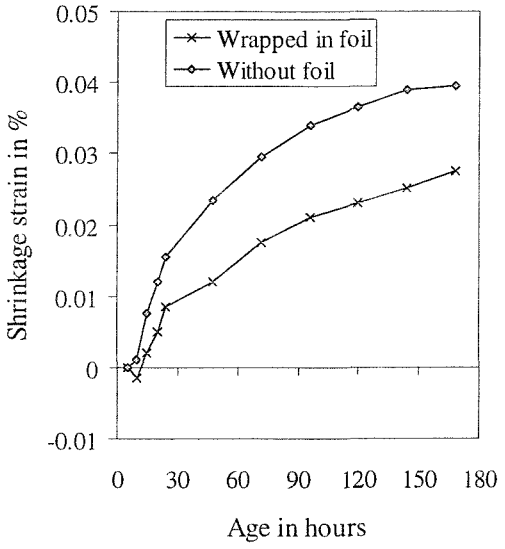

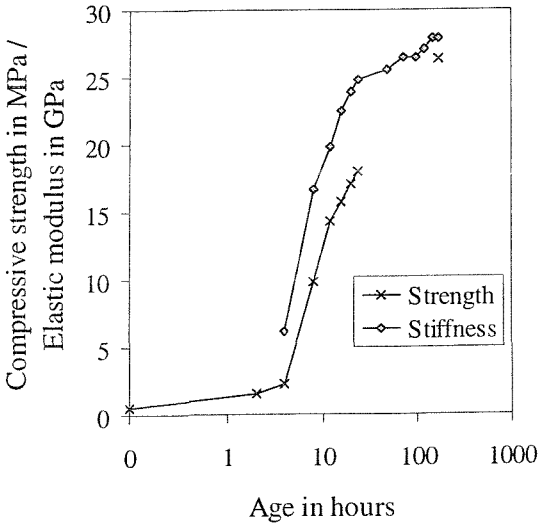

Figure 3.3 Comparison of elastic increments in creep test by Huber

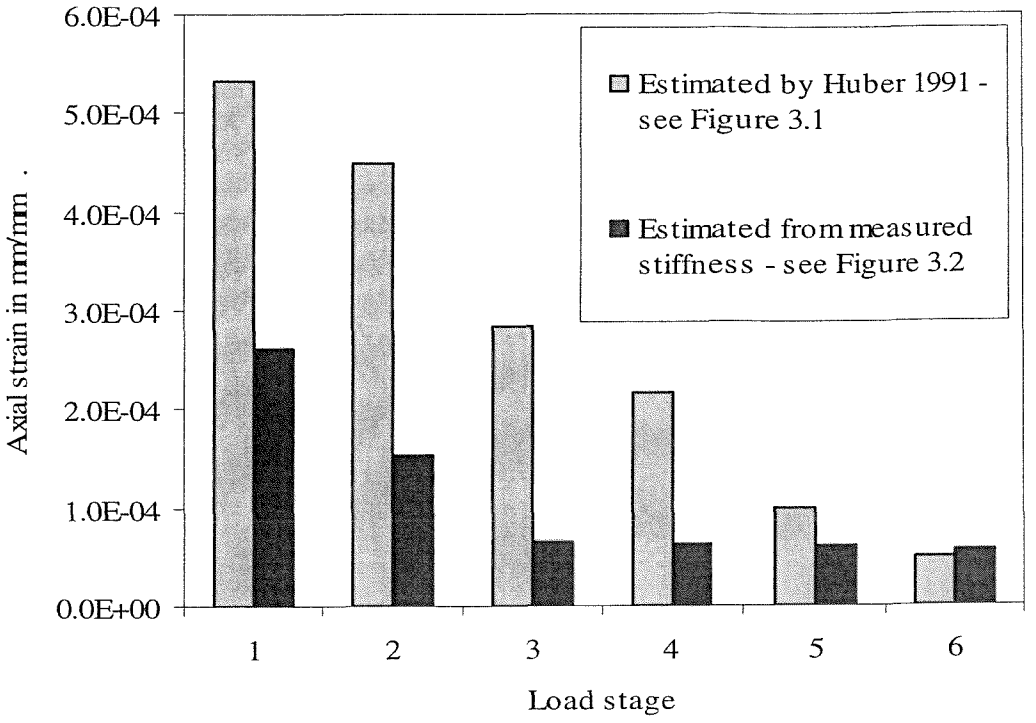

Figure 3.4 Uniaxial compression test on sprayed concrete (Brite Euram 1997)

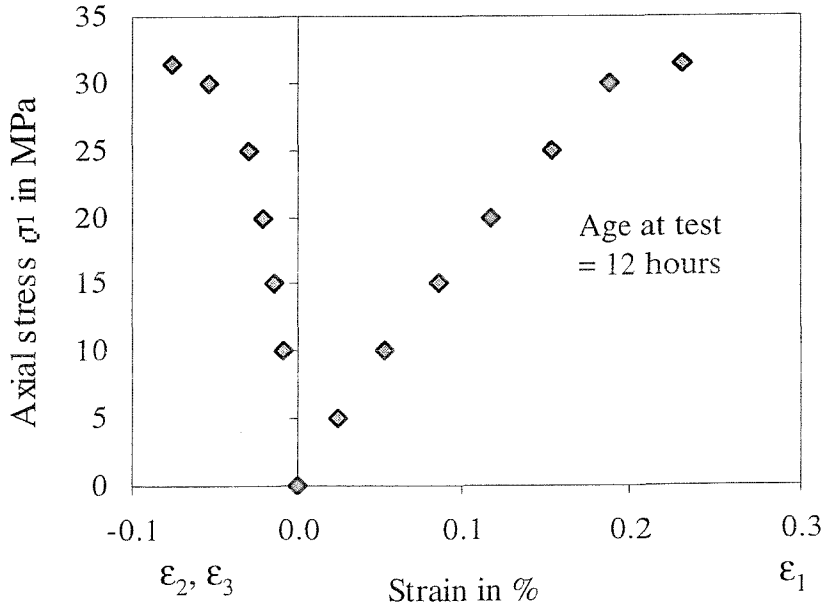

Figure 3.5 Triaxial compressive test on sprayed concrete($\sigma_2 = \sigma_3 = 1.0$ MPa) (Brite Euram 1997)

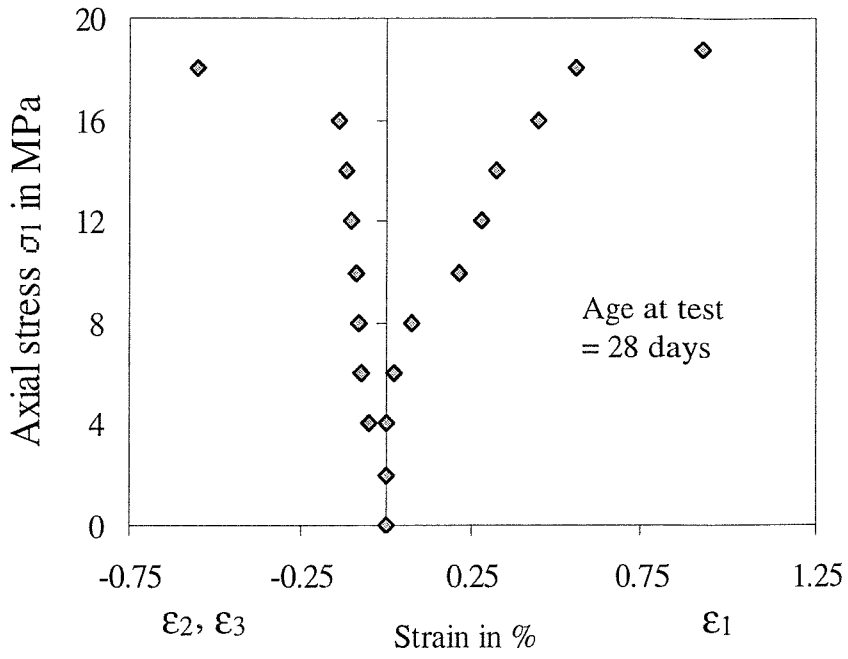

Figure 3.6 Schematic showing the cross-section of the large-scale load test with the monitoring points (Brite Euram 1998)

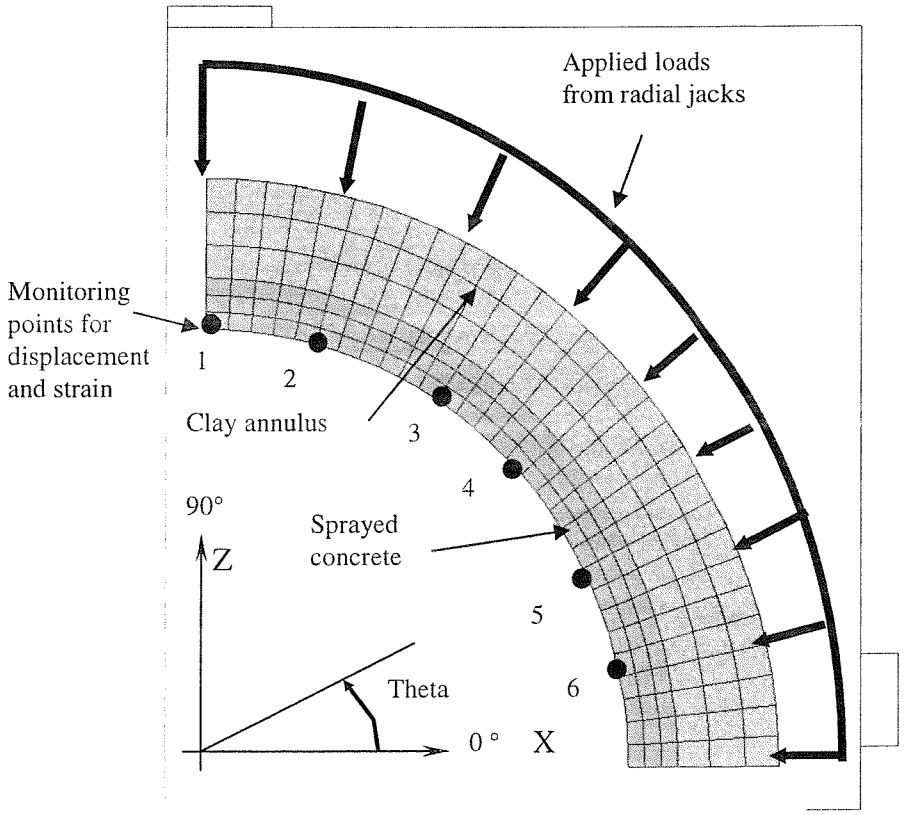

Figure 3.7 Variation of strength & modulus for SFRS mix IK013 and the applied load (normalized w.r.t. full overburden pressure) with age (Brite Euram 1998)

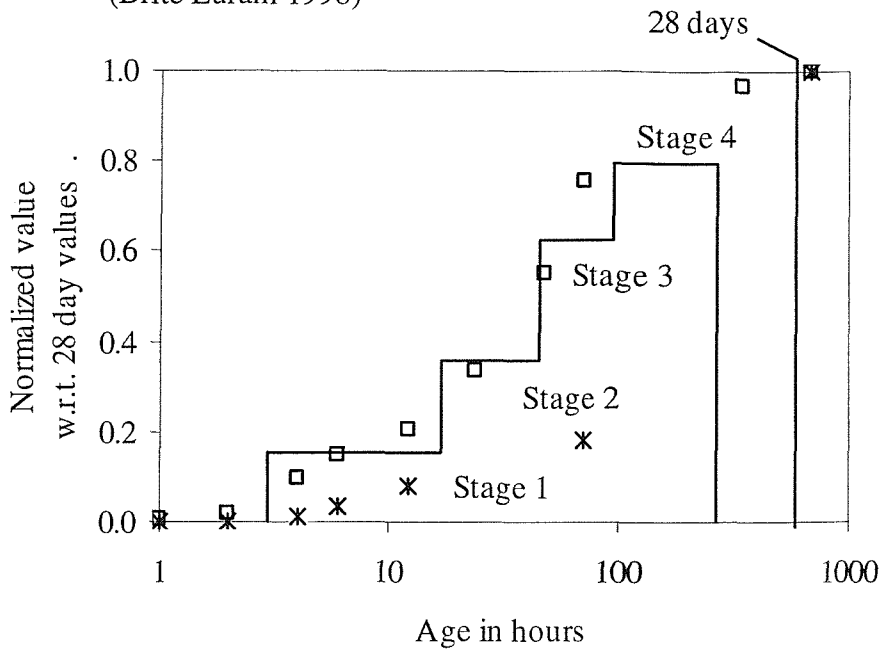

Figure 3.8 Radial displacements of monitoring pins, measured during the load test (see Figure 3.6 for location of pins) - Brite Euram 1998

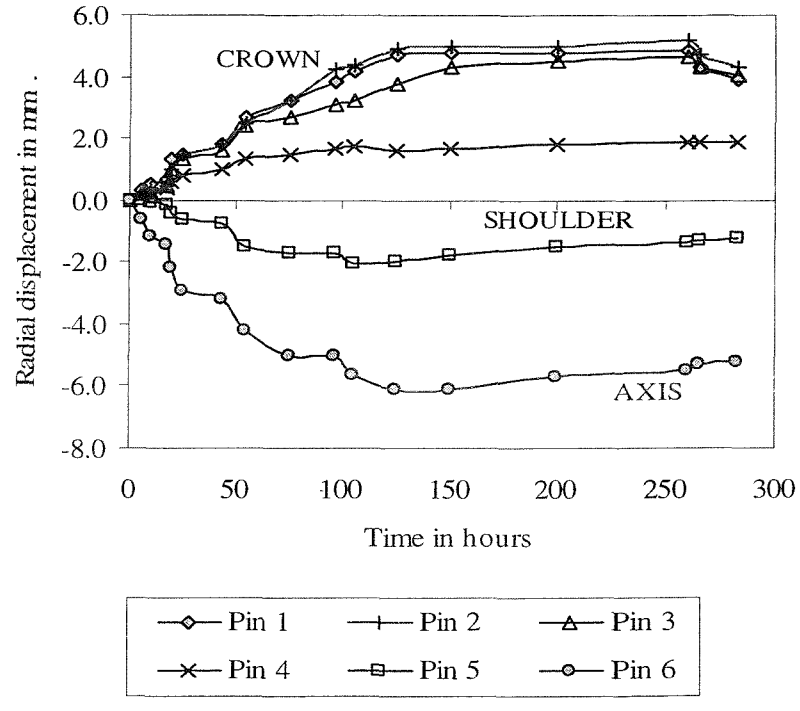

Inwards movement is positive

Figure 3.9 Strain gauge readings from the large-scale load test (Brite Euram 1998)

(a) Points 1 – 3

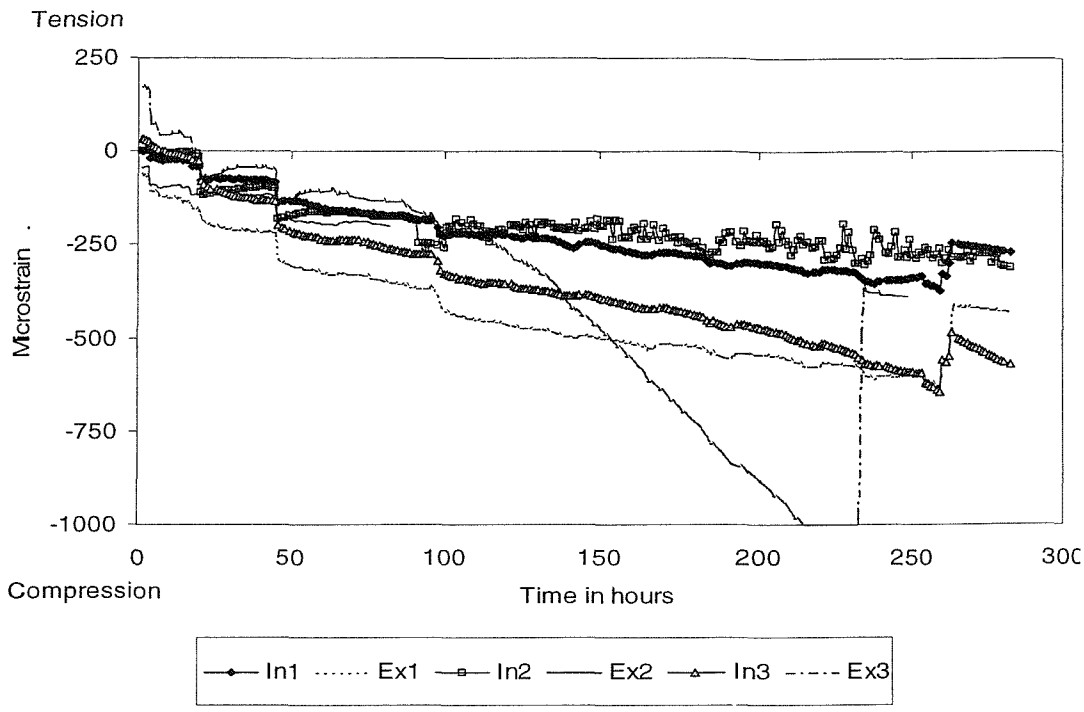

Positions of the gauges : IN = intrados; EX = Extrados – see also Figure 3.6

(b) Points 4 - 6

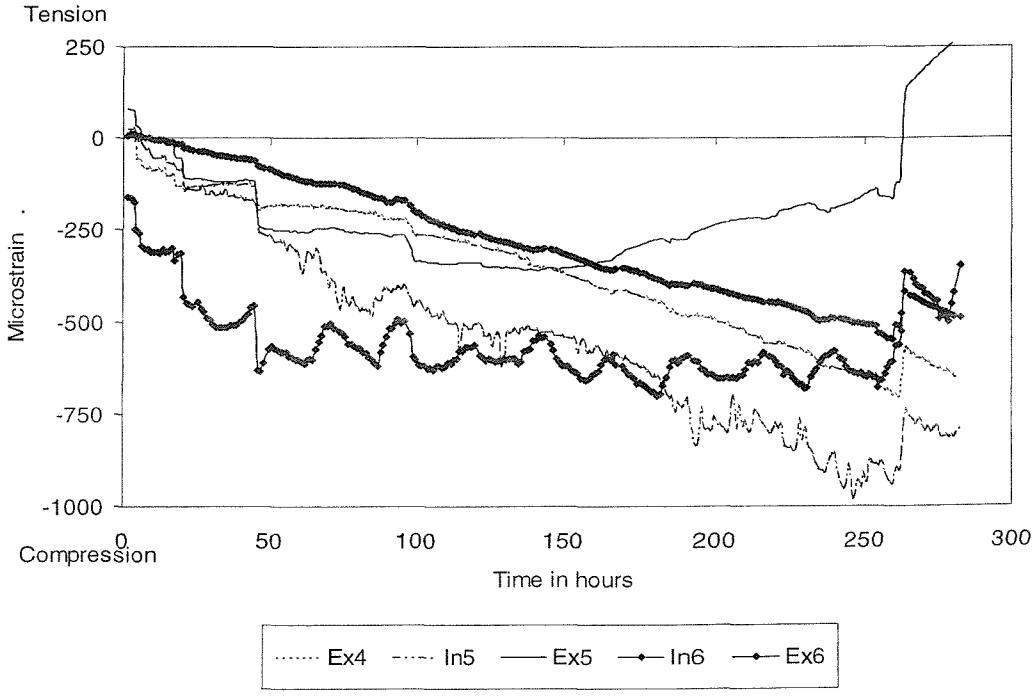

Positions of the gauges : IN = intrados; EX = Extrados – see also Figure 3.6

Figure 3.10 Plan of HEX T4 station tunnels showing location of monitoring sections (Mott MacDonald 1998)

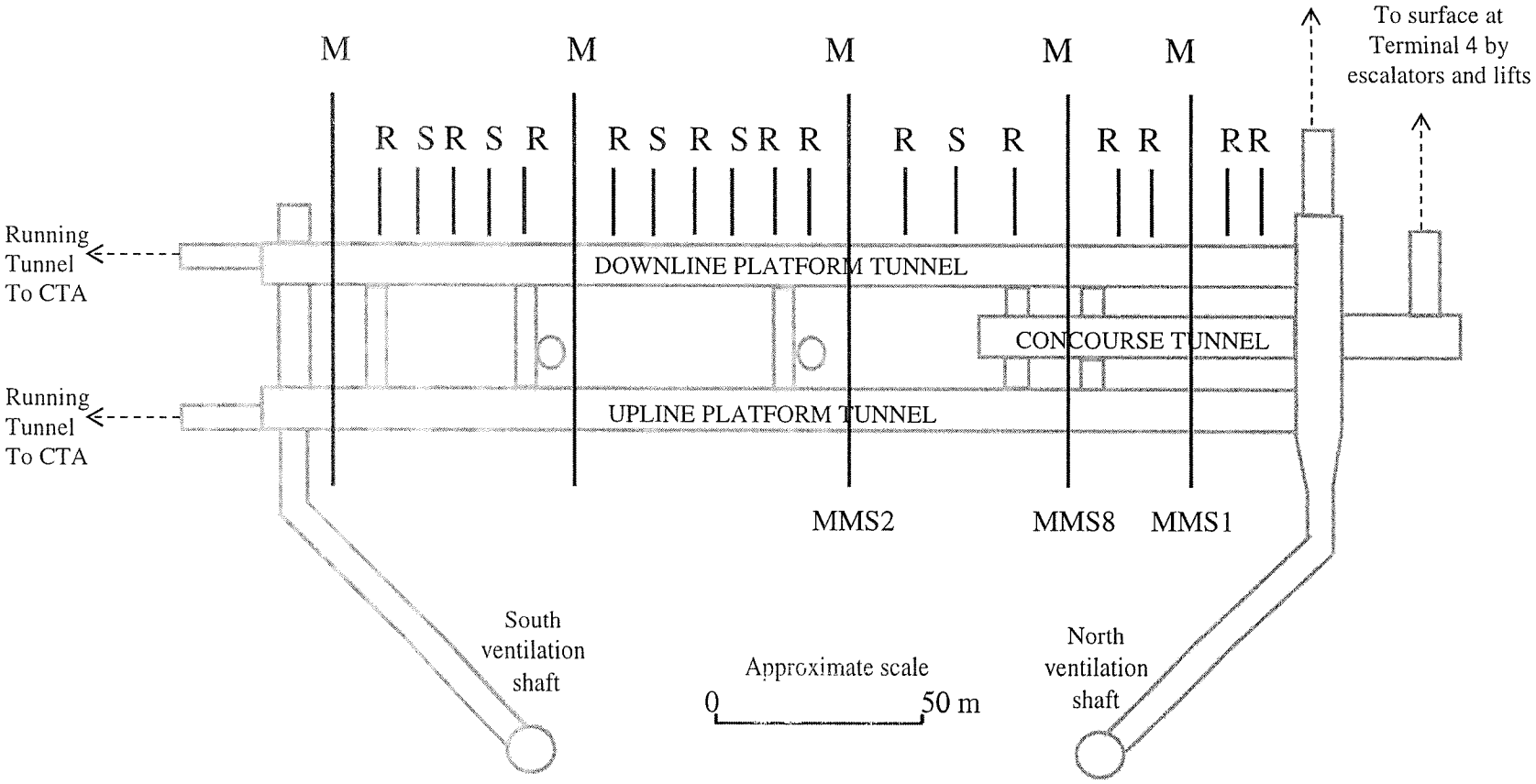

R – Regular monitoring @ ~20 m = In-tunnel deformation only

S – Stress monitoring @ ~20m = In-tunnel deformation plus piezometers, radial & tangential pressure cells

M – main monitoring @ ~40 m = As per S plus multiple rod extensometers (ID no. = MMS#)

Do not scale from this drawing

Figure 3.11 Cross–section through the HEX Platform tunnels, showing the geological section & instrumentation (Mott MacDonald 1998)

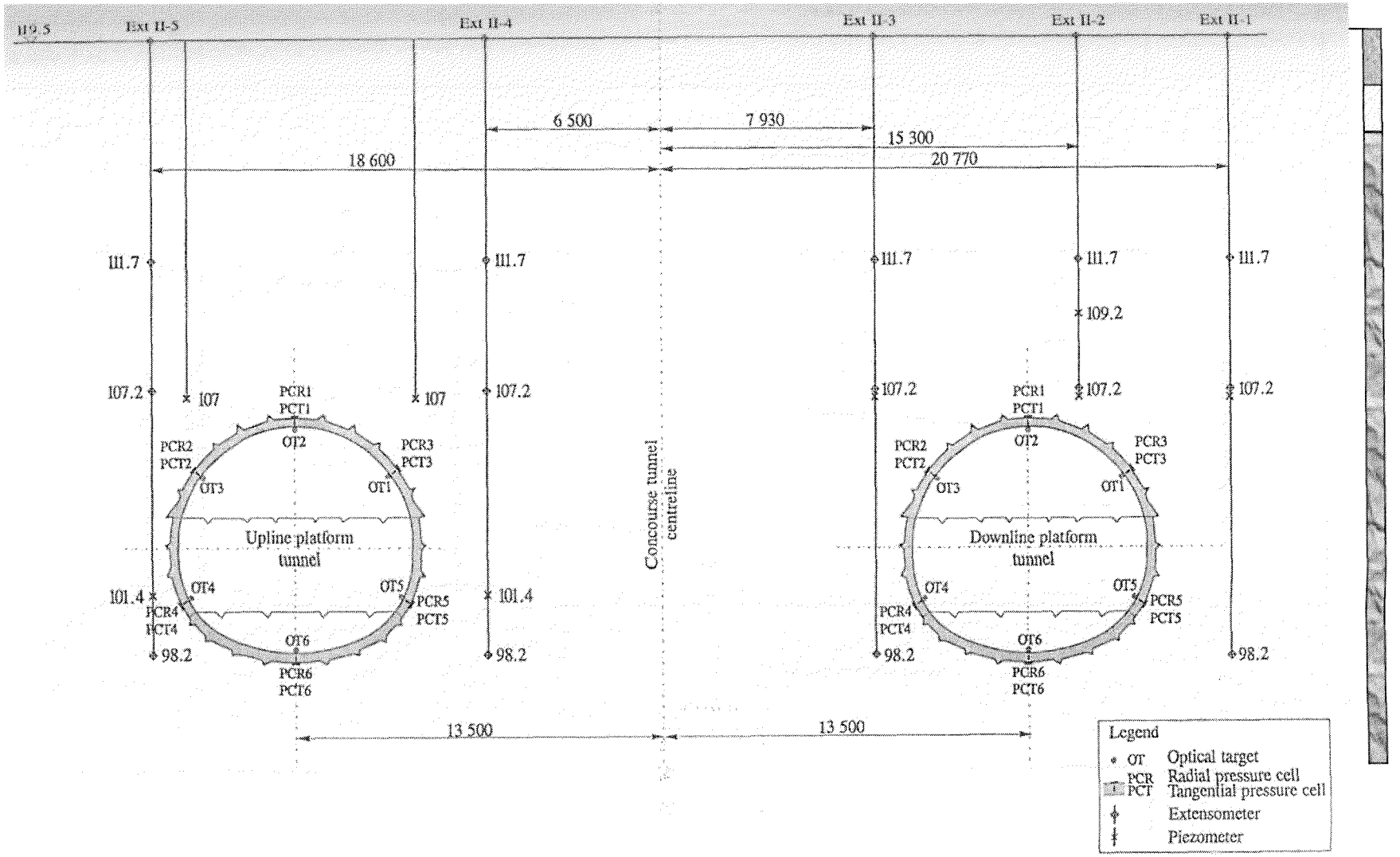

Figure 3.12 HEX platform tunnels excavation sequence

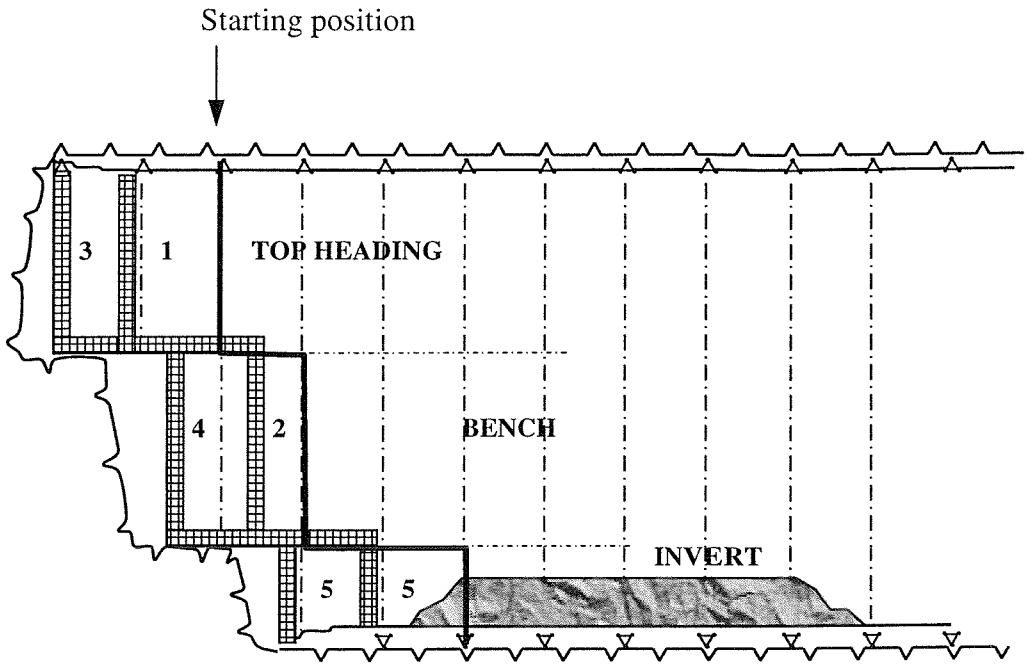

Figure 3.13 Isometric view of HEX Terminal 4 station

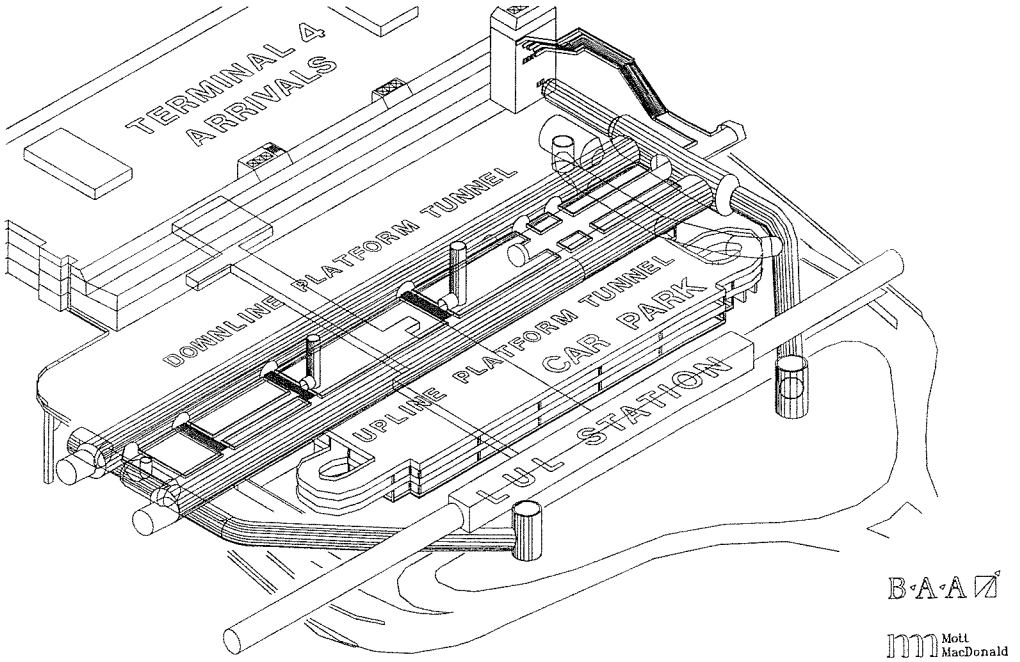

Figure 3.14 Tangential cell pressures (hoop pressures) in comparison to strength of cores of sprayed concrete (Bonapace 1997)

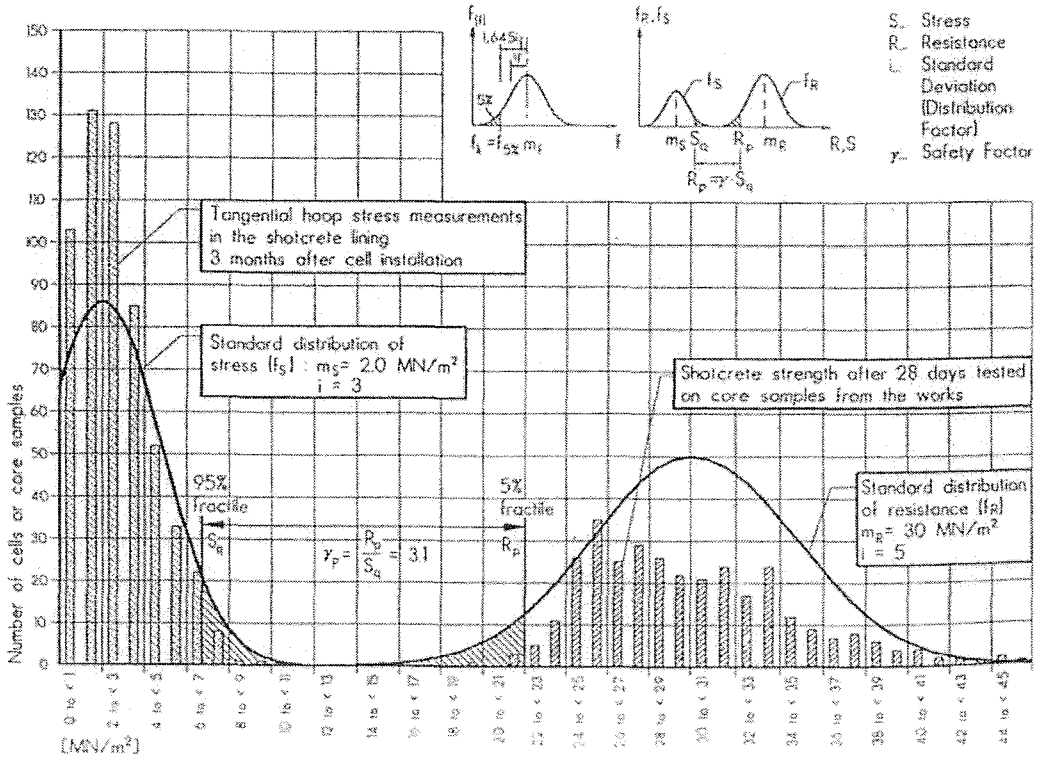

Figure 3.15 Tangential pressure cells from HEX Platform Tunnel at section MMS2 (for locations see Figure 3.17) - Mott MacDonald 1998

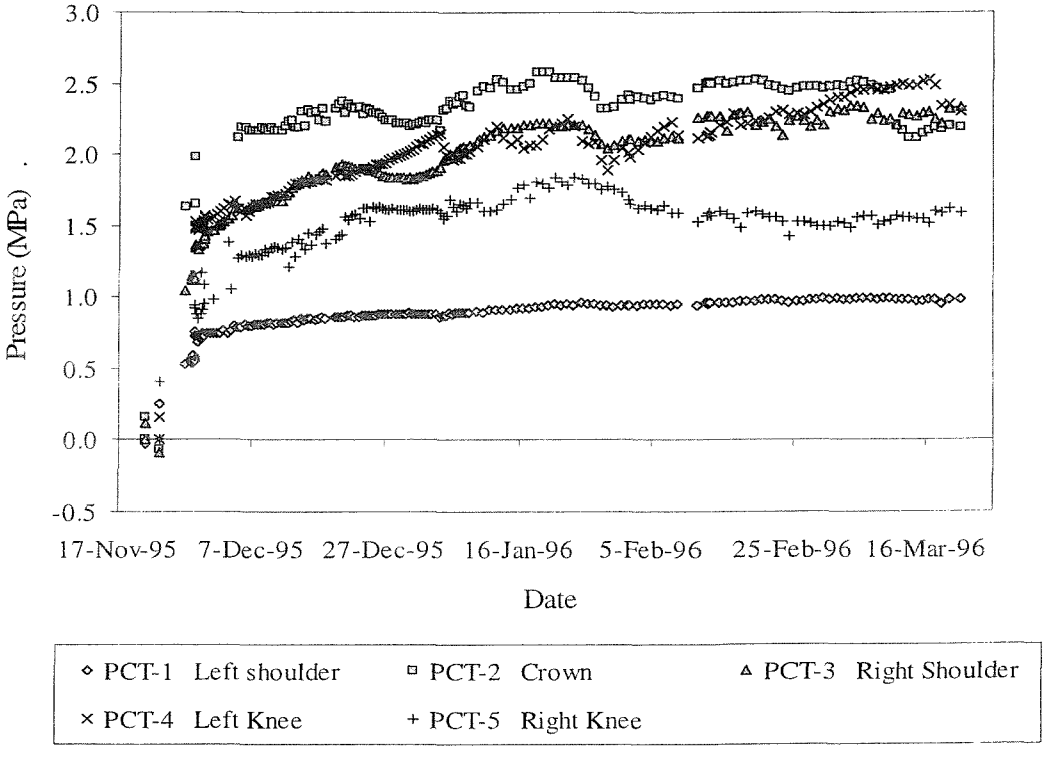

Figure 3.16 Strain gauge measurements from HEX Concourse Tunnel (for locations see Figure 3.17) - Mott MacDonald 1998

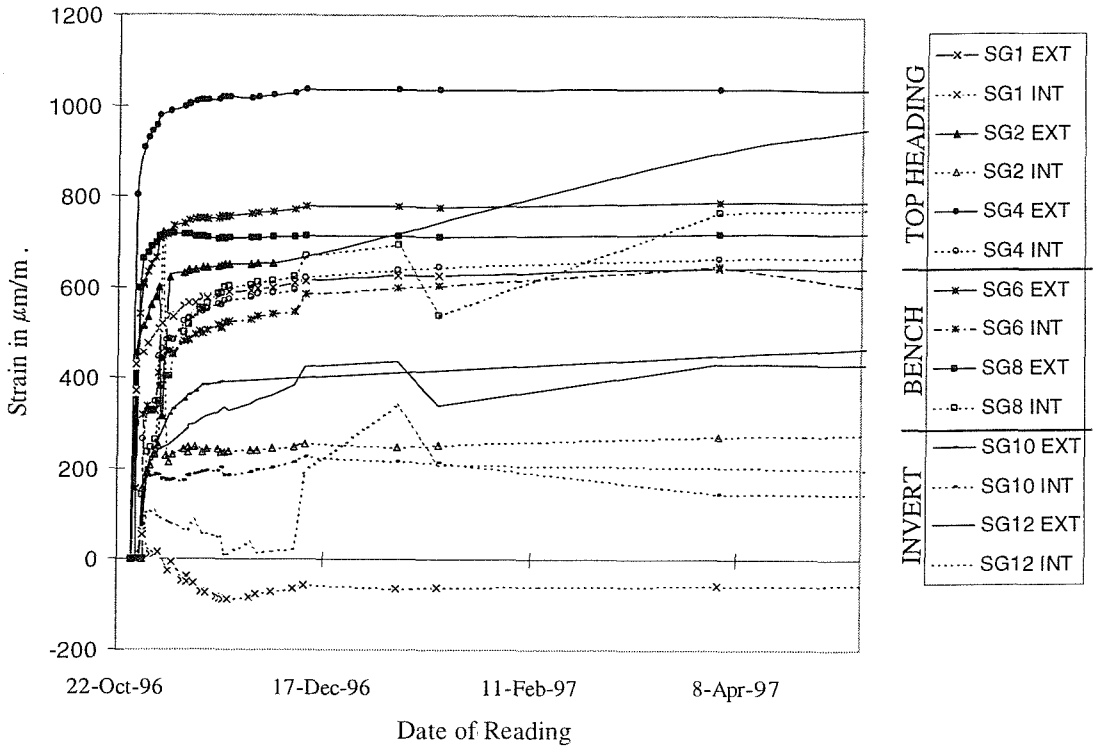

Figure 3.17 Average lining deformations for HEX Platform Tunnels (Mott MacDonald 1998)

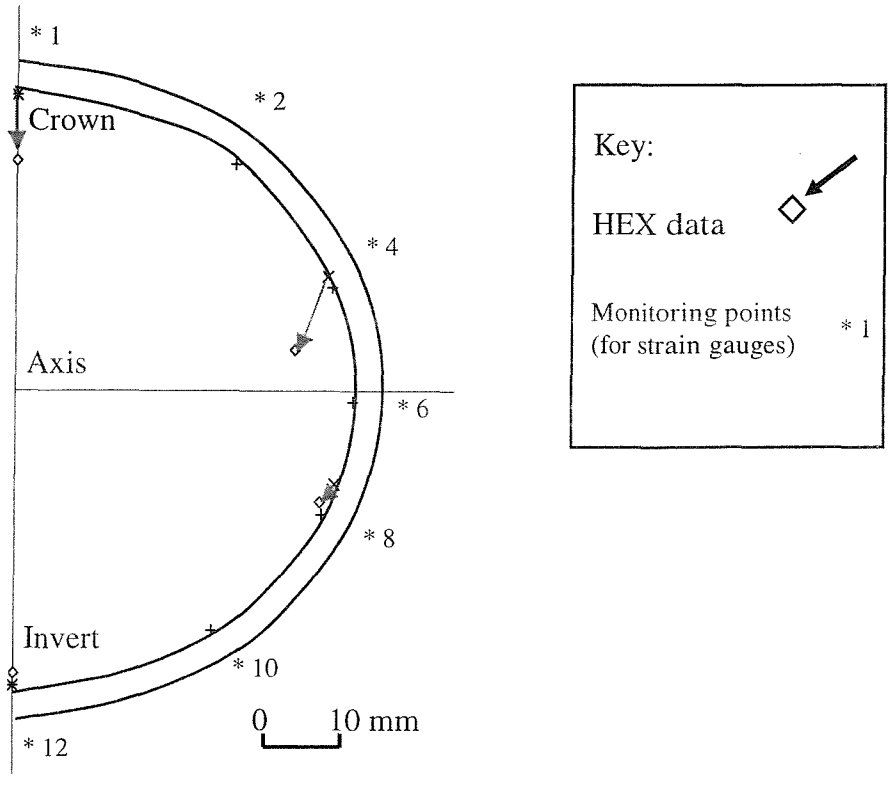

Figure 3.18 Pore pressure changes from 8m diameter HEX Trial Tunnel (Mott MacDonald 1998)

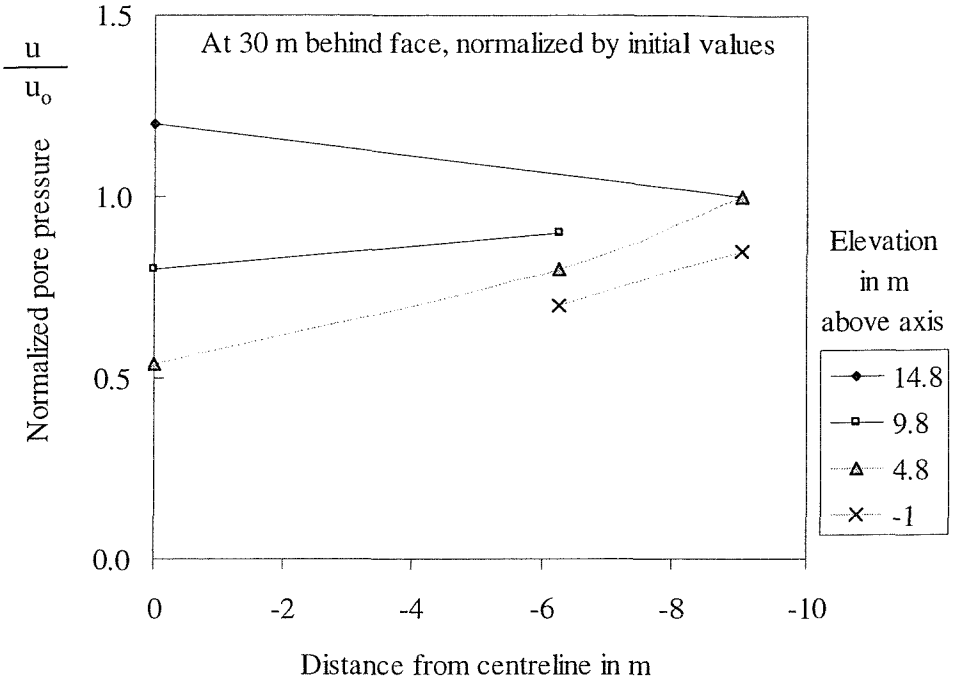

Figure 319 Longitudinal settlement profiles from HEX Concourse & Trial Tunnels at different elevations above axis level (Mott MacDonald 1998)

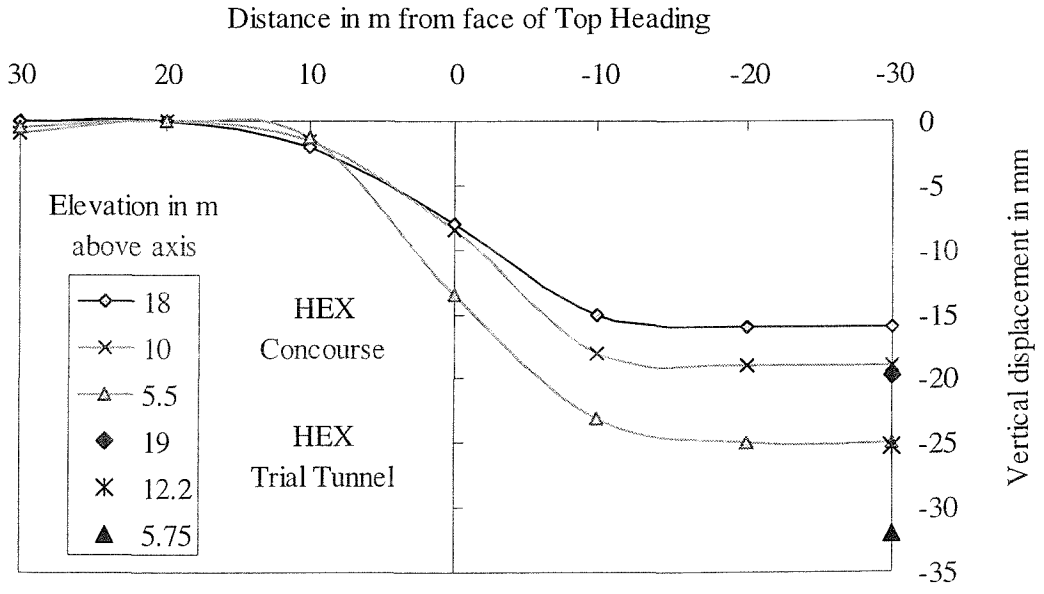

NB: Trial Tunnel values corrected for the difference in face area and volume loss; surface is 18 m or 19 m above axis

Figure 3.20 Transverse settlement profiles from HEX Platform & Concourse Tunnels and Trial Tunnels at 30 m behind the Top Heading (Mott MacDonald 1998)

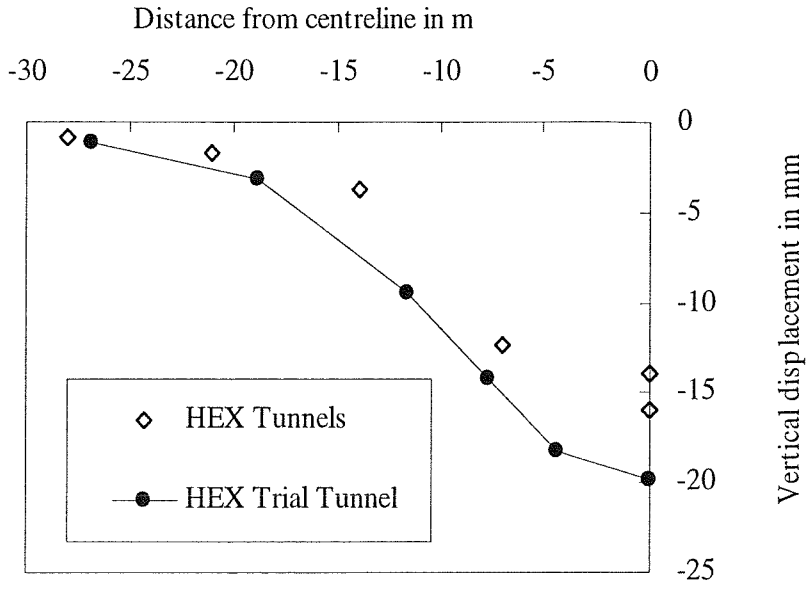

NB: Trial Tunnel values corrected for the difference in face area and volume loss

Figure 3.21 Vectors of ground movement around the HEX Trial Tunnel (Deane & Bassett 1995)

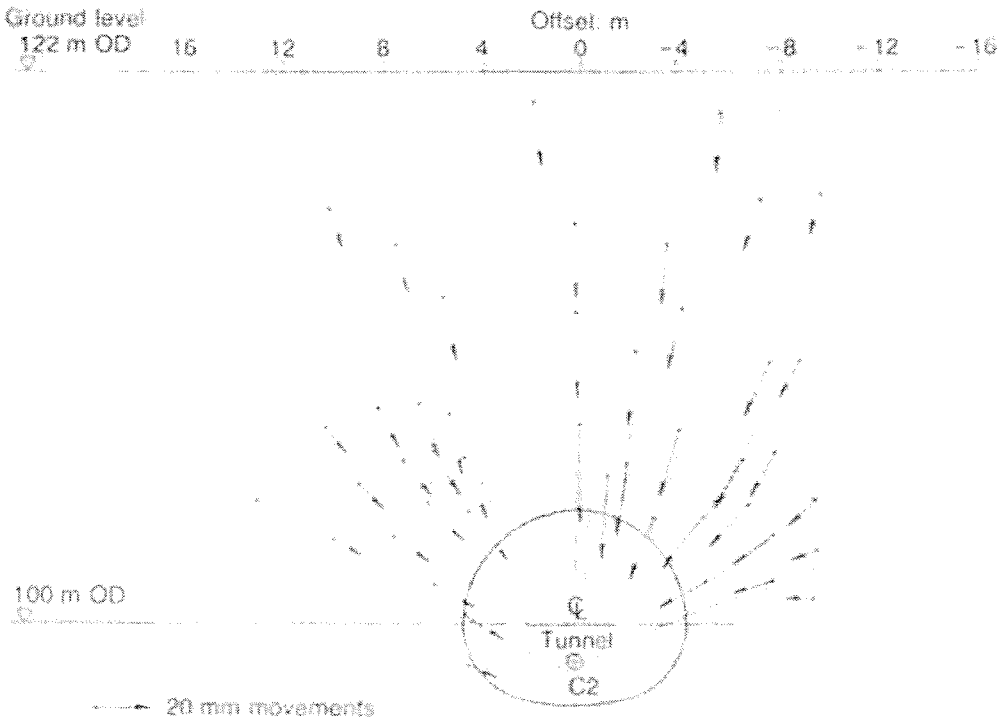

Figure 3.22 Longitudinal movement into the face of the HEX Concourse Tunnel (from inclinometer) - Van der Berg 1999

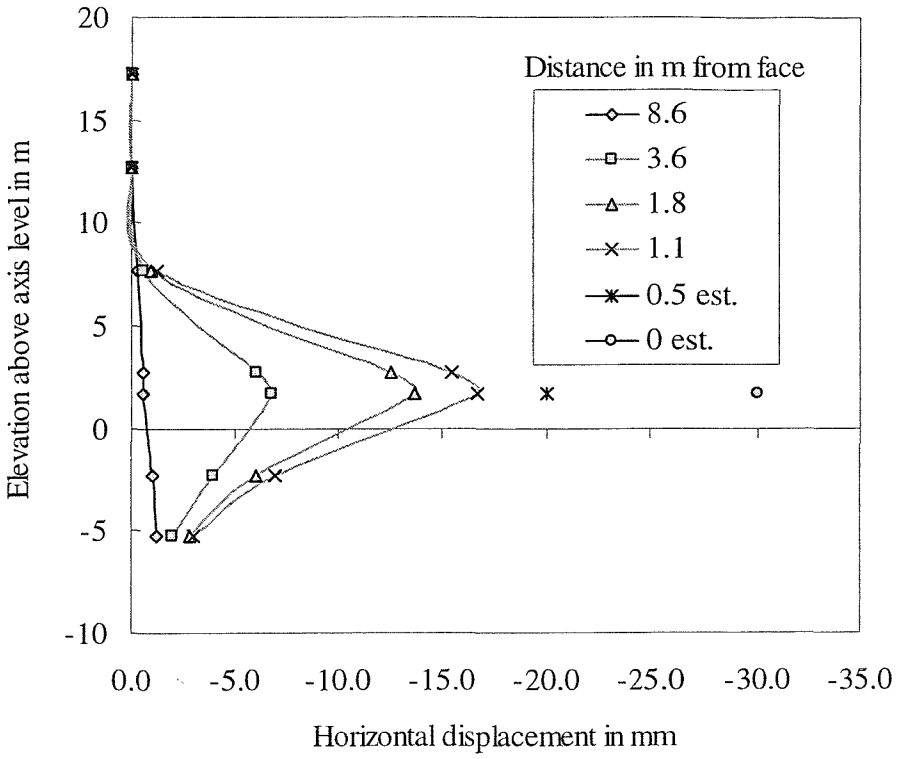

4 NUMERICAL MODELLING OF SPRAYED CONCRETE

4.1 Introduction

Having outlined the material behaviour of sprayed concrete in Chapter 2, the constitutive models that will be used in this study will now be presented. Before this, the primary tool for this research will be described.

4.2 The FLAC program

For the purposes of this work the numerical modelling program should be able to analyse complex continuum problems involving the nonlinear behaviour of the ground and structure within a relatively short time. This numerical study has used the FLAC (Fast Lagrangian Analysis of Continua) finite difference code (developed by ITASCA; www.itascacg.com) for the following reasons:

- The finite difference code is well suited to analysing nonlinear problems (see 1.2.3).
- FLAC incorporates a programming language, FISH, which *inter alia* enables the existing constitutive models to be customised easily.
- Both the industrial and academic partners in this research – Mott MacDonald Ltd and Southampton University – have considerable experience in using FLAC.
- FLAC can analyse both 2D and 3D problems.

A range of programs was considered. While finite element (FE) programs (e.g.: ABAQUS) are very popular, many were originally developed for mechanical engineering and therefore cannot be applied easily to geotechnical problems. Table 4.1 contains an assessment of the suitability of FLAC3D.

FLAC uses an explicit time-marching solution process which enables nonlinear problems to be analysed more quickly than in some FE programs. It does not need to store stiffness matrices, so requires only modest amounts of computer memory. A high processor speed is important because the solution process involves repeating a calculation cycle thousands of times, until the unbalanced forces in the model have reduced to an acceptably small size.

Preliminary work with FLAC established that a basic 3D model of the HEX Platform tunnel could be run on a desktop PC with a 300MHz processor in less than one day.

Finite elements (e.g.: shell and cable elements) can be used in FLAC in conjunction with the finite difference grid. The finite elements all have a linear elastic constitutive model.

Whenever the program has been updated with a new version, the verification examples provide by ITASCA have been run to verify that the program is functioning correctly.

Table 4.1: Assessment of FLAC3D (after Bond & MacLeod 2001)

Characteristic	FLAC3D
Functionality	Excellent - Designed for geotechnical problems, including tunnels; reasonable range of material models; can model fluid flow and creep problems; FISH language for customisation; Windows graphical user interface.
Reliability	Good - In operation since 1993; developed from ITASCA's well-established FLAC 2D program; supported by originators with regular updates.
Usability	Good – Clear explanation of theoretical basis & operation in manuals; input files have to be written in text editor in advance so slow to operate until the user is well acquainted with the commands; FISH is easy to learn.
Efficiency	Excellent – Rapid analysis of nonlinear problems; plotting can be automated as can extraction of data from specific points but this requires development of FISH routines
Maintainability	Excellent – Stable in Windows environment, stable while modelling nonlinear problems due to explicit solution method; instability in the analysis is easy to identify
Portability	Good – works under Windows 9x & NT.

4.3 Material behaviour of sprayed concrete

4.3.1 Stiffness

The first parameter used to characterise the behaviour of a lining material is its stiffness. To date most analyses of SCL tunnels have assumed isotropic linear elastic behaviour for the lining. Where experimental data exists for the stiffness (e.g.: Young's modulus, E, and Poisson's ratio, ν) at different ages of the sprayed concrete mix in question, this data can be

used to estimate how the stiffness varies with age. In practice, little or no information may exist. The Young's modulus may be estimated from the strength of the sprayed concrete (Chang & Stille 1993; see also Appendix A).

$$E = 3.86\sigma^{0.60} \qquad 4.1$$

where σ is the uniaxial compressive strength. If the Young's modulus is known at 28 days (E_{28}), the value at other ages may be estimated from any one of a number of equations (see Appendix A). In this study the relationship below, proposed by Aydan *et al.* (1992a), has been adopted (see Figure 2.15).

$$E = E_{28}.(1 - e^{-0.42t}) \qquad 4.2$$

where t is the age in days. It has been assumed that the Poisson's ratio, *v*, equals 0.2 and remains constant. This is reasonable except when the concrete is close to failure (Chen 1982).

4.3.2 Strength in compression & tension

Uniaxial compressive strength is the main parameter used during construction to assess the quality of concrete. In SCL tunnels, tests are typically performed at various ages (e.g.: 12 hours, 7 days, 28 days) and at a frequency of between 1 sample per 10 m^3 and 1 per 250m^3, depending on the type of project (Malmberg 1993). Again the strength values required for a model could be estimated directly from such data or one of many relationships (see Appendix A). In this study, the equation below (after Chang & Stille 1993) has been used to approximate the development of strength with age.

$$fcu_{(t)} = 1.1 \cdot fcu_{28}.e^{C} \quad \text{where} \quad C = \frac{-1}{t^{0.70}} \qquad 4.3$$

fcu_{28} is the strength at 28 days and t is the age in days. Strength tests are often carried out on cores of sprayed concrete whereas concrete design codes are usually based on characteristic cube strengths. The strengths from cores can be assumed to be 80% of the cube strengths for the same concrete (NCA 1993, BS 8110 1997). Design codes often stipulate further reductions in the design strengths, e.g.: BS 8110 (1997) defines the unfactored maximum strength in bending as 0.85 fcyl or 0.67 fcu. This additional factor has not been used in this study.

Tensile strength, f_{tu}, is rarely tested. Using the relationship for normal cast insitu concrete (Neville 1995), it has been assumed to be:

$$f_{tu} = 0.30.f_{cu}^{0.67} \qquad 4.4$$

4.3.3 Stress-strain behaviour

Nonlinearity in stress-strain behaviour can be implemented in the theoretical frameworks of either strain-hardening plasticity or nonlinear elasticity.

4.3.3.1 Strain-hardening plasticity

In a plasticity model, the material is assumed to behave in a linear elastic manner until the yield point is reached. Beyond that point the stress increases (or decreases) in accordance with a hardening (or softening) rule relating the cohesion to the plastic strain up to the peak plastic strain. The plastic strains occur according to a flow rule in addition to the elastic strains. In the generalised case, the yield point becomes a surface in 3D stress space (e.g.: see Figure 2.32) and is usually defined in terms of stress invariants (Chen 1982).

In this case it has been assumed that the concrete behaves in a linear elastic manner up to the yield strength, f_{cy}. The ratio f_{cy}/f_{cu} has been assumed to be 0.40 and f_{cu} can be obtained at any age from equation 4.3. Figure 2.17 shows the variation of peak strains (i.e. strain at peak stress) with age, t. There is considerable scatter. However, a possible relationship between age in hours and peak strain in % is:

$$\varepsilon_{peak} = -0.4142 \cdot \ln(t) + 3.1213 \qquad 4.5$$

Figure 2.18 shows the ultimate peak strain vs age. All the values are considerably larger than the 0.35% limit stated in design codes (e.g.: BS 8110 1997). In this study, it has been assumed that beyond the peak strength the concrete behaves in a perfectly plastic manner with no limit on ultimate strain. In FLAC, the standard strain-hardening model is based on the Mohr-Coulomb yield criterion, in which beyond yield the cohesion varies with plastic shear strain. Conveniently the yield surface of concrete at low hydrostatic stress agrees quite well with the Mohr-Coulomb surface (Chen 1982). A quadratic hardening law is used to

calculate the change in cohesion (after Meschke 1996 - see Figure 4.1). This agrees well with the idealised stress-strain curve proposed in BS8110 Part 2 (1985) [61].

$$f = f_{cy} + 2(f_{cu} - f_{cy}) \cdot \left(\frac{\varepsilon_{pl}}{\varepsilon_{pl.peak}} \right) - (f_{cu} - f_{cy}) \cdot \left(\frac{\varepsilon_{pl}}{\varepsilon_{pl.peak}} \right)^2 \qquad 4.6$$

The cohesion (on the compression meridian – Lode angle = 60°) is related to the uniaxial strength, f_c, by equation 4.7 taking $\phi = 37.43°$ [62].

$$cohesion = f_c . \frac{(1 - \sin\phi)}{2.\cos\phi} \qquad 4.7$$

Figure 2.13 suggests that this Mohr-Coulomb failure surface agrees reasonably well with experimental data along the compressive meridian but less well along the tensile meridian. Agreement is less good at hydrostatic octahedral stresses less than 0.33 f_{cu}. Finally, when any principal stress equals f_{tu}, a simple tension cut-off has been assumed. No allowance has been made for the effects of steel reinforcement.

4.3.3.2 Nonlinear elasticity

Alternatively the behaviour can be assumed to be nonlinear elastic. The model used here has been based on that by Kotsovos and Newman (1978) because of its relatively simple formulation (requiring only 3 input parameters: f_{cyl}, K_0 & G_0) and because it was found to agree well with recent data for sprayed concrete (Brite Euram C2 1997). The predicted failure surface agrees better than the Mohr-Coulomb model (see Figure 2.13). The formulae for the tangent moduli in this model can be found in Appendix E. This model has been implemented as a FISH routine that updates the moduli and is called at regular intervals during the analysis (see Appendix E)[63]. The standard FLAC constitutive models are called every cycle. The size

---

[61] NB: The maximum strength permitted by BS 8110 is 0.8 fcu (= fcyl) and this is only for the analysis of non-critical sections.

[62] From Chen (1982); Yin (1996) proposed 40°.

[63] In the first instance the model was updated every 100 cycles. Typically each stage of the basic 3D model of the HEX tunnel requires 3000 cycles to reach approximate equilibrium. This has since been modified so that the updating intervals starts at 2 cycles and increases to 100 cycles. The stresses changes are greatest at the start of each excavation stage / load increment so it is better to update more regularly then.

of interval for non-standard models is a trade-off between accuracy and speed (since it takes time to run the FISH function). Minor modifications have been made to the formulae to extend them to strengths less than 15 MPa. Since the shear modulus in the original formulation by Kotsovos and Newman does not decrease to zero at the peak strength, it has been reduced to 5% of G_0 (the initial shear modulus) as the actual shear stress approaches the peak shear stress. Above the same point the bulk modulus is reduced to 0.33 K_0 (the initial bulk modulus) (after Gerstle 1981).

Figures 4.2 and 4.3 suggest that the implemented form of this constitutive model functions well both under uniaxial and triaxial loading. Despite using the same input parameters as the strain-hardening plasticity model, the nonlinear elastic model agrees better with the test data in the triaxial case (see Figure 4.3). The nonlinear elastic model has been optimised to fit the test data by altering the point at which the moduli reduce to the low values. This leads to predicted stresses that exceed the model's own estimate of the strength of the concrete given the confining stresses and the uniaxial strength. This is permissible because it is an elastic model, whereas the strain-hardening plasticity model is capped at its predicted peak strength.

Since this is a tangent modulus model, its accuracy depends on the size of the load increments in comparison to the peak strength. Figure 4.4 suggests that a minimum of 7 equal increments is required for acceptable performance.

Ageing is a major complication in the implementation of the constitutive models for sprayed concrete. Since the strength increases with age, the τ_0/f_{cyl} ratio decreases with age. There is a sudden change in G_0/G_{tan} at the start of each increment in age (at each new load stage). Figure 4.5 shows values of the tangent shear modulus, G_{tan}, taken from the model of the creep test at different ages. The values agree well with the prediction according to the formulae (Equations 1 & 2 in Appendix E) despite the change in τ_0/f_{cyl} ratio.

Finally, the FISH function includes a check to determine whether loading, unloading or reloading is occurring (see Appendix E). While loading occurs, the moduli are calculated on

the basis of the current octahedral stresses. As soon as unloading (i.e. a reduction in deviatoric stress is detected), the moduli are reset to their initial values and then revised on the basis of the peak value of deviatoric stress minus the current value. If the deviatoric stress increases (i.e. reloading), the moduli are reset to their initial values and then revised on the basis of the current stress minus the lowest value in that unload-reload cycle, until the deviatoric stress exceeds the highest previous value. These are the Masing rules for loading cycles (Dasari 1996).

Unloading is probably of limited relevance to the lining of a single tunnel constructed on its own with a Top Heading, Bench and Invert excavation sequence, since one would not expect much unloading to occur. However, it is likely to be of relevance where other tunnels are constructed near to an existing tunnel, at junctions and in more complex excavation sequences. Since loading is determined on the basis of changes in octahedral deviatoric stress alone, changes in hydrostatic stress are not recognised in terms of loading / unloading. However, the lining is predominately in a biaxial stress state and so the most likely changes in load are primarily deviatoric ones, rather than purely hydrostatic.

4.3.4 Shrinkage

Figures 4.6 (a) & (b) show the variation of shrinkage strain with age. Given the scatter in experimental data, it appears that the simple ACI equation, with the constant B = 20 days and an ultimate shrinkage strain, ε_{shr00} of 0.1 %, may be used to predict the development of shrinkage with age (ACI 209R 1992) as a first approximation.

$$\varepsilon_{shr} = \frac{\varepsilon_{shr\infty} . t}{(B + t)} \qquad \text{where t is age in days} \qquad 4.8$$

4.3.5 Creep

4.3.5.1 Introduction

Figures 4.7 (a) to (f) show the data on creep strains versus age that has been collated during the course of this research. Over 200 results from 7 data sets have been presented in groups according to the age at loading. Interpretation of creep tests is complicated by the fact that

often the loads were applied incrementally at different ages. The total creep strain due to one load increment may not have developed before the next was applied. Furthermore the utilization factor may vary considerably during the test due to the ageing of the material (Huber 1991). From Figure 4.7, age is clearly a very important influence on specific creep strain (which is the creep strain divided by the magnitude of the load increment).

4.3.5.2 Generalised Kelvin model

As discussed earlier (see Chapter 2) the generalised Kelvin viscoelastic model (see Figure 2.40 (a)) is well suited to modelling the short-term creep of sprayed concrete. The Kelvin model requires 2 parameters, G_k and η, in addition to the normal elastic moduli, as below.

For a uniaxial case: $$\varepsilon_{xx} = \frac{\sigma_{xx}}{9.K} + \frac{\sigma_{xx}}{3.G} + \frac{\sigma_{xx}}{3.Gk}\left(1 - e^{-Gk.t/\eta}\right) \qquad 4.9$$

& in the 3D case: $$\dot{e}_{ij} = \frac{\dot{S}_{ij}}{2.G} + \frac{S_{ij}}{2} \cdot \frac{1}{\eta_k}\left(1 - e^{-Gk.t/\eta}\right) \qquad 4.10\ a$$

or $$\dot{e}_{ij} = \frac{\dot{S}_{ij}}{2.G} + \frac{S_{ij}}{2\eta_k}\left(1 - \frac{2Gk.e_{ij}}{S_{ij}}\right) \qquad 4.10\ b$$

where ε_{xx} and σ_{xx} are the strain and stress in the x direction, K is the bulk elastic modulus, G is the shear elastic modulus, t is time, S_{ij} is the deviatoric stress, $\dot{S}_{ij}$ is the deviatoric stress rate and $\dot{e}_{ij}$ is the deviatoric strain rate. Creep is generally assumed to occur under deviatoric loading only (Jaeger & Cook 1979, Neville *et al.* 1983). The following creep models are available in FLAC: Maxwell; Power Law; WIPP[64]; WIPP Viscoplastic model and Crushed Salt model (Itasca 1997). Unfortunately this list does not include the Kelvin model[65]. However, if one compares equations 4.10 (a) and (b) with the equation for the Maxwell model (equation 4.11), one can see that they have a very similar form.

Maxwell model: $$\dot{e}_{ij} = \frac{\dot{S}_{ij}}{2.G} + \frac{S_{ij}}{2} \cdot \frac{1}{\eta_M} \qquad 4.11$$

[64] This model was developed during research at the U.S. Department of Energy's nuclear Waste Isolation Pilot Plant (WIPP) in Carlsbad, New Mexico.

This fact has been exploited to create a "Kelvin" model in FLAC 3D by amending the viscosity of the Maxwell model. In the modified FLAC model, an "incremental" form has been used, as follows:

$$\eta_M = \frac{|S_{ij}|}{\Delta S_{ij}} \cdot \frac{\eta_k}{\left(e^{-Gk.t'/\eta_k}\right)} \qquad 4.12$$

where t' is the time from the start of the load increment and ΔS_{ij} is the deviatoric load increment and $|S_{ij}|$ is the magnitude of the deviatoric load.

Table 4.2: Specific creep strain increment, $\Delta\varepsilon_{xx\,\infty}$, in -/MPa

Age at loading in hours	Lower bound	Average	Upper bound
0 – 3.5	1.5e-3	4.0e-2	8.0e-2
3.6 – 6.0	5.0e-4	1.5e-3	2.5e-3
7 – 12	2.0e-4	6.5e-4	7.5e-3
13 – 24	2.0e-5	4.0e-4	8.0e-4
25 – 672	5.0e-6	1.0e-4	2.0e-4

Table 4.3: Relaxation time, B, in hours

Age at loading in hours	Lower bound	Average	Upper bound
0 – 3.5	0.50	0.75	1.00
3.6 – 6.0	1.0	3.0	10
7 – 12	5.0	14.0	25
13 – 24	10	30	50
25 - 672	100	500	1000

The two creep parameters for the Kelvin model can also be described as the specific creep strain increment, $\Delta e_{ij\,\infty} = 1/(2G_k)$, and the relaxation time, B, where $B = \frac{\eta_k}{G_k}$. In the

[65] Although the Kelvin model is available in the 2D version of the programme.

formulation of equation 4.10a the physical significance is clear. Namely, B is the time taken for 63.2% of the increment in creep strain to occur. When t' = B, $\Delta e_{ij\ \infty}.(2G_k)$ = $0.632 = 1 - e^{-t'/B}$ or when t = 3B, $\Delta e_{ij\ \infty}.(2G_k)$ = 0.95. Tables 4.2 and 4.3 summarise the data from Figures 4.7 (a) to (f) in terms of these parameters [66].

4.3.5.3 Ageing

Yin (1996) proposed formulae of the form, $X = \frac{X_{28}.a.e^{c/t^{0.6}}}{2(1+\upsilon)}$, in line with established equations for predicting the development of stiffness and strength with age (e.g.: Chang & Stille 1993). The parameters for the new model could be assumed to vary with age in this fashion, according to the equations below.

$$\eta_k = \frac{1.5 \cdot e^{11} \cdot 1.0 \cdot e^{\left(-1.5/\left(\frac{T}{24}\right)^{0.6}\right)}}{2(1+\upsilon)} \quad \text{in kPa.s} \qquad 4.13$$

$$Gk = \frac{8.0 \cdot e^{6} \cdot 1.0 \cdot e^{\left(-1.0/\left(\frac{T}{24}\right)^{0.4}\right)}}{2(1+\upsilon)} \quad \text{in kPa} \qquad 4.14$$

where T is the age of the sprayed concrete in hours, v is Poisson's ratio and the other parameters have been chosen to obtain a reasonable fit to the data (see Figures 4.8 & 4.9). The solid lines on Figures 4.7 a to f show the predicted specific creep strains from equations 4.13 and 4.14. Figure 4.10 shows the relaxation time calculated from data in Figures 4.7 (a) to (f), along with the prediction from equations 4.13 and 4.14.

Also plotted on Figures 4.8 and 4.11 are approximate lines of "best-fit" through the data:

$$\log_{10} Gk = a_g.\log_{10} T + b_g \qquad 4.15$$

[66] The data comes from uniaxial creep tests and therefore the parameters have been determined using equation 4.9. $\Delta\varepsilon_{xx\infty} = 1/3Gk$

$$\log_{10} \eta_k = a_\eta . \log_{10} T + b_\eta \qquad 4.16$$

where $a_g = 1.25$, $b_g = 4.50$, $a_\eta = 3.50$ and $b_\eta = 7.00$.

According to these equations, if T = 100 hours, $G_k = 1.0e^7$ kPa, which equates to a uniaxial specific creep strain, $\Delta\varepsilon_{xx\infty}$, of $3.33e^{-5}$ -/MPa (from equation 4.9), and B = 2780. The modified "Yin" formula predicts quite different values of $G_k = 1.89e^6$ kPa (equivalent to $1.76e^{-4}$ -/MPa) and B = 5. Experimental data suggests that the specific creep strain is about $1.0e^{-4}$ -/MPa and B = 500 (see Tables 4.2 & 4.3). One should bear in mind that the majority of the data points for the loading age range of 25 to 672 hours refer to tests that were started at ages less than 80 hours.

Given the scant data for loading at ages greater than 100 hours, it would seem reasonable to assume that the sprayed concrete obeys the existing predictions for the creep of mature concrete. According to the ACI method (ACI 209R 1992), one would expect specific creep strains of about $1.08e^{-4}$ -/MPa and $0.68e^{-4}$ - /MPa after 700 hours for loading at an age 168 and 672 hours respectively. BS8110 predicts a specific creep strain of about $0.43e^{-4}$ -/MPa after 700 hours, for normal C25 concrete, loaded at 168 hours.

From a visual inspection of Figures 4.8 & 4.9, it would seem that the ageing formulae after Yin overestimate how fast the creep occurs (i.e. underestimate B) at all ages, and the magnitude of the creep increment for ages greater than 100 hours. The logarithmic ageing formulae agree better, except in the age range greater than 100 hours where the creep increment is probably underestimated and the relaxation time overestimated. Therefore, these formulae have been capped at 72 hours [67]. Creep models with both ageing formulae have been used in this study.

[67] Obviously creep remains age-dependent beyond the age of 72 hours and the logarithmic ageing formula could be amended to reflect ageing in line with published formulae or data (eg: BS8110 or ACI 209R).

4.3.5.4 Loading / Unloading

In the case of varying loads, superposition is normally assumed (Neville *et al.* 1983). Unloading can be modelled as the addition of a negative load increment. FLAC uses the total stress in a zone in creep calculations so unloading a zone only reduces the total stress used in the calculation.

If the duration of each load increment is longer than 3B, each load increment could be treated separately, since the creep due to that increment would be complete before the next one is added. If the load duration is shorter, one is faced with the question of whether to use the total stress in a zone or the stress increment during the creep calculation for each advance. Applying the normal principle of superposition would be very complicated. Even if one assumed that the creep strain increment during the advance of the tunnel face could be calculated individually for each load increment due to all the previous advance lengths, this would overlook the fact that, in this soil-structure interaction problem, the applied stress is not necessarily constant during the time-step of an advance.

Therefore the approach adopted here has been that when the time duration of each advance was greater than 1.5 B [68], only the increment in stress for that advance was used in the creep calculation. If the duration was less, it was assumed that the time was insufficient for most of the creep strain increment to occur and so the increment in stress was allowed to accumulate.

4.3.5.5 Stress dependency

It has been widely reported that the creep strain rate is more than directly proportional to the applied stress for stresses greater than 0.5 f_{cu} (Rokahr & Lux 1987, Pöttler 1990, Aldrian 1991). A stress dependence is discernible in Figure 4.11 but, due to the large scatter, its exact nature is unclear. The exponential stress dependence proposed by Aldrian would appear to overestimate the dependence for values of utilization factors, α, of 0.45 to 0.75 and underestimate it for $\alpha > 0.75$. Based on Figure 4.11, as an initial estimate of the stress

[68] 1.5 B = the time for 0.78 of the creep strain increment to occur

dependence, the following relationship for predicting the specific creep increment has been proposed for $\alpha > 0.45$.

$$\Delta e_{ij\,\infty} = (1 + 2.5*(\alpha - 0.45)/0.55) / (2Gk) \qquad 4.17$$

4.3.5.6 Verification

This new model has been implemented as a FISH routine that updates the moduli and at regular intervals, like the nonlinear elastic model (see section 4.3.3.2). The model was used to simulate the uniaxial creep test by Huber (see section 3.1.1). The model (with parameters chosen to match the test data – "VE matched") agrees to within -5 % of both the analytical solution and the experimental data – see Figure 4.12 [69]. Knowing the creep strain increment (from each stage in the experiment) one should be able to match the parameters of the creep model for each stage. Encouragingly, Figure 4.12 also shows that the model (with the average parameters based on results of different researchers – "VE Kelvin") agrees reasonably well with the experimental data. Also shown is the simulation with the ageing, isotropic linear elastic model, Et.

4.3.6 Hypothetical Modulus of Elasticity (HME)

As far as the author can tell, there is no generally accepted method for determining the values of HME to be used in modelling. One complicating factor is that it was originally developed for 2D numerical modelling and hence the reduction in modulus was intended to correct for 3D effects as well as creep, shrinkage and the ageing of the sprayed concrete.

$$E_{HME} = E_T.f_v.f_{s,k}.f_{vv} \qquad 4.18$$

Since the numerical modelling in this study has used using 3D analyses f_{vv} = zero (see 2.3.3.2). The time dependent elastic modulus has been divided by a factor of 2.4 for zone A and 1.8 for zone B (see Figure 4.13), to account for creep, shrinkage and the ageing of the stiffness during the period (i.e. factors $f_{s,k}$ and f_v in equation 4.18 (Pöttler 1985)). As

[69] At first sight this may seem to be a large error but it is largely due to the fact that it takes a finite time for the stress in a zone to rise to the value determined by the load increment. Therefore during this time in the creep calculation, the stress is lower than it should be. This can be avoiding by cycling to mechanical equilibrium first and then starting the creep calculation. However, the size of the error has not been deemed sufficient to warrant the additional calculation time required for this.

explained earlier, there is no established means of determining these parameters but, based on the material properties and prior experience, it seems reasonable to suggest that creep and ageing could reduce the stresses in lining by a factor of between 1.8 and 2.4. BS 8110 (Part 2: 1985) suggests that the creep coefficient would be about 2.10 [70]. The ultimate strengths in each zone have been set at 0.67 * fcu (t), in line with section 2.5 of BS 8110 (Part 1: 1997). The values used in the analyses are the same as those used in the design of the CTRL North Downs Tunnel (Watson *et al.* 1999), which one could take as representing the state-of-the-art of SCL design in the UK.

[70] Based on 60% of creep deformation occurring in the first 6 months after loading, for a 300 mm thick section loaded at an age of 1 day and stored in 50% RH.

Figure 4.1 Theoretical strain hardening curves

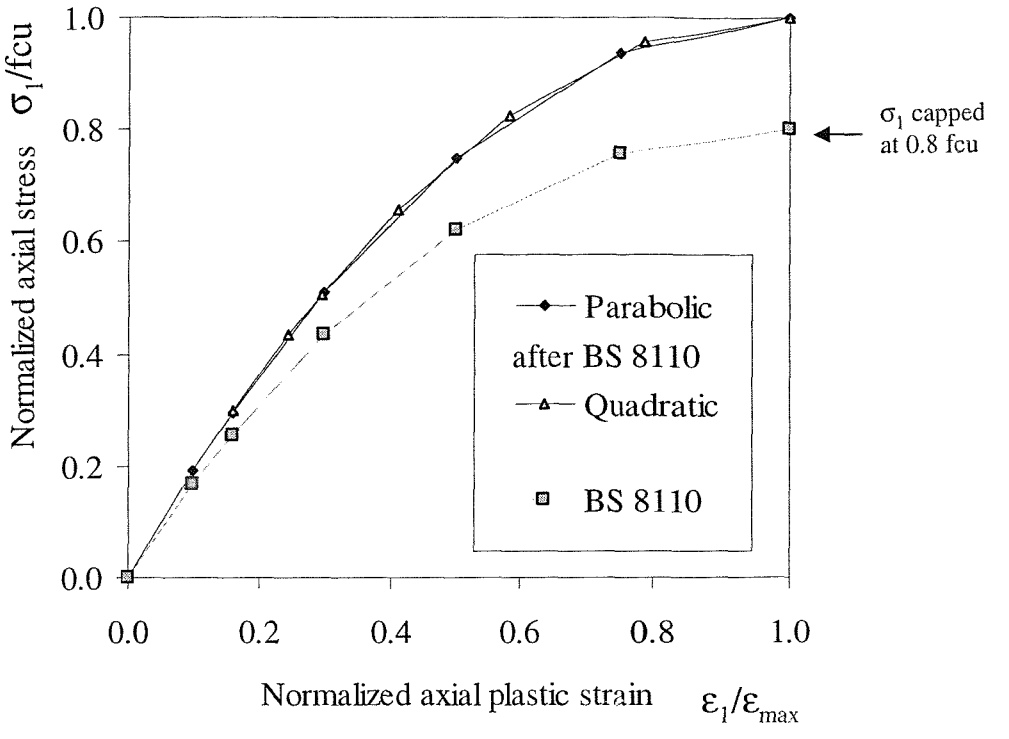

Figure 4.2 Uniaxial compression test on sprayed concrete

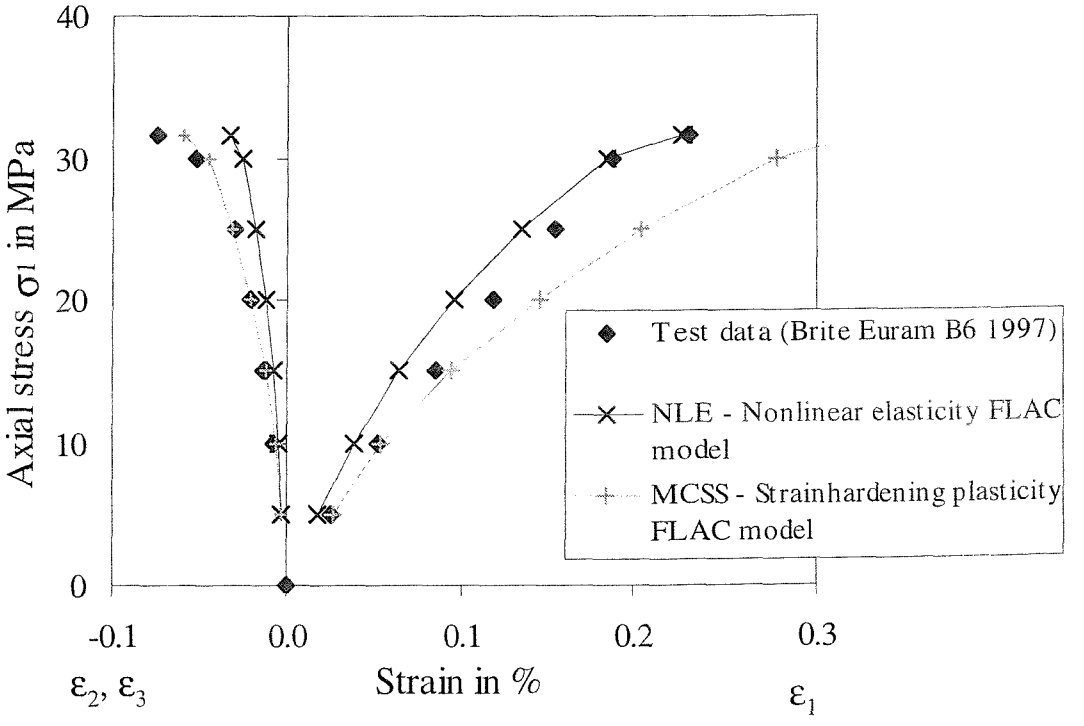

Input data for both models: f_{cyl} = 31.5 MPa, v = 0.2, E_0 = 18.80 GPa

Figure 4.3 Triaxial compressive test on sprayed concrete ($\sigma_2 = \sigma_3 = 1.0$ MPa)

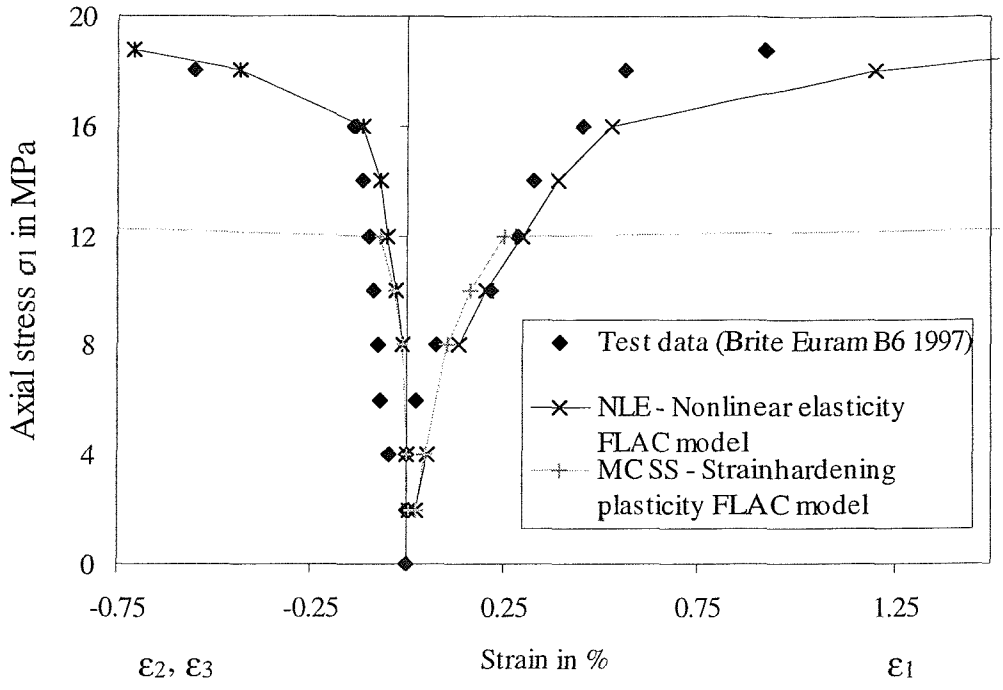

Input data for both models: $f_{cyl} = 9.5$ MPa, $\nu = 0.2$, $E_0 = 8.45$ GPa

Figure 4.4 The influence of load increments on the results of the non-linear elastic model

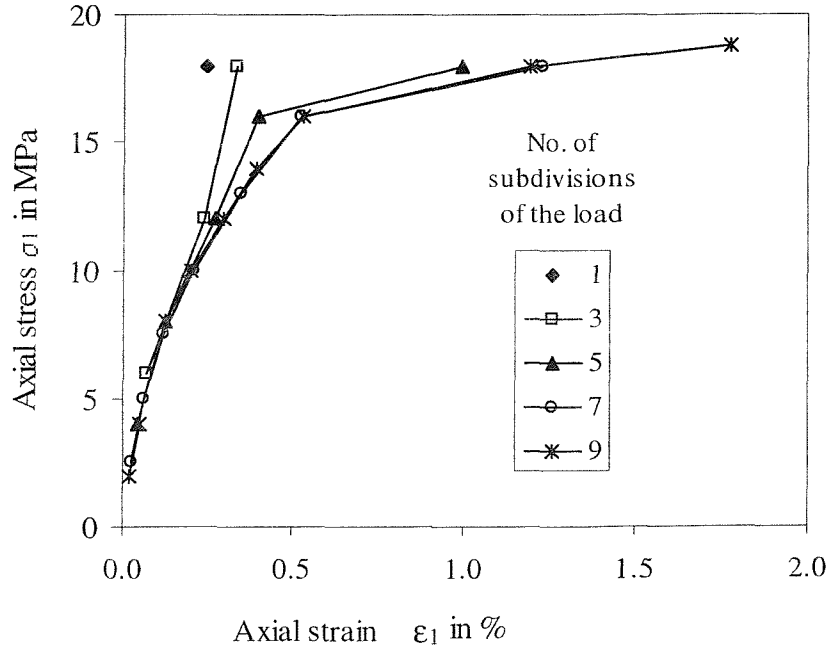

Figure 4.5 Normalized tangent shear modulus vs normalized shear stress

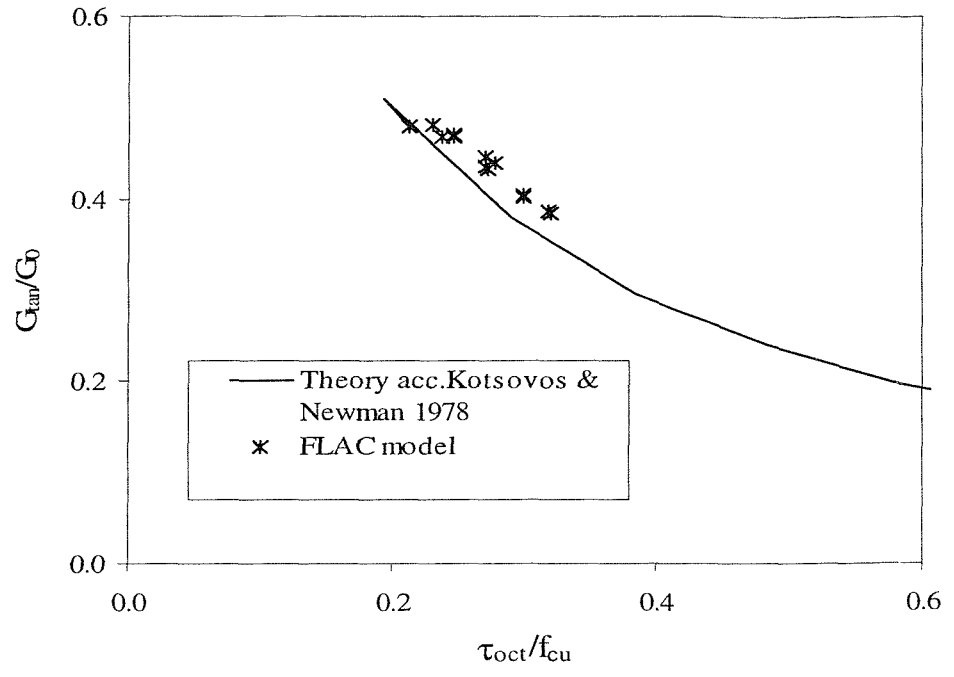

G_0 = initial tangent shear modulus; fcu = uniaxial compressive strength

Figure 4.6 Shrinkage of sprayed concrete

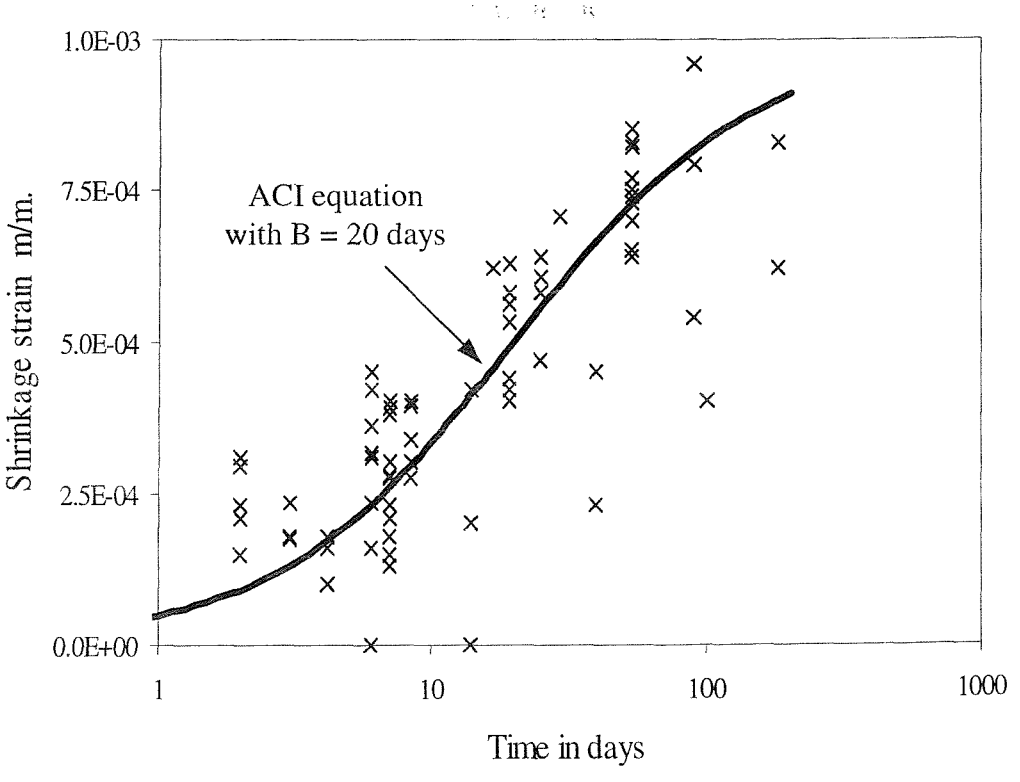

x Data from Abler1992, Cornejo-Malm 1995, Ding 1998, Golser et al. 1989, Schmidt et al. 1987, Pichler 1994,Rathmair 1997

Figure 4.7 Specific creep strain of sprayed concrete, loaded at different ages

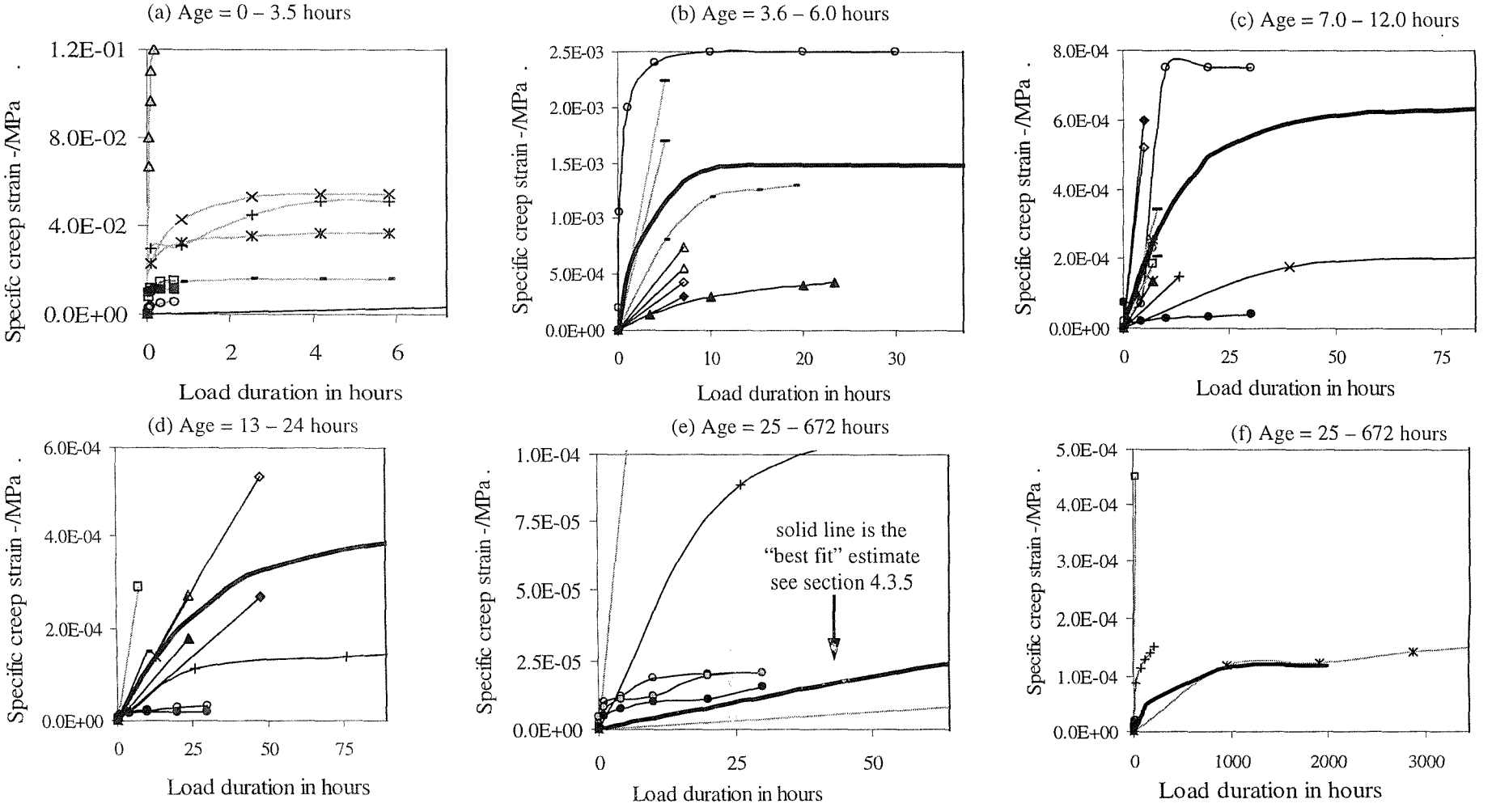

(Data from: Brite Euram B6 1997; Ding 1998; Huber 1991; Kuwajima 1999; Probst 1999; Rokahr & Lux 1987; Schmidt et al. 1987)

Figure 4.8 Shear stiffness (of spring in Kelvin rheological model), Gk, vs age

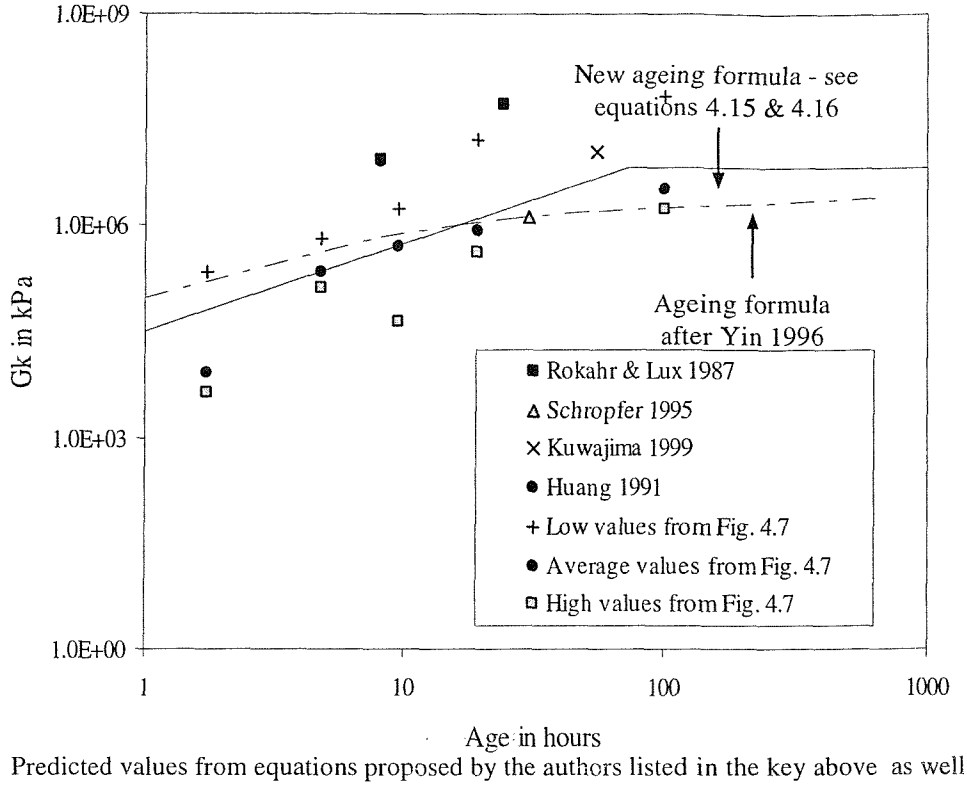

Predicted values from equations proposed by the authors listed in the key above as well as estimated values from the experimental data in Figure 4.7.

Figure 4.9 Viscosity of damper (in Kelvin rheological model) ,η_k, vs age

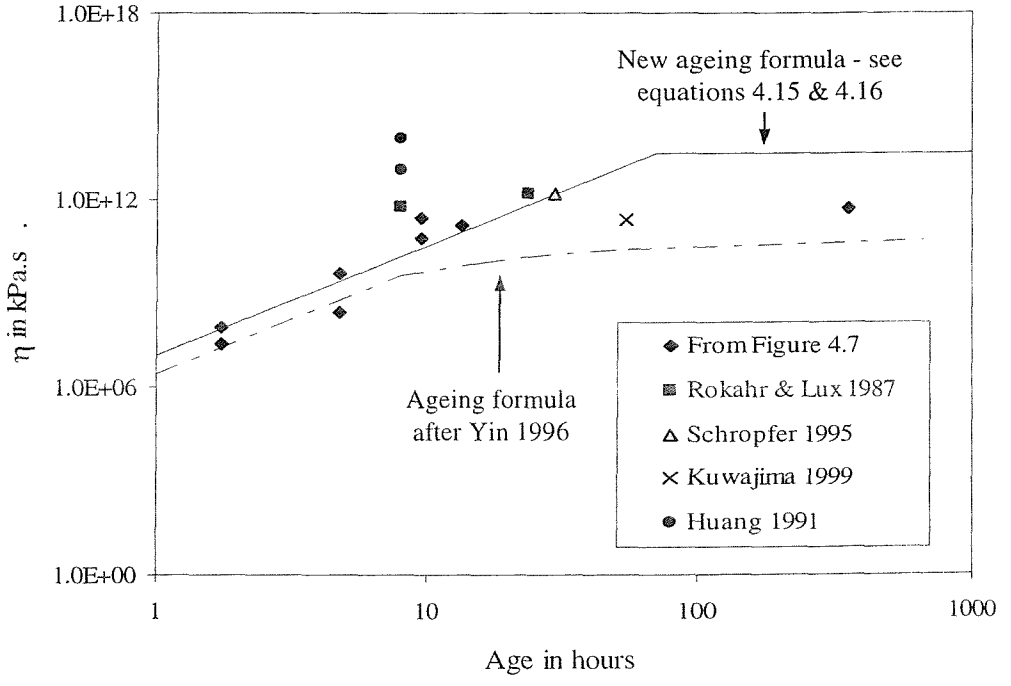

Predicted values from equations proposed by the authors listed in the key above as well as estimated values from the experimental data in Figure 4.7.

Figure 4.10 Relaxation time, B, vs age - $B = \eta_k/Gk$

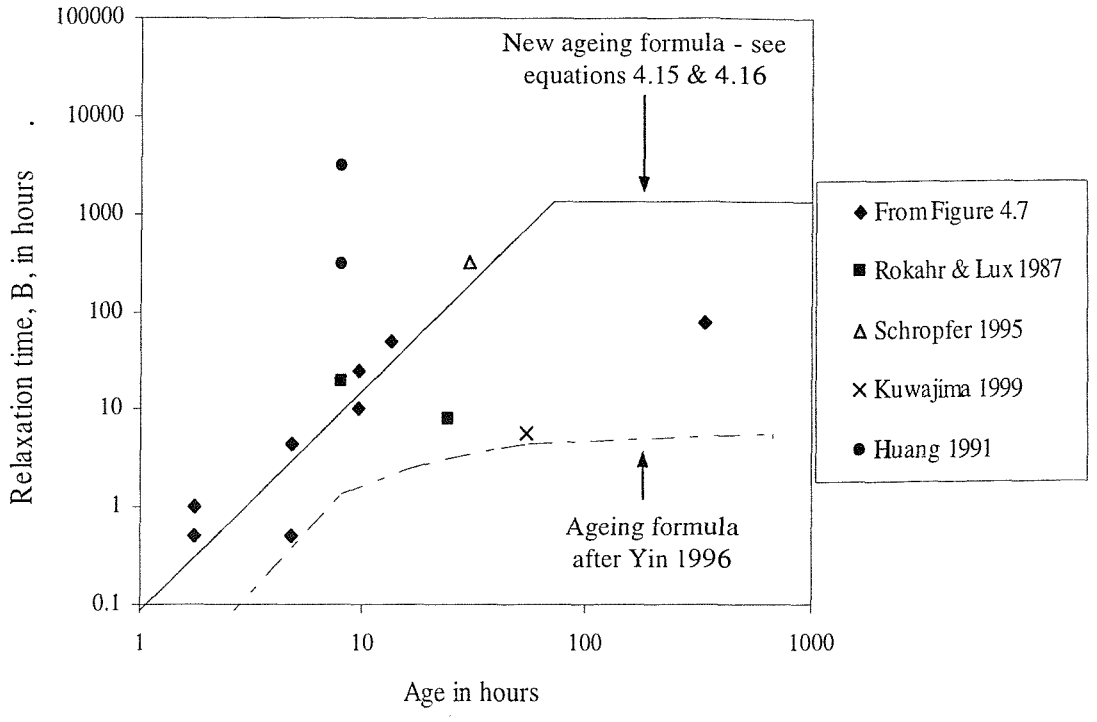

Predicted values from equations proposed by the authors listed in the key above as well as estimated values from the experimental data in Figure4.7.

Figure 4.11 Specific creep strain increment vs utilization factor

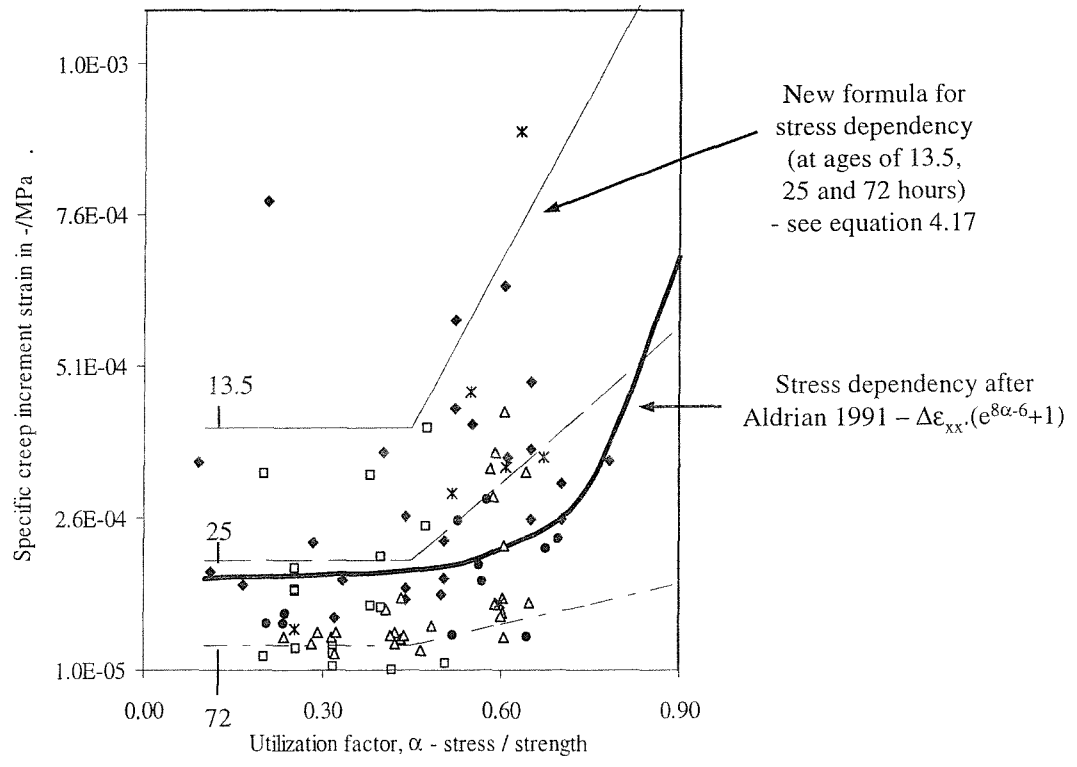

Data from Ding 1998, Huber 1991, Schmidt et al. 1987, Probst 1999

Figure 4.12 Comparison between FLAC models and test data from Huber 1991 (see Table 5.2 for key to models)

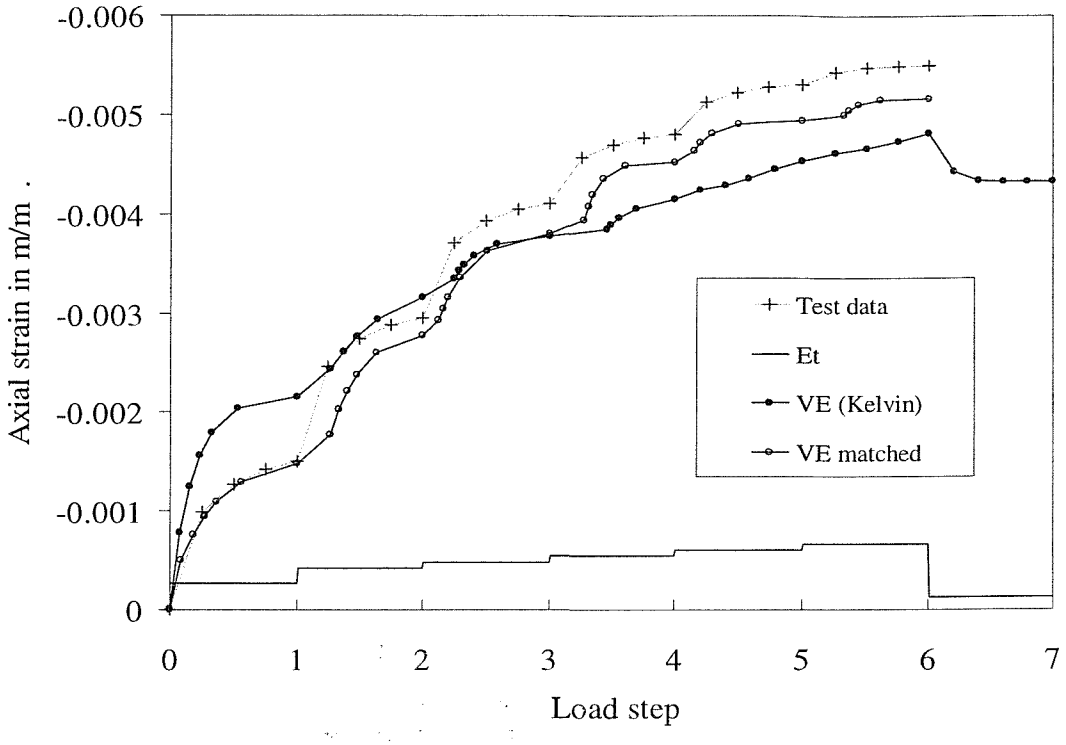

Figure 4.13 Hypothetical Modulus of Elasticity

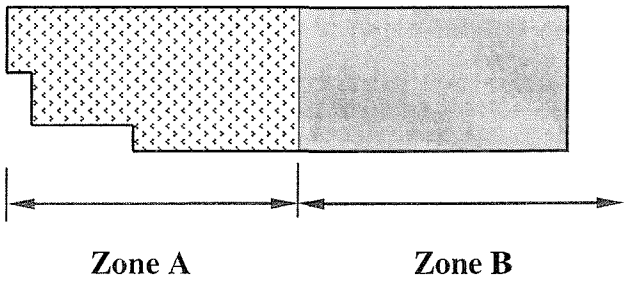

Zone A (from face to 1 diameter behind invert closure. This is the same as Zones I & II in the HEX monitoring system which were the areas of "Green" sprayed concrete) Here the concrete is young (aged less than 125 hours).

E = 7.5 GPa ~ E_T at 60 hours / 2.4
fc = 5.0 MPa ~ 0.67 x characteristic strength at 60 hours

Zone B (from 1 diameter behind invert closure. This is the same as Zone III in the HEX monitoring system which was the areas of hardened sprayed concrete). Here the concrete is aged more than 125 hours.

E = 15.0 GPa ~ E_T at 60 hours / 1.8
fc = 16.75 MPa ~ 0.67 x characteristic strength at 28 days

5 NUMERICAL MODELLING OF LABORATORY TESTS

The aims of this stage of the research were:

- to demonstrate the viability of modelling a tunnel lining ring using zones and
- to examine the effects of modelling the sprayed concrete with different constitutive models,

using the simplified case of a large-scale laboratory load test on a ring of sprayed concrete (see Chapter 3). Following from the conclusions of Chapter 2, as a step to improve the numerical analysis of tunnel linings, it is logical to investigate the role of the constitutive model for the sprayed concrete. From the literature review, the key aspects of the material behaviour appeared to be:

- ageing of material properties;
- nonlinear stress-strain behaviour;
- creep and
- shrinkage.

A secondary purpose of this modelling was to test and de-bug the new user-defined constitutive models in FLAC3D. Chapter 4 contains details of the chosen constitutive models.

5.1 Model development

5.1.1 Geometry & boundary conditions

Making use of symmetry, one quadrant of the ring was modelled (see Figure 5.1).

Boundary conditions - The 3D plane strain model, which lay in the X-Z plane, was supported with rollers at both ends and restrained from moving in the Y-direction on the top and bottom surfaces. As a general check, the test was also modelled using the 2D version of FLAC. The 2D and 3D models were found to agree to within 5 % (for axial loads in the ring and for radial displacements).

In the actual experiments a heavy steel top-plate provided the vertical confinement. So a more accurate modelling would have been to apply the dead-weight to the top of the mesh.

Discretization - (Finite element) Shell elements are available in FLAC but only as linear elastic elements. Therefore zones were used to model the lining. The use of zones leads to errors in the bending stiffness, in addition to the geometrical error that one would expect due to modelling a circle as a series of straight-sided elements. These errors were examined using a simpler model – a weightless circular ring, loaded at top and bottom by a point load under plane stress conditions. In the model the ring has an external radius of 1.375 m, a thickness of 0.145 m and a depth of 0.05 m. The Young's modulus is 25 GPa, Poisson's ratio of 0.2 and the point load is 100 kN. Figure 5.2 shows the variation in error depending on discretization, compared to the analytical solution by Sturmath (1993). By interpolation from the data, a discretization of 3 zones radially and 30 circumferentially per quadrant for the sprayed concrete was chosen as a reasonable compromise, bearing in mind that this discretization was to be used later in a full 3D model of a tunnel. Table 5.1 summarises the expected errors. The aspect ratios of the zones range between 1:1.4 to 1:2.

Table 5.1: Estimated errors (at axis) due to discretization with 3 zones radially & 30 zones circumferentially

Hoop axial force [71]	Bending moment	Radial displacement
-10 %	-30 %	-20 %

For the chosen discretization, the errors when using shell elements (compared to an analytical solution) were less than 1% for displacements and axial force and about 12 % for bending moments. The errors in the model of the load test should be less than the values in Table 5.1 since the ring is thicker and bending is a secondary effect, in comparison to the overall compression of the ring.

Table 5.2 List of analyses run

Analysis ID	Sprayed concrete model	Description
E-	E-	Linear elastic, constant stiffness = 26.0 GPa (28 day value)
Et	Et	Age dependent elastic modulus acc. to Aydan *et al.* (1992a) - see 4.3.1
DP	DP	Ageing linear elastic perfectly plastic model (Drucker-Prager); yield strength = 0.40 ultimate strength - see 4.3.2
MC	MC	Ageing linear elastic perfectly plastic model (Mohr-Coulomb); yield strength = 0.40 ultimate strength - see 4.3.2
MCSS	MC SS	Ageing strain-hardening plasticity model (Mohr-Coulomb) - see 4.3.2 and 4.3.3.1.
NLE	NLE	Ageing nonlinear elastic model after Kotsovos & Newman (1978) - see 4.3.3.2
VE1	VE 1	Viscoelastic Kelvin creep model – "best fit" ageing, acc. to equations 4.15 & 4.16
VE2	VE 2	Viscoelastic Kelvin creep model, VE1, with stress dependency, acc. to equation 4.17
VE3	VE 3	Viscoelastic Kelvin creep model – ageing after Yin (1996) acc. to equations 4.13 & 4.14
SHR	SHR	Ageing elastic model with shrinkage; ultimate shrinkage strain = 0.1 % - see 4.3.4
Et_e	Et	Exact dimensions of the ring - see 5.2.6
MCSS_e	MC SS	Exact dimensions of the ring - see 5.2.6
MCSS_r	MC SS	Peak strength factored by 0.45 in line with BS8110
E-_s	E-	Age-independent elastic model with shell elements
Et_lg	Et	3 reinforcing bars added to mimic a lattice girder
Et_c	Et	Stiffness of clay reduced to 25 MPa from 100 MPa

5.1.2 Analyses

The constitutive models for the sprayed concrete have been given abbreviations which will be used from this point on (see Table 5.2 & Chapter 4). Where possible the parameters for the models were taken from other Brite Euram tests on the same mix. Otherwise they were based

[71] The hoop force at the crown should be zero but the numerical model predicts compressive forces, i.e. overestimates the load there.

on a review of published data. In this work a single ("best estimate") set of material parameters has been used. A parameter study has not been undertaken since it is believed that the results are intuitively obvious in most cases. For example, increasing the creep strain rate would increase deformation.

5.2 Results & interim discussion

5.2.1 General behaviour

Figure 5.3 shows the deflected shape of the ring. Due to the asymmetrical load the ring deformed in bending as well as compressing. Figures 5.4 and 5.5 show the development of axial force and displacement with time. The load on the ring was increased in 4 increments at different ages (see Figure 3.7). Considering the end of load stage 4, Figures 5.6 – 5.8 show the variation in radial displacements, axial forces and bending moments around the ring. The values in these figures have been multiplied by correction factors to account for discretization errors (see Table 5.1).

There was little scope for stress redistribution within the system represented by the numerical model (& real test) since the clay annulus was thin and had a much lower stiffness than the sprayed concrete. Consequently one would not expect much variation in axial forces (see Figure 5.9). However the use of the different constitutive models for the sprayed concrete resulted in quite different predictions of bending moments and displacements (see Figure 5.9). Varying the constitutive model effectively changed the stiffness of the sprayed concrete. In this case, since features such as plasticity, ageing or creep led to a more "flexible" material, one would expect the bending moments to be lower and the displacements higher than the base case, E- model. This was observed to be the case.

5.2.2 Ageing elasticity

Figure 5.9 shows that, in this case, the increase of stiffness with age was one of the most influential factors on the axial forces and bending moments in the sprayed concrete. This was not surprising since the loads in the test were designed to keep the stresses well below the strength at all ages, for fear of failing the ring prematurely. However, it is worth noting that

the load at stage 4 corresponded to 80% of the full overburden pressure for a tunnel at a depth of 30m and so the loads were representative of the likely loading on a real tunnel lining. The effect of ageing was most noticeable during the first 3 load stages, i.e. while the ageing stiffness was less than 60% of the 28 day value - see Figure 5.10. This corresponded to the first 48 hours of the life of the sprayed concrete.

5.2.3 The effects of plasticity

During the load tests the loads were deliberately kept well below the failure strength of the sprayed concrete to prevent the ring collapsing. Therefore, if a linear elastic – perfectly plastic constitutive model with the yield strength set at the peak failure strength was used, there would be no yielding and the results would be the same as the linear elastic model. To investigate the effects of plasticity a set of three analyses were run with the yield strength set to 40% of the peak (uniaxial compressive) strength. The first two (DP and MC) were linear elastic – perfectly plastic (i.e. no hardening above 40% of the peak strength) while the final one was a linear elastic – strain hardening plastic model (MCSS), with strain hardening from 40% to 100% of the failure strength.

Despite the low utilization factors, the analyses performed using a Mohr-Coulomb yield criterion resulted in significant additional deformation (twice as much as the other models). The results from the Drucker–Prager model were basically the same as the age-dependent elastic model (Et), indicating limited yielding. Given that the concrete was generally under triaxial compression, one would expect the discrepancy between the Drucker-Prager and Mohr-Coulomb perfectly plastic models to be small (- the parameters for the former were set to match the Mohr-Coulomb model on the compressive meridians where the Lode angle = 60°). However, as Figure 5.11 shows the Lode angle is about 50°. At this angle the Mohr-Coulomb yield strength is about 85% of the Drucker-Prager yield strength. So a small difference in the constitutive model can have a considerable impact on the results of the model. As was explained in Chapter 2, the Drucker-Prager yield criterion is often used because it is simpler to implement in numerical models but the Mohr-Coulomb criterion reflects better the observed behaviour of concrete at low hydrostatic stress.

Adding strain-hardening behaviour to a plasticity model resulted in less deformation and higher loads in the lining compared to the linear elastic-perfectly plastic model (see Figure 5.9). In the perfectly plastic (MC) model, once the stress reached 40% of the strength the concrete yielded perfectly whereas in the strain-hardening model the stress continued to rise up to the peak strength. The effect of this yielding may also have been accentuated by the nature of the model, in that there was little scope for redistribution of the load from the lining back into the ground around it. The annulus of clay was quite thin and much softer than the sprayed concrete.

The utilization factor, α, (which was equal to the deviatoric stress, r, divided by current yield strength) was highest in the early load stages (Figure 5.11). The Et model predicted utilization factors of 0.46 in stage 1, falling to around 0.39 in the stages 2 to 4. The yield strength was set at 40% ultimate strength. Hence the behaviour was largely elastic and yielding in the plasticity models was most pronounced at the early ages - i.e. Load stages 1 & 2 (age = 0 to 17 hours) - see Figure 5.11. Unfortunately this is the time period for which the least information exists and therefore there is the most uncertainty about the material behaviour. The models and key parameters (e.g.: peak strain; ratio of yield strength to peak strength) have been shown to be suitable for sprayed concrete at ages above 12 hours (see section 4.3.3).

5.2.4 Nonlinear elasticity

There were two reasons for implementing a nonlinear elastic model. Firstly, it was thought that, despite being run as a FISH function, it might run faster than the strain-hardening plasticity model. The run times were 70% longer than the strain-hardening plasticity model, although the models required about the same number of cycles to reach equilibrium. Secondly, the nonlinear elastic model could be incorporated into other models, principally the creep models.

In the single-element models of triaxial and uniaxial compression tests (see Chapter 4), the nonlinear elastic model was seen to have a "stiffer" response to loading than the strainhardening plasticity model (MCSS). Broadly speaking this was also the case in the

numerical models of the large-scale load test. The axial forces and displacements were lower for the nonlinear elastic model (see Figures 5.6 & 5.7). The "softer" response of the strain-hardening model may be due to the high peak strains at early ages, which led to a more ductile behaviour above the yield point, compared to the nonlinear model.

5.2.5 Time-dependent behaviour

Despite the low utilization factors, the **creep** models predicted much larger deformations and lower bending moments. Once again, the axial force was only slightly reduced. As noted in section 4.3.5, there is considerable uncertainty over the creep capacity of sprayed concrete. The results of the numerical models varied significantly depending on the chosen model and its parameters (see Table 5.3). While the results here confirm the suggestion by advocates of sprayed concrete linings (e.g.: Rabcewicz 1969) that creep in the concrete reduces stress concentrations and bending moments, the challenge of quantifying this benefit with confidence remains. Bending moments are often the governing parameter in tunnel lining design.

It is worth noting that adding in stress dependency did increase deformations considerably (by 25 %) even at these relatively low utilization factors. The load in the lining was only slightly altered due to the limited scope for stress redistribution in the ground/lining system - see Table 5.3.

Table 5.3: Results of creep models normalised w.r.t. E- model

	Description of Kelvin model	Axial force in crown	Bending moment in crown	Radial displacement in crown
VE 1	"Best fit" ageing	0.90	0.64	4.80
VE 3	Ageing after Yin	0.83	0.47	5.79
VE 2	"Best fit" plus stress dependency	0.88	0.67	5.70

Shrinkage appeared to have little effect in the X-Z plane, although large tensile stresses were induced in the Y direction due to the enforced plane strain condition. Therefore shrinkage was not investigated any further.

5.2.6 Construction defects

Considering the middle of the test ring, the difference between the real dimensions of the ring and the design thickness was at most –19 % and was on average –6 % - see Table 5.4. Using a mesh with the real dimensions (i.e. the as-built dimensions at the middle of the ring) resulted in slightly more deformation – about 10% at the crown and 3% at the axis. The outcome was the same when both the linear elastic (Et) and plastic (MC SS) models were used. In this case the deviation from the exact dimensions does not seem to have had a significant impact on the predictions.

Table 5.4: Exact dimensions of the test ring

Angle	0	16.36	32.73	49.09	65.45	81.82	98.18
Radius in m	Crown					Axis	
Intrados	1.2770	1.2845	1.2620	1.2670	1.2670	1.2545	1.2470
Extrados	1.3995	1.4020	1.4070	1.4045	1.3920	1.4045	1.4020

5.2.7 Behaviour in tension

The ring in the Et model was in compression at all times except for the final load stage, when the load was removed completely. Even then the tensile stresses were less than the tensile strength. In the shrinkage model there was more tension but it was limited and always remained less than 50 % of the tensile strength. Therefore the behaviour in tension has not been investigated in more detail.

5.2.8 Reinforcement

The test ring was reinforced with steel fibres only. Tunnel linings often include lattice girders, which are used to support steel mesh and to ensure that the tunnel profile is correct (see Figure 1.6). The girders are not normally included in design calculations because, if one

considers the whole advance - typically 1.0 m or more - the girder only contributes about 10 % to the bending stiffness at an age of 1 day (and progressively less thereafter). At earlier ages the girder makes a larger contribution. Model Et_lg included a scaled down version of a lattice girder modelled by 3 sets of cable elements - see Figure 5.12. The elements represented steel bars of 9 and 12 mm in diameter embedded in the concrete. The stiffness of the steel was 210 GPa and a perfect bond to the concrete was assumed. Figures 5.12 and 5.13 show that the lattice girder made little difference at any age and the stresses in the lining remained fairly uniform.

5.2.9 Behaviour of the clay annulus

As was mentioned earlier, there were doubts about the mechanical properties of the clay annulus around the ring. In the base case the material properties of the clay were assumed to be as follows: a Young's modulus of 100 MPa and a Poisson's ratio of 0.15. Model Et_c had an age-dependent elastic model for the concrete like the base case (Et) but the stiffness of the clay was reduced from 100 MPa to 25 MPa. Because of the limited scope for redistribution of stress, the axial loads in the ring only increased slightly. The bending moments increased by 30 % and the deflections of the ring increased by 50 to 100 % compared with Et.

5.2.10 Comparison with test results

The irregular pattern of measured deformations (see Figure 5.6) suggests that the actual loading applied may have been less uniform than intended. Specifically the radial movement between 60 and 90° from the axis was almost constant. One would have expected an even variation in deformation with the angle from the axis. This may have been because of irregularities in the clay annulus or the loading apparatus. No cracking that might have led to localisation of deformation was observed.

While the displacements predicted by the numerical models were of the right order of magnitude, none of the models predicted the pattern of movement correctly (see Figure 5.6). The change from convergence (positive radial displacement) to divergence (negative radial displacement) occurred at about 30° from the axis in the real case, whereas the elastic models (E- & Et) predicted it at about 38 to 40° and the MCSS plasticity model predicted it at 28°.

One may note that the displacement measurements (and the strain gauges) appear to show a considerable amount of time-dependent movement. Typically this may be more than 50% of the total movement. However, the creep models overpredicted the displacements of the ring. Therefore one could speculate that the elastic stiffness of the sprayed concrete and / or the clay in the numerical model was too low (particularly at early ages – see Figure 5.10).

Considering the strains in the sprayed concrete ring in the hoop direction, the age dependent elastic model (Et) generally predicts strains that were higher than those recorded by the strain gauges (see Figure 5.14). However, the Et model appeared to slightly underpredict the displacements, compared to the recorded values. Some of the strain gauges failed completely and the pattern of results seems incoherent. If one assumes that the deformation results were more reliable (given the simpler measurement method), one might conclude that the strain gauges underestimated the actual strain in the ring.

5.3 Interim conclusions

The conclusions below were carried forward to next stage. Firstly, regarding modelling of sprayed concrete linings:

- A ring of sprayed concrete can be modelled using zones;
- The use of zones introduces discretization errors – see Table 5.1 & Figure 5.2 – but these can be estimated and corrected for.

Secondly regarding the influence of the constitutive model:

- The constitutive model of sprayed concrete can have a large influence over the predicted behaviour – even at low utilization factors;
- The influence of the constitutive model is most pronounced at the early ages – i.e. ages less than 48 hours;
- The details of the constitutive model can be as important as the type of model - e.g.: the choice of yield criteria; the hardening behaviour above the yield point; the ageing

of creep parameters - and can lead to large differences between models of the same type;

- Bending moments and displacements may be influenced more than axial forces;
- The more "flexible" the constitutive model of sprayed concrete, the more displacement is predicted and the lower the loads in the lining;
- Incorporating the ageing of the elastic stiffness, the nonlinear stress-strain behaviour and creep into the constitutive model for sprayed concrete all lead to more "flexible" behaviour;
- (In general) the lowest bending moments and axial forces and the highest deformations were predicted by the viscoelastic creep model (VE3) with ageing, after Yin (1996).

Finally, regarding possible simplifications:

- The contribution of the lattice girder can be ignored;
- Shrinkage and the tensile behaviour of sprayed concrete beyond the tensile strength can be ignored.

Given the uncertainties surrounding the original test (e.g.: concerning the loading, the reliability of the instrumentation and properties of the two materials in the test), it is impossible to make any firm conclusions about which constitutive model is best. The experimental data suggests that creep is a significant factor.

Figure 5.1 FLAC mesh for Brite Euram ring

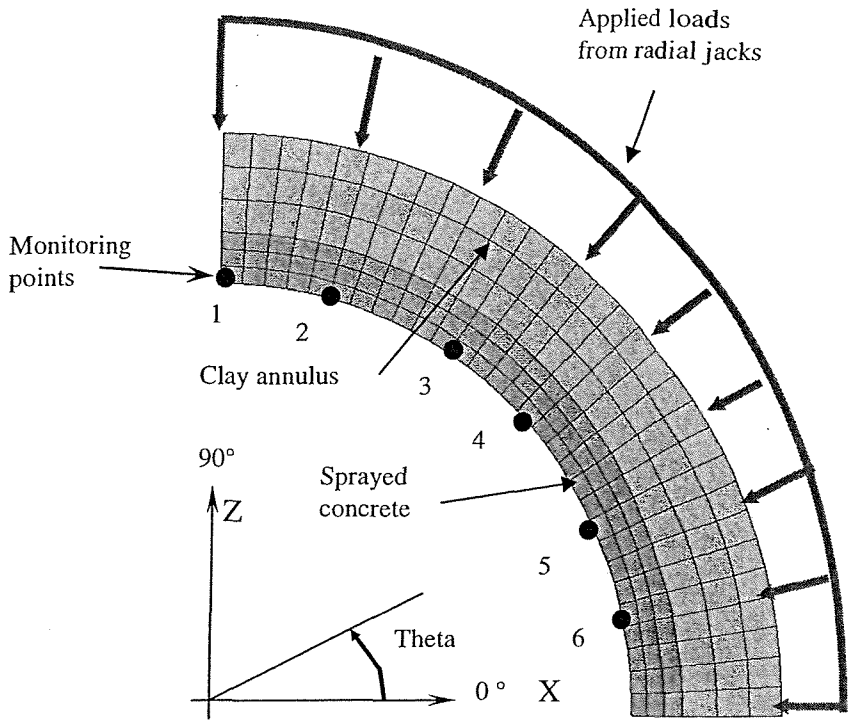

Figure 5.2 Point load on a circular ring under plane stress and error in FLAC predictions vs analytical solution at axis

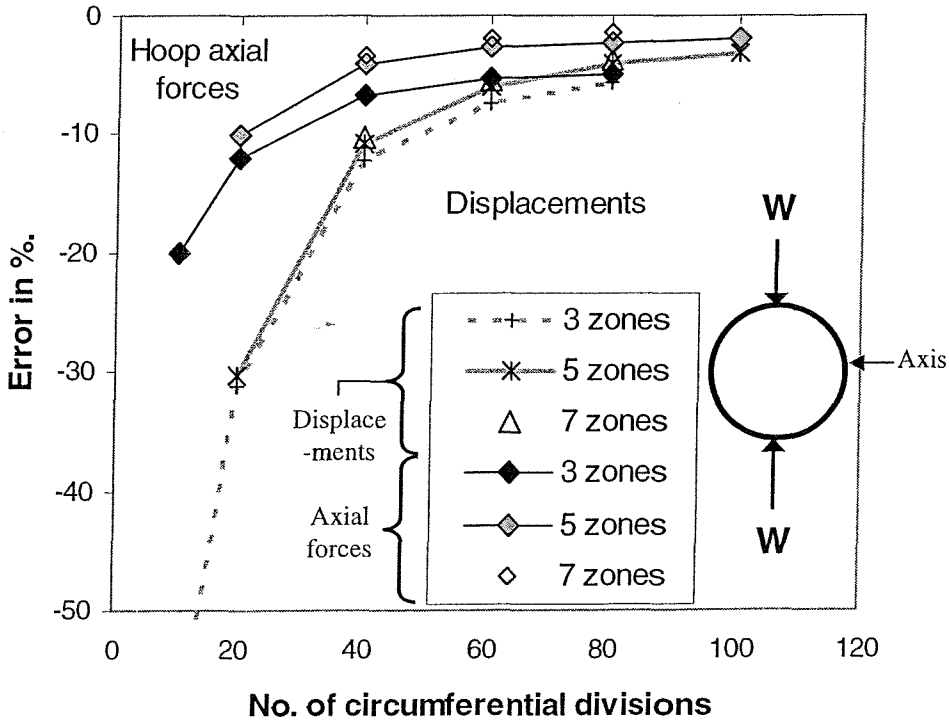

Figure 5.3 Distorted shape of the FLAC mesh

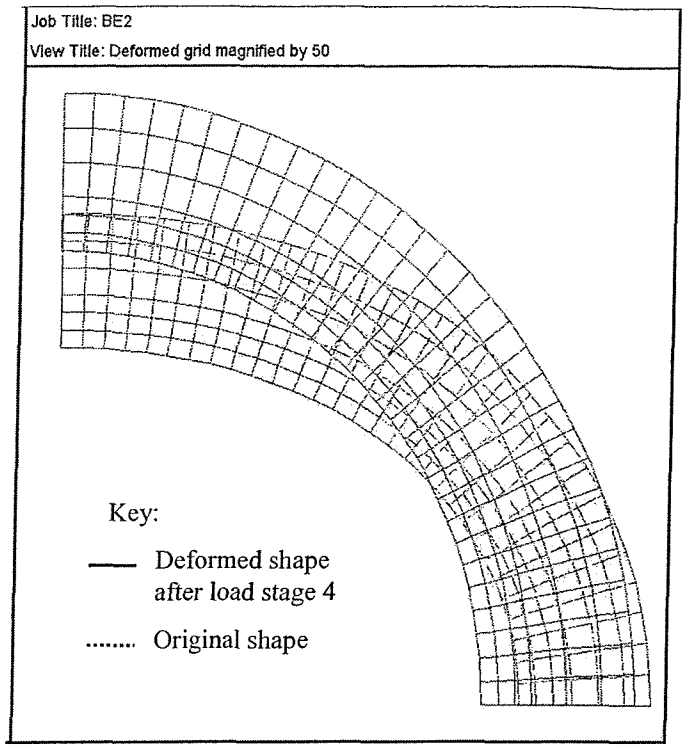

Figure 5.4 Predicted axial force in circumferential (hoop) direction vs time

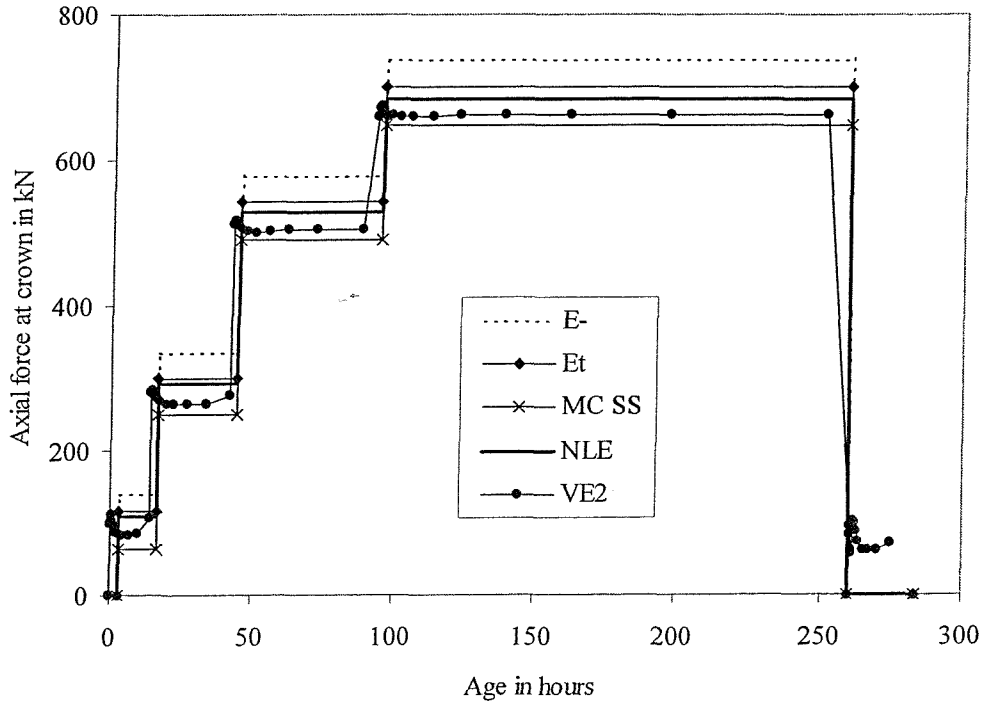

Figure 5.5 Predicted radial displacement at crown vs time

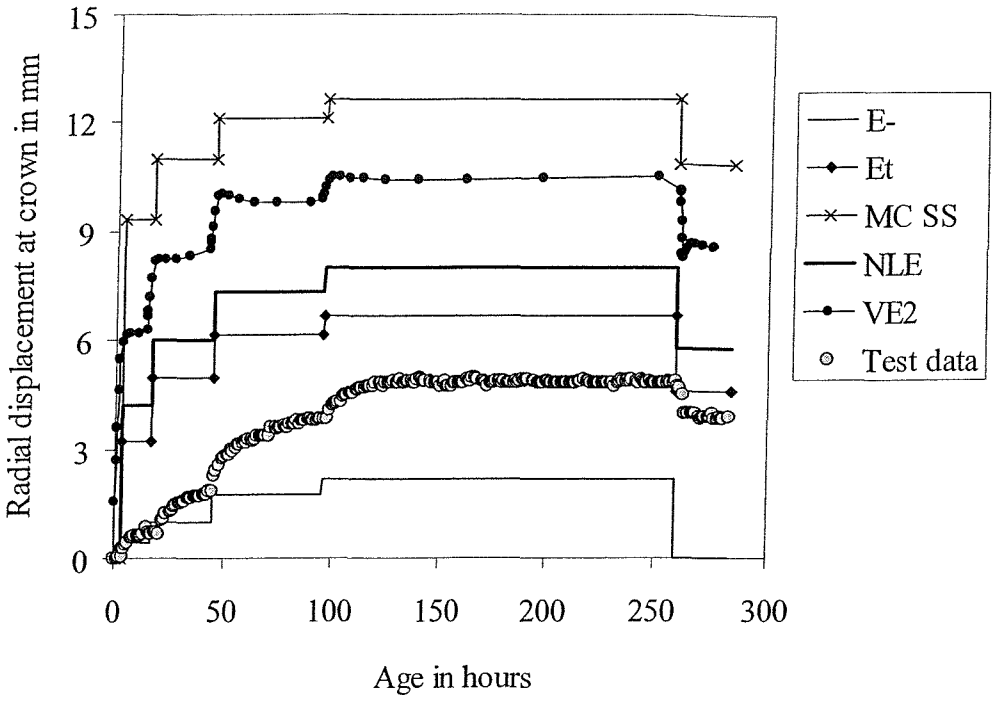

Figure 5.6 Predicted radial displacements at the end of load stage 4

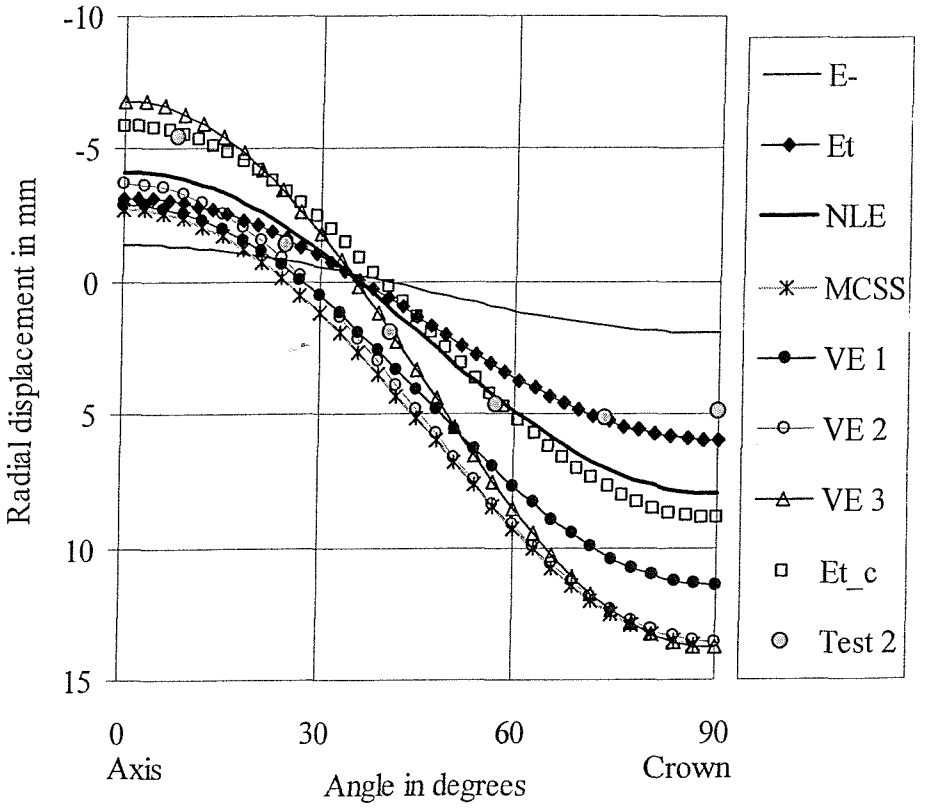

Figure 5.7 Predicted axial forces at the end of load stage 4

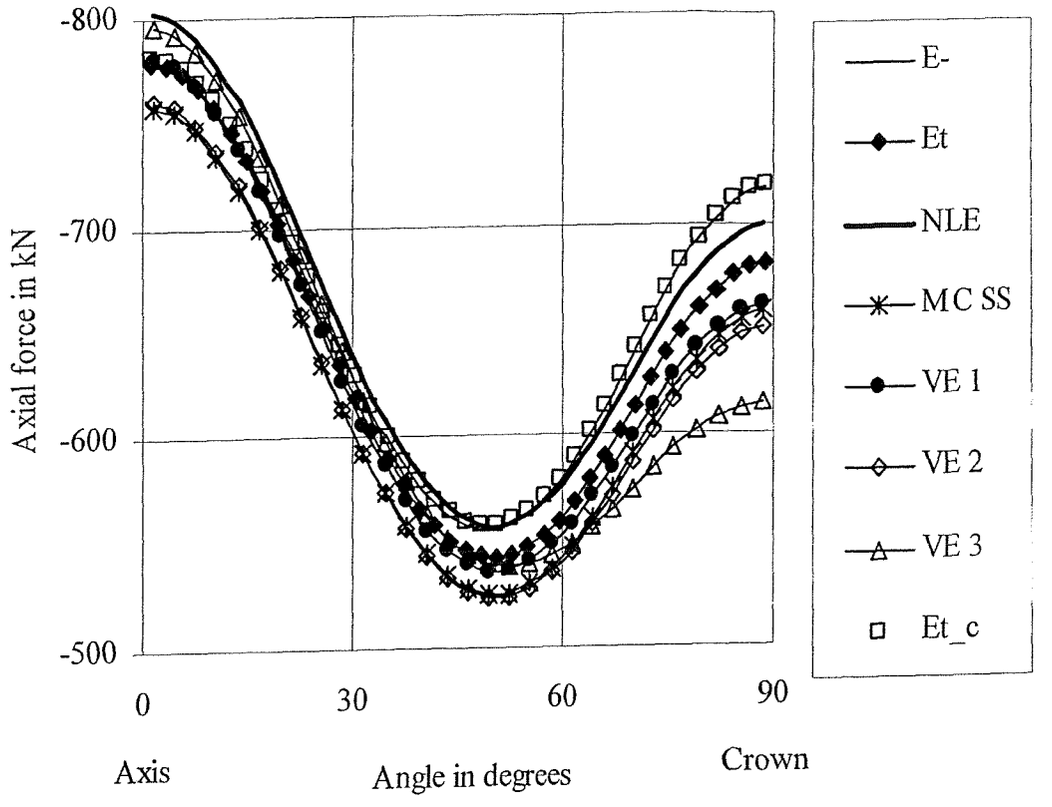

Figure 5.8 Predicted bending moments at the end of load stage 4

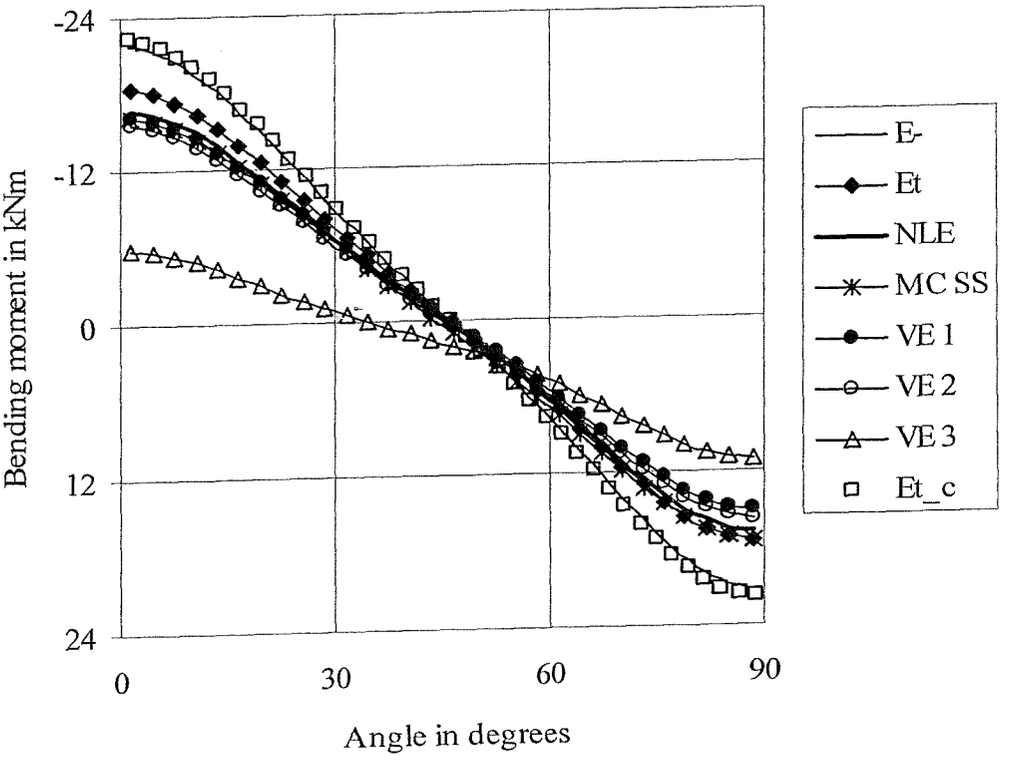

Figure 5.9 Results at the end of load stage 4, normalized w.r.t. model E- (sprayed concrete model = age independent stiff elastic model)

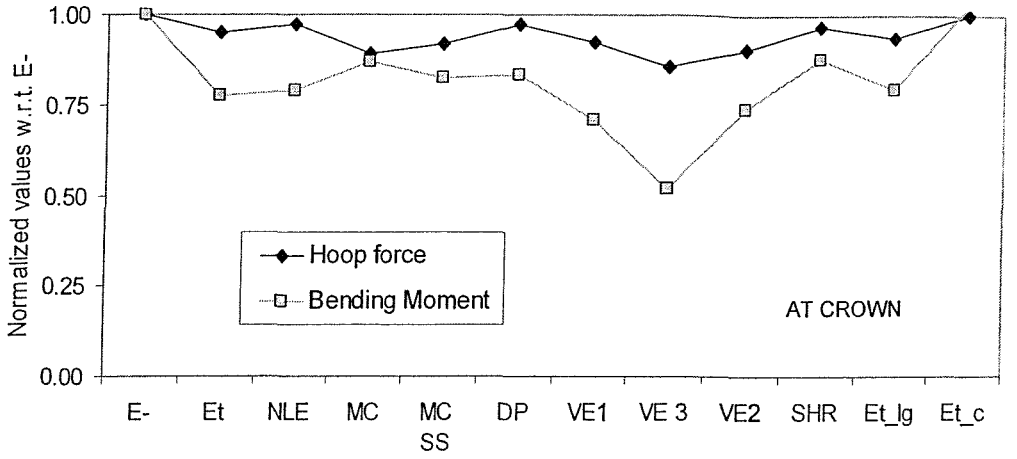

(a) Axial forces & bending moments in circumferential direction at the crown

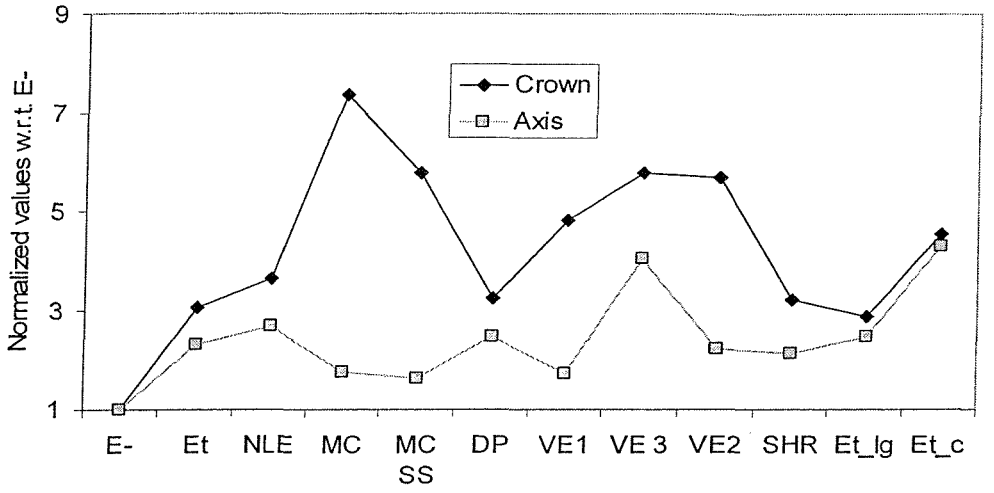

(b) Radial displacements at the crown & axis

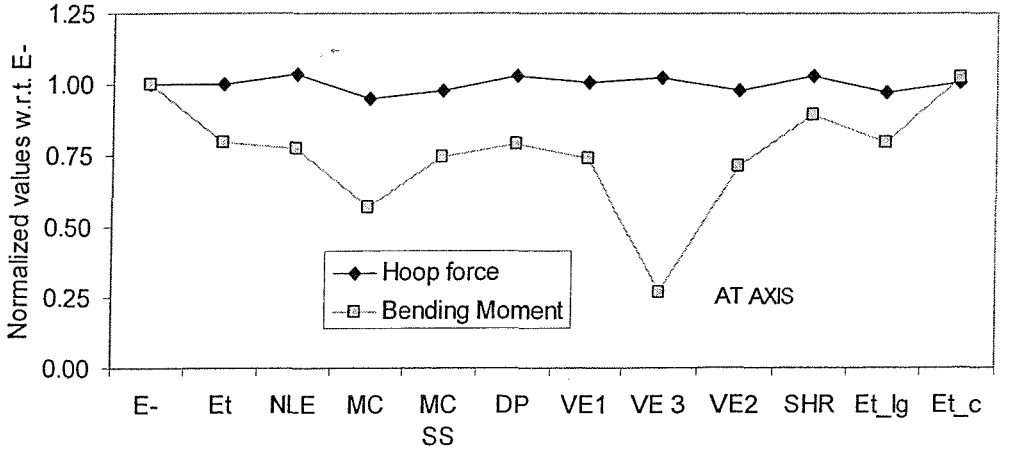

(c) Axial forces & bending moments in circumferential direction at axis

Figure 5.10 Increments in radial crown displacements - predicted & actual

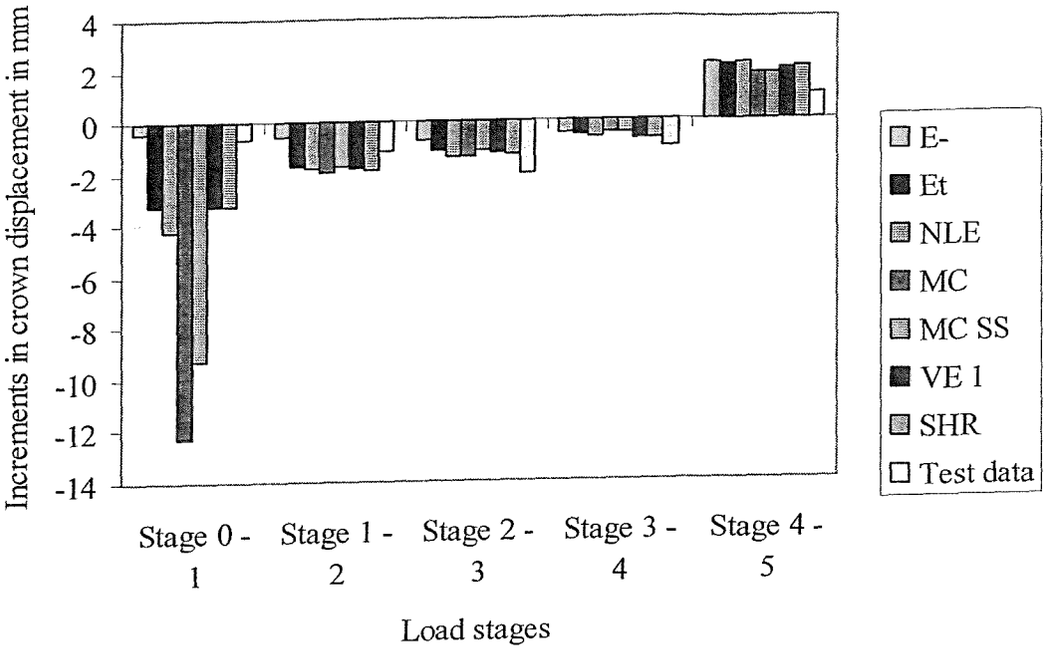

Figure 5.11 Yield surfaces in the deviatoric stress plane at different load stages and predicted stresses from FLAC models

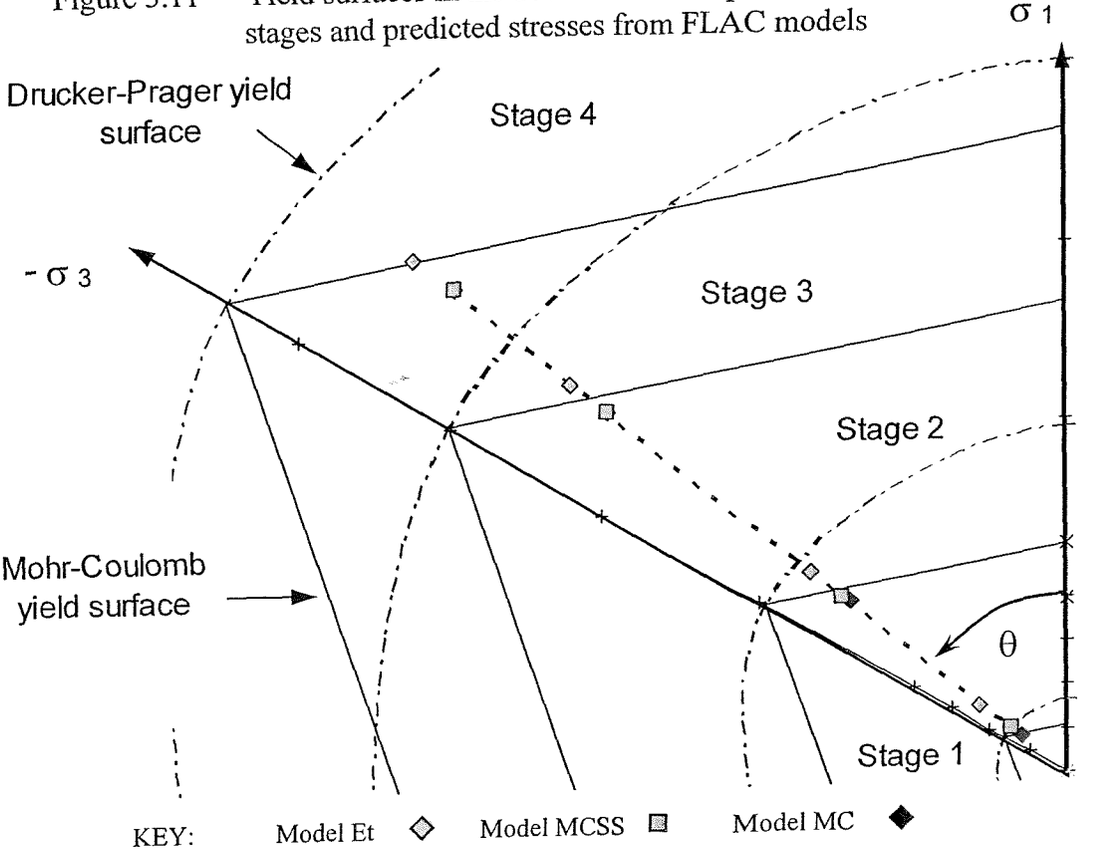

Figure 5.12 Predicted hoop stress in a ring with a lattice girder

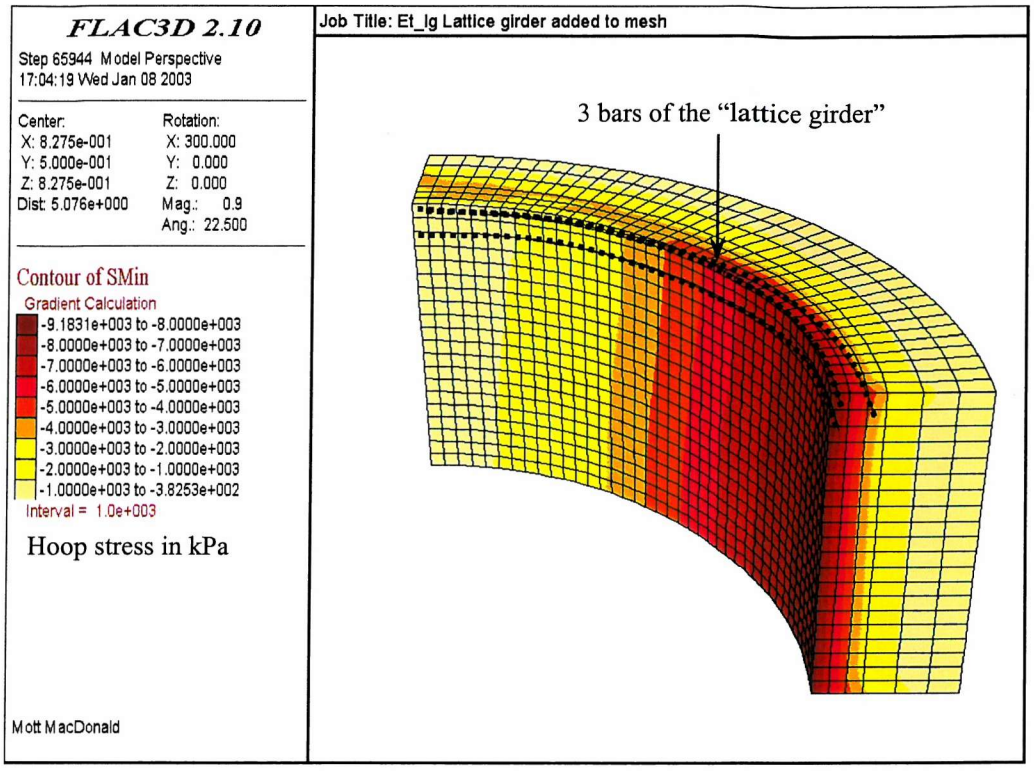

Figure 5.13 The effect of a lattice girder on displacements of the ring (at the end of load stage 4)

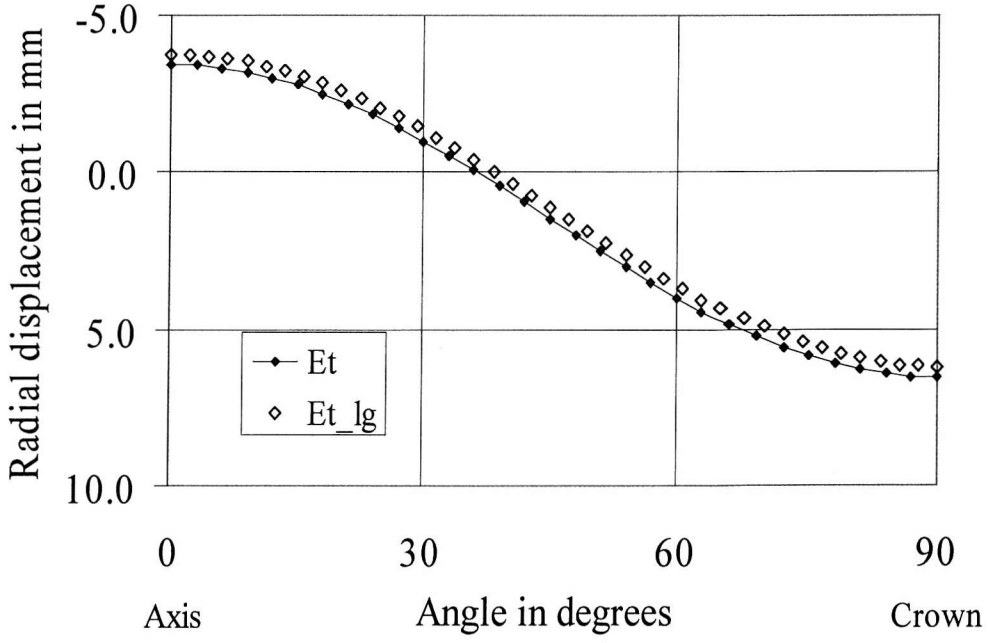

Figure 5.14 Circumferential strain after load stage 4 - predicted & actual

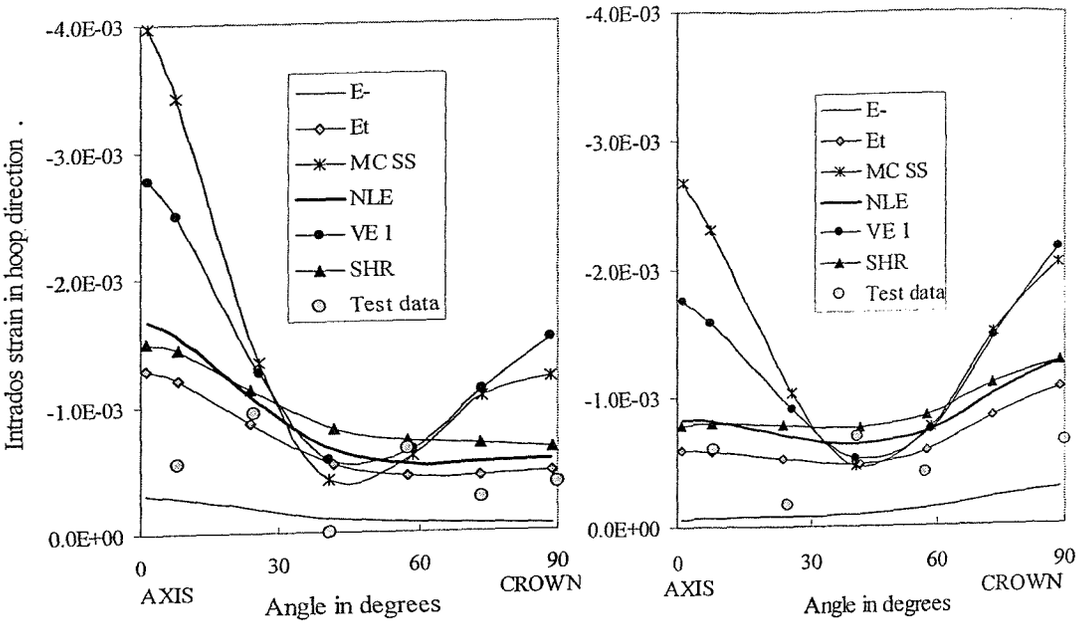

(a) Intrados

(b) Extrados

6 NUMERICAL MODELLING OF TUNNELS

6.1 Introduction

The goal of this second set of numerical analyses was to assess, in a semi-quantitative manner, the influence of different sprayed concrete material models and the influence of construction defects on the behaviour of a SCL tunnel in a full 3D numerical model. To date few similar comparative studies have been done (e.g.: Duddeck & Erdmann 1985 or Yin 1996 for single tunnels and Soliman *et al.* 1994 for two adjacent tunnels). No previous work has examined the question of material models for sprayed concrete as thoroughly. The constitutive model for the ground was also varied. This chapter will presents the numerical models used, the analyses performed, and typical results from the base case model. Results from the other models will be presented and discussed in the following chapter.

The individual analyses have been assigned a code as follows (see Tables 6.1 – 6.4):

(Geometry) _ (Lining model id) _ (Ground model id no.) (**)

e.g.: H_Et_4 = Hex exact geometry, age dependent elastic lining & ground model 4.

Where necessary additional letters or numbers have been added (**) to distinguish the analyses. These have been added only where differences from the base cases exist. Appendix G contains a complete list of the analyses run. The abbreviations for the constitutive models for the sprayed concrete may be used in the text and figures.

Table 6.1: Model tunnel geometry

Abbreviation	Description
H	The exact cross-sectional geometry for the HEX platform tunnel; face area = 61 m^2; lining thickness = 0.30 m
N	Circular cross-sectional geometry with the same face area as the HEX platform tunnel; external radius = 4.40 m; lining thickness 0.30 m
N* [72]	Circular cross-sectional geometry with the same radius as HEX concourse tunnel top heading – face area = 54 m^2; external radius = 4.15 m; lining thickness 0.30 m

Table 6.2: Sprayed concrete constitutive models

Abbreviation	Description – see also Chapter 4
E-	Linear elastic, constant stiffness = 28 day value
Et	Linear elastic, age-dependent stiffness – see 4.3.1
HME	Hypothetical Modulus of Elasticity – see 4.3.6
MCSS	Strain-hardening plasticity model (Mohr-Coulomb) – see 4.3.3.1
NLE	Nonlinear elastic model - Kotsovos & Newman (1978) – see 4.3.3.2
VE 1	Visco-elastic "Kelvin" creep model - stress independent – see 4.3.5.3
VE 2	Visco-elastic "Kelvin" creep model - stress dependent – see 4.3.5.5
VE 3	Visco-elastic "Kelvin" creep model after Yin (1996) – see 4.3.5.3
JR	MCSS model but strength reduced by 50% on radial joints
JL	MCSS model but strength reduced by 50% on longitudinal joints
J	MCSS model but strength reduced by 50% on radial & long. joints

[72] In the early part of the study a simpler model was used – see section 6.2.

Table 6.3: Geotechnical constitutive models

Abbreviation	Description – see 6.3.3
0	Isotropic linear elastic – "soft" – Eu = 600*Cu
1	Isotropic linear elastic perfectly plastic (Tresca) – Eu = 600*Cu
2	Transversely anisotropic linear elastic – Evu = 600*Cu
3	Transversely anisotropic nonlinear elastic – Evu max ~ 1500*Cu
4	Isotropic nonlinear elastoplastic (Tresca) – Emax = 1500*Cu
5	Isotropic linear elastic perfectly plastic – "stiff" – Eu = 1500*Cu

Table 6.4: Variations in construction sequence

Abbreviation	Description – see 6.3.2
A_0.5	Advance length of 0.5 m
K_1.5	Constant K_0 value = 1.5
S_2.0	Advance rate = 2.0 m / day
X_4.5	Ring closure distance = 4.5 m

6.2 Base case

The base case was: **H_Et_4**

This simulated a tunnel with the exact HEX Platform tunnel cross-section (see Figure 3.10) and a lining thickness of 0.30 m. The construction sequence is shown in Figure 6.1– an advance length of 1.0 m and a rate of 1.20m per day, with the invert closed in an average of 5 m from the Top Heading. The lining model was an age-dependent linear elastic model - Et. The ground model – 4 - was a strain-softening elastoplastic isotropic soil model with properties that vary with depth. The behaviour was assumed to be undrained (see 6.3.3). The initial stress state in the ground was based on a non-uniform K_0 distribution – see Figure 6.2.

The N* runs differed from the base case in more than just the geometry. To simplify matters, a constant K_0 of 1.50 was adopted. The 2.0m of gravels above the London Clay were modelled as a uniform surcharge. To reduce the number of calculation steps the advance

length was 1.5 m. Based on the Concourse tunnel, the distance to ring closure was 7.5 m and the advance rate was 3.0 m/day.

6.3 Model development

6.3.1 Geometry, boundary & initial conditions

Geometry

Figure 6.3 shows the mesh around the tunnel and Figure 6.4 shows the cross-section of the tunnel. The boundaries were set in line with the recommendations in Table 2.8. The X, Y, Z dimensions, in multiples of the tunnel radius, are 13, 21 & 10 respectively, where the Z dimension is the depth of the mesh below tunnel axis. If the boundaries were too close they would have affected the results at the point of interest – the tunnel face. This was checked by performing a simplified axisymmetric FLAC analysis (see Figure 6.5 & FLAC Manual Example 8 (Itasca 1998)) and comparing the results with an analytical solution (Panet 1979). The average errors for radial displacement of the ground ahead of the tunnel and the unlined tunnel itself were less than 0.25 % (see Figure 6.6), indicating that these boundary locations were far enough away.

Discretization

The base case model had 32000 zones and took between 1 ½ and 3 days to run on an 800 MHz PC, depending on the constitutive models used. Since computing power is still limited, when choosing the level of discretization a compromise must be struck between the desire to minimise discretization errors and the need for reasonably short run-times. Figure 6.4 shows the mesh around the tunnel in detail. Significant re-meshing of the basic FLAC3D "primitives" – the building blocks of zones for 3D meshes - was required using FISH routines to optimise the shape and number of the zones near to the tunnel. Since the changes in strain are greatest around the tunnel the mesh should be finest in this area.

The tunnel lining was modelled with 40 zones in the circumferential direction per quadrant and 3 zones in the radial direction. According to the earlier investigation of discretization (see 5.1.1), the errors due to this discretization have been estimated (see Table 6.5). Circular

geometries for the lining were used as well as the exact shape, in order to determine the importance of this approximation. Modelling the exact shape increases the time required for pre- and post-processing.

Table 6.5: Estimated errors due to discretization with zones (at axis)

Axial force	Bending moment	Radial displacement
-7 %	-20 %	-12 %

The discretization was also checked using a simplified, plane strain FLAC model (see Figures 6.7 & 6.8 and Flac3D Manual Verification Example 8 (Itasca 1997)) for which an analytical solution exists (Einstein & Schwartz 1979). Both shells and zones were used to model the lining (see Table 6.6). Compared to the basic FLAC mesh, the new mesh performed marginally better in matching the analytical solution. This was despite the use of the Attach command, which allows regions of different grid densities to be joined together. No adverse effects due to the use of the Attach command were observed.

Table 6.6: Average errors compared to analytical solution

Lining [73]	Axial force	Bending moment	Radial displacement
Shells	-0.8 %	-19.7 % [74]	-0.6 %
Zones	9.7 %	-22.7 %	-6.5 %

In terms of longitudinal discretization there was a finer region with 0.5m long zones in the centre of the mesh. This region was sized at about 4 tunnel diameters in length so that it was long enough for the steady state stress distribution to be established before the change to the coarser longitudinal discretization. The effects of this discretization were checked using an

[73] With 40 divisions circumferentially and, for the zones, 3 zones radially.

[74] The relatively large error in bending moments is to a large degree due to the size of the model in comparison with the analytical solution which assumes an infinite continuum (Itasca 1998).

axisymmetric analysis (see Figure 6.5 & FLAC Manual Example 8 (Itasca 1998)). No adverse effects were observed.

Boundary conditions

Movement perpendicular to the X and Y boundaries was fixed. Both fixed stress and displacement boundary conditions were used in the axisymmetric test case and the results were found to be the same. Displacements at the bottom of the mesh were fully fixed. A uniform surcharge of 60 kPa was applied to the top of the mesh to represent the loading from buildings above.

Initial stress state

Before the tunnel was excavated the initial stresses in the ground were introduced and the model cycled to equilibrium. A non-linear K_0 distribution was used based on the actual and maximum overconsolidation ratio experienced by the ground (see Figure 6.2), after Mayne & Kulhawy (1982). This produced a K_0 profile that initially increased with depth from the low K_0 of 0.40 in the overlying gravels to a peak value of 1.43 and then declined with increasing depth. This is consistent with the experience of London Clay, which has been overconsolidated by overburden that has since been removed.

The N* runs used a constant K_0 value of 1.50 which is at the higher end of the range measured (see Figure 2.37). Gourvenec *et al.* (1999) recommended an average value of 1.30; Harrison (1995) recommended 1.50. Other authors have examined the effect of K_0 at values less than 1.50 (e.g.: Gunn 1993, Addenbrooke 1996, Krenn 1999, van der Berg 1999). Typically SCL designers adopt a constant K_0 value of between 0.8 and 1.2 for London Clay.

6.3.2 Construction sequence

Figure 6.1 shows the construction sequence for the base case. The advance length was 1.0 m and the distance from the Top Heading face to the closed Invert (the Ring Closure Distance – RCD) varied from 4.0 to 6.0 m. The advance rate was 1.2 m/day. The sequence differed from the HEX Platform tunnel in a few respects.

Firstly, the sequence was simplified to reduce the number of calculation steps. In the numerical model one Top Heading and one Bench section were excavated together, followed by another Top Heading and Bench and then a double Invert section was excavated.

During an excavation stage, the ground zones in the next advance length were nulled and lining zones were activated in the advance length behind it. If the lining had been activated within the new advance length, this would have been similar to "wishing-in-place" [75] the lining, which would have reduced the predicted ground movements. The sequential construction of the lining increased the computing runtime by a factor of 11 times compared to an analysis in which the lining is "wished-in-place" in one stage.

Three key parameters of the construction sequence were varied – advance rate (AR), advance length (AL) and ring closure distance (RCD) – within realistic ranges.

The advance length was varied between 0.50m and 2.00m to see if there is an optimum advance length that minimises load on the lining. Table 6.7 contains additional information on these runs. In the main series of analyses, the advance rates were adjusted to account for the increased volume of each round. It was assumed that the time to fix the mesh and set the lattice girder was constant and the remainder of the cycle time was scaled proportionally according to the volume excavated.

While the advance length was varied the ring closure distance was maintained at an average of 4 advance lengths (and therefore varied). The ring closure distance was also varied at constant advance rate and constant advance length (see Table 6.7). On average at the HEX Platform tunnels the ring closure distance was 4.5 m (in 4.65 days). A variety of different advance rates and ring closure distances were used in the initial N* analyses too.

Table 6.7: Variations in advance rate, length & distance to ring closure

Run	Advance rate in m/day	Advance length in m	Average distance to closure of ring in m
H_Et_4_A_0.5	1.00	0.5	2.0
H_Et_4 ***(base case)***	1.20	1.0	4.0
H_Et_4_A_2.0	1.33	2.0	8.0
H_Et_4_X_6.0	1.20	1.0	6.0
H_Et_4_X_8.0	1.20	1.0	8.0
N*_Et_4	3.00	1.5	7.5
N*_Et_4_S_1.2	1.20	1.5	7.5
N*_Et_4_S_0.5	0.50	1.5	7.5
N*_Et_4_X_4.5	3.00	1.5	4.5

6.3.3 Constitutive modelling of the ground

As Figure 6.3 shows, the basic numerical model includes the London Clay and overlying gravels (see Figure 3.11 for the HEX geological strata). In keeping with the construction period of the tunnel and the low permeability of London Clay ($k \sim 10^{-10}$ m/s), the analyses assumed undrained behaviour. This study was concerned with only the short-term case. Total stress analyses only were performed. Calculating information on pore pressures and effective stresses increases the run-time.

Section 6.3.1 includes a description of the initial stress state in the ground. The K_0 profile varied with depth, with the highest values in the region between the tunnel and the surface (see Figure 6.2). Before the tunnel was excavated these initial stresses are introduced and the model was cycled to equilibrium. The displacements were checked to ensure that no yielding occurred during this stage.

[75] i.e. inserting the lining into the ground without permitting any movement or stress relief first.

Table 6.3 contains a brief description of the geotechnical models that have been used in this study. The nonlinear models 3 and 4 have been tested in a single element FLAC model representing a uniaxial compressive test, in order to compare their performance with experimental data (see Figures 2.33 & 2.36). Where relevant, the main properties of all the models varied with depth. The models are outlined below, with a complete listing of the properties in Appendix F.

Geotechnical model 0 – Linear elastic isotropic (soft)

The simplest model was a linear elastic model, with an isotropic stiffness that increased with depth. The stiffness was that measured at a deviatoric strain of approximately 0.1% (Eu = 600*Cu).

Geotechnical model 1 – Linear elastic perfectly plastic isotropic (soft)

In this model, a Tresca yield criterion was added to linear elastic model, with the undrained strength according to equation 2.4 (Cu = 0.67*(50+8z)). The stiffness was that measured at a deviatoric strain of approximately 0.1% (Eu = 600*Cu).

Geotechnical model 2 – Linear elastic transversely anisotropic (soft)

The clay particles in London Clay tend to be orientated perpendicularly to the direction of consolidation. This leads to anisotropic mechanical properties. The Young's modulus in the horizontal plane is higher than the stiffness in the vertical plane. This anisotropy has been quantified in the laboratory and found to be an important influence on the results of numerical models of tunnels (Addenbrooke 1996, Lee & Rowe 1989). The anisotropic properties have been taken from van der Berg (1999) and Lee & Rowe (1989), while the vertical stiffness was the same as in Models 0 and 1, ie. Evu = 600*Cu.

Geotechnical model 3 – Nonlinear elastic transversely anisotropic

In this model (after Dasari 1996), the stiffnesses varied according to the deviatoric strain in the ground. The variation in stiffness with depth was calculated in a different way to the other models (depending on the effective mean stress instead of depth) so at very small strains this

model behaves more stiffly than Model 4 (see Figure 2.36). However, in general, under uniaxial compression it agreed with the average experimental data for London Clay. Masing rules have been applied to produce a nonlinear response during unloading-reloading cycles as well as during loading (see Figure 2.33).

Geotechnical model 4 – Isotropic strain-hardening plastic

Using the strain-hardening plasticity model in FLAC offers a more reliable means of incorporating the nonlinear behaviour of the clay, since, after yield, there is a unique relationship between shear strength and the plastic deviatoric strain under loading. On unloading the response is elastic and uses the initial (high) stiffness. This means that the nonlinear behaviour on unloading is not replicated. However, in general, the model agreed very well with the experimental data (see Figures 2.33 & 2.36) and has been found to perform well in full 3D numerical analyses (Pound 1999). The strain-hardening model was applied to a zone around the tunnel while outside it the behaviour was linear elastic with Eu = 1500*Cu. Figure 6.9 shows that typically the dimensions of the nonlinear zone were adequate. The dividing line between linear and nonlinear behaviour was a deviatoric strain of $1.0e^{-5}$. The angles of friction and dilation are set to zero since this model is for undrained behaviour.

Geotechnical model 5 – Linear elastic perfectly plastic isotropic (stiff)

This model was essentially the same as model 4, except that the strain-hardening function was not activated. The behaviour up to the undrained shear strength was linear elastic, with a high stiffness of Eu = 1500*Cu.

The gravels were modelled as an elastoplastic material with a Mohr-Coulomb yield criterion. The angle of friction was chosen to be 36° and the shear and bulk moduli were 42 and 56 MPa respectively (Mott MacDonald 1990).

6.3.4 Constitutive modelling of the lining

Table 6.1 contains a list of the constitutive models that have been used for the lining. The parameters are the same as in the earlier numerical models (see section 4.3) except that f_{cu28} = 35.0 MPa and E_{28} = 27.0 GPa.

Defects Concerns have been raised over possible construction defects in SCL tunnels, particularly at the joints (HSE 2000). Analyses have been run with weakened zones along the radial joints, the longitudinal joints and both (see Figure 6.10). To do this, the strength in the zones at the joints was reduced by 50%.

6.4 Typical results

Considering the base case model H_Et_4 – strain-hardening plastic isotropic ground (Model 4) with an age-dependent linear elastic lining – one can make the following general comments.

6.4.1 Behaviour of the ground

In terms of a qualitative assessment first, one can say that the numerical model replicated the real behaviour of tunnels reasonably well (e.g.: in comparison to field data from HEX project – Mott MacDonald (1998)). As Figures 6.9, 6.11 and 6.12 show the 3D re-orientation of stress around the tunnel occurred predominately within 1 diameter of the face. The stresses were virtually unchanged at more than 2 diameters away from the tunnel in all directions. The largest strains (and therefore movements) occurred near the base of the Top Heading face which was the point that had least support from either the adjacent ground or the tunnel lining.

Figure 6.13 shows the stress paths undergone by elements in the ground at various points around the lining. Initially, when the tunnel face was about 2 diameters away, the stresses were close to the initial insitu stresses. As the tunnel approached, the deviatoric stress increased while the mean stress decreased due to unloading in the direction of the tunnel face. As seen qualitatively in Figure 6.12, arching around the tunnel occurred. The vertical stress increased beside the axis while the horizontal stress decreased (and the deviatoric stress, q, became positive[76]). The opposite occurred above and below the tunnel. The minimum mean stress occurred at the point closest to the face of the Top Heading and thereafter the mean

[76] q is positive if the vertical stress is greater than the horizontal stress and negative if vice versa.

stress generally increased while the deviatoric stress remained unchanged. None of the points reached failure. The undrained shear strength of the ground was set according to the depth of the point in question. It did not vary during the analysis so, although some points in Figure 6.13 appear to exceed the strength, in fact they did not. A "steady-state" condition was attained at approximately 2 diameters behind the closure of the invert.

Figure 6.14 shows that there is more unloading in the face of the tunnel (i.e. the area that was least supported) than around the extrados. At a distance of about 1 diameter from the tunnel (both ahead and to the side) there was a slight increase in the minimum (i.e. most compressive) stress due to the "arching" around the cavity and within 1 diameter there was a rapid drop in stress.

Table 6.8 contains results from the base case model and field measurements. Although the predictions were of the correct order of magnitude, they differed considerably from the field measurements.

There is most confidence in the field measurements for ground and lining displacements. Although the volume loss predicted by the model was close to but lower than the field data, the settlement trough was much wider and shallower than the real case (see Figures 6.15, 6.16 & 6.17). Numerical models have often been found to overpredict far-field settlements (Gunn 1993). It is possible that this effect could have been reduced by using a non-linear (or simply a stiffer model) for the gravels as has been proposed by Standing *et al.* 1998.

In contrast field observations and centrifuge models, the numerical model predicted relative heave above the centreline of the tunnel and actual heave above the face of the Top Heading. The transverse shape of the trough was not an inverted Gaussian curve. This pattern of behaviour has been observed before in numerical models with K_0 greater than 1.0 due to yielding in the ground (e.g.: Addenbrooke 1996, van der Berg 1999). Similarly relative heave seemed to affect the longitudinal settlement profile 10m either side of the face. Considering

the ground movements in the transverse plane, there seemed to be a much larger horizontal component that is observed in the field (see Figures 6.18 & 3.21).

Table 6.8: Results from the Base Case – H_Et_4[77]

Parameter (Ground)	Model	Field data	Parameter (Lining)	Model	Field data[78]
Volume loss in %	0.51	0.85	Crown displacement in mm	-6.0	-8.4
Max. surface settlement over centreline in mm	-2.6	-14.0	Displacement at 60° from crown (horizontal) in mm	-5.9 est.	-3.0
Width of settlement trough in m ($\delta v > 0.1$ mm)[79]	>54	33	Displacement at 60° from crown (vertical) in mm	-5.8 est.	-6.0
% of surface settlement ahead of face	N/A	50	Crown hoop force in kN	1370	932 (1036)
Radial stress at crown in kPa	225	207	Hoop bending moment at crown in kNm	14.8	- (21)
Radial stress at axis in kPa	381	195 est.	Hoop force at 60° from crown in kN	1334	864 (1044)
Max. horizontal disp. in mm at 1.5m from face	39	16	Hoop bending moment at 60° from crown in kNm	10.0	- (23)

As Figure 6.19 shows the numerical model underpredicted how much the stresses in the ground relax due to excavation. This was most noticeable around the axis. On average the radial stresses were 48% of the initial stresses, at a distance of 2 diameters back from the face, compared an average reading of 35% from the pressure cells. Therefore the loads on the

[77] NB: the values from the numerical model have not been corrected to account for discretization errors.

[78] The field data are averages of measurements from the HEX tunnels (Mott MacDonald 1998); the loads are estimated from radial pressure cells and strain gauges; the estimates from strain gauges are in brackets and assume a concrete stiffness of 15 GPa; the tangential pressure cells recorded much lower loads, e.g. 412 kN in the crown & 549 kN at 60° from the crown.

[79] δ_v is the vertical deformation of the ground surface.

lining in the numerical model were probably 30% higher than the loads applied to the real lining.

At the transition from the coarse to fine regions of the mesh, the number of radial zones in the lining increased from 1 to 3 and the length of each lining zone increased from 0.5 to 1.0m – i.e. from half to one advance length. The coarser mesh behaved more stiffly and hence the ground movements were lower (e.g.: Figure 6.11). This transition was sufficiently far away to assume that it did not have any influence on the "steady-state" condition formed at about 1 diameter from the closure of the invert.

6.4.2 Behaviour of the lining

The behaviour of the lining reflected the loading from the ground. As the ground attempted to close the cavity, the shell structure of the lining was compressed and bent. The arching of the stresses in the ground around the face meant that the load on the lining was initially small and then built up with distance from the face

Considering Figure 6.20, one can see that the lining acted as a shell structure with the stresses arching within the lining around the corners of the heading. In the crown and invert, the stresses were predominately orientated along the axes of the lining, with the most compressive stress aligned in the hoop direction.

Figure 6.21 shows that much of the upper part of the extrados was in tension in the longitudinal direction. Sometimes these tensile stresses were significant, i.e. more than 50% of the tensile strength. This appeared to be due to the relative rotation of the ground displacement vectors towards the tunnel face, after the lining had been placed (Pound & Beveridge 2001). Initially they were angled at about 45° to the vertical axis. 20m behind the face the angle was about 30° to the vertical. This small relative longitudinal displacement of the ground "pulls" the lining towards the face, inducing tensile stresses that reached up to 2.5 MPa.

A useful measure of the intensity of stresses in tunnel linings is the utilization factor, α, which is the current deviatoric stress divided by the current deviatoric strength[80]. Figures 6.22 and 6.23 show that α varied considerably with distance from the tunnel face. Initially it could be as high as 60%. Several diameters away from the face, after the new state of equilibrium had been established, α generally lay between 30 and 40%. The stresses were more intense at the leading edge of each advance length than the trailing edge, often more than 50% higher. Consequently the hoop force was lower at the trailing edge. Bending moments were lower too by up to about 20%. There was also a concentration of stress at the radial joint between the Top Heading and Bench and to a lesser extent at the same joint between the Bench and Invert.

The hoop stresses on the inner part of the lining (intrados) tended to be higher than in the outer part (extrados). Typically the final stresses in the crown were 3.9 and 5.3 MPa for the extrados and intrados respectively. In contrast field measurements using flat-jacks suggested that the loads near the intrados were much lower - less than 1 MPa (Hughes 1996).

In lining design calculations the main parameters are the hoop force and hoop bending moment. Figures 6.24 and 6.25 show how these parameters varied with distance from the face of the Top Heading. At all points the stresses were low when the lining was first installed and then rose rapidly. At a distance of about one diameter after the closure of the ring the stresses in the lining had stabilised. Consequently both hoop forces and bending moments rose and then stabilised. In the final state the hoop forces were fairly uniform but were somewhat lower at the shoulder and knee. Near the face the forces were greatest in the Top Heading, especially the crown. The values were larger than the forces estimated from field data (see Table 6.9) although there is some doubt over the interpretation of the field data, as discussed in section 3.2.2.

[80] Utilization factor can also be defined as the current hoop stress divided by the uniaxial strength.

The hoop bending moments were highest just below the axis and lowest at the knee. The bending moments were generally hogging above axis and sagging below axis[81]. In terms of magnitude the bending moments were quite low, even when allowing for the correction for the discretization error. There was a shift in the pattern of bending in the Top Heading from sagging at the footing to hogging within the first few metres from the face (see Figure 6.25).

Considering lining deformations, Figures 6.26 and 6.27 show that deformations were generally vertical in the upper part of the ring, while at the axis and in the Bench the movements were largely horizontal. Deformations were smallest in the invert. All movements stabilised rapidly and ceased to increase as soon as the invert was closed. Convergence data from HEX showed that movements continue at a decreasing rate for about 2 diameters behind the leading edge of the invert whereas the numerical model predicted that the deformations stabilised within about 1 diameter (see Figure 6.28).

At first glance (e.g.: Table 6.8), the movements predicted by the numerical model appeared to agree quite well with those observed at HEX. However, because there was a delay in installing the convergence pins in the real tunnel, the recorded movements were only a fraction of the actual movements. The values from the numerical model represented total lining deformations. As a first approximation the field data has been multiplied by a factor of 2 in Figures 6.27 and 6.28.

The model predicted very high radial movements at the base of the Top Heading (up to 16mm). It appeared that this was due to the fact that one of the zones at the axis remained connected to the zones representing the ground (see Figure 6.4). The grid-points that are shared by the ground and the lining basically seem to have retained most of the displacements generated in the ground before the lining was placed. There was a peak in radial deformation at the bottom corner leading edge of the Bench for the same reason. Elsewhere the lining was formed of zones that were nulled during excavation (re-setting the displacements to zero) and

[81] Hogging corresponds to a higher stress at the intrados than at the extrados of the lining.

then reactivated. Therefore the displacements were a true reflection of the lining movements. This may in part also explain why there was a concentration of stress at the joints.

Finally, Figures 6.29 and 6.30 show the stresses in the longitudinal direction. In the literature review little information was found on this subject. In general the predicted forces here were compressive but there was some tension in the crown. The forces were about 66% of the hoop forces while the bending moments were up to twice the hoop bending moments. The forces continued to increase with distance from the face while the bending moments stabilised after a distance of about 2 diameters.

6.4.3 Summary

While the base case numerical model replicated most aspects of the general behaviour of the ground and tunnel lining, there were certain aspects that it did not model accurately (in comparison with field data). Specifically, considering the base case model – H_Et_4:

- The volume loss was underestimated – suggesting that overall the ground / tunnel model was too stiff. Also the amount of stress relaxation at the tunnel appears to have been underestimated;
- Far-field ground movements were over-estimated – suggesting that the ground model was too soft in the far-field;
- There was heave above the tunnel face and relative heave above the centreline, leading to a settlement trough that does not match the inverted Gaussian shape observed in the field;
- The lining deformations stabilised almost immediately after ring closure. This was much more quickly than field measurements suggest;
- The magnitude of the lining deformations was less than the field measurements – suggesting that the lining was too stiff.
- Since the radial stresses acting on the lining in the model were about 1.3 times greater than those recorded by the radial pressure cells at HEX, the predicted lining loads were probably overestimates.

From the point of view of this study the most important thing was to obtain a reasonably realistic loading on the lining. This was achieved, although the loads may be overestimated slightly as noted above. The effects of varying the constitutive model for the lining and other aspects of the numerical model will be presented in the next chapter.

Figure 6.1 Excavation sequence

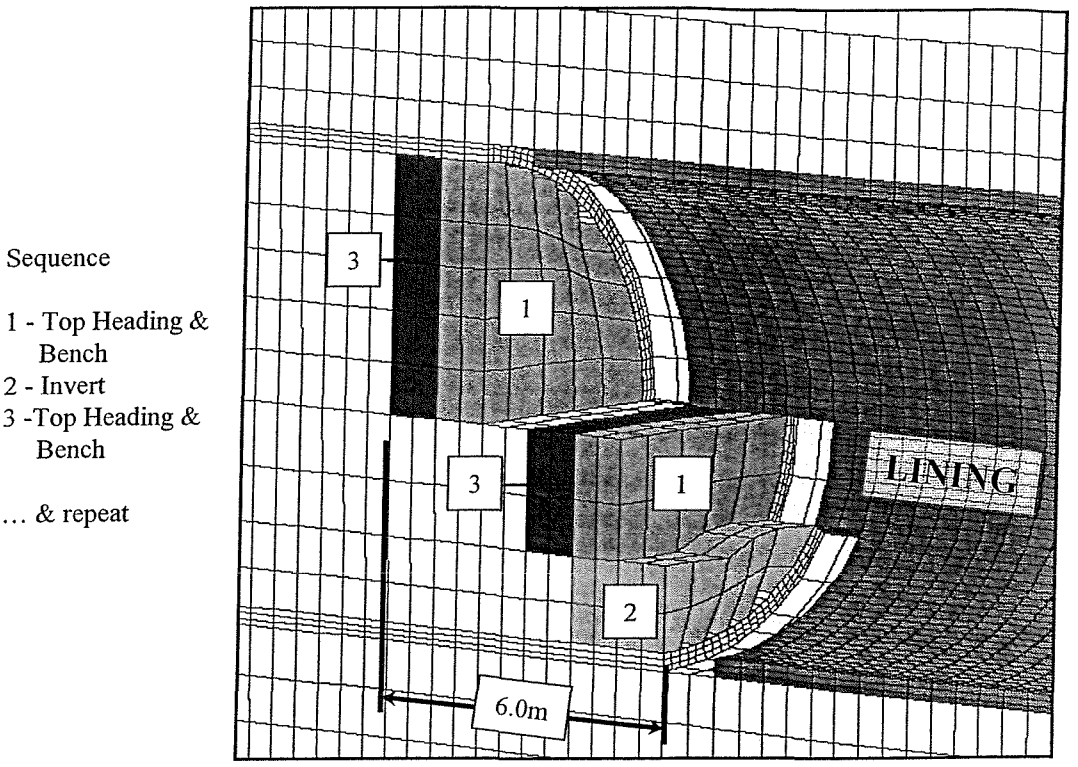

Figure 6.2 K_0 distribution with depth

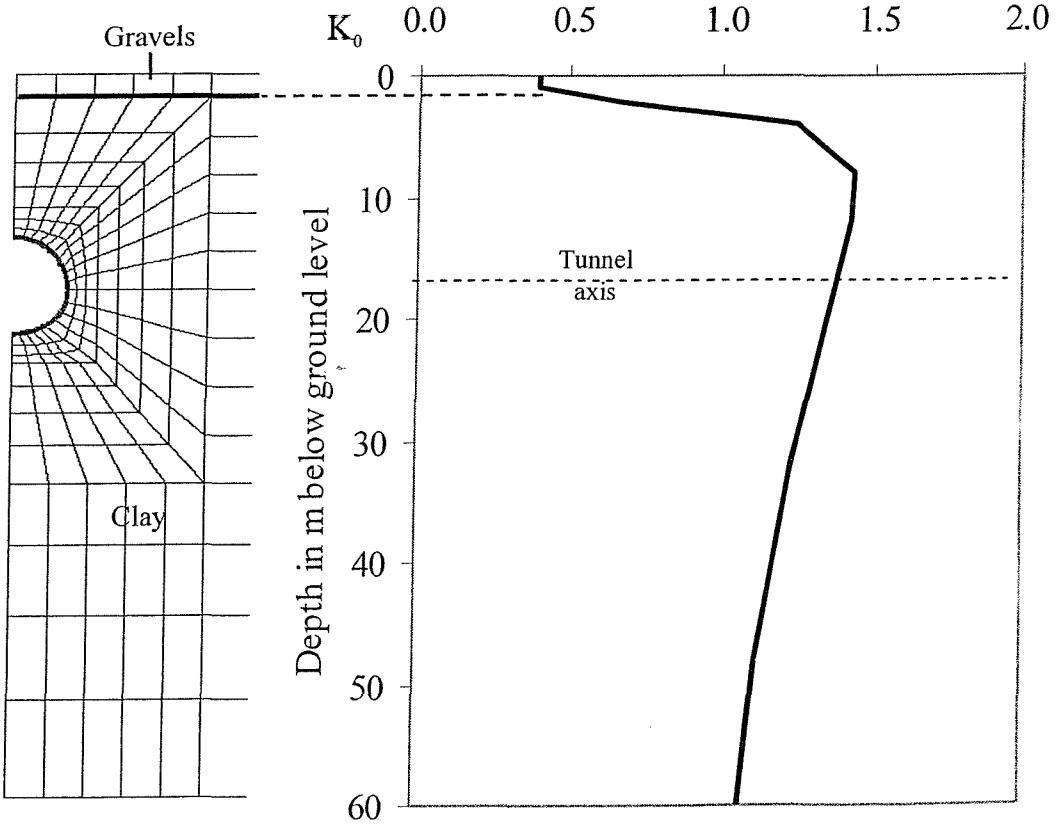

Figure 6.3 Base case mesh

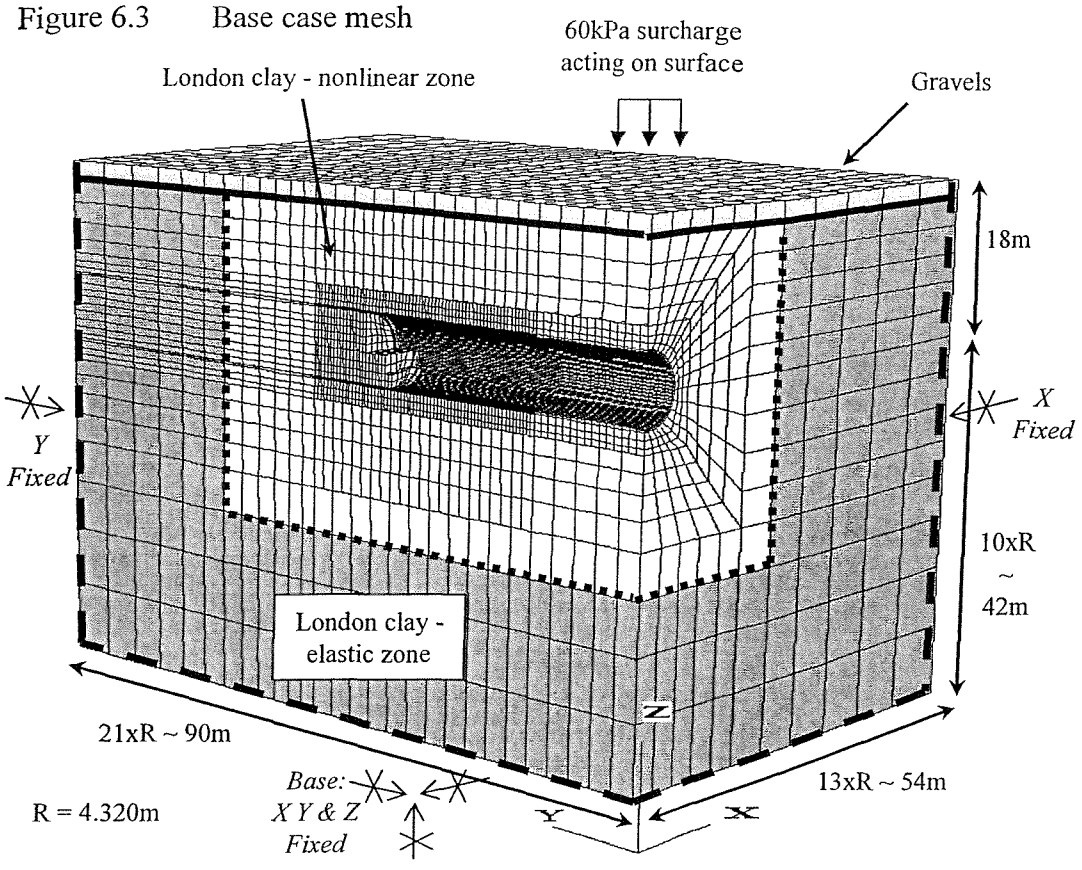

Figure 6.4 Enlarged view of tunnel mesh

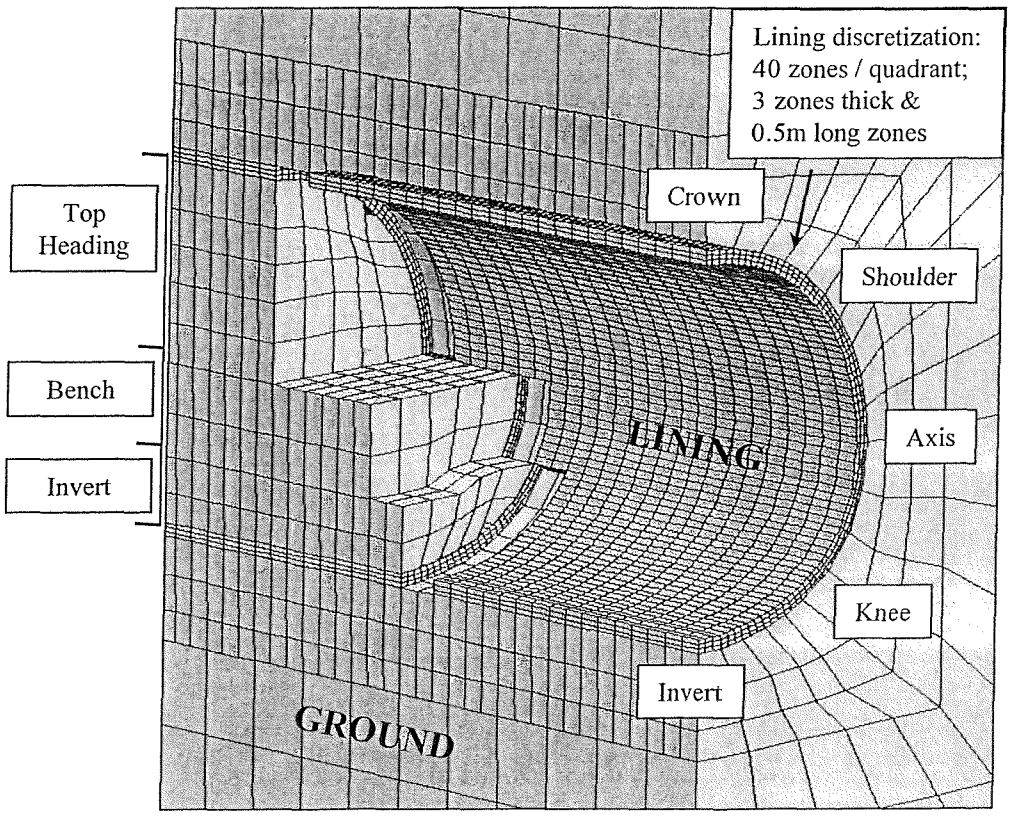

Figure 6.5 Axisymmetric model for boundary conditions study (showing contours of displacement in X direction)

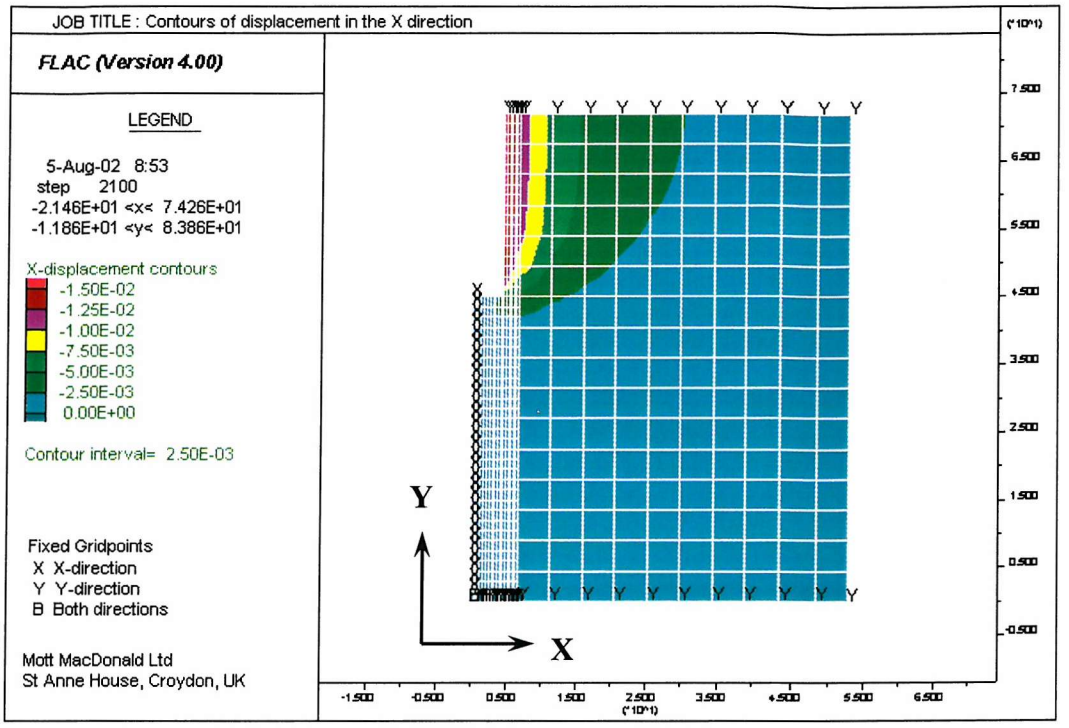

Figure 6.6 Errors in FLAC model w.r.t. CCM analytical solution for axisymmetric model for an unlined tunnel

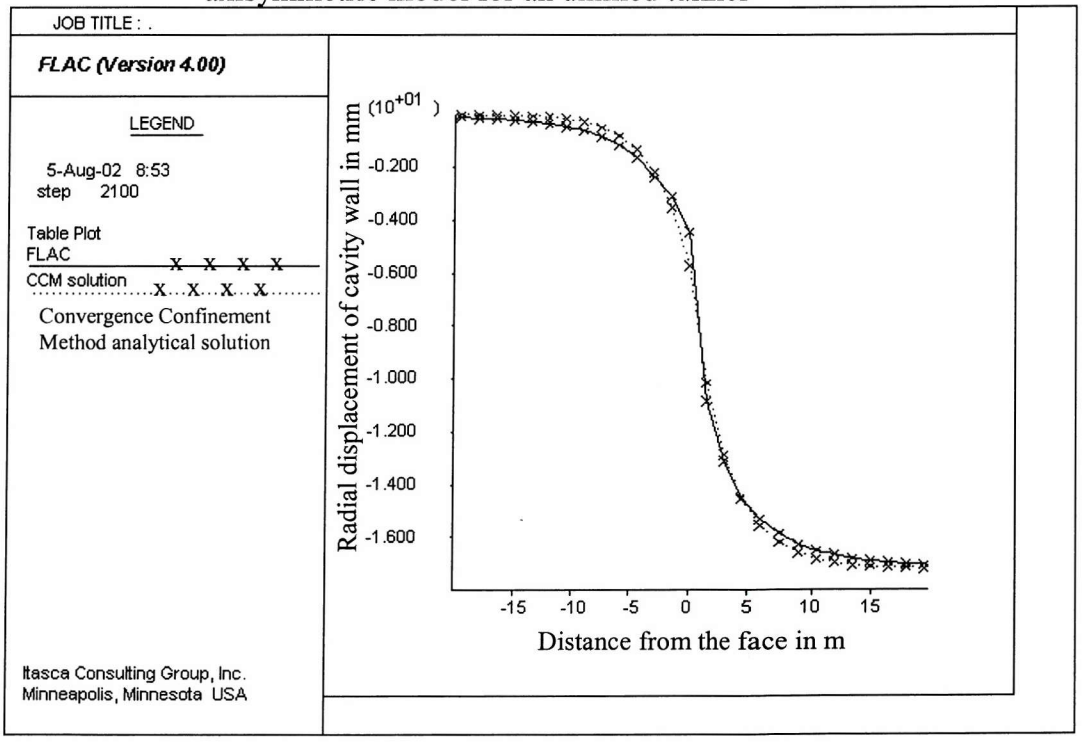

Figure 6.7 Plane strain model for comparison with analytical solution

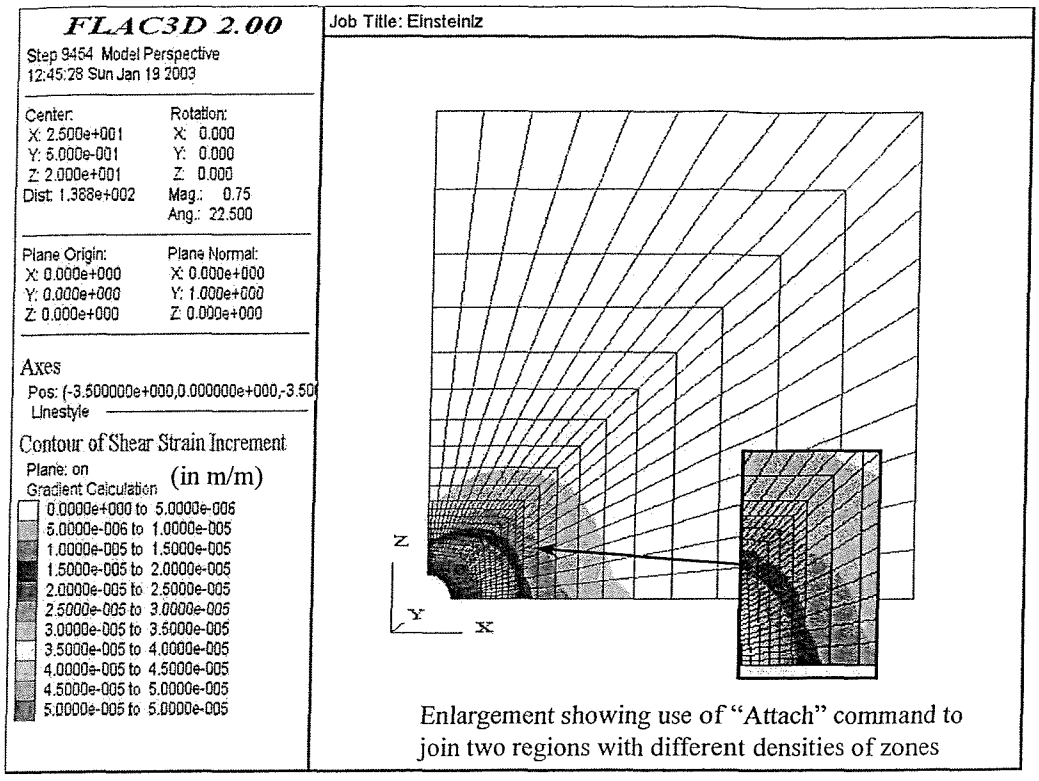

Enlargement showing use of "Attach" command to join two regions with different densities of zones

Figure 6.8 Plane strain model - normalized results for forces & moments

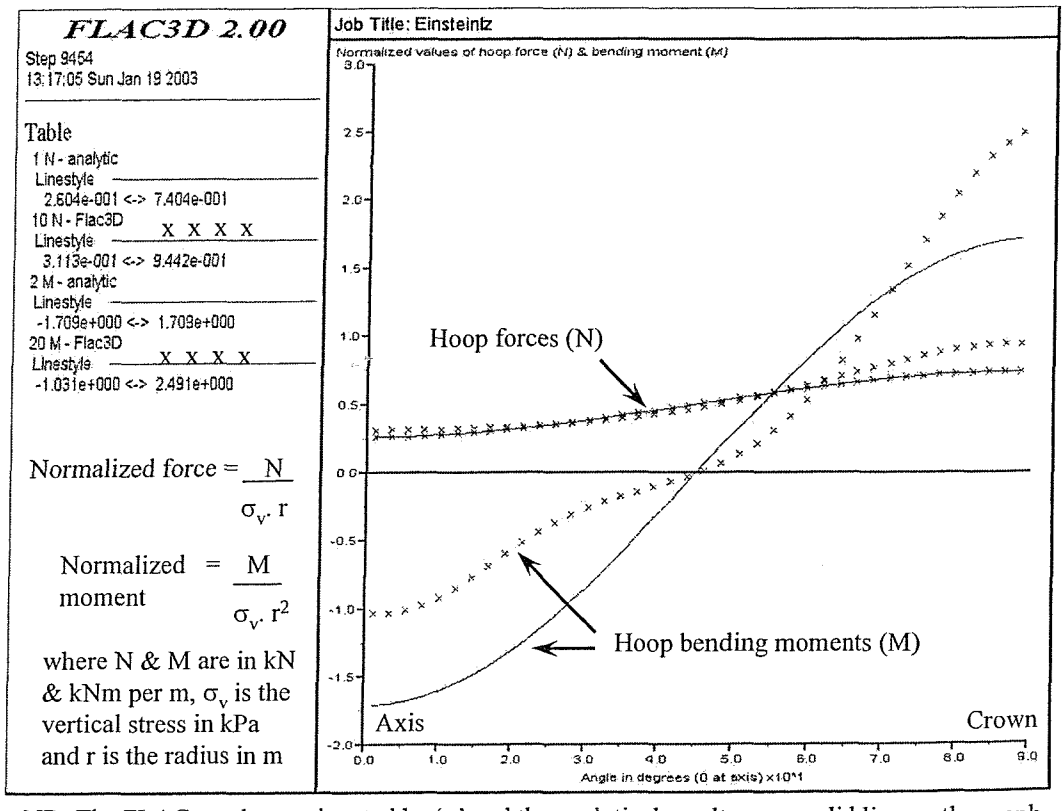

NB: The FLAC results are denoted by 'x' and the analytical results are a solid line on the graph

Figure 6.9 Deviatoric strain contours

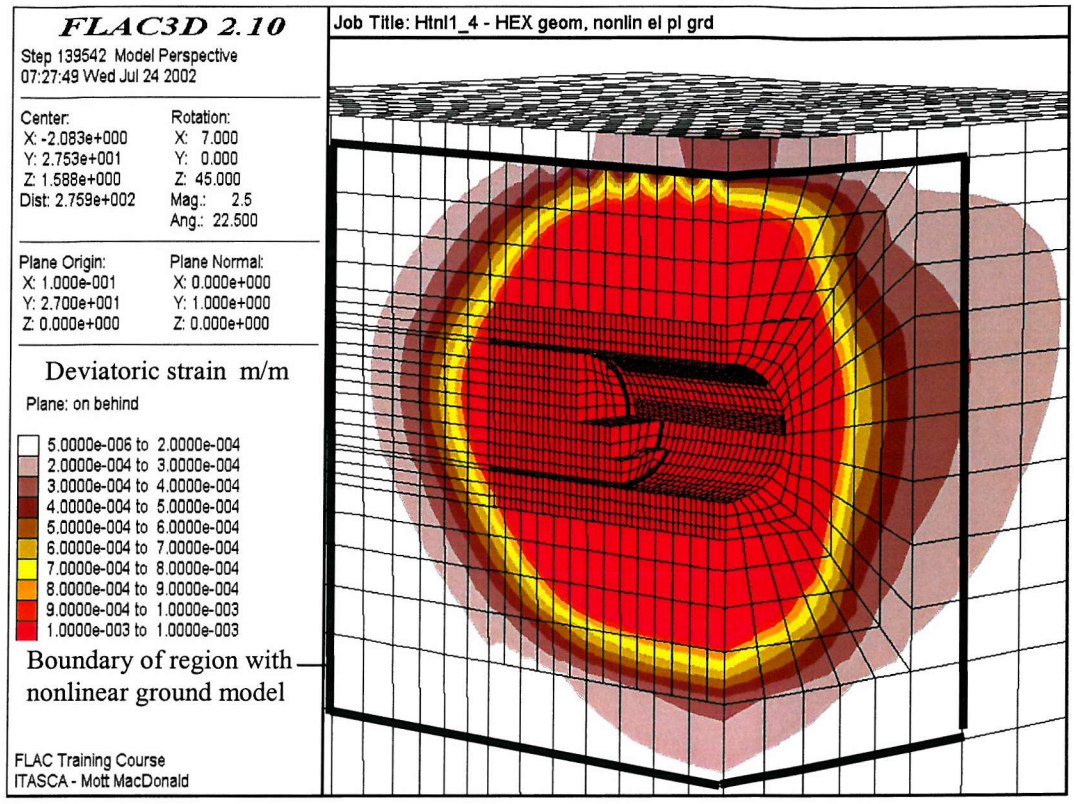

Figure 6.10 Locations of joints in mesh

(a) Radial (b) Longitudinal

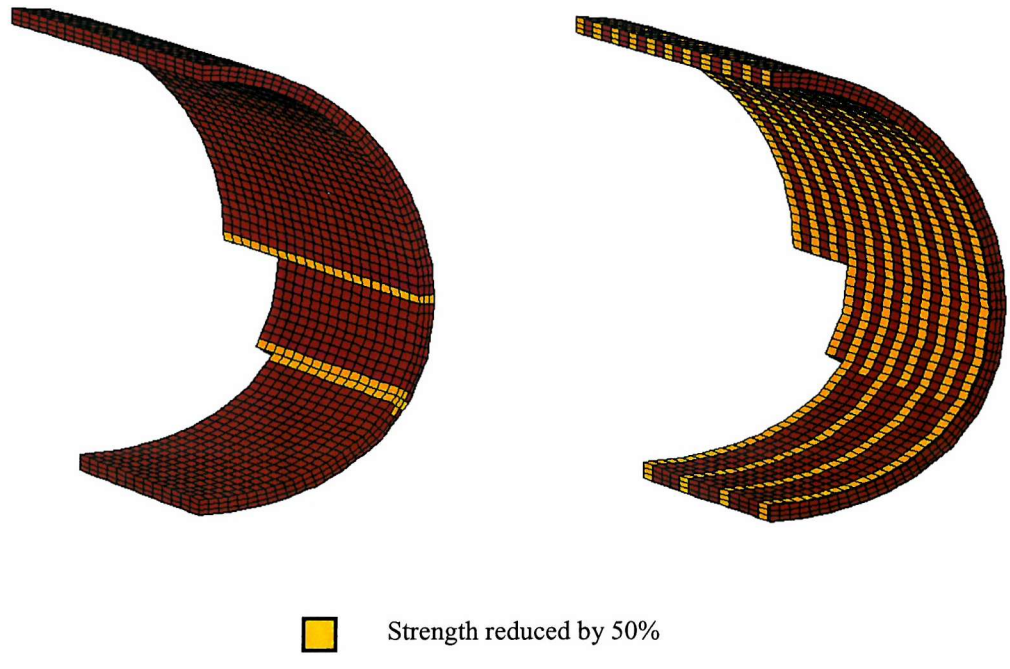

Figure 6.11 Displacement vectors on plane of centreline of tunnel

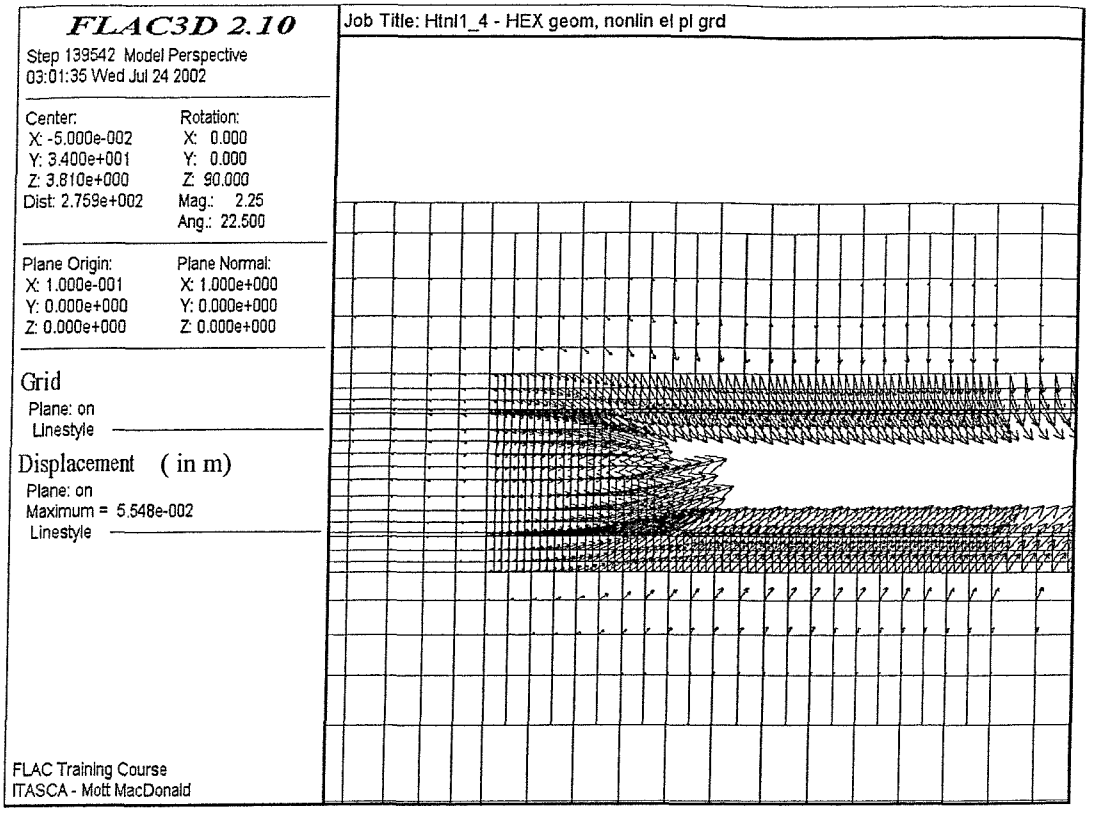

Figure 6.12 Principal stress tensors in ground

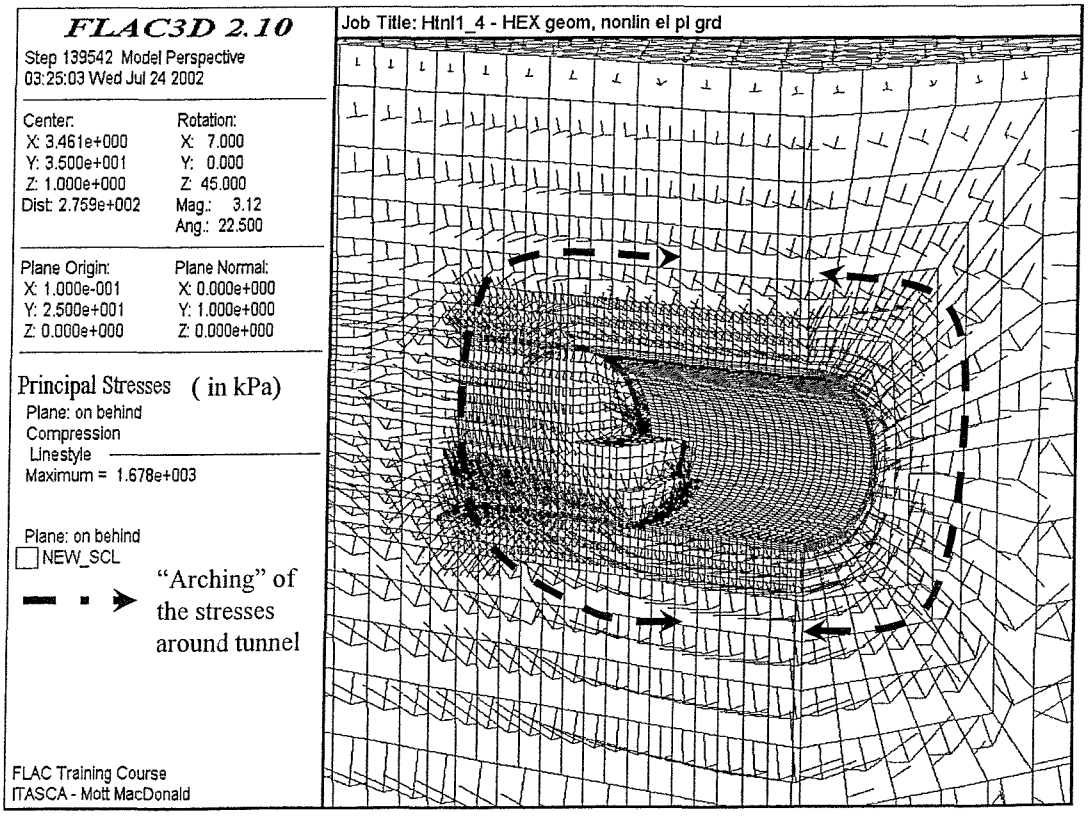

Figure 6.13 Stress paths in ground near tunnel - 0.5m from extrados

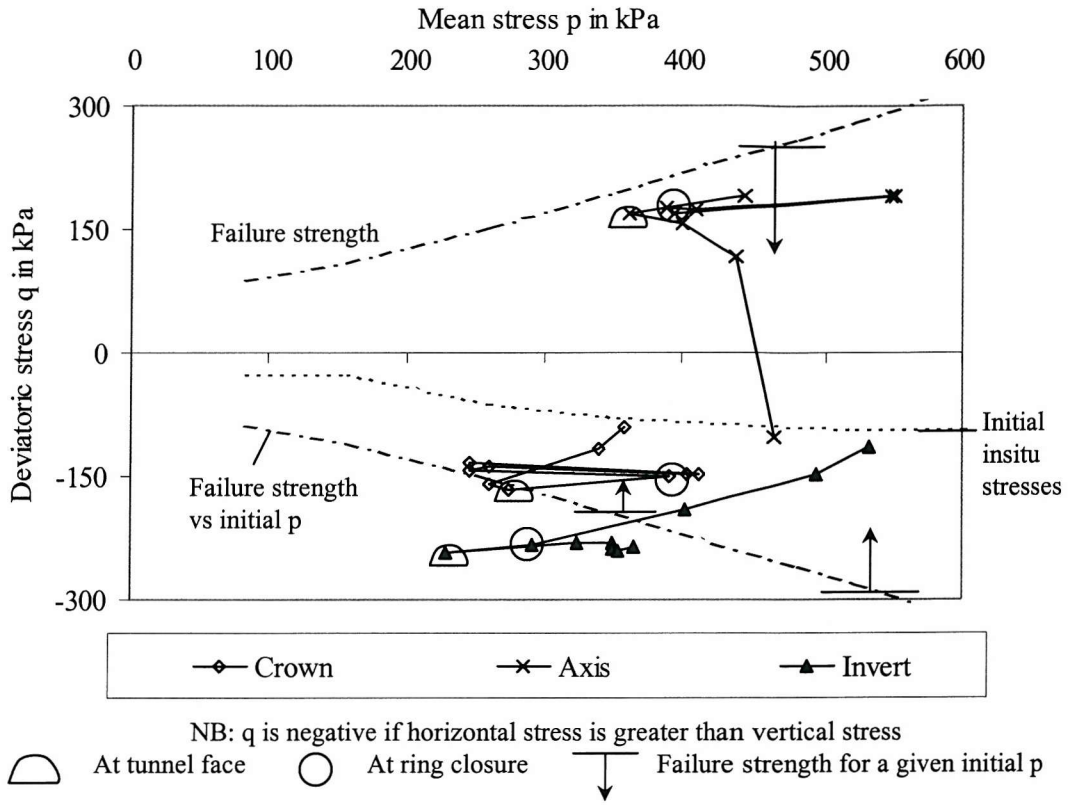

Figure 6.14 Contour plot of minimum (most compressive) principal stress

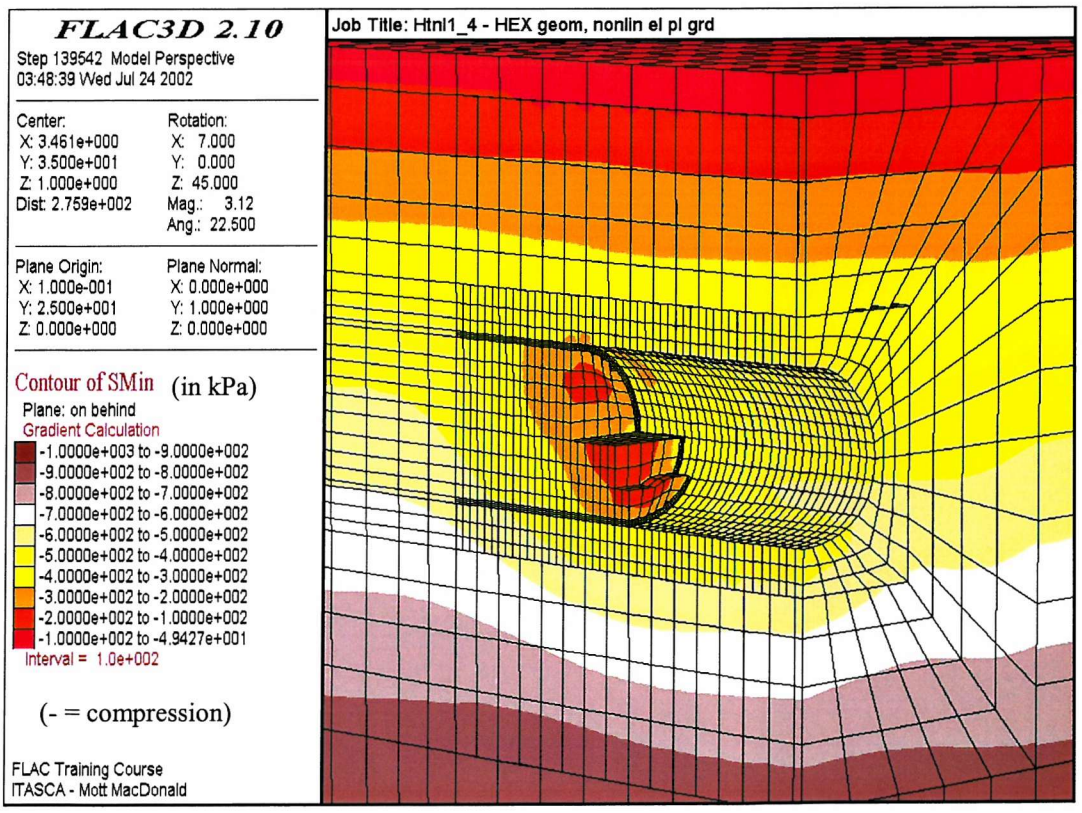

Figure 6.15 Longitudinal surface settlement trough (on centreline)

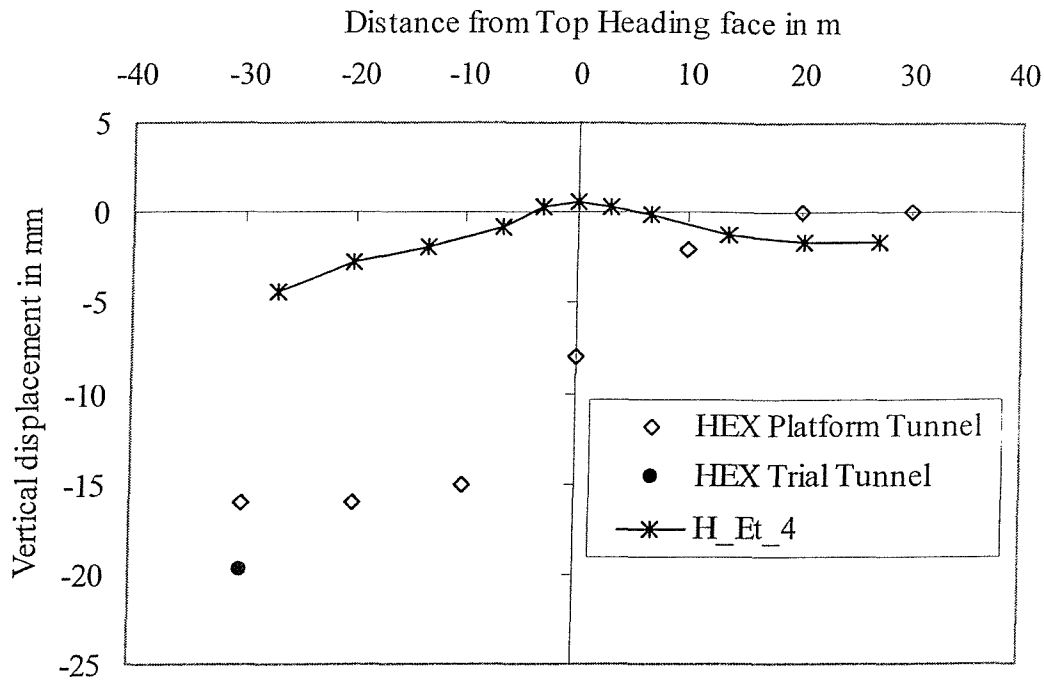

NB: Trial Tunnel values corrected for the difference in face area and volume loss; surface is 18 m or 19 m above axis

Figure 6.16 Transverse surface settlement trough (18m from face)

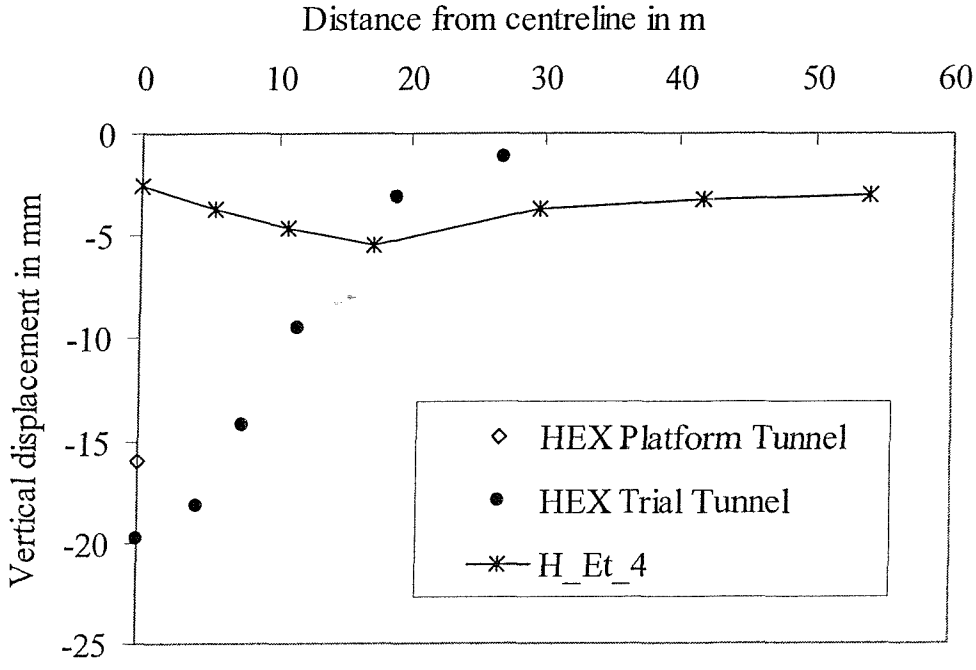

NB: Trial Tunnel values corrected for the difference in face area and volume loss; surface is 18 m or 19 m above axis

Figure 6.17 Surface settlement trough

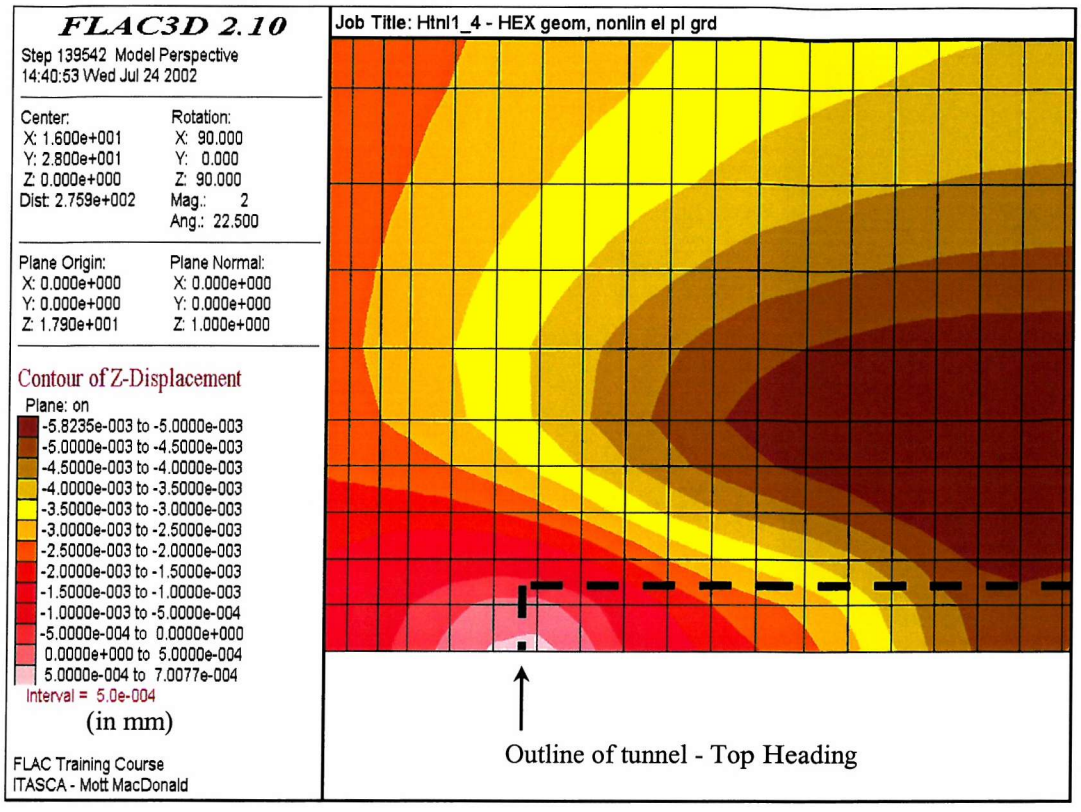

Figure 6.18 Displacement vectors on a transverse plane to the tunnel

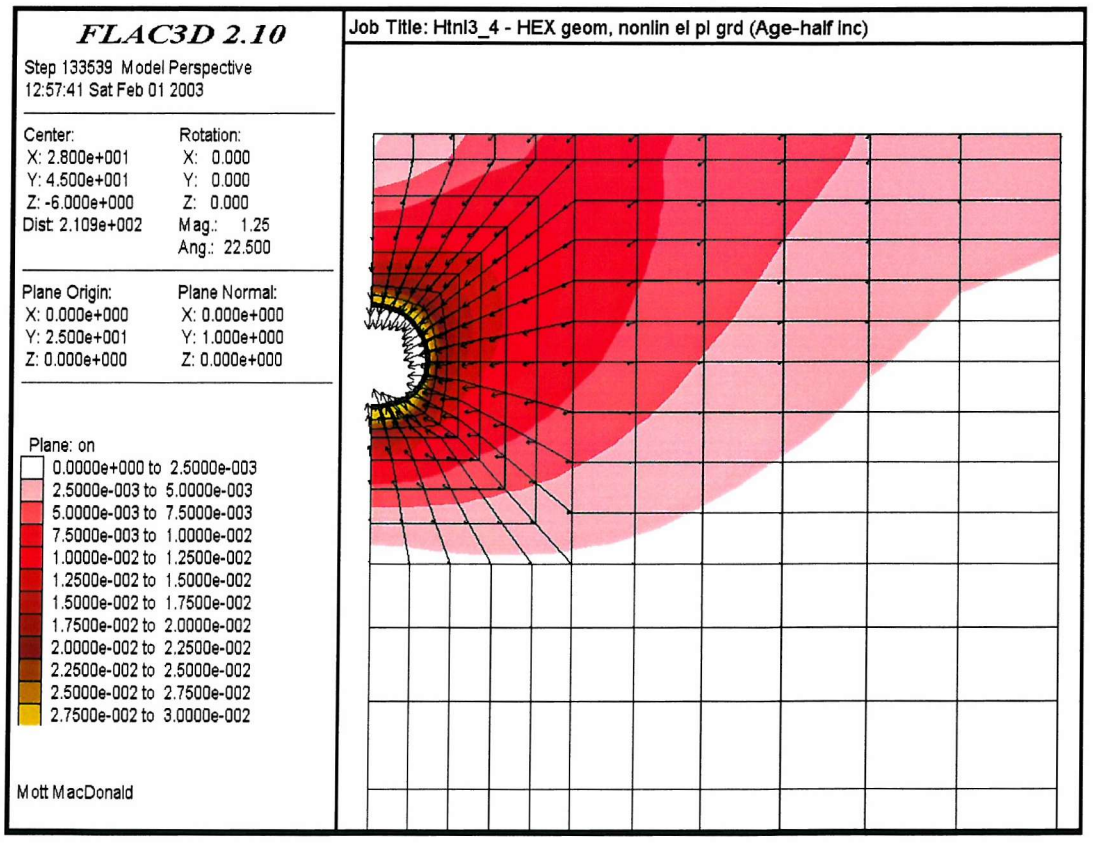

Figure 6.19 Radial stresses in the ground acting on the tunnel lining

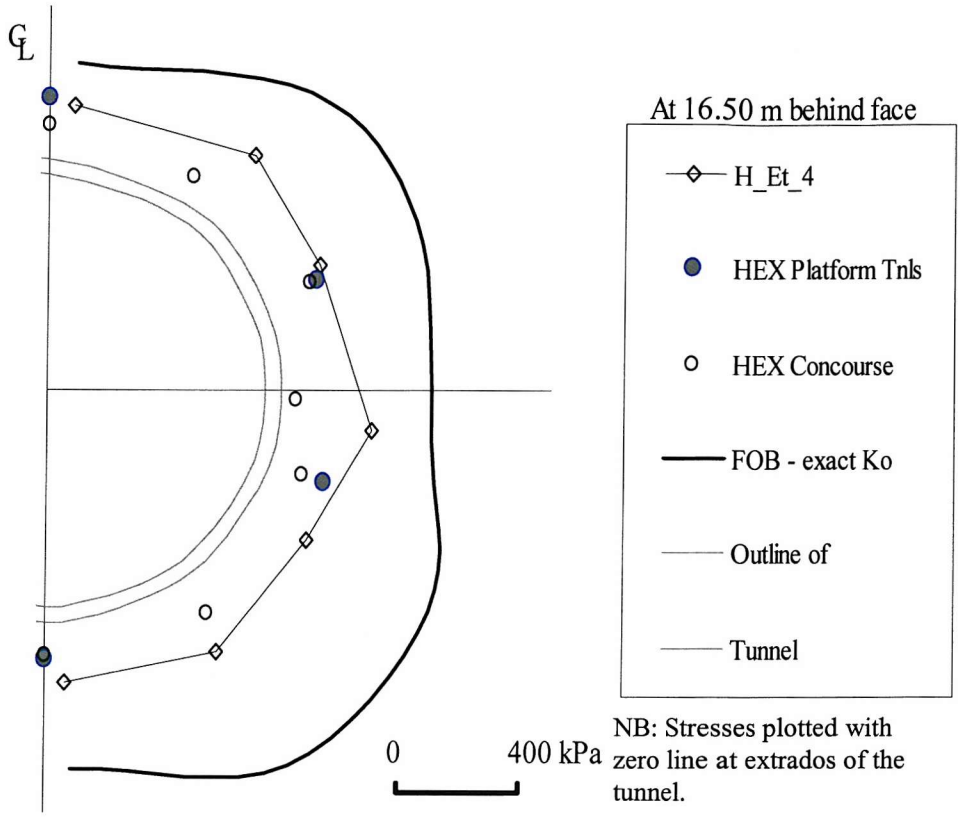

Figure 6.20 Principal stress tensors in tunnel lining - intrados

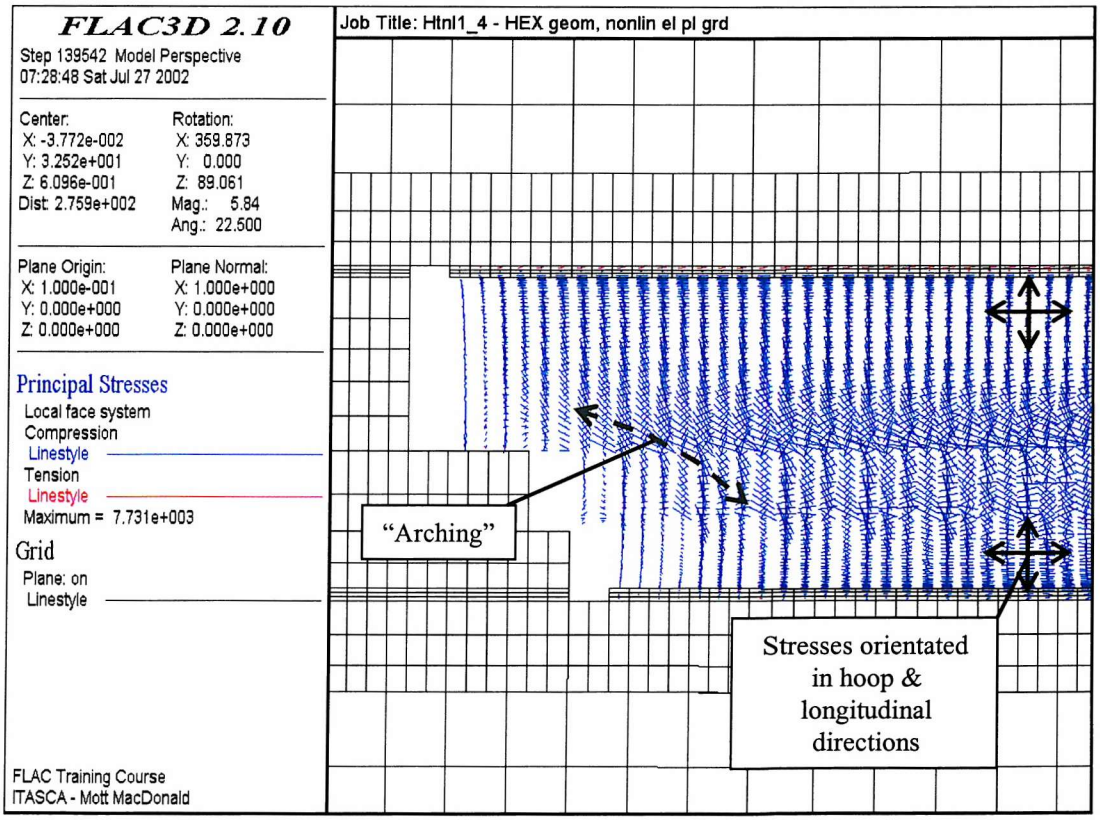

Figure 6.21 Principal stress tensors in tunnel lining - extrados

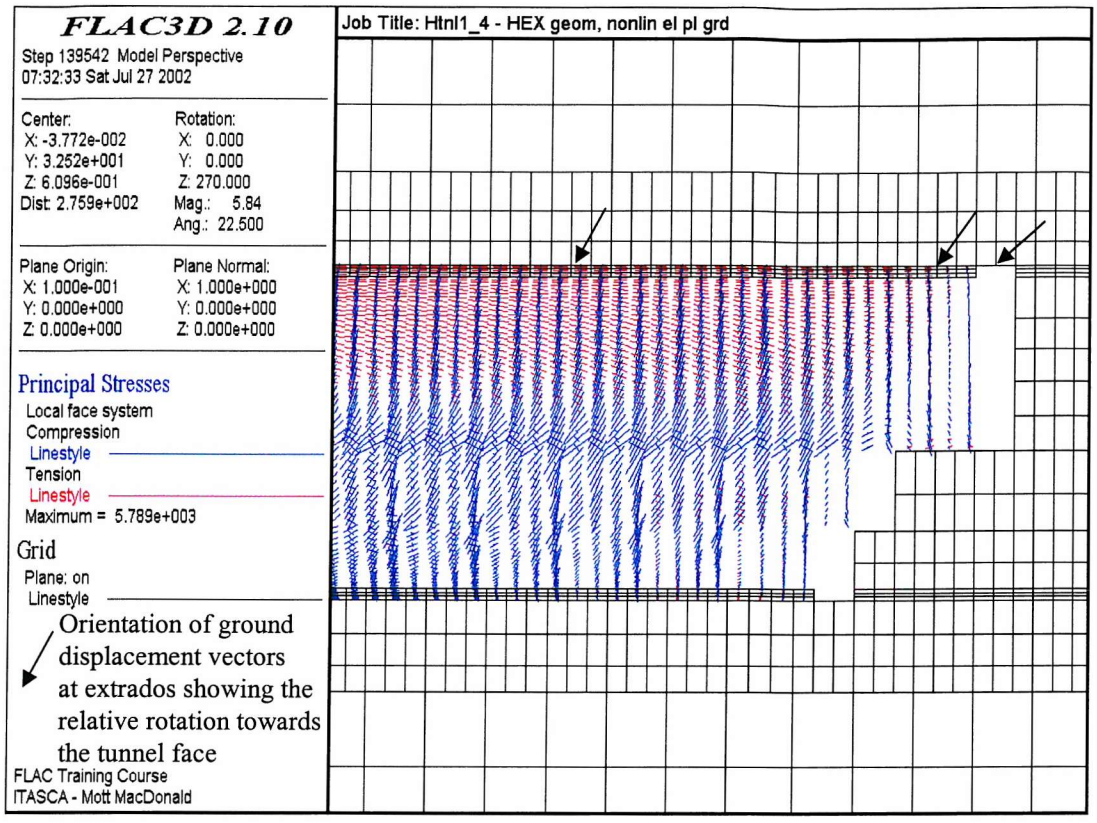

Figure 6.22 Utilization factor in lining - intrados

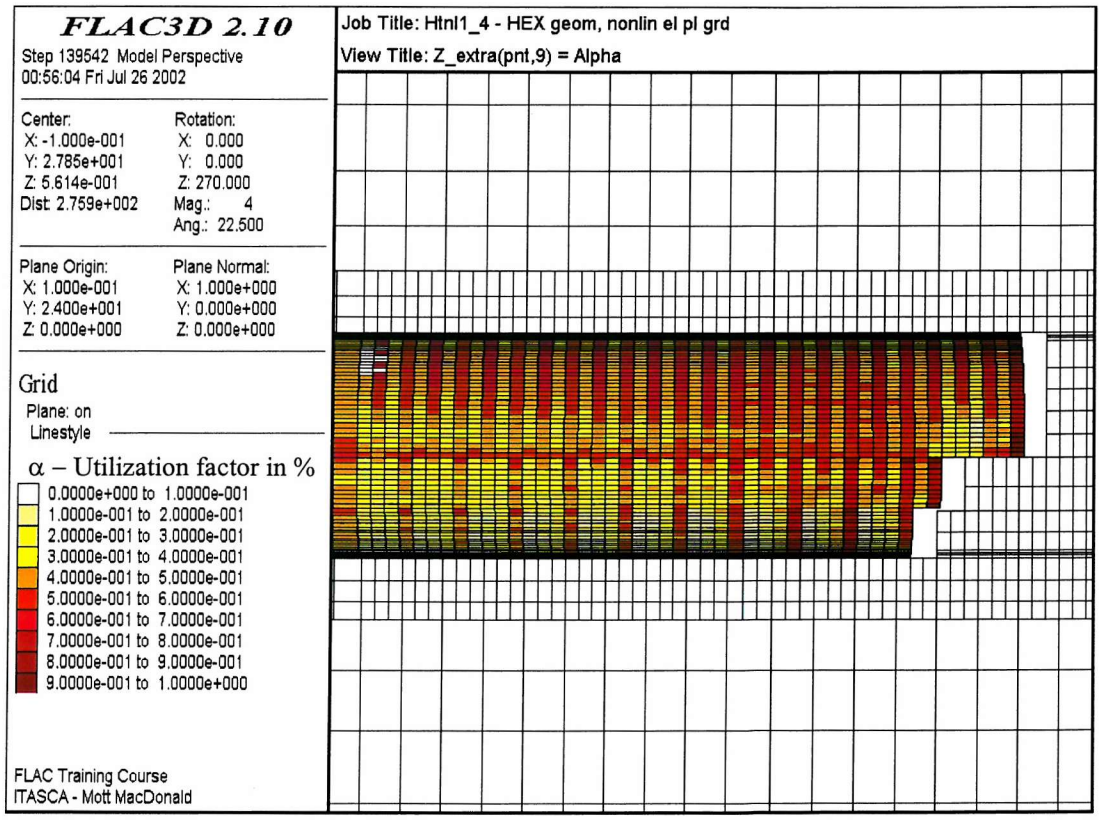

Figure 6.23 Utilization factor in lining - extrados

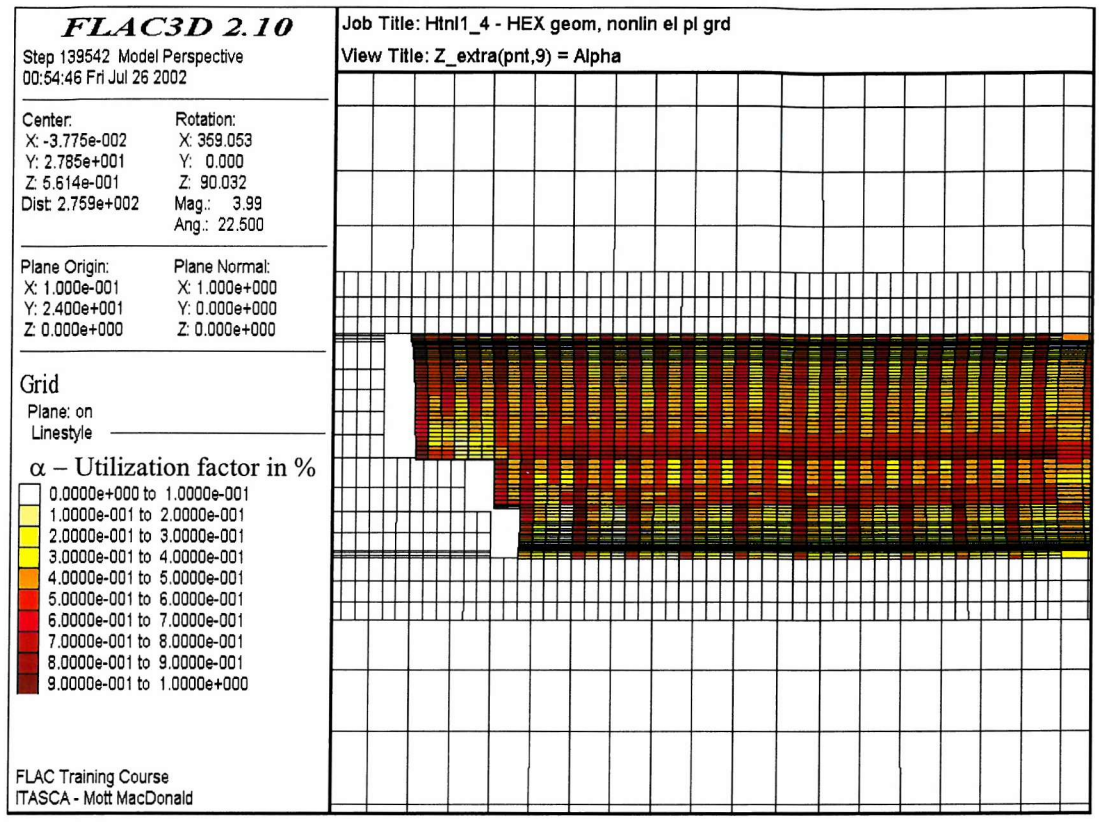

Figure 6.24 Hoop axial force vs distance from face

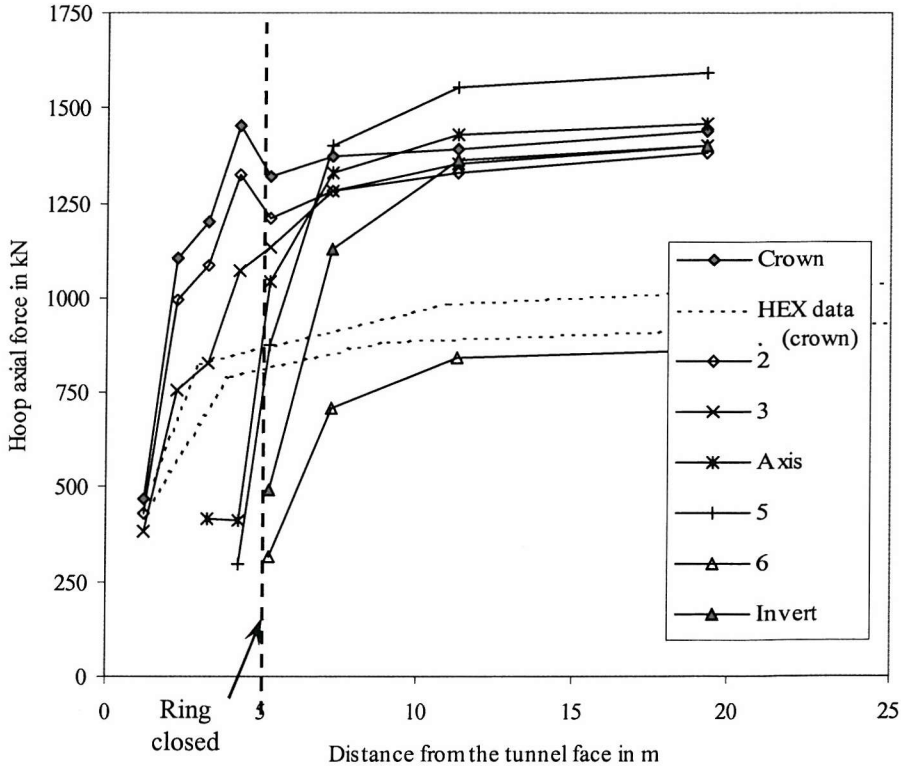

Figure 6. 25 Hoop bending moment vs distance from face

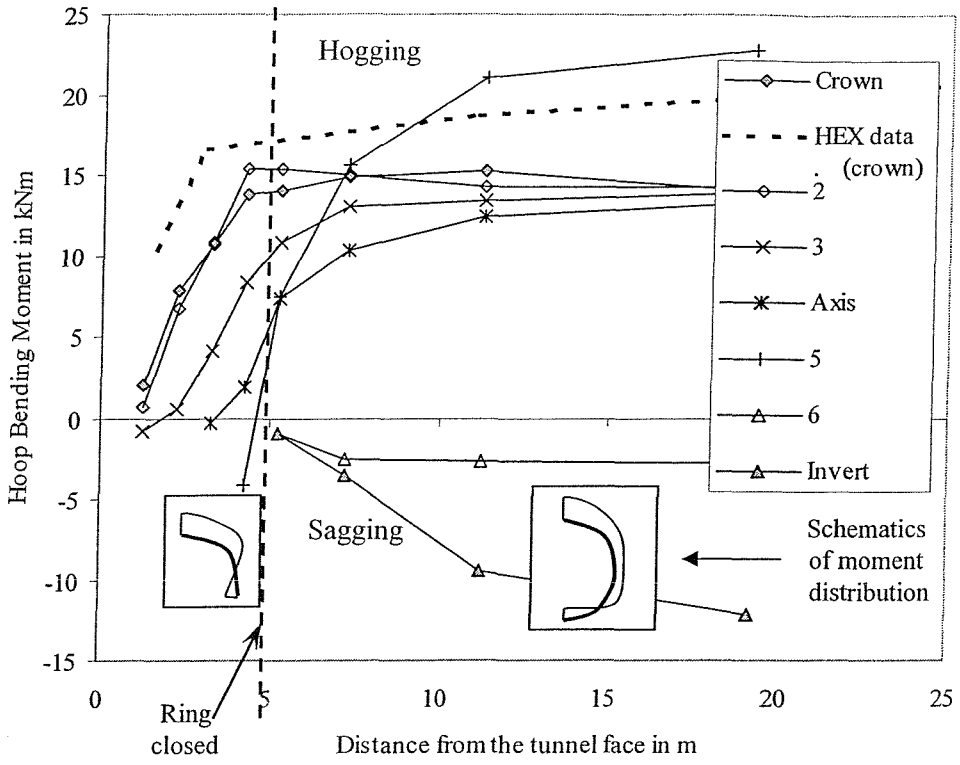

Figure 6. 26 Radial deformation vs distance from face

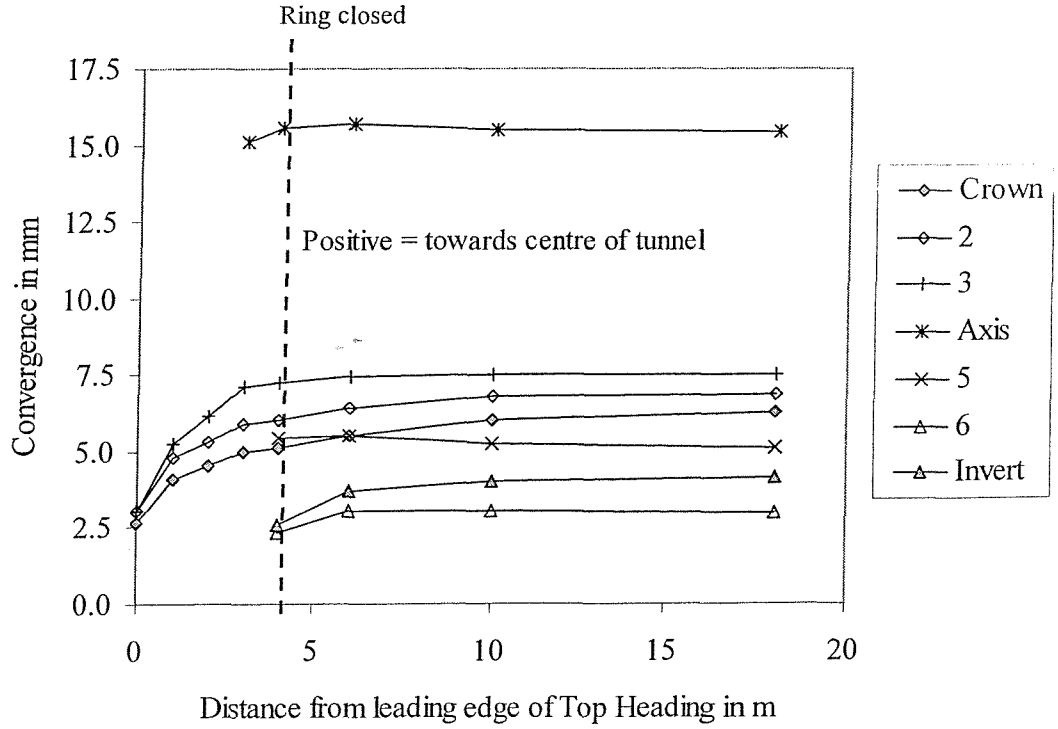

Figure 6.27 Lining deformation 18m from leading edge of Top Heading

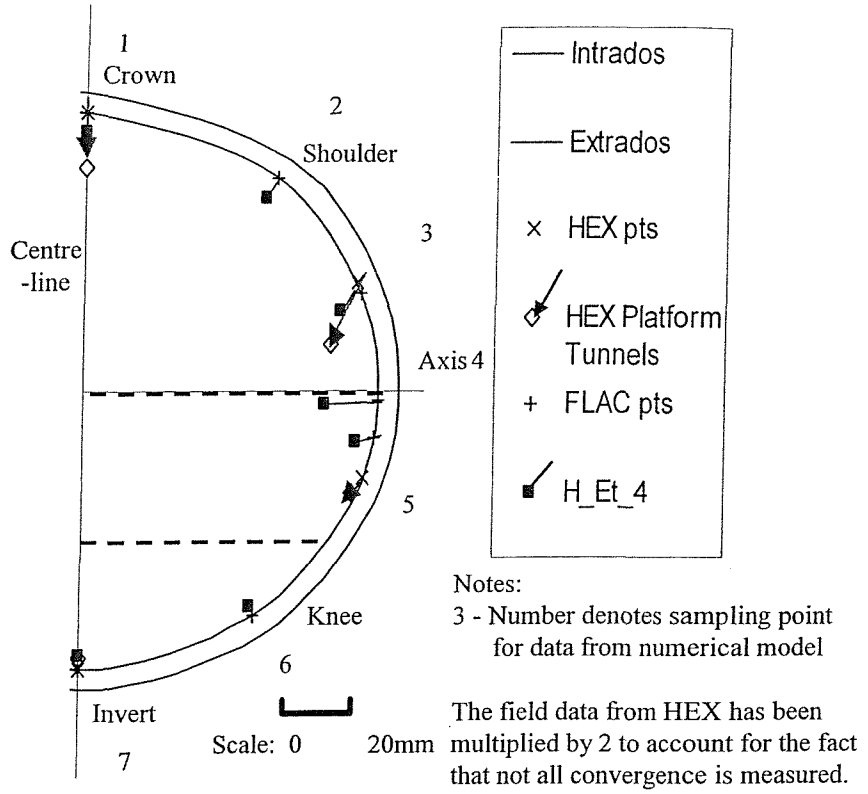

Figure 6.28 Vertical deformation vs distance from face

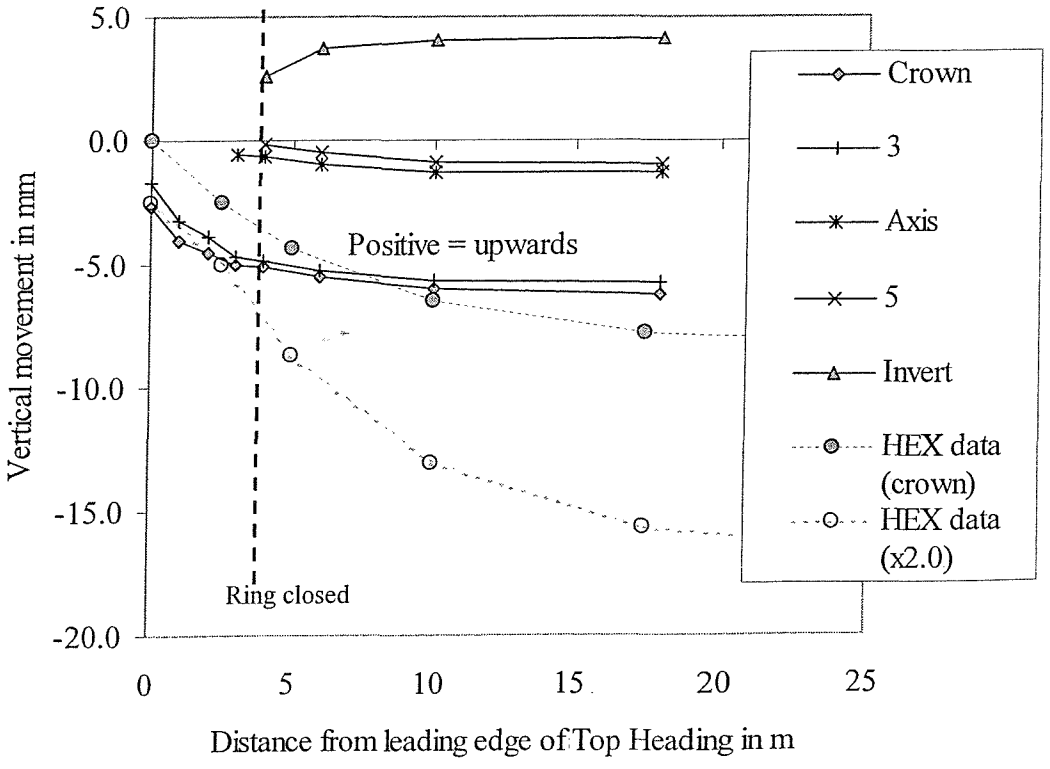

Figure 6.29 Longitudinal axial forces vs distance from the face

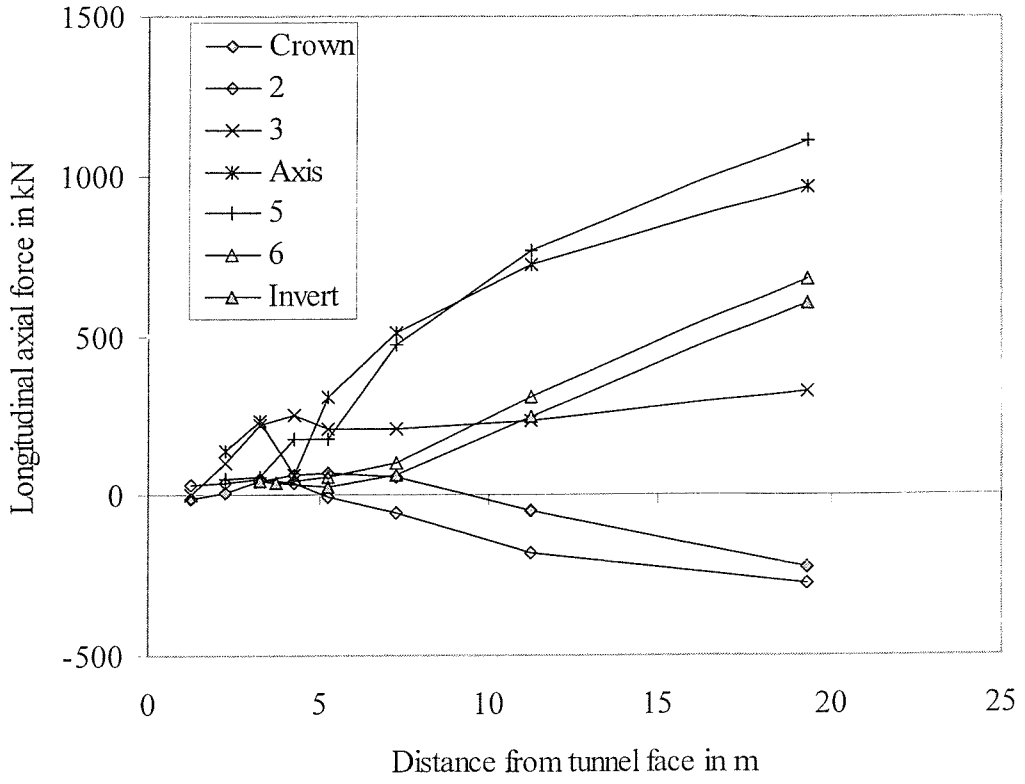

Figure 6. 30 Longitudinal bending moments vs distance from the face

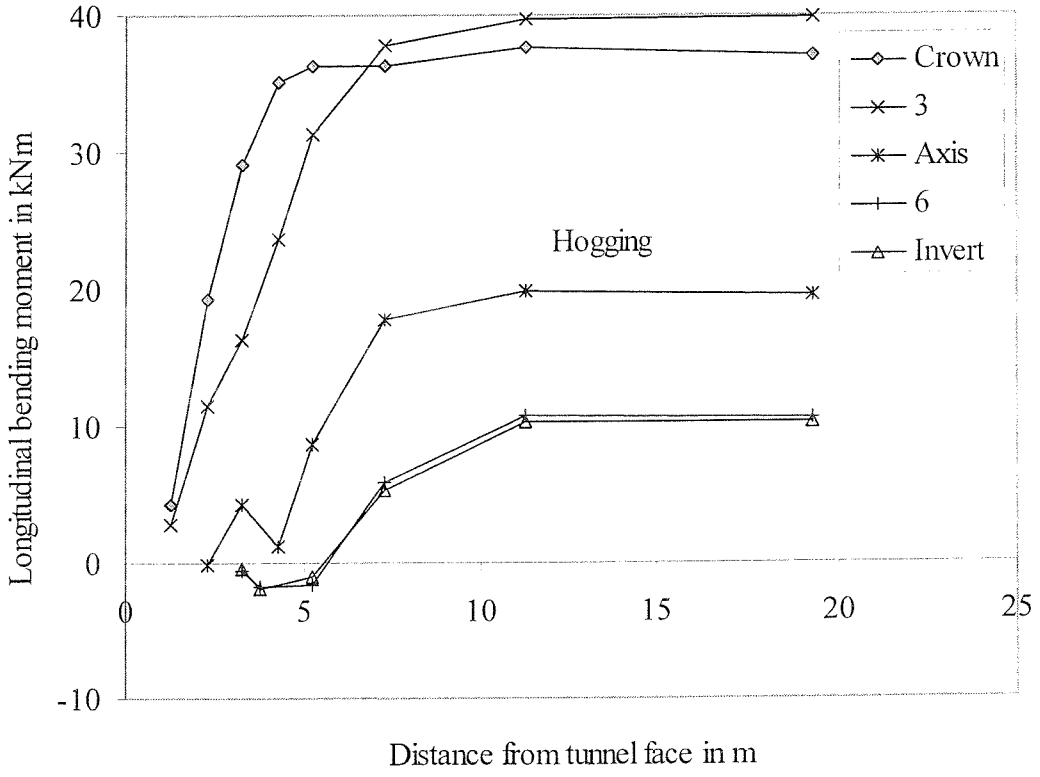

7 DISCUSSION

The purpose of this thesis has been to examine the influence of the modelling of the sprayed concrete lining in design analyses of SCL tunnels. This was born out of the observed discrepancy between the performance of real tunnels and their design predictions. It was established in the literature review that sprayed concrete exhibits a complex material behaviour and that this is rarely modelled fully in design analyses. A suite of constitutive models was developed to simulate various aspects of the material behaviour of sprayed concrete (e.g. ageing, nonlinear stress strain behaviour & creep). The influence of these different models has been examined in simple numerical models of laboratory tests (see Chapter 5). The results suggest that the constitutive model of the sprayed concrete can have a large influence on design predictions. In the final part of the research the influence of the constitutive behaviour, along with other aspects of construction, were examined in a numerical model of a single, shallow SCL tunnel in clay.

In this section a selection of results from the analyses listed in Appendix G will be presented to illustrate the impact of variations in certain key elements of the numerical model. These key elements are:

- the constitutive model of the sprayed concrete;
- the geotechnical constitutive model;
- the construction sequence and
- the lining geometry.

The identification codes for the analyses are contained in Tables 7.1 to 7.4.

Table 7.1: Model tunnel geometry

Abbreviation	Description
H	The exact cross-sectional geometry for the HEX platform tunnel; face area = 61 m^2; lining thickness = 0.30 m
N	Circular cross-sectional geometry with the same face area as the HEX platform tunnel; external radius = 4.40 m; lining thickness 0.30 m
N* [82]	Circular cross-sectional geometry with the same radius as HEX concourse tunnel top heading – face area = 54 m^2; external radius = 4.15 m; lining thickness 0.30 m

Table 7.2: Sprayed concrete constitutive models

Abbreviation	Description – see also Chapter 4
E-	Linear elastic, constant stiffness = 28 day value
Et	Linear elastic, age-dependent stiffness – see 4.3.1
HME	Hypothetical Modulus of Elasticity – see 4.3.6
MCSS	Strain-hardening plasticity model (Mohr-Coulomb) – see 4.3.3.1
NLE	Nonlinear elastic model - Kotsovos & Newman (1978) – see 4.3.3.2
VE 1	Visco-elastic "Kelvin" creep model - stress independent – see 4.3.5.3
VE 2	Visco-elastic "Kelvin" creep model - stress dependent – see 4.3.5.5
VE 3	Visco-elastic "Kelvin" creep model after Yin (1996) – see 4.3.5.3
JR	MCSS model but strength reduced by 50% on radial joints
JL	MCSS model but strength reduced by 50% on longitudinal joints
J	MCSS model but strength reduced by 50% on radial & long. joints

[82] In the early part of the study a simpler model was used – see section 6.2.

Table 7.3: Geotechnical constitutive models

Abbreviation	Description – see 6.3.3
0	Isotropic linear elastic – "soft" – Eu = 600*Cu
1	Isotropic linear elastic perfectly plastic (Tresca) – Eu = 600*Cu
2	Transversely anisotropic linear elastic – Evu = 600*Cu
3	Transversely anisotropic nonlinear elastic – Evu max ~ 1500*Cu
4	Isotropic strainhardening plastic (Tresca) – Emax = 1500*Cu
5	Isotropic linear elastic perfectly plastic – "stiff" – Eu = 1500*Cu

Table 7.4: Variations in construction sequence

Abbreviation	Description – see 6.3.2
A_0.5	Advance length of 0.5 m
K_1.5	Constant K_0 value = 1.5
S_2.0	Advance rate = 2.0 m / day
X_4.5	Ring closure distance = 4.5 m

As noted earlier, such a comprehensive study of the influences on the loads in a SCL tunnel has never been performed before using a 3D numerical model of an advancing tunnel. The focus of the discussion is the impact on the lining design parameters – i.e. the forces, bending moments and displacements of the tunnel lining. Having established the overall stability of a tunnel the main focus of interest for a designer is usually the determination of the loads in the tunnel lining. The prediction of ground behaviour is of secondary interest. In the context of this case study – a shallow tunnel in London Clay – empirical methods are often more reliable than 3D numerical methods in predicting surface settlement (e.g.: van der Berg 1999). Various corrections can be employed to improve numerical predictions – for example, an unrealistically long unlined length can be used (e.g.: Sharma *et al.* 2000) or K_0 can be reduced beside the tunnel (e.g.: Addenbrooke 1996).

Unless otherwise stated the values for forces and bending moments below have not been corrected for the errors listed in Table 6.6. The data in the figures refer to the H-series, unless otherwise noted.

7.1 Influence of the constitutive model for sprayed concrete

The base case was analysis H_Et_4 – i.e. the exact geometry of the HEX tunnel with an age-dependent linear elastic lining and a linear elastic strainhardening plastic model for the clay.

The influence of the constitutive model for the sprayed concrete depended heavily on the magnitude of the stresses in the lining. Even within this limited study, changes in the modelling of the ground and excavation sequence produced sufficient variations in the loading to alter the influence of the constitutive model considerably. For the N* series the constitutive model had a large influence whereas for the H and N series the influence was less pronounced (see Figure 7.1 & 7.2). In the N* series the insitu stresses, the advance length and rate of advance were larger, leading to much higher hoop loads in the lining – near the face which proved to be the critical area (see Figures 7.3 & 7.4).

The following discussion will concentrate on the loads in the crown at the Leading Edges of each ring since the stresses in the lining were generally greatest there.

7.1.1 Hoop forces in the tunnel lining

As the "stiffness" of the constitutive model of the lining decreased, the loads in the lining decreased. In other words as the strains predicted by the constitutive model increased, the loads decreased. This is a well-established phenomenon (e.g.: Peck *et al.* 1972 and Soliman *et al.* 1993). Ageing of the elastic moduli (in which the moduli rise from a low initial value), nonlinearity of stress strain behaviour and creep all lead to more strain for a given load, compared to the constant, high stiffness model (E-). Because the lining deforms more, in these particular ground conditions, the stresses in the ground are relaxed. Consequently the loads in the lining decrease.

Figures 7.5 and 7.6 show the utilization factor at the intrados and extrados of the lining – which is the current stress divided by the strength – and illustrate this reduction in loads. It is also clear that the utilization factors are highest at the face – since the strength is lowest here – and they decrease rapidly. This is in line with findings by others – e.g.: Rokahr & Zachow 1997. As a result the effect of the different constitutive models for the sprayed concrete was noticed mainly within the first few metres of lining – see Figure 7.7. Beyond this point there was generally little difference in the development of the load except that the peak in axial load ahead of the invert closure was not observed in the constant, high stiffness model (E-).

Figure 7.7 clearly demonstrates that the ageing of the stiffness of the lining is an important factor in determining the loads in the lining, if one compares the constant stiffness (E-) and age-dependent stiffness (Et) models. This contradicts findings by some (e.g.: Bolton *et al.* 1996 & Sharma *et al.* 2000) who have rejected the importance of ageing on the basis of a review of its effect on surface settlement – see 7.1.6. However, others have highlighted the significance of the lining stiffness (e.g.: Berwanger 1986, Huang 1991, Moussa 1993, and Cosciotti *et al.* 1999 – see also section 2.3.3.1).

The base case (Et) model predicted loads which were less than 50% of those predicted by a commonly-used analytical solution[83] and which were generally higher than the estimates of hoop loads from the strain gauges and radial pressure cells in the HEX tunnel linings (Mott MacDonald 1998).

In general the variations in hoop forces were small for the nonlinear elastic and elastoplastic models in the H and N series models (see Figure 7.1). The two-stage Hypothetical Modulus of Elasticity model showed a larger reduction – 14 to 18% - compared to the ageing elastic model (Et), because the elastic modulus grew rapidly with age. Initially the HME stiffness is twice that of the age-dependent model and as a result the forces and moments are higher. At ring closure in the Top Heading the HME stiffness is only 20% of the age-dependent

[83] Analytical solution by Einstein & Schwartz (1979), assuming stiffness of the ground is 100MPa, the lining is 15GPa and $K_0 = 1.50$, predicted a hoop force of 2500 kN and a bending moment of 38 kNm.

stiffness. Hence the lower ultimate values for forces and moments in the invert. At the Trailing Edge the hoop forces are higher initially and remain slightly higher. This leads to a more even distribution of stress in the lining.

The creep models predicted some of the lowest hoop forces. The reduction increased with increasing creep capacity. Model VE2 incorporated a stress dependent function that produced a linear increase in creep parameters with utilization factor above a utilization factor of 45%. Consequently in general VE2 predicted lower loads than the stress-independent model (VE1) – see 4.3.5 – although since the utilization factors were mostly below 45% in the analyses of the tunnel, the difference here was small (see Figure 7.7). The creep model with ageing after Yin (1996) - VE3 - had the greatest creep capacity at early ages (see 4.3.5.3) and so it predicted the lowest hoop forces and utilization factors (see Figure 7.8). Creep of sprayed concrete has long been regarded as being a beneficial phenomenon which leads to lower lining loads (e.g.: Rabcewicz 1969, Huang 1991, Schropfer 1995 and Yin 1996 – see also 2.3.3.6), although this depends on the ability of the ground to carry the remainder of the load (Pöttler 1990). Figure 7.8 shows how creep can "smooth" out the stress distribution in the lining (as suggested by Rokahr & Lux (1987)).

7.1.2 Hoop bending moments in the tunnel lining

The distribution of bending moments is governed by the shape of the tunnel – both the shape of subdivisions of the heading and the final completed cross-section. Sudden changes in shape and tight radii, such as those seen when a tunnel is constructed using side-galleries (see Figure 1.4), can lead to concentrations in bending moments. In this case study the tunnel cross-section was almost circular and a Top Heading, Bench and Invert sequence was adopted. Therefore there are no local high concentrations in bending moments (see also 6.4.2). Ahead of ring closure, the crown experiences hogging due to the large horizontal loads on the Top Heading arch while there is a small amount of sagging at the axis level (see Figure 7.9). After ring closure most of the ring experiences hogging bending moments. The discussion below concentrates on hoop bending moments in the crown.

The hoop bending moments tended to be more strongly affected by the constitutive model for the sprayed concrete than hoop forces because the effect of the lever arm in the moment calculation was to magnify changes in stress.

In all cases the models with a constant high stiffness (E-) predicted much higher bending moments than the base case of the age dependent (Et) models (see Figures 7.2 & 7.9). The base case was also much lower than a commonly used analytical solution, which predicted a bending moment of 38 kNm [83]. The predictions from the numerical models were generally less than the estimates of bending moments from strain gauges in the HEX tunnel lining. However these estimates used a simplistic conversion of the recorded strain into stress with a relatively high stiffness (15 GPa) and therefore may not be reliable.

Where the loading was lower – i.e. the N and H series – nonlinearity of stress-strain behaviour had little effect because up to utilization factors of 50% the behaviour of the models was basically the same as the linear elastic model (Et) (see Figure 7.9 a & 4.3). However, in the N* series in the first 2 metres the utilization factor was generally well above 50% (see Figure 7.4). Hence the "softer" stress-strain response at this higher loading led to more deformation, a favourable redistribution of stresses and lower loads. This echoed the findings of the earlier work on the numerical modelling of the large-scale laboratory tests – see 5.2.3 – and the findings of others (e.g.: Moussa 1993, Hafez 1995 and Hellmich *et al.* 1999c).

The Hypothetical Modulus of Elasticity (HME) models for the sprayed concrete predicted higher bending moments than the age dependent (Et) models due to the relatively high stiffness in the first few metres of lining (see Figure 7.9).

In a similar manner to the hoop forces, the creep models predicted some of the lowest bending moments (see Figure 7.2). The beneficial effects of creep depend on the level of loading and any stress-dependency, as well as the specific creep capacity. Although there was no difference in the bending moments at the crown between the stress-independent (VE1) and

stress-dependent (VE2) models, above and below the axis level, the moments are reduced – by between 10 and 33%.

7.1.3 Tunnel lining deformations

As before the constitutive model has a significant influence on the results of the numerical modelling. The "softer" the model, the more deformation occurred (see Figure 7.10). For example, the nonlinear elastic and strain-hardening plasticity models predicted higher displacements by about 6 and 10% respectively compared to the base case, linear elastic (Et) model.

In general the models predicted that the displacement of the crown would stabilise within about 1.5 tunnel diameters of the face. However, for the high creep capacity model, VE3, even at large ages there was considerable creep capacity, and so the lining deformations continued to increase with time and showed no sign of stabilising even 20m from the face. Pöttler (1990) and Yin (1996) have noted that creep in the lining may adversely interact with the ground, rather being a beneficial phenomenon. If the ground cannot cope with the load that is transferred into it, more yielding will occur and deformations will increase. The results run counter to the measured convergence at HEX, which showed a stabilisation of movements within about 2 diameters of the face. This suggests that the ageing function used in the high creep capacity model (VE3) overestimates the actual creep of sprayed concrete.

In general the numerical models predicted more deformation at early ages and less at later ages than was measured in HEX tunnels (see Figure 7.10). However, one must bear in mind that the in-tunnel convergence measurements only capture a fraction of the deformation due to the delay in installing the convergence pins (see 3.2.2). The values from the numerical models represent the total deformation. At Hex the measured lining deformations were estimated to be about 50% of the total displacements so points have been added to Figure 7.10 showing the measured values multiplied by a factor of two.

Figure 7.11 shows the movements around the cross-section predicted by the models together with the measured values. The patterns are broadly similar. The high lateral movements

predicted at the axis level seem to be largely due to the fact that the Leading Edge of the lining at this point shared a node with the ground.

7.1.4 Longitudinal forces and bending moments in the tunnel lining

Longitudinal stresses in tunnel linings have rarely been examined in detail. Figures 7.12 and 7.13 show that the constitutive model of the sprayed concrete has a large influence on the predicted longitudinal forces. In general the longitudinal forces are small if the age-dependent stiffness is incorporated into the model (e.g.: Et or MCSS). However the bending moments were high for all models, except the HME model.

In the top part of the lining – i.e. above axis – the extrados of the lining was in tension due the relative movement of the ground towards the face – see 6.4.2. The intrados was in compression. This process continued far back from the face and therefore it was the stiffness here that helped to determine the longitudinal forces and bending moments in the final situation. The tension cut-off in the plasticity model (MCSS) and creep in the VE models helped to reduce the tension and therefore the bending moments. The lowest loads were predicted by the HME model because of its relatively low stiffness throughout the lining.

In the absence of field data on longitudinal loads it is not known how realistic these predictions are. Since the tension is on the extrados, cracking would be hidden from view. Potentially this could cause a durability problem as it would permit water access into the body of the lining. There is some anecdotal evidence from segmentally lined pilot tunnels that longitudinal movements in the ground can drag tunnel linings into tension, causing the joints between rings to open.

7.1.5 Ground stresses

The ground stresses acting radially on the tunnel lining govern the loads in it. The predicted radial stresses acting on the lining after it has been built are about 50% of the initial insitu stresses (see Figures 7.14 & 7.15). This is in line with suggestions by others for the short-term loads on shallow tunnels in London Clay (e.g.: Muir Wood 1975). The constitutive model of the sprayed concrete generally had a moderate effect on the ground stresses acting

radially on the tunnel. However, the radial stresses ahead of the face are not affected by the constitutive model of the lining (see Figure 7.14).

All of the models show a peak in radial stress on the lining after ring closure but this is not apparent in the field data from HEX (Mott MacDonald 1998). The field data and predicted values near the face and far from it agree quite well (see Figures 7.14 & 7.15).

Unlike the other models, the model with a constant high stiffness (E-) predicted a more extreme pattern of radial stresses, with a high peak in radial stress after ring closure but the lowest stresses further from the face.

7.1.6 Ground movements

Table 7.5 shows that the age-dependency of the elastic stiffness of the sprayed concrete had a large influence on the overall volume loss, again contradicting the findings of Bolton *et al.* 1996 and Sharma *et al.* 2000. The volume loss was generally higher by 0.08% for the age-dependent elastic models (Et), compared to the age-independent elastic model (E-). Nonlinearity of the sprayed concrete behaviour (i.e. the MC or NLE models) had virtually no effect on the predicted volume losses.

Table 7.5: Volume losses in percent

	E-	Et	HME	MCSS	NLE	VE1	VE2	VE3
H series	0.43	0.51	0.53	0.52	0.52	0.51	0.51	-
N series	0.34	0.42	0.42	0.42	-	-	0.42	-
N* series	0.52	0.59	0.55	0.58	-	0.56	-	0.87

The high-creep capacity model VE3 (in the N* series) predicted large lining displacements and ground movements that showed no sign of stabilising. Hence it predicted a highest volume loss.

With the exception of the age-dependence of the stiffness, the constitutive model of the sprayed concrete did not have any significant influence on the magnitudes of ground movements ahead of the tunnel face (either near the tunnel or far away) or the shape of the surface settlement troughs (see Figures 7.16 & 7.17). The surface settlement troughs for all of the models did not look realistic compared to actual field measurements (Mott MacDonald 1998) and the volume losses were less than the estimated value of 0.85% for the HEX Platform tunnels (except for VE3). It is believed that this is due to deficiencies in the modelling of the ground (see 7.2.6).

7.1.7 Summary of effects of sprayed concrete constitutive model

The patterns of behaviour outlined above were observed to be the same both at the Leading and Trailing Edges of each ring and regardless of the different constitutive models for the ground. This suggests that the constitutive model of the sprayed concrete is an important consideration, especially when trying to predict the forces and bending moments in a tunnel lining.

Another important conclusion is that the ageing of the stiffness of the sprayed concrete should be modelled since this has a large influence on the results of the numerical model. While the stiffness of sprayed concrete is not often a parameter that is measured in the normal course of pre-construction trials or quality testing, as a first approximation it is reasonable to assume that stiffness grows at the same rate as compressive strength. Strength data normally exist or can be assumed for a given mix. Alternatively, there are numerous relationships for predicting the growth of stiffness with age – see Appendix A. Therefore this is easy to incorporate into a 3D numerical model.

The HME approach has been used very successfully as a "numerical short-cut" in 2D analyses – see 2.3.3.2. However, these results suggest that this constitutive model overestimates hoop bending moments. These are often the governing design parameter in shallow SCL tunnels. The choice of stiffness values is critical to the predictions of the models. A "coarse" two or three stage HME model is not recommended. The usage of the HME approach should be updated. The stiffness at all ages in the age-dependent model (Et)

could be reduced by a factor to account for creep and nonlinear effects, thereby producing a "finer" HME. The only remaining problem would be how to determine the reduction factor, without performing a full creep analysis. A first approximation could be to estimate the creep capacity from the mix design using existing codes of practice (e.g.: as in section 4.3.6).

From the practical stand-point of deciding whether or not to use a more sophisticated model than the elastic ones above, a decision could be made after examining the extent of high utilization factors (i.e. >70%) predicted by an age-dependent elastic model.

The nonlinear elastic model by Kotsovos and Newman (1978), chosen for this study, is not offered as standard in commercial numerical modelling programs. The process of implementing the nonlinear model in the full analysis of the advancing tunnel proved to be time-consuming because of the added complication of zones of material with different ages that change their age with each advance of the tunnel. The difficulty of debugging numerical models increases with their complexity. The run times were also longer. Hence only one run was completed with the nonlinear elastic model for the sprayed concrete lining. For these reasons it may be better to choose a standard strain-hardening plasticity model to replicate the nonlinear stress-strain behaviour, unless there are special conditions which suggest that it would be preferable, e.g.: if it was deemed necessary to add nonlinear elasticity to a creep model.

If creep effects are believed to be important, either because of high early loading or a high creep capacity in the sprayed concrete, it is recommended that a full creep analysis is done since the creeping lining may interact in a detrimental way with the ground as noted above in the case of model VE3. Because of the risk of an unfavourable interaction with the ground, one cannot assume that creep is always beneficial. In general the stress-dependent viscoelastic model (VE2) is recommended.

Finally the ground behaviour is markedly influenced by the elastic stiffness of the lining. Incorporating the ageing of the stiffness leads to more realistic predictions of radial stresses

and higher volume losses. Apart from this the constitutive model of the lining generally has a small influence ground movements and stresses. The constitutive model for the lining has very little influence on the predictions of ground movements ahead of the face.

7.2 Influence of the constitutive model of the ground

Table 7.3 summarises the ground models used in this study (see Appendix D for full details). As before the base case was H_Et_4. This had a K_0 profile that varied with depth (see Figure 6.2). Models were also run with constant profiles of K_0 = 1.0 (H_Et_4_K1 & H_Et_5_K1) and K_0 = 1.5 (N*_Et_4_K1.5). The following discussion will concentrate on the loads in the crown at the Leading Edges of each ring, since the stresses in the lining were generally greatest there. The model for the sprayed concrete was the age-dependent elastic model (Et). Unless otherwise stated the values in the Figures 7.18 to 7.26 come from the H series runs.

7.2.1 Hoop forces in the tunnel lining

Figure 7.18 shows that the ground model had a moderate influence on the hoop forces in the crown of the tunnel. In general the nonlinear elastic transversely anisotropic model (3) was the "softest" model and gave the highest forces while the stiff elastoplastic model (5) predicted the lowest forces. This is in keeping with the established belief that the relative stiffness of the ground and structure is important in determining the behaviour. The perceived wisdom is that the stiffer the ground is the lower the loads in the structure as a consequence of soil-structure interaction. As Table 7.6 shows, the pattern was similar at the axis. Comparing the linear isotropic and anisotropic elastic models (0) and (2), it appears that anisotropy did not have much effect on the hoop forces at the crown. The vertical stiffnessses were the same in both models. The loads were lower at the axis because it was stiffer in the horizontal plane. The horizontal stiffness was 1.6 times the vertical stiffness in the anisotropic model.

Plasticity in the ground model generally led to lower loads because there was more relaxation of the ground stresses in comparison to an equivalent elastic analysis (*cf.* models 0 and 1). In contrast, Yin (1996) and Oettl *et al.* (1998) found that adding plasticity led to higher lining loads in 2D numerical models. The difference may be related to the fact that these were 2D

models and therefore the modelling of the stress redistribution may be different (Lee & Ng 2002) – see also 7.2.5.

Table 7.6: Hoop loads at crown and axis level, normalised w.r.t. the base case

Ground model	0	1	2	3	4	4_K1	5	5_K1
Elastic stiffness	*soft*	*soft*	*soft*	-	-	-	*stiff*	-
Plasticity in the model ?	*no*	*yes*	*no*	*no*	*yes*	*yes*	*yes*	*yes*
Hoop force – crown	1.08	1.00	1.07	1.20	**1.00**	1.07	0.88	0.73
Hoop force – axis	0.97	0.94	0.89	1.00	**1.00**	1.10	0.73	0.67
Bending moment – crown	1.82	1.32	1.79	3.57	**1.00**	1.26	0.67	0.62
Bending moment – axis	0.56	1.08	0.30	0.68	**1.00**	0.99	0.70	0.57

The loads were not necessarily lower when the lateral earth pressures were lower (i.e. when K_0 was lower) – see Table 7.6. It seems that this factor cannot be separated from the stress-strain behaviour of the ground model. Models 4 and 5 produced apparently contradictory results, with the former predicting higher loads when K_0 is lower and the latter predicted the opposite.

Table 7.7: Results for a variable K_0 profile compared to a constant profile (K_0 = 1.5)

	% change		% change
Hoop force in crown	-1	Radial displacement in crown	-3
Hoop moment in crown	-12	Radial displacement at axis	-9
Hoop force at axis	0	Radial stress on lining at crown	-2
Hoop moment at axis	+44 [84]	Radial stress on lining at axis	-5

The use of a K_0 profile that varied with depth had very little impact on the tunnel lining compared to the constant K_0 profile – *cf.* the base case, N*_Et_4 and N*_Et_4_K1.5 (see

[84] The difference appears to be large but the actual numbers were small; 7.8 and 5.4 kNm respectively.

Table 7.7). This is because the difference in horizontal stresses at the level of the tunnel was small. The stresses were about 5% lower in the model with the variable K_0 profile.

The development of the loads in the lining with distance from the face followed the same pattern in all models as was seen in the base case (see Figure 7.7).

7.2.2 Hoop bending moment in the tunnel lining

The constitutive model of the ground influenced the bending moments more than the hoop force (see Figure 7.18). Apart from the nonlinear anisotropically elastic model (3), one can see that the elastic ground models (0 & 2) produced higher bending moments in the crown than the plastic models (1,4 & 5). The opposite was true at the axis (see Table 7.6). The predicted bending moments were low for the anisotropic models (2 & 3) because the stiffness in the horizontal plane was higher than the vertical plane.

7.2.3 Tunnel lining deformations

Figures 7.19 and 7.20 show the predicted lining deformations for different ground models. Although it predicted the lowest settlements of the tunnel crown, overall the nonlinear anisotropic elastic model (3) predicted the largest movements. In particular it predicted very large horizontal movements near the axis, in contrast with the measured values from the HEX tunnels.

Considering the whole ring, the stiff elastoplastic model (5) predicted the smallest deformations for the runs with variable K_0 profile. These deformations were even smaller for model 5 when K_0 was 1.0. This is in line with the effects of the ground model noted above on the hoop loads.

7.2.4 Longitudinal loads in the tunnel lining

All of the elastic models (0,2 & 3) predicted very high tensile forces in the longitudinal direction – up to more than 1000 kN in the crown. The bending moments were very high too, exceeding 50 kNm in the crown. Introducing plasticity into the ground model reduced these loads considerably. For example, the loads in the linear elastic perfectly plastic model (1)

were about 20% lower than in the linear elastic model (0). The strain-hardening plasticity model (4) predicted the lowest forces and moments – typically 50% lower than the linear elastic model 0.

The initial K_0 value had little influence on the longitudinal forces in the Top Heading.

7.2.5 Ground stresses

Figure 7.21 shows the radial stress acting on the tunnel lining. The constitutive model of the ground had a moderate influence on the radial stress. The radial stresses were about the same irrespective of the initial stress state (K_0 value) – i.e. they differed by less than 10% (see Figure 7.21). This may suggest that the final stress state at the tunnel is governed more by the yield strength of the ground and the tunnel dimensions than the initial stress state.

Table 7.8: Average radial stress as a percentage of full overburden pressure

Ground model	0	1	2	3	4	4_K1	5	5_K1
Elastic stiffness	*soft*	*soft*	*soft*	-	-	-	*stiff*	*stiff*
Plasticity in the model ?	*no*	*yes*	*no*	*no*	*yes*	*yes*	*yes*	*yes*
Ave. radial stress at 16.5 m from the face	0.36	0.31	0.44	0.31	0.45	0.49	0.34	0.31

Figure 7.22 shows the stress paths in the ground near the crown of the tunnel. In general the pattern was similar for all models but there were some differences. As one would expect, the most extreme changes in stress were observed in the elastic models (0, 2 & 3) since there is no yield surface to limit this. The linear elastic models predicted increases in the mean stress whereas the nonlinear and plastic models exhibited stress paths in which the mean stress fell as tunnel approached and then recovered. This leads to quite different distributions of pore pressure changes with the elastic models showing only positive pore pressure changes and the plasticity models showing some negative pore pressure changes near the face. Therefore plasticity models should be used if a realistic pore pressure distribution is required.

For clarity some of the models have been omitted from Figure 7.22. Model 1 – the "soft" linear elastic perfectly plastic model – showed stress paths that were almost identical to its "stiff" counterpart, model 5, although the changes in mean stress were slightly larger. H_Et_4_K1 was similar to H_Et_4 but there were larger increases in mean stress because, when the K_0 value was 1.0, the initial stress state in the ground was further from the yield surface.

Figure 7.23 shows the stress strain behaviour in the ground at the tunnel crown. A similar pattern of behaviour was observed at the axis but there the nonlinear elastic anisotropic model (3) predicted more strain than the other models (see Table 7.9) – hence comment in 7.2.1 that overall this model produced the "softest" response.

Table 7.9: Max. deviatoric strain in ground at various levels around the tunnel

Ground model	0	1	2	3	4	5	4_K1	5_K1
Deviatoric strain in % at crown	0.56	1.34	0.40	1.22	1.03	0.58	1.16	0.34
Deviatoric strain in % at axis	0.57	0.90	0.44	1.19	0.80	0.40	0.91	0.35

7.2.6 Ground movements

Figures 7.24 and 7.25 show the surface settlement curves for the various ground models. The results from this study followed the pattern seen in other numerical models- namely: the far-field surface settlements are overestimated; the settlement above the centreline is underestimated and, due to the K_0 values greater than 1.0, there is relative heave above the centreline (e.g.: van der Berg 1999 and Lee & Ng 2002). The overall volume losses were within a realistic range (see Table 7.10) but they are lower than the measured values at HEX of about 0.85%. Apart from the models with "unrealistically" low K_0 values, only the anisotropic nonlinear elastic model (3) predicted realistic surface settlements. However, this model overestimated the movements ahead of the face (see Figure 7.26). This led to an overestimate of the overall volume loss.

Adding a Tresca yield criterion to the isotropic linear elastic ground model increased the amount of ground movement (both at surface and near the tunnel) due to yielding, as would be expected (*cf.* models 0 and 1).

Table 7.10: Volume losses in % for different ground models

Ground model	0	1	2	3	4	4_K1	5	5_K1
Elastic stiffness	*soft*	*soft*	*soft*	-	-	-	*stiff*	*stiff*
Plasticity in the model ?	*no*	*yes*	*no*	*no*	*yes*	*yes*	*yes*	*yes*
Volume loss in %	0.43	0.66	0.32	0.74	0.51	0.58	0.51	-

Comparing the two runs with an elastoplastic ground model but different stiffnesses (models 1 & 5), one can see that increasing the stiffness by a factor of 2.5 reduced volume loss by a fifth and halved the surface settlement on the centreline. The movements towards the face were much reduced. Of all the models, the stiffer elastoplastic model (5) predicted the movements towards the face most accurately. The other models overestimate the displacements into the face, above and below the tunnel (see Figure 7.26).

Comparing models (0) and (2) it appears that anisotropy reduced both the near and far-field predicted ground movements, in line with the findings of others (van der Berg 1999 and Lee & Ng 2002). At the face the longitudinal movement was reduced by about 33% (see Figure 7.26).

The K_0 profile had a large influence on the predicted surface settlement. It is well established that the shape of the settlement trough depends heavily on the K_0 value and that a high K_0 leads to relative heave above the centre-line of the tunnel and high far-field surface settlements (e.g.: Addenbrooke 1996, van der Berg 1999, Krenn 1999 and Lee & Ng 2002). Compared to the base case - variable K_0 profile – a constant K_0 value of 1.0 produced a much more realistic prediction of settlement (see Figures 7.24 & 7.25 and Addenbrooke (1996)), although the far-field surface settlements were still overestimated.

7.2.7 Summary of influence of ground model

The modelling of the ground – its constitutive model and the initial stress state - had as important an influence over the loads in the lining and the ground behaviour as the constitutive model for the lining itself. In general the magnitude of the influence was the same.

Considering the predicted ground movements only, then the results from this study confirm that the initial stress state has a profound influence. Plasticity should be included since simple elastic models underestimate the movements and some form of nonlinearity should also be included since this produces more localised deformation in line with observations from the field. However, the initial stress state – often characterised by the K_0 value – is probably the single most important factor. Unrealistically low K_0 values have to be used in order to get realistic surface settlement predictions. This suggests that some aspect of the behaviour of the ground is still not being modelled well enough.

7.3 Influence of tunnel geometry & construction defects

7.3.1 Cross-sectional geometry

In general, whether the exact geometry or an equivalent circular geometry was used had no effect on the general pattern of behaviour in the crown of the tunnel when constitutive model for the sprayed concrete was varied (see Figures 7.1 & 7.2). However, the stress distribution was quite different depending on the shape of the lining. Figures 7.7 and 7.9 show that while the hoop forces were generally little changed, the pattern of bending was reversed below the axis. In the final case the entire ring (for the circular geometry – N series) was in hogging. The greatest change occurs in the Bench where the moments were about 25% of the values in the base case - H_Et_4 - and the hoop force was doubled. This behaviour was observed at both the Leading and Trailing Edges of the rings.

However, the volume loss was 20% lower for the equivalent circular geometry. There was a reduction in surface settlements both ahead of and behind the face. The ground movements into face and the lining deformations were both smaller. The root cause of this may lie partly

in the fact that the circular lining is an inherently stiffer shape. The pattern of the displacement vectors in the ground did not appear to be affected by the difference in shape of tunnel lining.

7.3.2 Doming of the face

Sometimes due to concerns over face stability, the face of a tunnel is domed so that the concrete sprayed on the face can act as an arch. In addition to doming, a berm may be left to help support the face (see Figure 7.27 and Pound & Beveridge 2001). Doming the face in the numerical model led to a very slight reduction in the stresses in the lining (both in the hoop and longitudinal direction). The stresses in the ground appeared to be virtually unchanged but the strains were higher. In reality the doming undermines the ground above the crown with the risk of worsening face stability. In the numerical model the undermining was counteracted by the berm.

7.3.3 Construction defects – at joints

Poor construction at radial joints has been established as a contributory factor in tunnel collapses (HSE 2000). The results of this study confirm that the presence of weak joints does influence the predicted behaviour of the lining. The effect on the final stress state in the lining was arguably less dramatic than one would expect given the large reduction in strength. At the weakened joints the strength was 50% of the normal strength. Furthermore the effects in this particular case were not always negative.

Weak radial joints did not lead to much change in the stress state in the lining. The hoop bending moments at the shoulder and knee were increased and decreased respectively by large amounts (i.e. more than 33%) but otherwise hoop forces and moments remained the same. The deformation of the lining was basically unaltered, as was the longitudinal behaviour. This may be because the tendency of each ring / partially complete section of the lining to converge was restricted by the previous ring which, being older, was stiffer. As Figure 7.28 shows the utilization factors in the lining were about 4% lower than the base case - H_Et_4, except right at the face where they were about 4% higher. Weak radial joints might have had a greater effect if the hoop loads had been greater

Weak longitudinal joints in general led to lower forces in the Top Heading and Bench and higher deformations at the Leading Edge in the final case. Near the face the bending moments in the crown were up to 50% lower. The hoop forces were about 10% lower. Radial displacements increased by a similar percentage. Longitudinal bending moments were considerably lower (down by a third) above axis. In longitudinal direction the whole lining remained in compression. In contrast the base case predicted tensile axial forces in the Top Heading. In this respect the yielding in the longitudinal direction was beneficial. It appeared that the weaker joints permitted a small amount of additional movement and therefore more relaxation in the ground. Hence the lower hoop forces. Figure 7.28 shows that there is a more even distribution of load in the lining. This occurred throughout the Top Heading.

Although the additional deformation permitted by the weak longitudinal joints, in this model, led to some improvement in the performance of the lining, this may not be the case in a real tunnel. These results suggest that the proper formation of circumferential joints and the continuity of longitudinal reinforcement across those joints may be as important as the formation of sound radial joints.

Weakening joints both radially and longitudinally resulted in a combination of the effects noted above. Near the face in the Top Heading the stresses were higher (see Figure 7.29 & 7.30). Hoop forces were increased by up to 15% and bending moments by 50% in the crown. Soon after the closure of the invert there was a sudden drop in the loads, particularly bending moments (see Figure 7.30) and an increase in convergence. The stress distribution was markedly altered by the weak joints, although overall, in this case, the final utilization factors were lower than the base case (see Figure 7.28) – i.e. the final situation was better.

As well as confirming that weak joints may affect the stress distribution in the lining adversely, the results above demonstrate the potentially beneficial effects of limited stress redistribution by permitting more movement in the ground. This is a well-established principle in rock NATM tunnelling (e.g.: Rabcewicz 1969). However, in shallow soft ground

tunnels – such as the HEX Platform tunnels - the margin of error / timeframe between acceptable and unacceptable strains is so small that this phenomenon should not be used in design. One should note that the volume loss predicted by these analyses was only 0.5%, which was about 50% lower than the actual volume loss. Figure 6.9 shows the resulting strain in the ground. The danger in a strain-softening material is that permitting even a small amount of additional movement could led to the plastic zones in the ground around the tunnel that extend to the surface. Then the lining must carry the entire dead weight of the ground above. To avoid this linings are designed to resist movements rather than permit them.

7.4 Influence of construction sequence – advance rate, advance length & ring closure distance

These three parameters are considered together because in reality varying one will affect the others. While it is a fundamental tenet of the NATM that the lining loads depend on the time of ring closure, the effects of varying advance rate and advance length are rarely discussed (e.g.: Cosciotti *et al.* (2001) and Pöttler (1990) – see also 2.3.1.3).

Closing the ring forms a structure that is considerably stiffer than an open arch. In shallow soft ground SCL tunnels, the aim is usually to close the ring quickly to restrict ground movements (and therefore settlements) – e.g. Thomas *et al.* 1998. This implies that there will be less stress relief and higher loads on the lining, although the sprayed concrete (at least in the invert) may be soft at the time of ring closure because it is fresh. It has occasionally been suggested that one can optimise the loads in an SCL lining of a soft ground tunnel by delaying ring closure, as is commonly done in deep rock tunnels, (e.g. Negro *et al.* (1998)). As noted above, in shallow tunnels the proximity of the surface means that this is a very risky strategy. Failure to close the ring quickly enough is a classic cause of tunnel collapses (HSE 1996).

Increasing the advance length (AL), increases the initially unsupported area which the ground must arch around. Conventional wisdom maintains that this will lead to higher loads on the lining and the results from this study echoed this, as did the work of Kropik (1994). However, this also delays the ring closure, which may lead to lower loads in the invert of the tunnel.

Simple economics dictate that tunnellers try to maximise advance rates (AR). In SCL tunnels high advance rates lead to concerns about overstressing of the young sprayed concrete.

Table 7.11: Variations in advance rate, length & distance to ring closure

Run	Advance rate in m/day	Advance length in m	Average distance to closure of ring in m
H_Et_4_A_0.5	1.00	0.5	2.0
H_Et_4 ***(base case)***	1.20	1.0	4.0
H_Et_4_A_2.0	1.33	2.0	8.0
H_Et_4_X_6.0	1.20	1.0	6.0
H_Et_4_X_8.0	1.20	1.0	8.0
N*_Et_4	3.00	1.5	7.5
N*_Et_4_S_1.2	1.20	1.5	7.5
N*_Et_4_S_0.5	0.50	1.5	7.5
N*_Et_4_X_4.5	3.00	1.5	4.5

Plotting data from the models listed in Table 7.11 against the individual parameters – AR, AL & RCD (Ring Closure Distance) - led to a somewhat contradictory picture because more than one parameter varied between the models. Prompted by this the key factors were re-examined and grouped in the following form.

RCD/AR - ring closure distance/advance rate ~ the time taken to close the ring

E_x / E_{28} - the ratio of Young's modulus of the sprayed concrete at ring closure to the 28-day value ~ a measure of how stiff the ring is in compression at closure

AL/R - advance length / tunnel radius ~ a measure of the relative size of the unsupported length during excavation

Figures 7.31 to 7.33 show that this produced a slightly more consistent picture. As each of these parameters increased one would expect the loads in the lining to increase. However there was still a lot of scatter.

Flexibility ratios (for flexure and compression) have been derived for simplified "closed-form" calculations for loads in closed, circular tunnel linings in order to assess the effects of soil-structure interaction.

$$C = \frac{\dfrac{E_m}{(1+v_m)\cdot(1-2v_m)}}{\dfrac{E_l \cdot t}{(1-v_m^2)} \cdot \dfrac{1}{R}} \qquad 7.1$$

$$F = \frac{\dfrac{E_m}{(1+v_m)}}{\dfrac{6E_l I}{(1-v_l^2)} \cdot \dfrac{1}{R^3}} \qquad 7.2$$

where C = compressibility ratio, F = flexibility ratio, E_m = the Young's modulus of the ground, v_m = the Poisson's ratio of the ground, E_l = the Young's modulus of the lining, v_l = the Poisson's ratio of the lining, t = lining thickness, I = the second moment of area of the lining and R = tunnel radius (Peck *et al.* 1972).

Considering typical equations for flexibility ratios (see Equations 7.1 & 7.2), one can see that the difference in tunnel radius between runs H and N* may also affect the stiffness of the completed ring. The data for normalised loads in the closed ring – at about 2 diameters behind the face – were replotted against the following factor: $\left(\frac{RCD}{AR} \cdot \frac{Ex}{E_{28}} \cdot \frac{AL}{R}\right)$ multiplied by $\left(\frac{4.4}{R}\right)$ or $\left(\frac{4.4^3}{R^3}\right)$ for hoop forces and bending moments respectively (see Figure 7.34). Here this factor has been called the "Sequence Factor". The data was normalised against the results from the base case, H_Et_4.

Despite the fact that the data comes from two different series – H and N* - there is a general agreement on the trends for hoop forces and bending moments (both in the crown and axis). Data from a separate independent study on the effects of advance rates and ring closure distance also appears to follow the same trend (Mott MacDonald 2002). The results show that increasing the time to close the ring, the stiffness at closure or the advance length while maintaining the other factors constant led to an increase in the lining loads. This pattern of behaviour was most clearly visible for hoop forces and bending moments in the crown. There did not appear to be a pattern for bending moments in the invert. The "Sequence Factor" may offer a simple way to evaluate the effects of changes in advance rates, advance lengths and ring closure distances but this requires further investigation.

7.5 General issues

7.5.1 Stress distribution within the lining

One benefit of 3D numerical models is that they provide detailed information on the stress distribution in the lining and its deformation at all times (e.g.: Figures 7.3 & 7.4). This eases the assessment of the factor of safety and determination of Trigger / Limit values (for the monitoring performance during construction).

This study has shown that in some cases the constitutive model or excavation sequence may have a significant influence on the lining loads (see Figure 7.35). The results from the more sophisticated 3D numerical models were lower than the predictions from simpler methods. This was particularly true for bending moments (see section 7.1.2).

If these predictions can be relied upon, this may permit the support to be optimised further. For example, steel fibre reinforcement alone may be adequate. Advanced surveying equipment is already in use that can ensure that the correct profile and thickness are sprayed. This means that lattice girders can be omitted. Not only would the omission of lattice girders and steel mesh reduce material costs significantly but this would also reduce the amount of time spent by operatives at the partially supported face. Furthermore a major durability

concern - the corrosion of incompletely encased steel bars - would also be removed, thereby opening the way for the primary sprayed concrete lining to be used as the permanent lining.

These advances in SCL technology would significantly improve the cost-effectiveness of this method (and to a lesser extent the safety too).

7.5.2 Code compliance

Design codes for reinforced concrete are written for conventionally placed concrete at ages greater than 7 days. To comply with the normal factors of safety and the stress-strain behaviour set out in the codes, typically the utilization factors [85] in the tunnel lining should be less than 38 % ($0.8\ f_{cu} \div \{1.4\ (\gamma_f) * 1.5\ (\gamma_m)\}$). While some codes (e.g.: BS8110 Part 2 1985) permit some latitude on the basis of experimental data and engineering judgement, it would still be difficult to justify utilization factors that exceed 55 % ($1.0\ f_{cu} \div \{1.2\ (\gamma_f) * 1.5\ (\gamma_m)\}$) for short-term loads near the face [86]. As Figures 7.4 shows the utilization factor in the lining may be greater than 55 % within the first few metres of the lining. The concrete here is less than 7 days old.

This raises two questions. Should normal design codes be applied at these ages? How can one prove the safety of the tunnel in this critical area?

One could assume that the codes do not apply and resort to other means to prove the stability of the tunnel, e.g.: empirical methods based on the stability number, N, or limit equilibrium solutions. The limitations of this approach and the difficulty in application to SCL tunnels have been discussed in section 1.2.3. One could strengthen this approach by combining it with a process of risk management which culminates in the use of monitoring data during construction to verify that the tunnel is behaving as intended in the design (Powell *et al.* 1997) although one does not have the opportunity to take many readings in the critical area

[85] NB: the calculated utilization factors from the numerical model are based on deviatoric stresses whereas BS8110 considers stress components in each direction separately – e.g. the hoop axial load vs f_{cu}

[86] A partial factor of safety of 1.20 is commonly used for temporary loads.

which is near the tunnel face. The differences between this approach and the classical NATM are discussed in the BTS Lining Design Guide (BTS 2004).

Alternatively one could use some of the more elaborate constitutive models such as those presented in this study. By taking advantage of factors such as creep, the numerical models may predict utilization factors that are low enough to comply with the codes (e.g.: Figure 7.35). However, this approach is vulnerable to scrutiny. Few projects can afford an extensive pre-construction test programme. At the same time, there is currently an insufficient pool of data from which to determine many of the model parameters with the certainty normally required. The results from this study have shown that small variations in key parameters (e.g.: advance rate or creep parameters) may have significant effects on the results. Therefore the results of the design analyses might remain open to question.

This problem of code compliance has been concealed to a degree in the past since designs were usually based on 2D analytical methods with empirical correction factors (such as in the Hypothetical Modulus of Elasticity approach). The complete stress history of the lining and variations in stress within each ring were rarely investigated. Furthermore the primary lining was often regarded as part of the temporary works.

A pragmatic approach may be:

- to acknowledge that, while the principles of conventional design codes apply to the heading of an SCL tunnel, the detail may not at very early ages;
- to embrace the new information provided by 3D numerical analyses as a complement to existing design approaches &
- to accept that numerical models are still only an approximation of reality – so sound engineering judgement remains as important as ever.

7.5.3 The role of numerical modelling in design

7.5.3.1 Advanced numerical modelling vs rule of thumb

Given our imperfect understanding of geotechnics and construction techniques, such as SCL tunnelling or compensation grouting, and our limited ability to model them, numerical modelling should not be used in isolation to design tunnels. As designers, we are still faced with the conundrum that in the cases where we have a lot of experience of tunnelling, we can calibrate our design tools sufficiently well to obtain reliable predictions of behaviour. However, in those cases the experience from other tunnelling, combined with simple design tools might suffice without recourse to sophisticated numerical modelling. In cases where we do not know how the ground will behave, even our most sophisticated design tools can only offer a suggestion of how the ground might behave. Yet this is where additional (reliable) information would be most useful. It would be foolhardy to rely on numerical modelling alone without calibration against data from the laboratory or the field and other design tools, and preferably all three.

7.5.3.2 2D vs 3D

There seems to be a logical flaw in the view that a single 3D numerical model can be run to obtain the relaxation factor for subsequent use in a series of 2D analyses (e.g.: Cosciotti *et al.* (2001)). In order to develop a reliable 3D model, considerable preliminary work with simplified 2D and 3D models is required, together with whatever calibration is possible. Even with modern computing power, it is the time required for this development work, along with the time for post-processing that discourages or even prohibits the more widespread use of 3D models, rather than the run times themselves (see Table 7.12). Having taken the trouble to develop a 3D model, it is arguable that one might as well continue using it for the routine analyses. In practice, on commercial projects there is rarely the time or budget for a 3D analysis and so the relaxation factor is estimated by other means and 2D analyses are used alone.

Another argument against 3D modelling is that the increased costs for licences for 3D programmes and the computers on which to run them [87]. This is true but developing more sophisticated numerical models in 2D can become very difficult too. For example, if a cross-section of a tunnel is divided into many headings, it is quite difficult to determine the relaxation factor associated with each individual construction stage of each heading. Similarly, to investigate how stress state in the lining develops during the whole life of the lining, some mechanism is required of gradually applying the load to the lining, in line with the way the load develops with time due to each subsequent construction stage (Shin 2000).

Table 7.12: Time demands of 3D numerical models

Stage	Model of single circular tunnel	Model of asymmetric shaft with adjacent structures
Pre-processing: - mesh generation; selection of constitutive models.	84 hours	120 hours
Validation: - of mesh and constitutive models.	84 hours	84 hours
Runtime: - for a single run.	72 hours	96 hours
Post-processing: - extracting results; interpretation – for a single run.	24 hours	32 hours
Total time in man hours	264 hours	332 hours

7.5.4 The development of SCL design

Finally this section reviews the purpose of this study and its outcomes in the broader context of the SCL tunnelling today.

London Clay is a relatively well-understood medium for tunnelling. Many shallow tunnels have been successfully constructed in this clay under London. However, even with this high

[87] The computers used for this study were standard (albeit high performance) PC's – 256 MB RAM; 800MHz processors.

level of understanding of the material and extensive precedent practice, the experience of applying a new tunnelling technique in London – namely, SCL tunnelling – has revealed the limitations of that knowledge and the risks when one strays beyond the boundaries of precedent practice. Despite all the safeguards and the body of knowledge of SCL tunnelling in soft ground elsewhere, fundamental mistakes were made and went undetected for long enough for a critical situation to develop and a collapse to occur. The collapse at Heathrow in 1994 is not an isolated incident (HSE 1996) nor do such accidents only occur with this tunnelling method (e.g.: BTS 2003).

The collapse at Heathrow, like all major accidents, was caused by a combination of factors – some obvious errors, some subtle and deep-seated flaws. The civil engineering profession has taken steps to address many of the issues related to project management and construction procedures. The question of whether or not the design of the tunnel was adequate is difficult to answer. On one level, the design may have been adequate in that the lining thickness and reinforcement was sufficient to carry normal loads. On a broader level, the design was probably inadequate in that, for example, joint details were difficult to construct and therefore vulnerable to poor workmanship, and the potential loads from compensation grouting and adjacent tunnelling were not fully appreciated (HSE 2000).

The prevailing view at the time was that the primary sprayed concrete lining of a tunnel is temporary works. Therefore, not only is the contractor free to amend it as he sees fit but also the temporary nature of the structure means that poor construction quality or small variations in the design are not important. In the author's experience this view still persists in some quarters and there is a very real risk that the mistakes made at Heathrow and other collapses could be repeated due to the inexperience of the designers or contractors. Indeed some in the insurance industry (which holds the most comprehensive database on construction failures) believe that the inability of the tunnelling profession to reduce this risk may make insurance costs prohibitively expensive (BTS/ABI 2002). Potentially this could prevent new construction projects from using SCL techniques.

After the collapse at Heathrow, the project team had to convince the HSE that the new management systems and redesigned SCL tunnels could be constructed safely. Submissions were made by the HEX team and critically examined by the HSE. Design assumptions were strongly challenged, in a way that rarely happens on a normal project. Under such scrutiny, the choice of key design parameters (such as ground loads or HME values) on the basis of precedent practice would be hard to justify if previous projects were in different environments. Equally, simplistic design methods are hard to defend since they cannot account for the complicated loading or geometry of the real tunnels. Despite their limitations (see section 1.2.3), numerical models have the ability to consider more factors explicitly (e.g.: loads from adjacent structures) and require fewer empirical corrections. Therefore they are capable of bolstering the design and demonstrating more clearly its safety. Most projects are not subjected to the level of examination seen at HEX but the independent checks are increasingly required for major projects. It is arguable that such scrutiny should promote good practice in design.

Therefore the principal general conclusion of this study is that there is merit in considering the behaviour of SCL tunnels – whether temporary primary linings or permanent works - in detail, with due regard to their complexity since apparently minor changes in design or behaviour may have large impacts on the performance of the tunnel.

Figure 7.1 Normalized hoop axial forces in the crown at 8m from the face

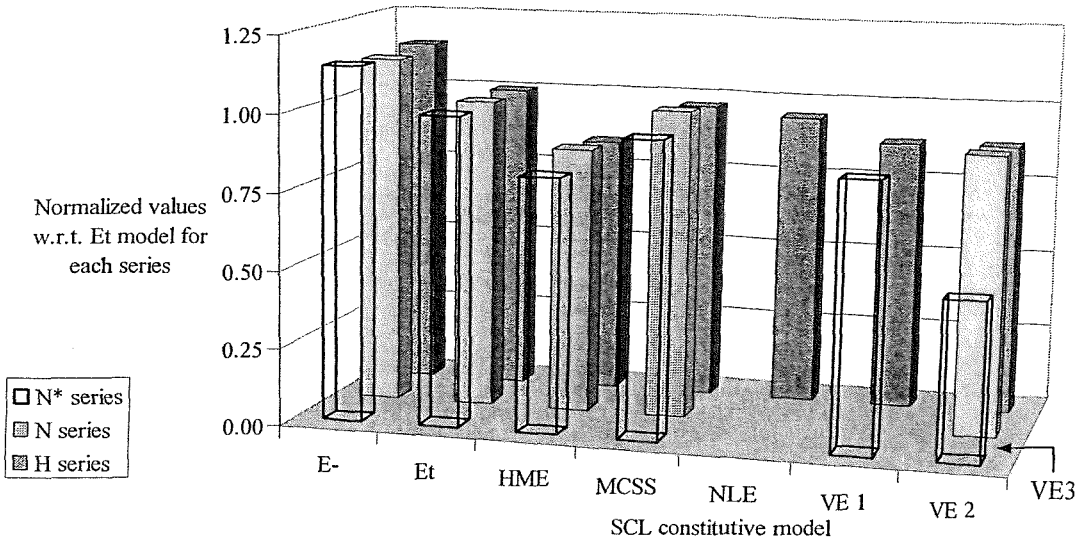

	E-	Et	HME	MCSS	NLE	VE 1	VE 2
N* series	1.15	1.00	0.82	0.95		0.86	0.50 *
N series	1.13	1.00	0.86	0.99			0.90
H series	1.15	1.00	0.84	0.97	0.95	0.88	0.88

* - Model VE3

Figure 7.2 Normalized hoop bending moments in crown at 8m from face

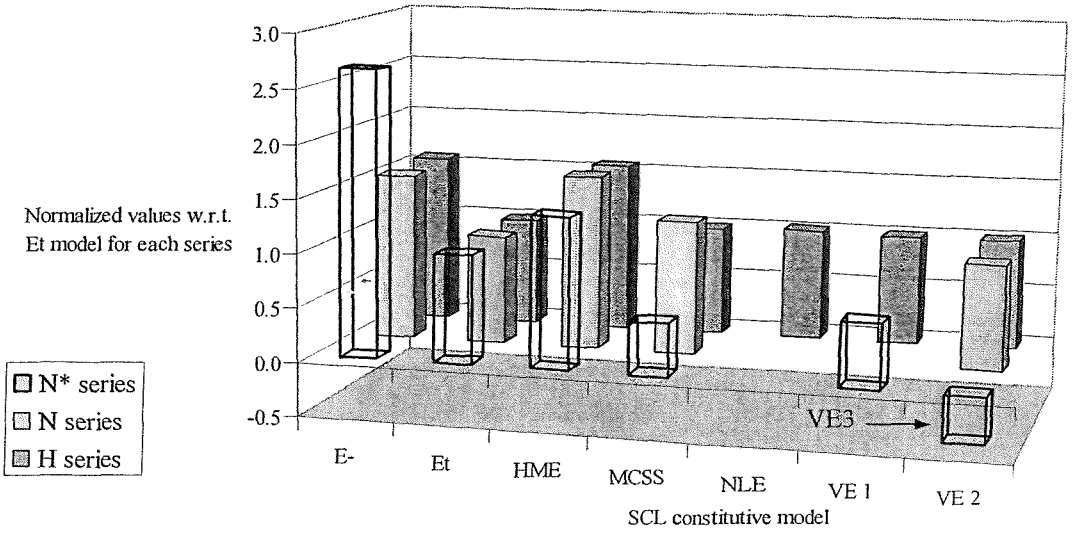

	E-	Et	HME	MCSS	NLE	VE 1	VE 2
N* series	2.66	1.00	1.39	0.49		0.59	-0.42 *
N series	1.54	1.00	1.61	1.23			0.96
H series	1.58	1.00	1.57	1.00	1.02	1.00	1.01

* - Model VE3

Figure 7.3 Utilization factor, α, in H_Et_4

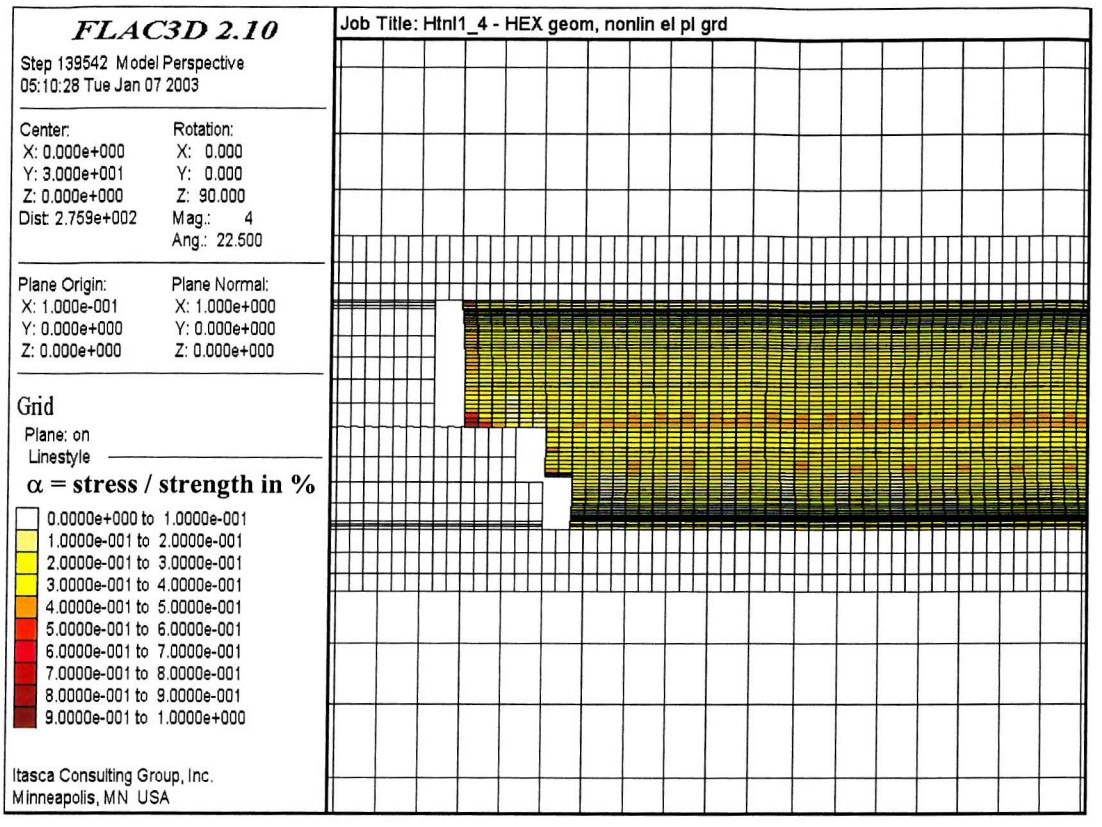

Figure 7.4 Utilization factor, α, in N*_Et_4

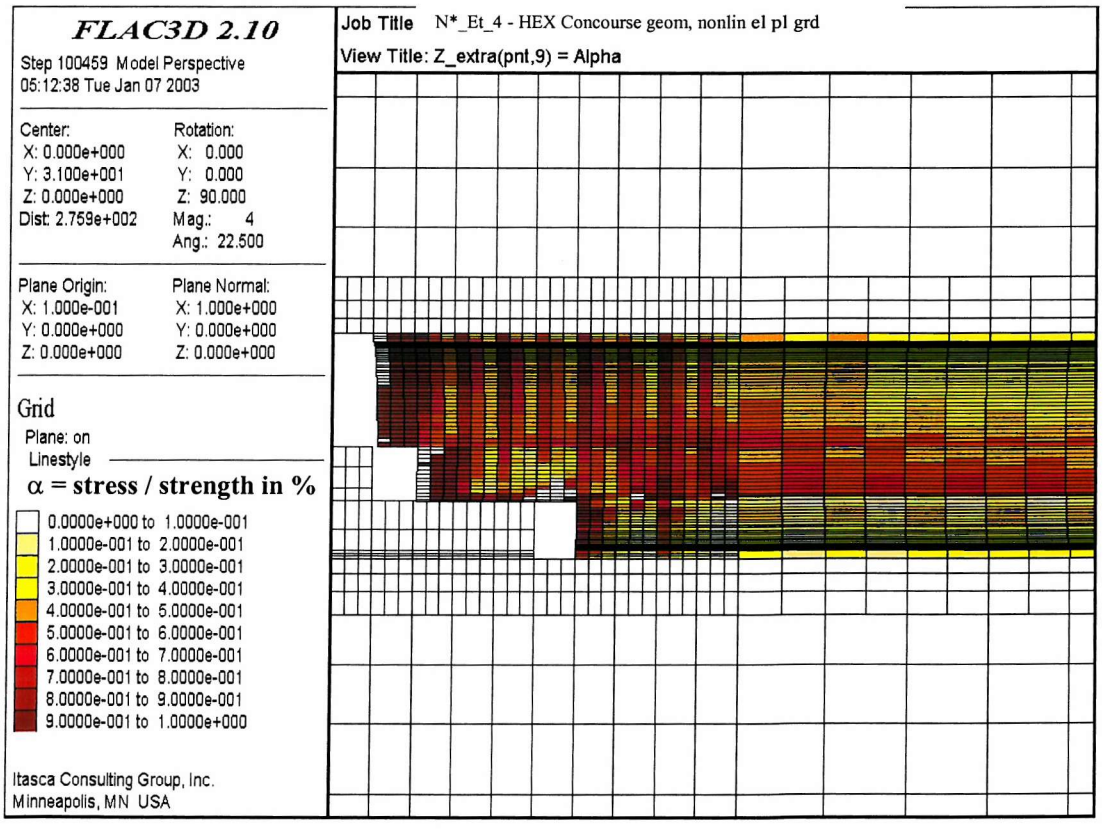

Figure 7.5 Utilization factors at intrados vs distance from Leading Edge

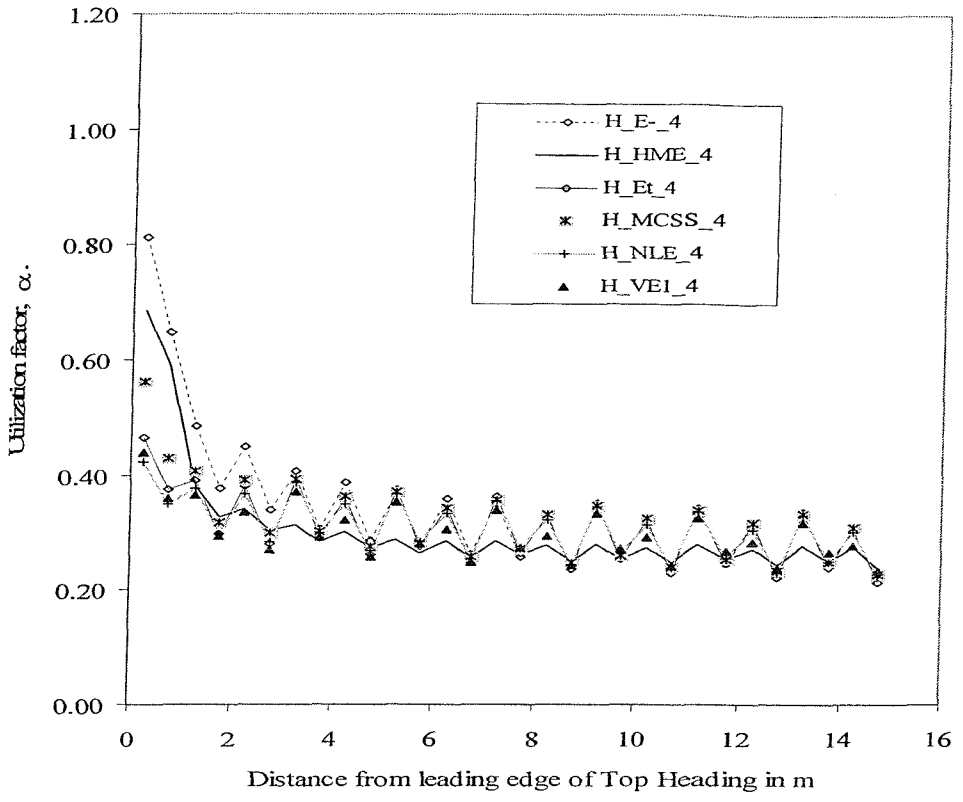

Figure 7.6 Utilization factors at extrados vs distance from Leading Edge

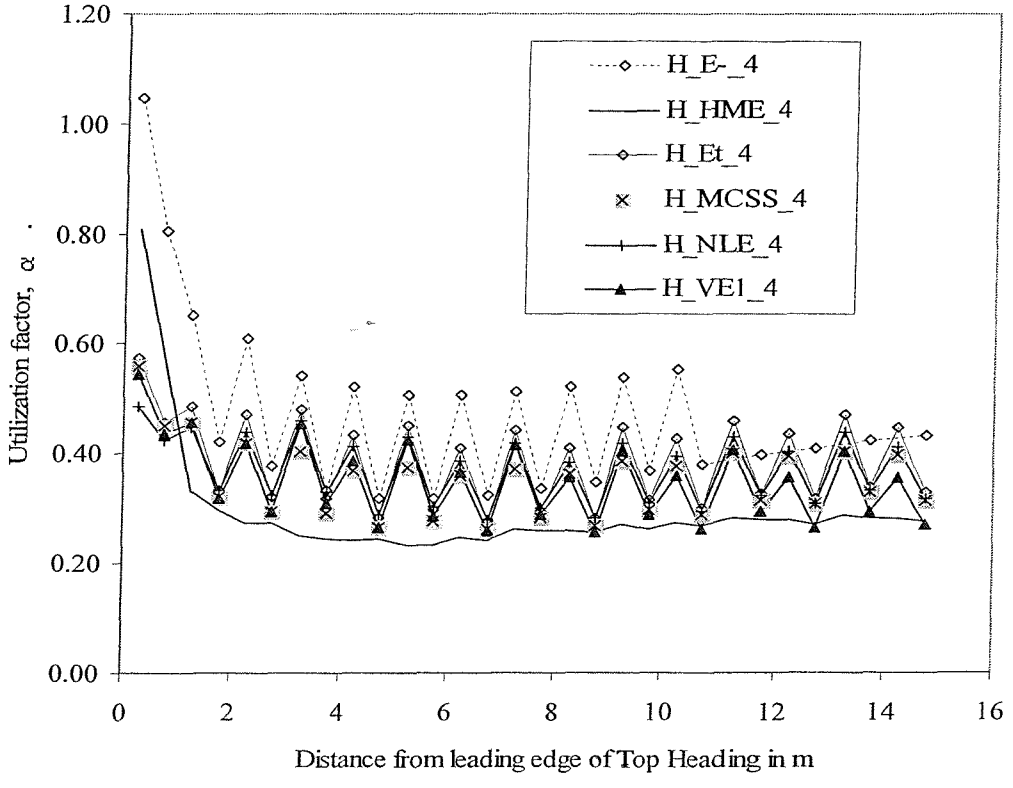

Figure 7.7 Hoop axial force in crown vs distance from face
(a) for different sprayed concrete models

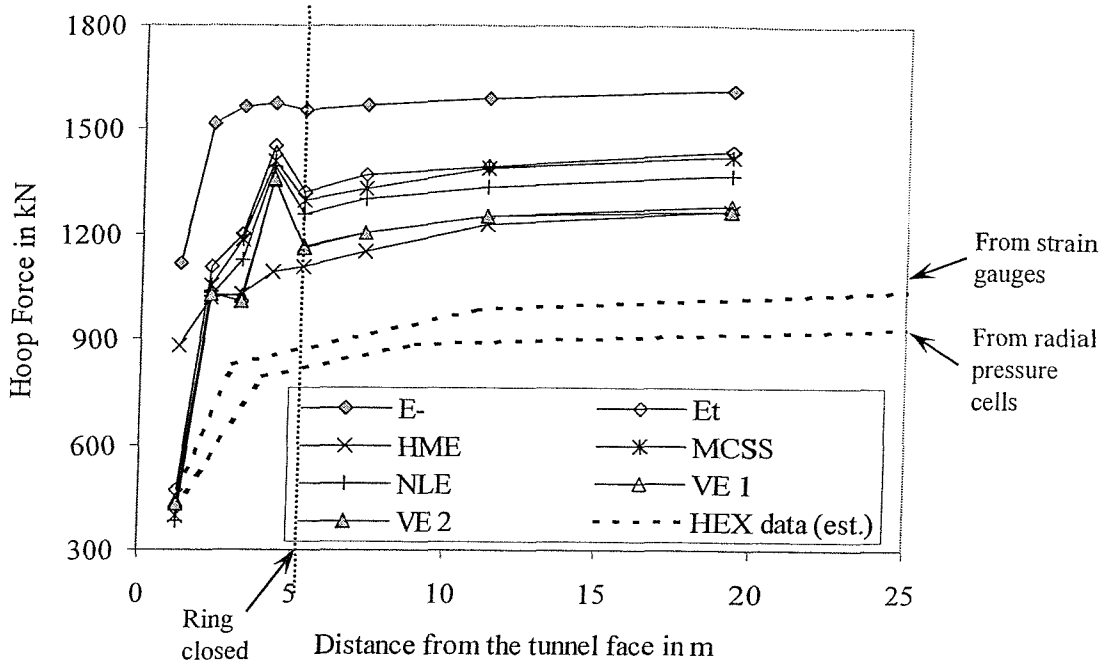

NB: Compressive forces are positive

(b) variation around the ring for different models

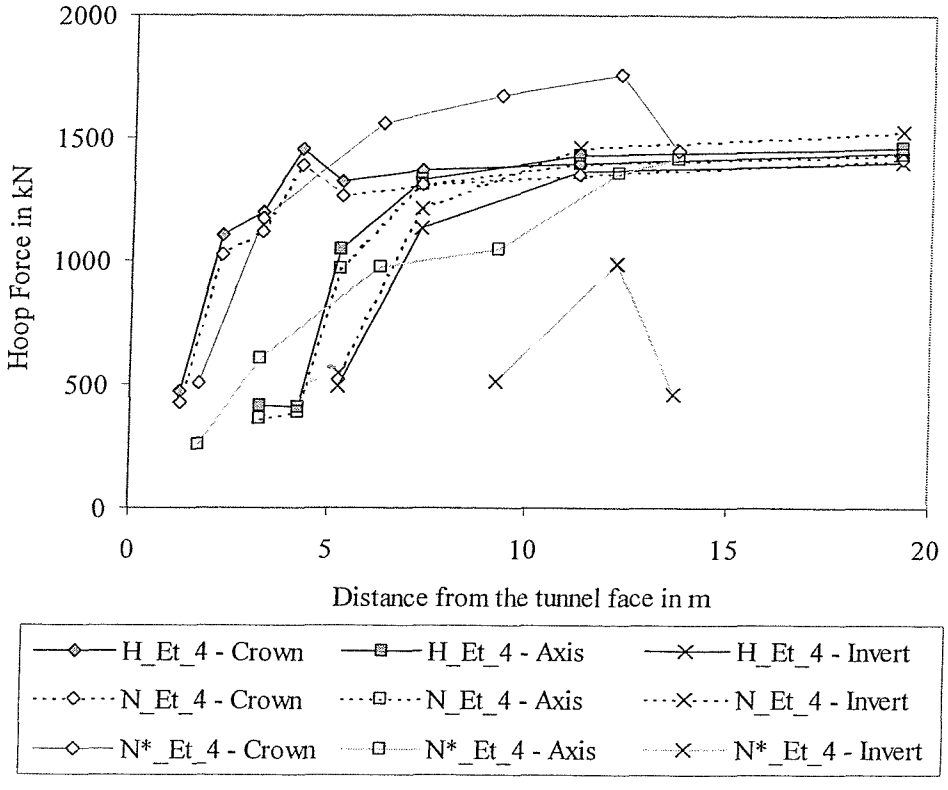

NB: Compressive forces are positive

Figure 7.8 The effect of creep on utilization factors

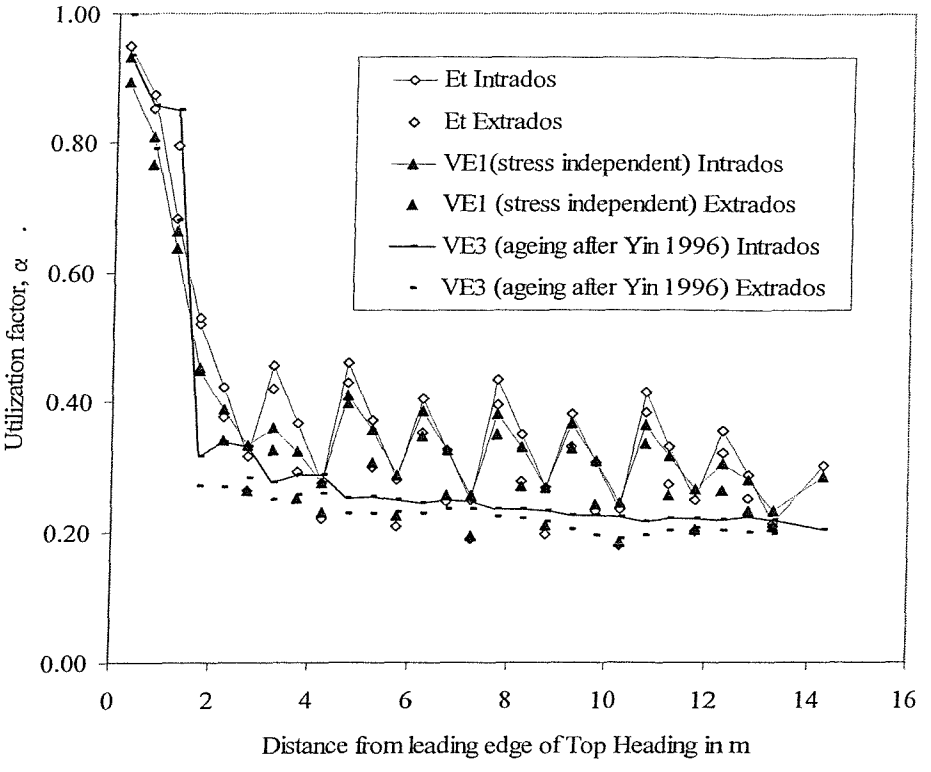

Results from N* analyses: N*_Et_4; N*_VE1_4 & N*_VE3_4

Figure 7.9 Hoop bending moment in crown vs distance from face
(a) for different sprayed concrete models

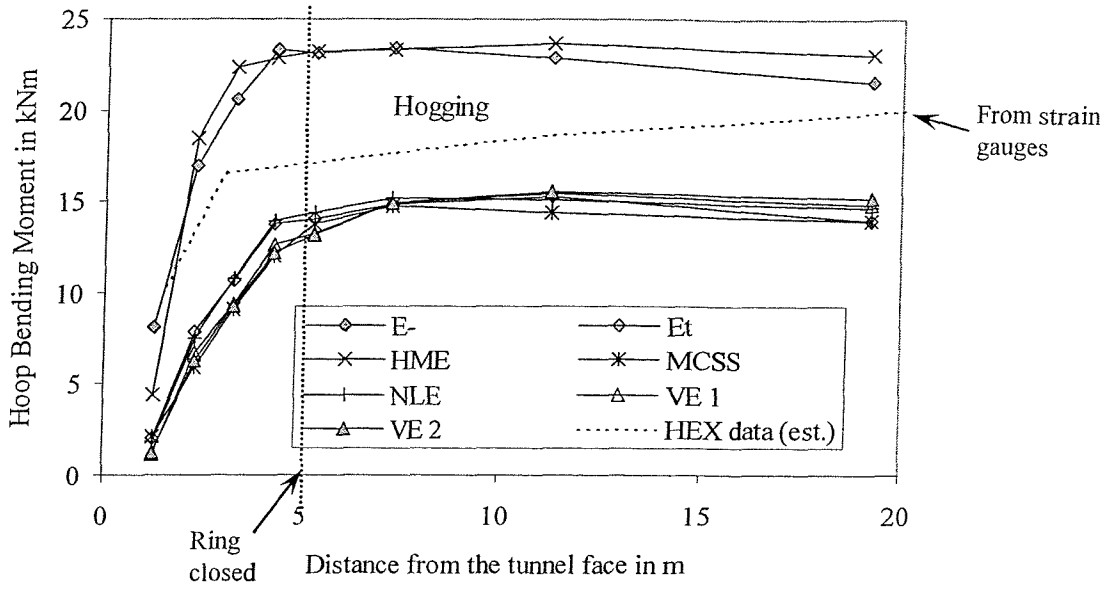

(b) variation around the ring for different models

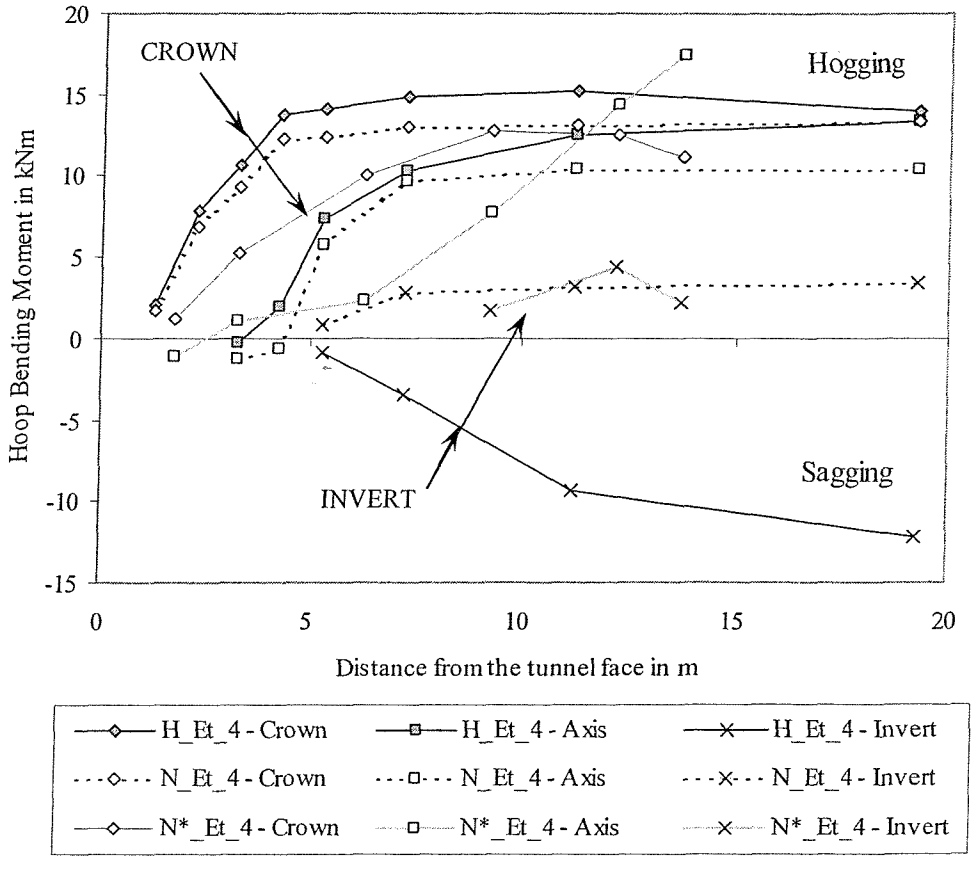

Figure 7.10 Crown displacement vs distance from leading edge of Top Heading

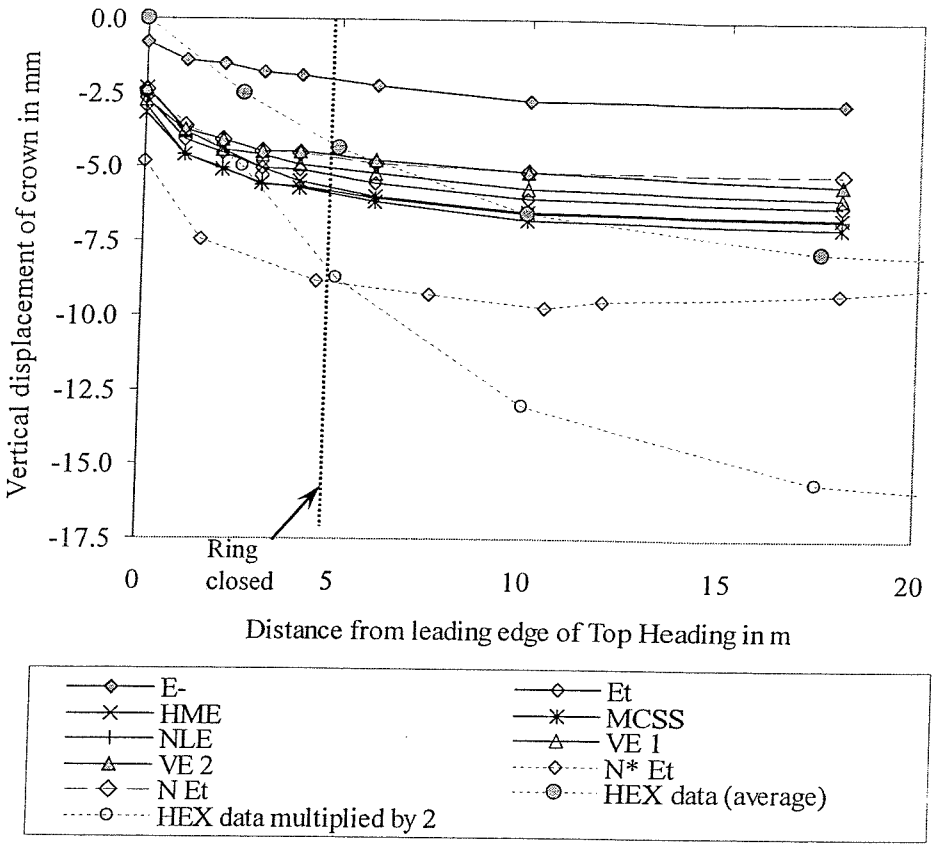

Figure 7.11 Lining deformation at 10m from Leading Edge of Top Heading

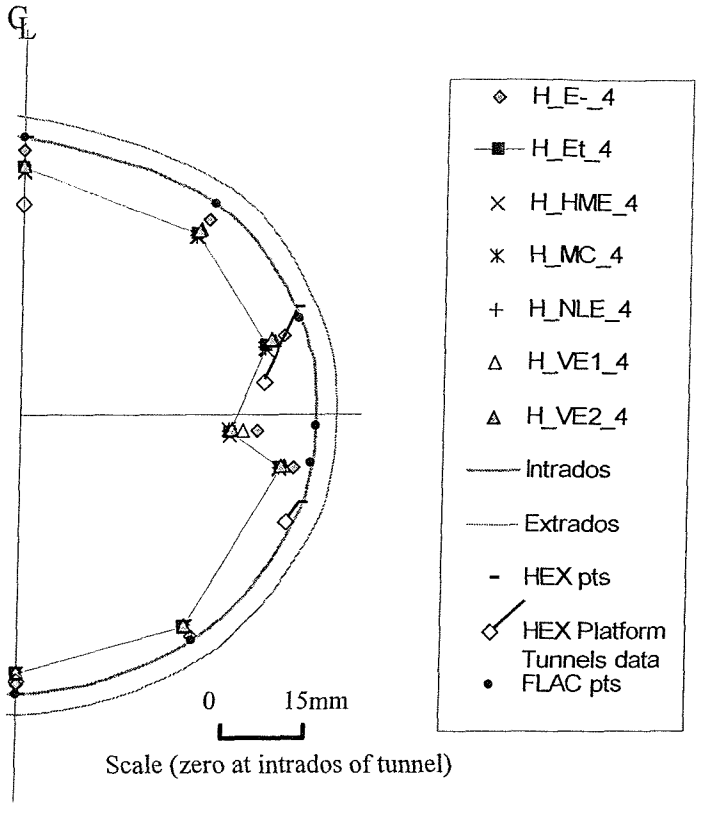

Figure 7.12 Longitudinal axial forces vs distance to face

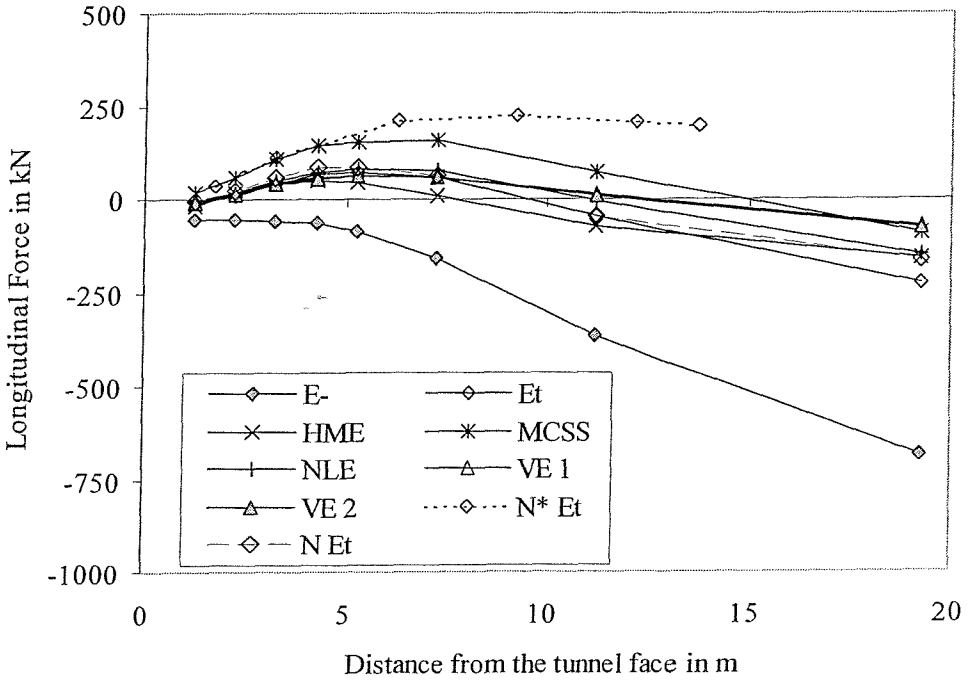

NB: Compressive forces are positive

Figure 7.13 Longitudinal bending moments vs distance to face

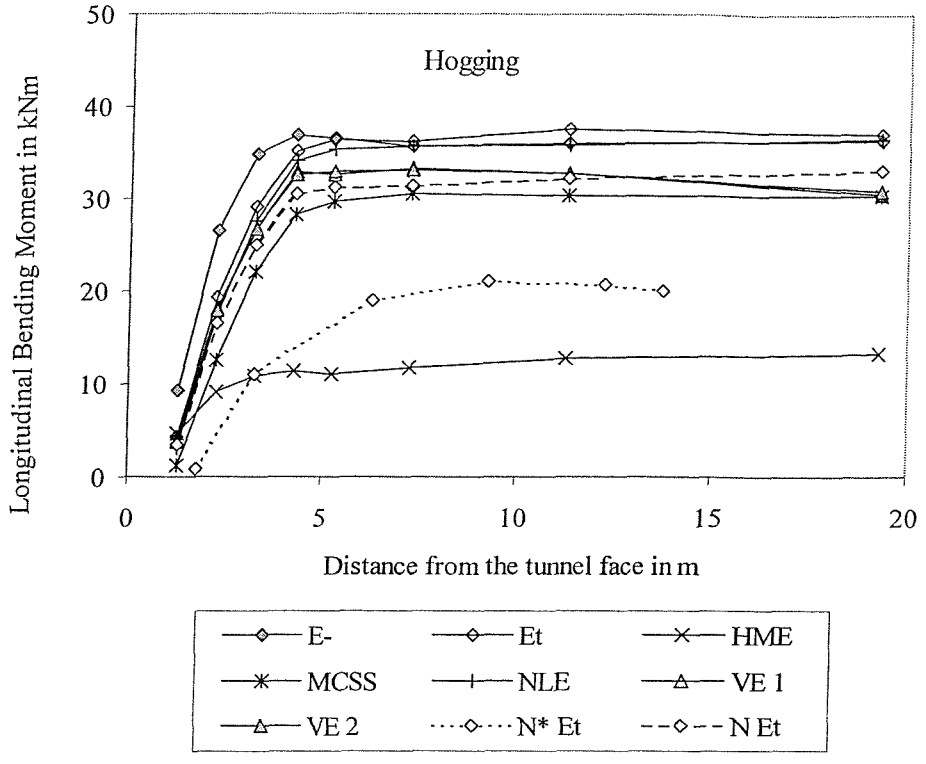

Figure 7.14 Radial stress in crown vs distance to the face

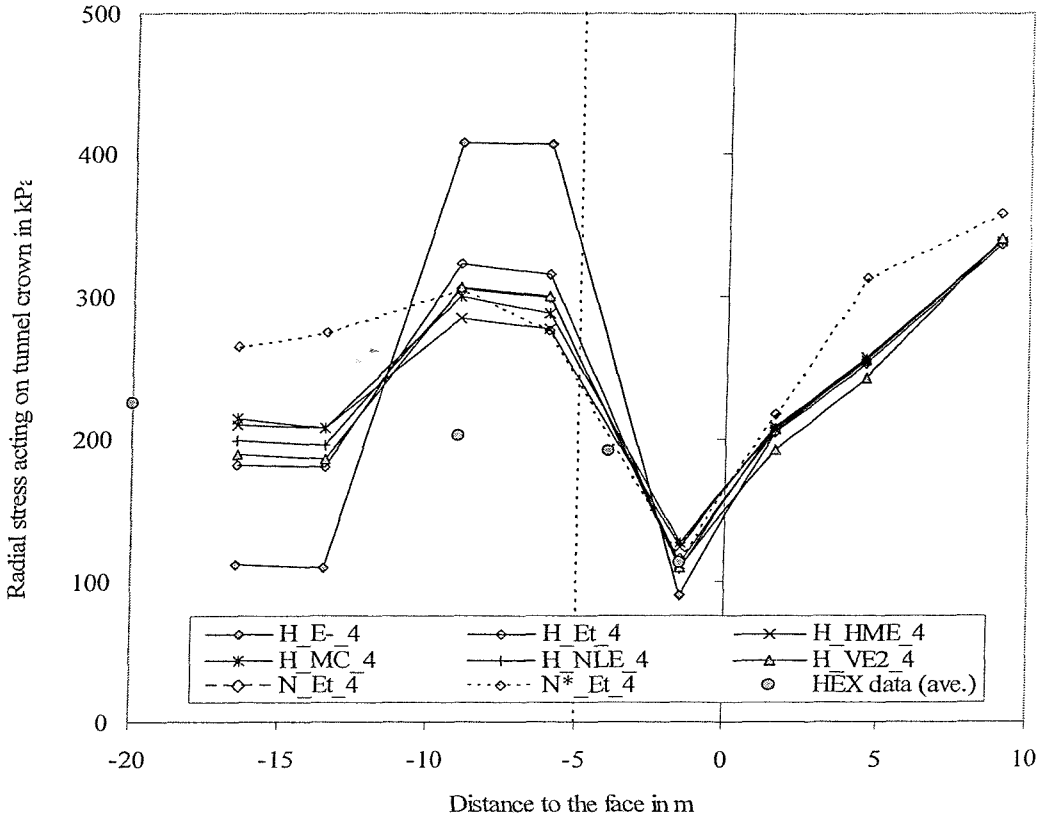

Figure 7.15 Radial stresses in the ground acting on the tunnel extrados

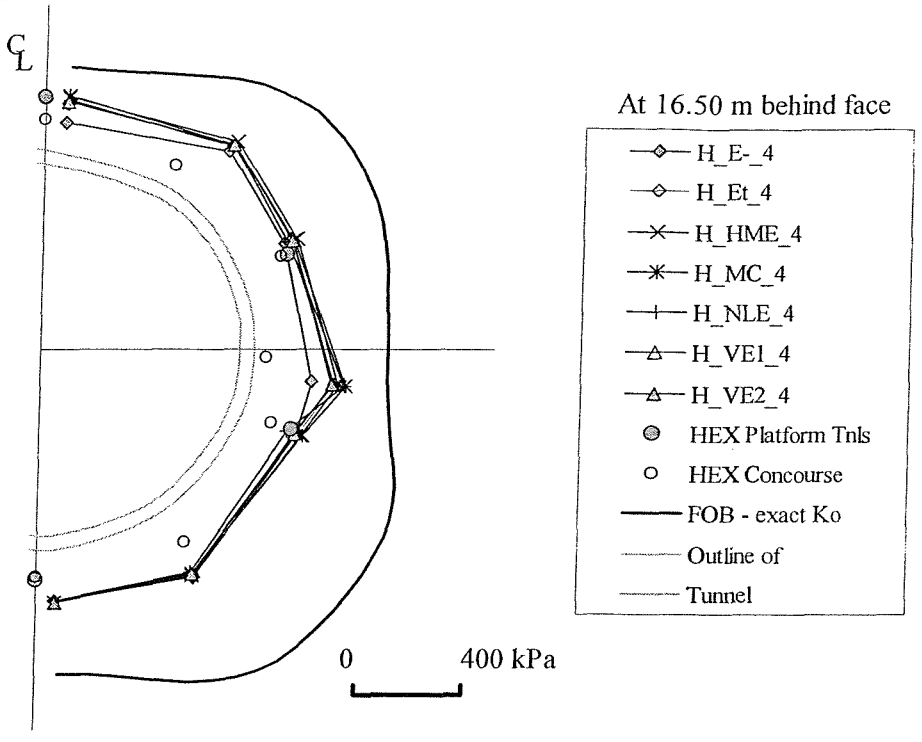

Figure 7.16 Transverse surface settlement profile at 18m from the face

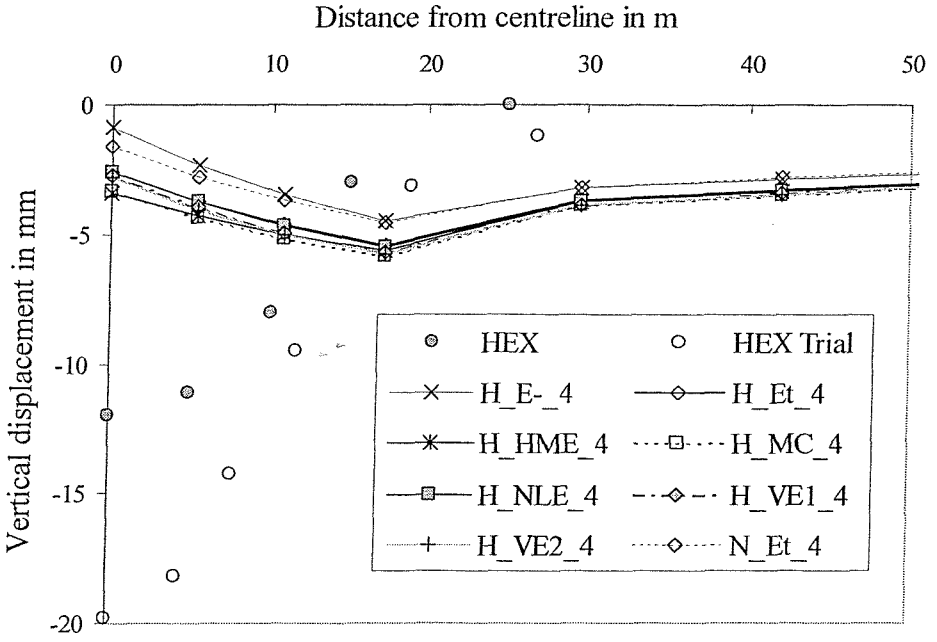

Figure 7.17 Longitudinal surface settlement profile above the tunnel centreline

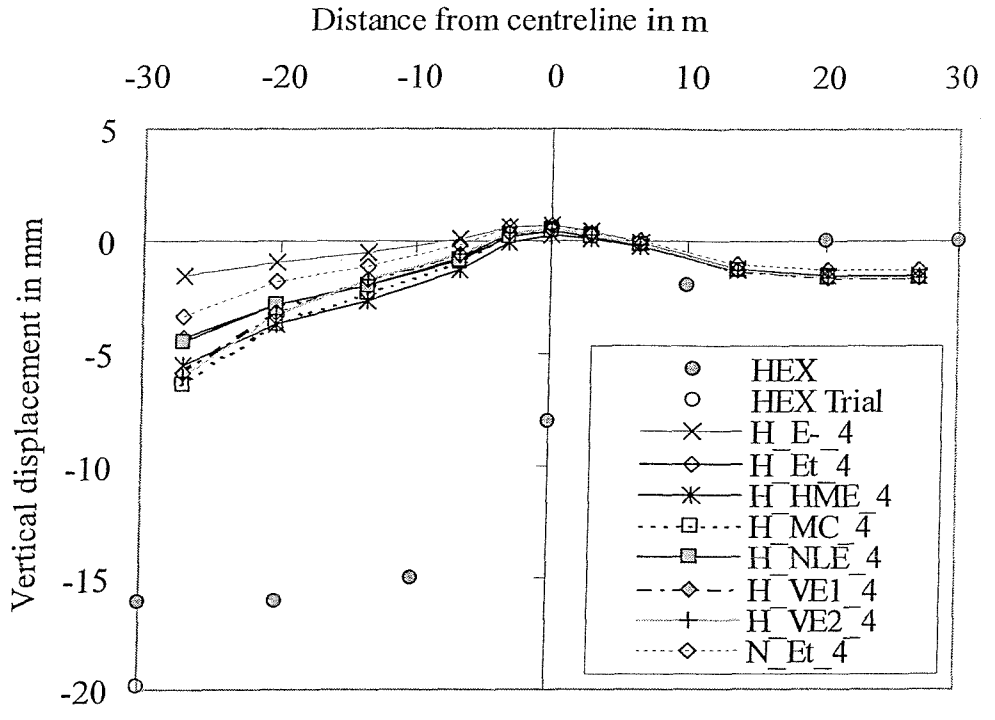

Figure 7.18 Normalized hoop forces (N) & bending moments (BM) in the crown at 8m from the face for different ground models

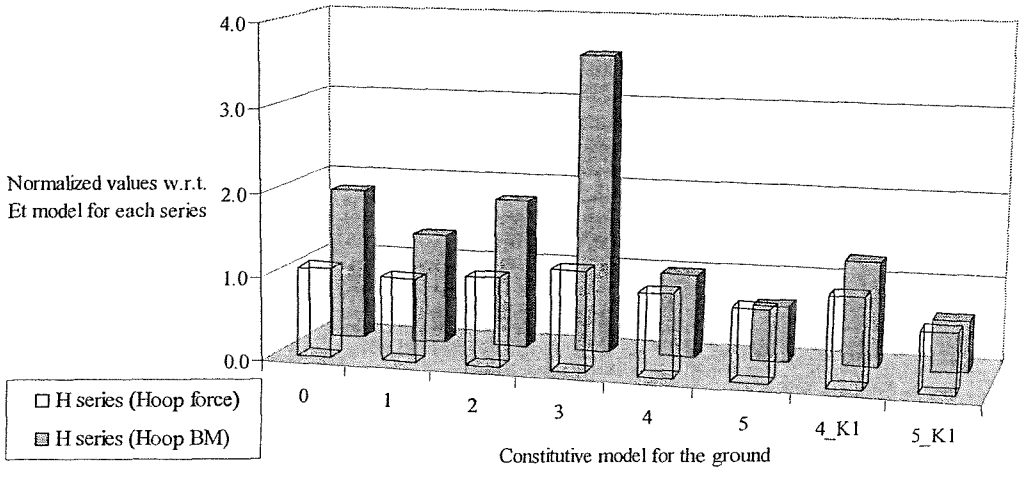

	0	1	2	3	4	5	4_K1	5_K1
H series (Hoop force)	1.08	1.00	1.07	1.20	1.00	0.88	1.07	0.73
H series (Hoop BM)	1.82	1.32	1.79	3.57	1.00	0.67	1.26	0.62

Figure 7.19 Normalized vertical displacements of the crown of the tunnel and normalized volume losses for different ground models

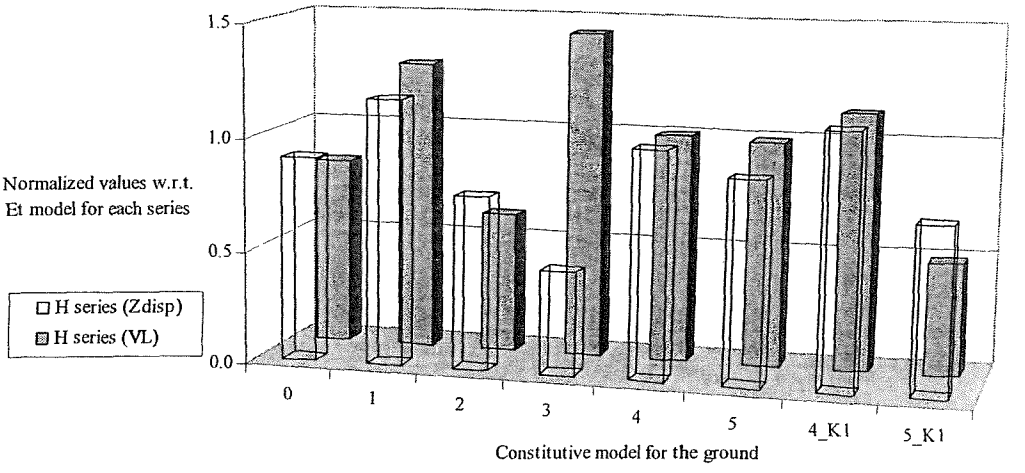

	0	1	2	3	4	5	4_K1	5_K1
H series (Zdisp)	0.91	1.17	0.76	0.45	1.00	0.89	1.11	0.73
H series (VL)	0.83	1.28	0.62	1.43	1.00	0.99	1.13	0.49

Figure 7.20 Lining deformation at 10m from Leading Edge of Top Heading

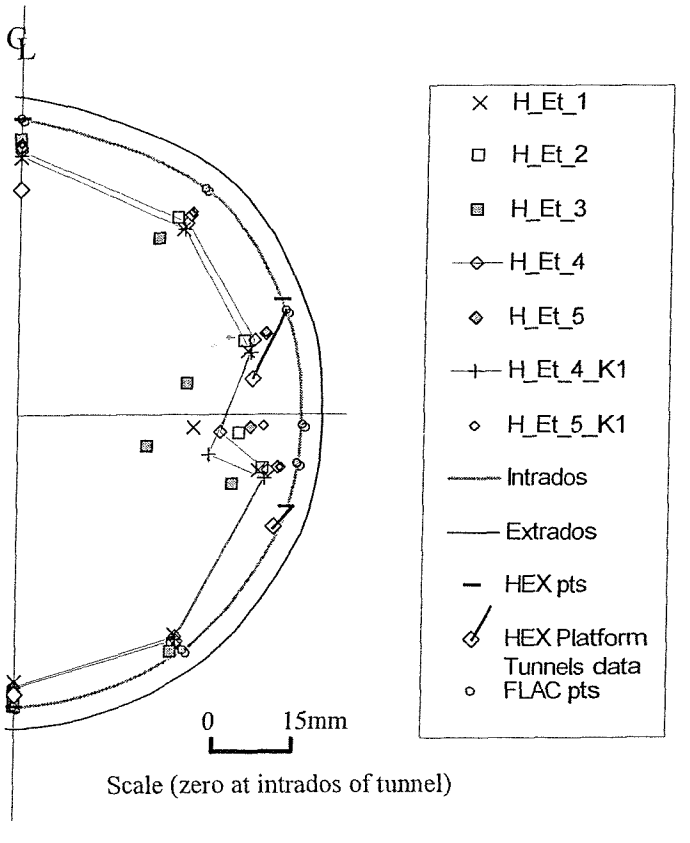

Figure 7.21 Radial stresses in the ground acting on the tunnel extrados

(a) The effect of the ground model on radial stresses

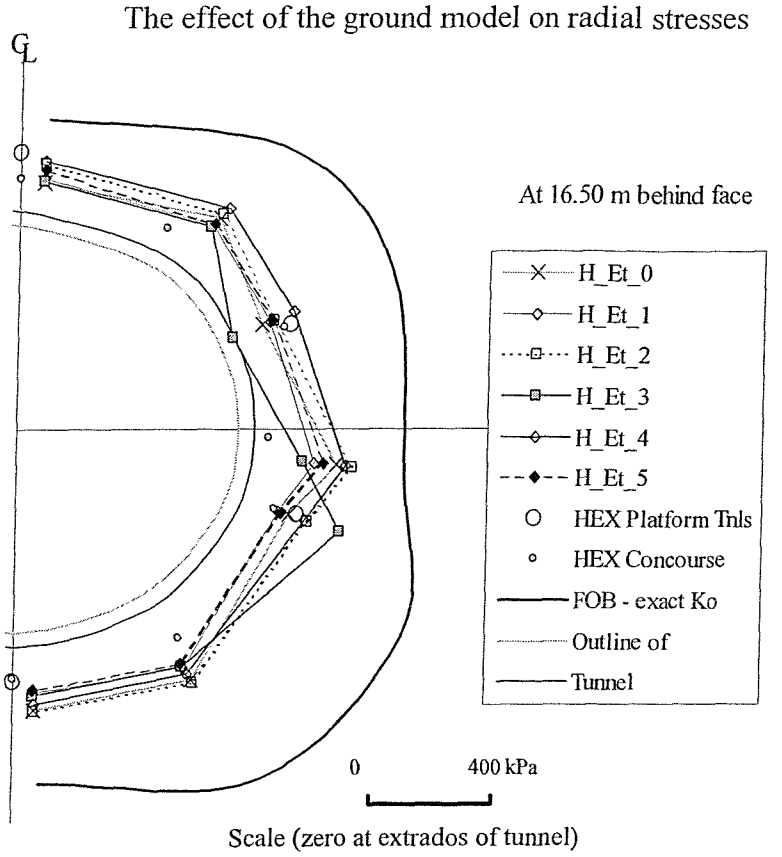

Scale (zero at extrados of tunnel)

(b) The effect of tunnel geometry, Ko and joints

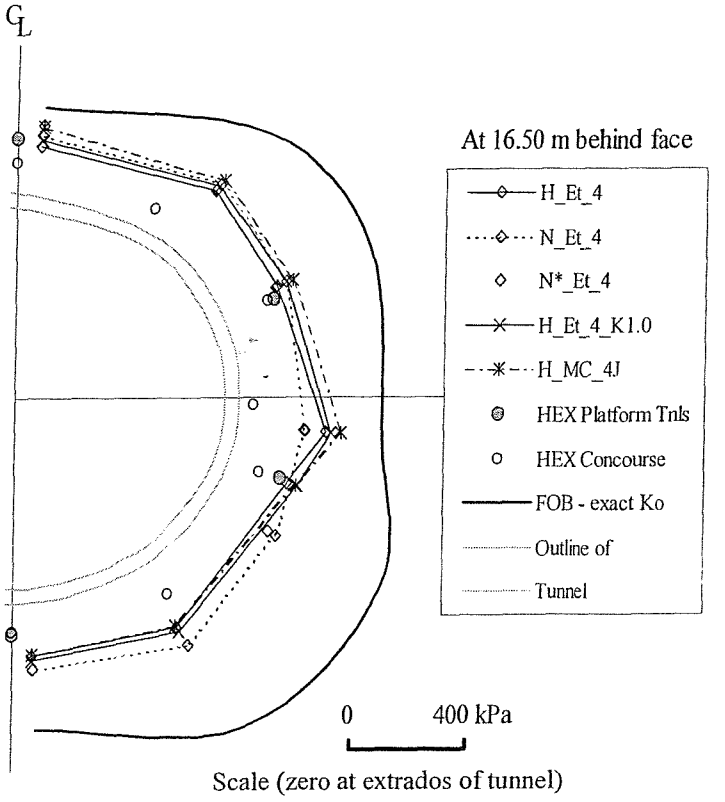

Scale (zero at extrados of tunnel)

Figure 7.22 Stress paths in the ground near the tunnel extrados – at axis and crown – for different ground models

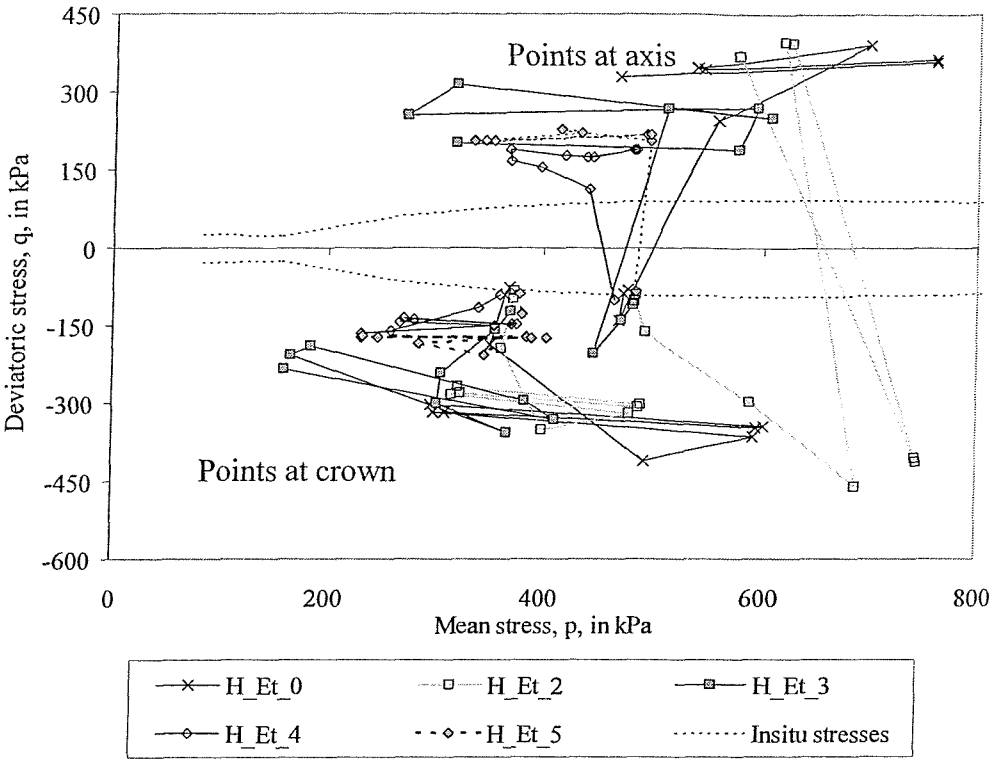

Figure 7.23 Deviatoric stress vs deviatoric strain in the ground near the tunnel extrados above the tunnel crown

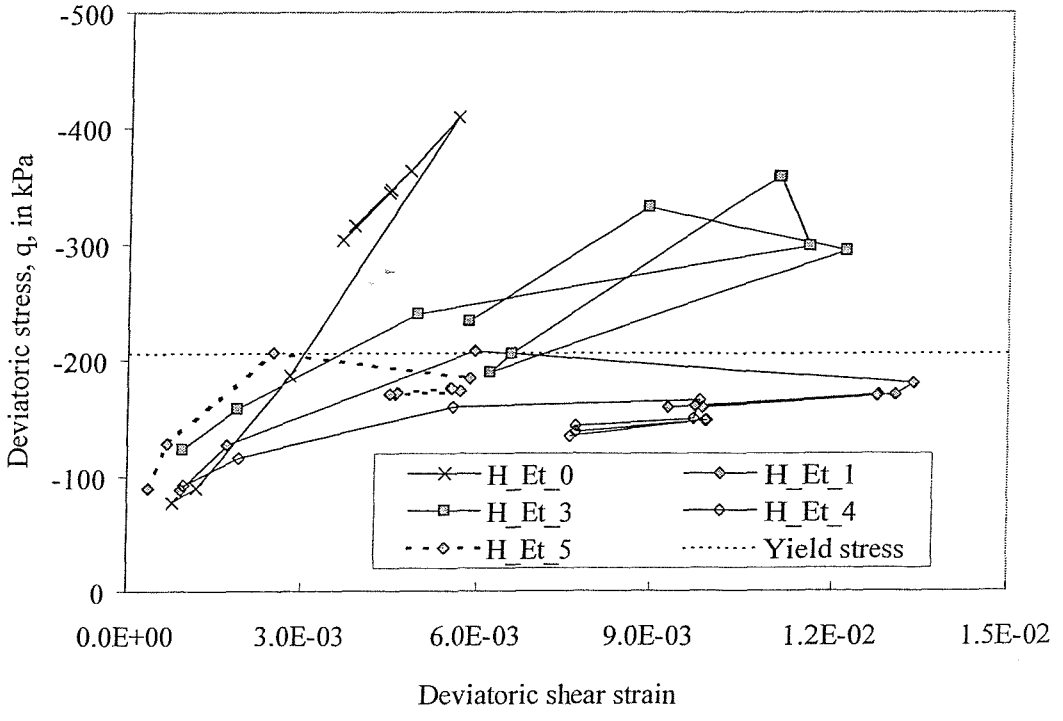

Figure 7.24 Transverse surface settlement profile at 18m from the face

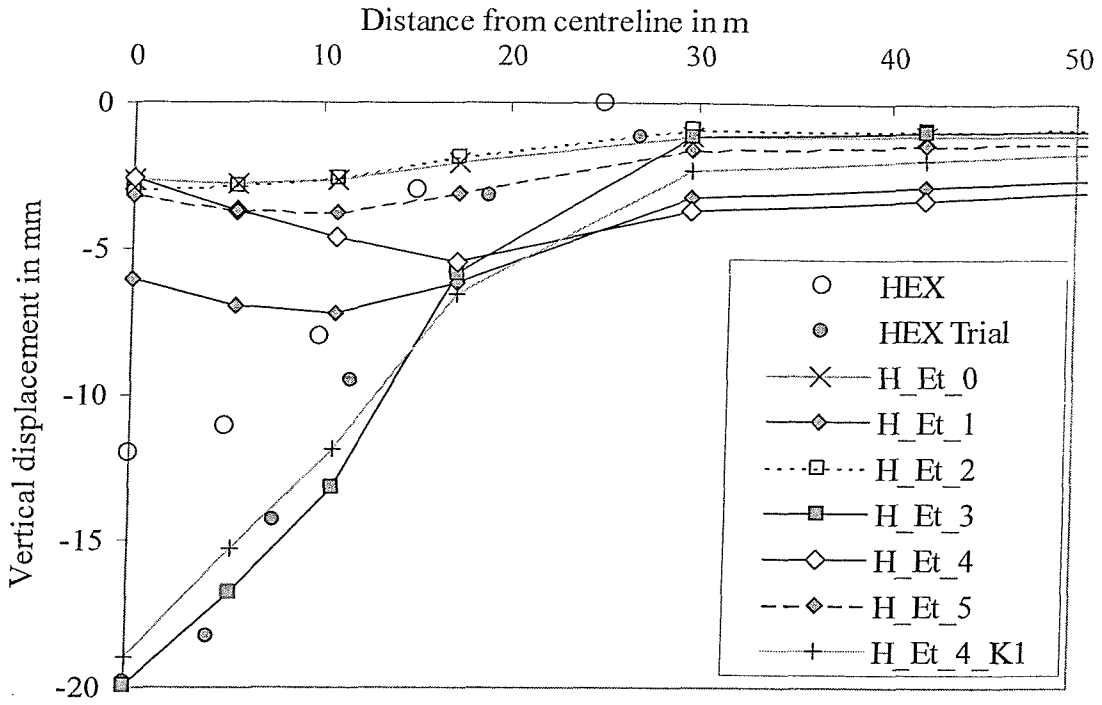

Figure 7.25 Longitudinal surface settlement profile above tunnel centreline

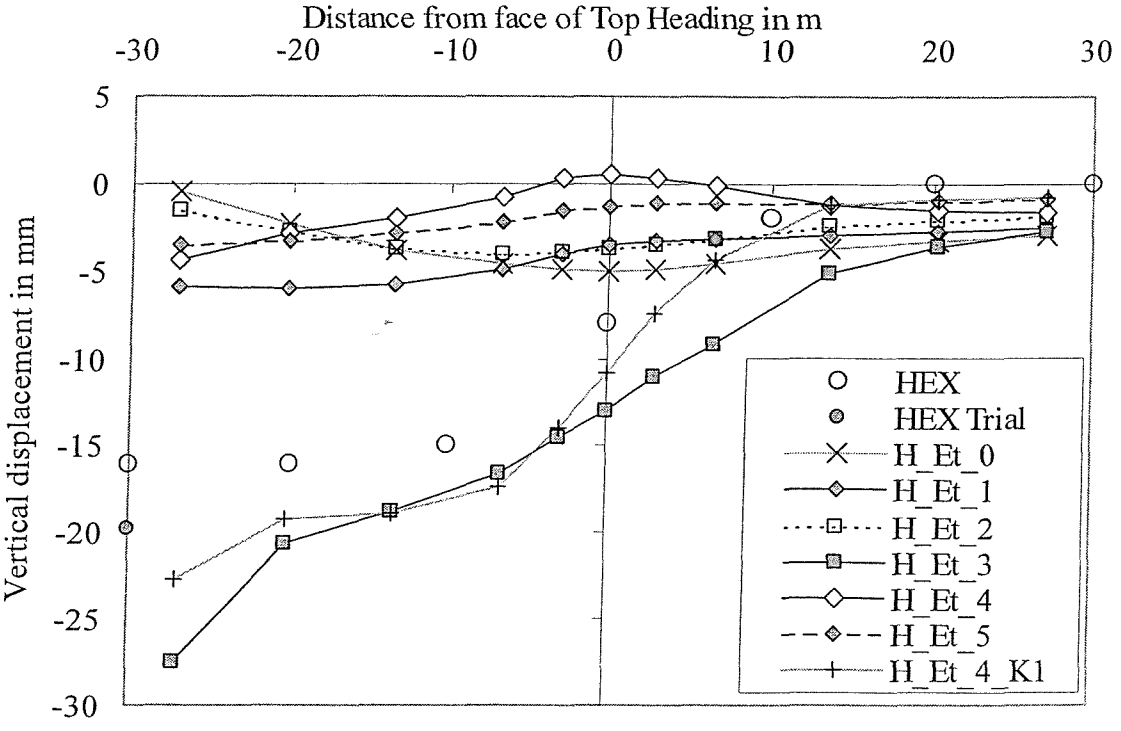

Figure 7.26 Longitudinal movement at 1.5m ahead of the face on the tunnel centreline

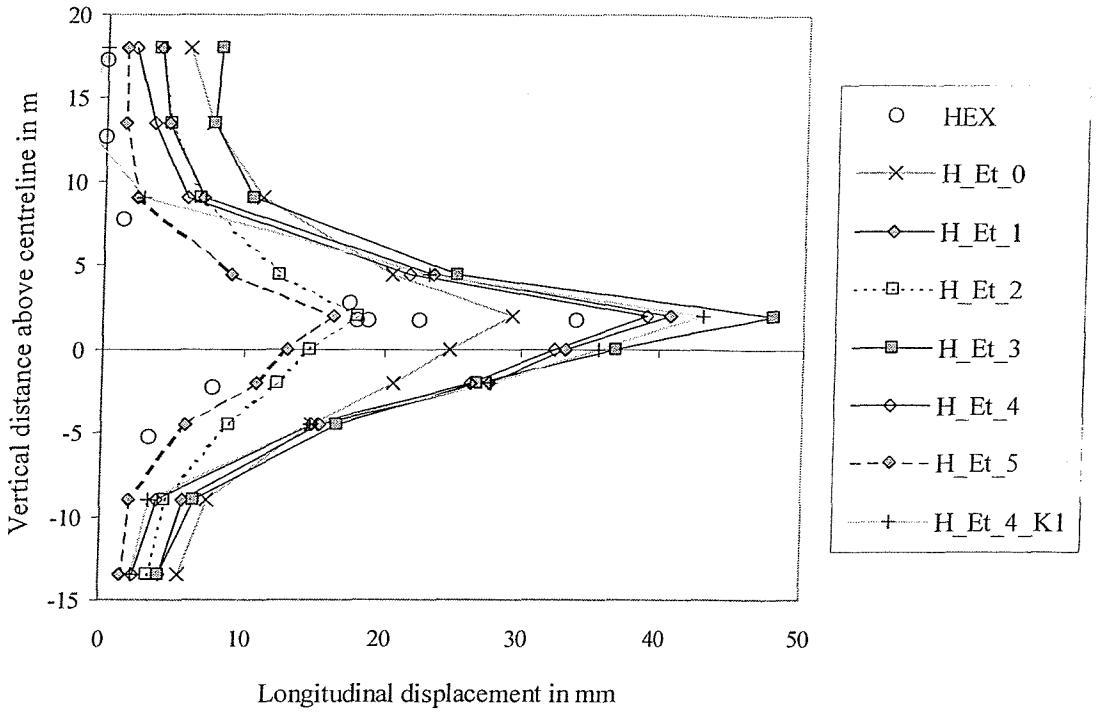

* HEX results from inclinometer located ahead of Concourse tunnel

Figure 7.27 Close-up of mesh for domed face

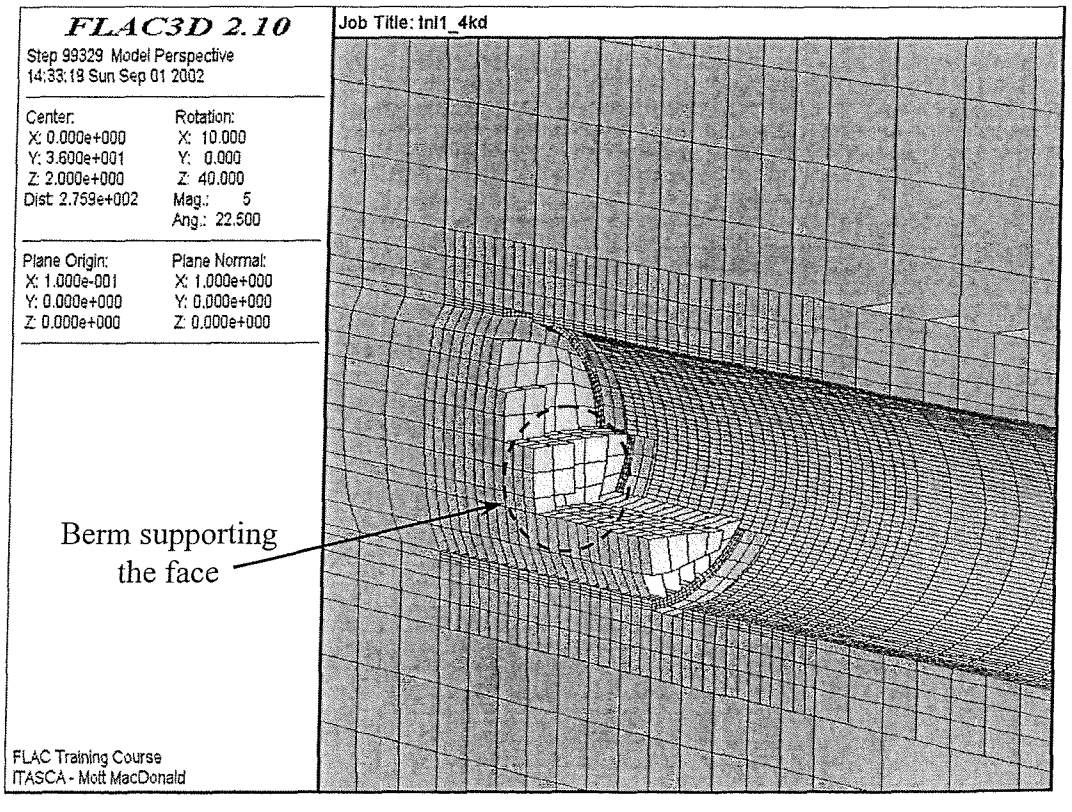

Figure 7.28 Utilization factors vs distance from Leading Edge (for models with weak joints)

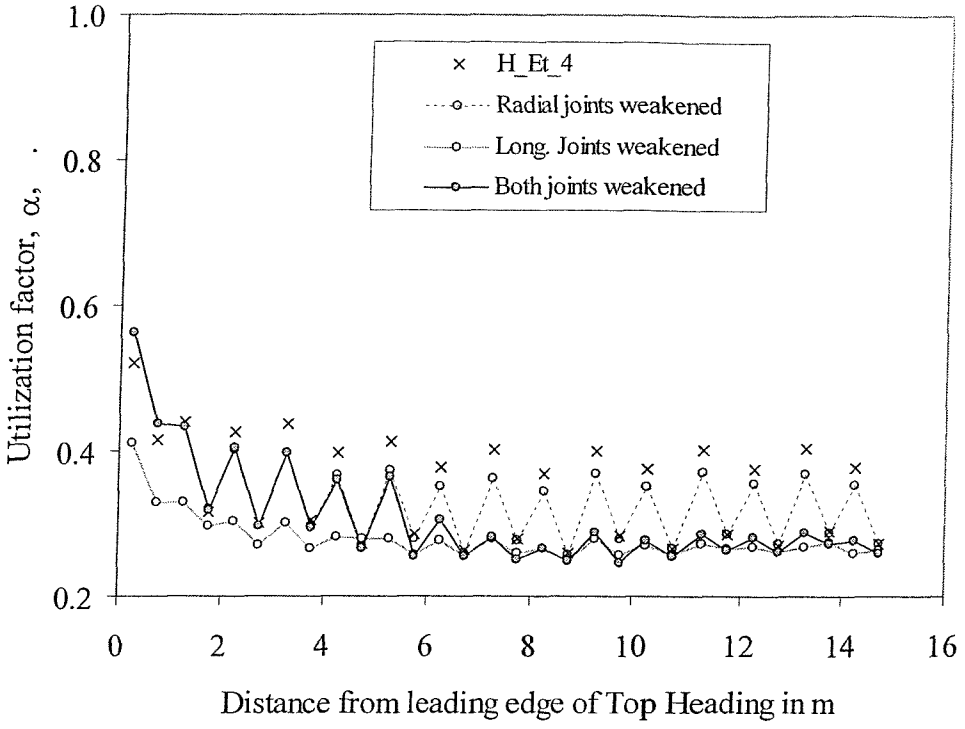

Figure 7.29 Hoop force in crown vs distance from face

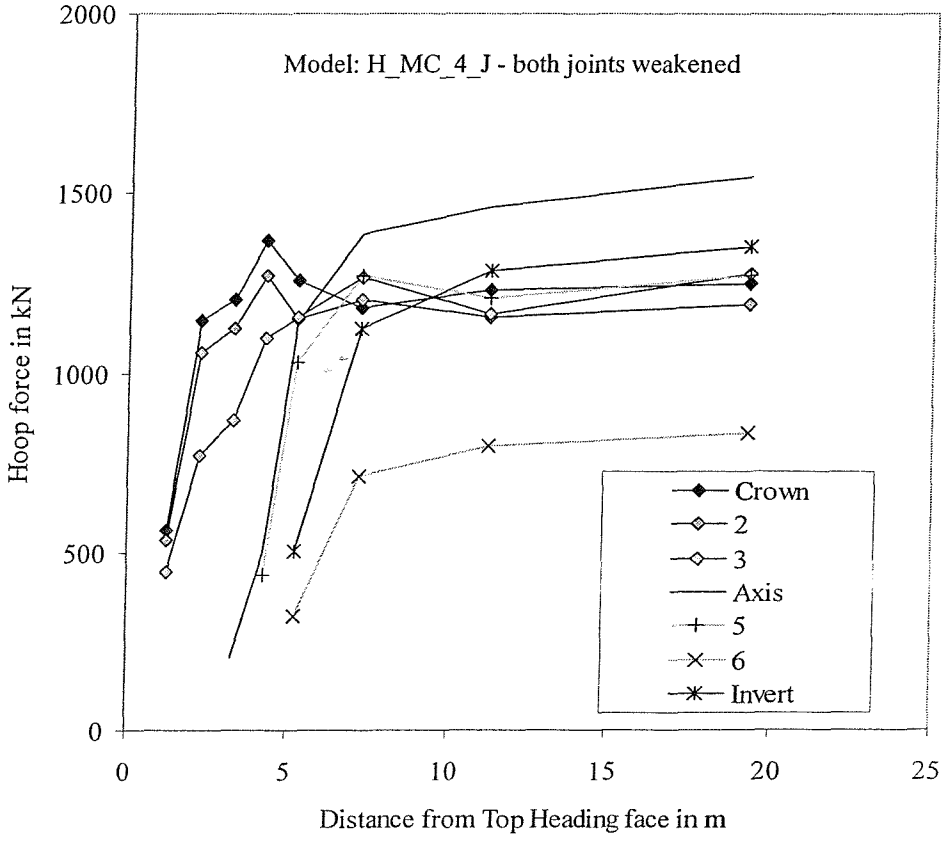

Figure 7.30 Hoop bending moment in crown vs distance from face

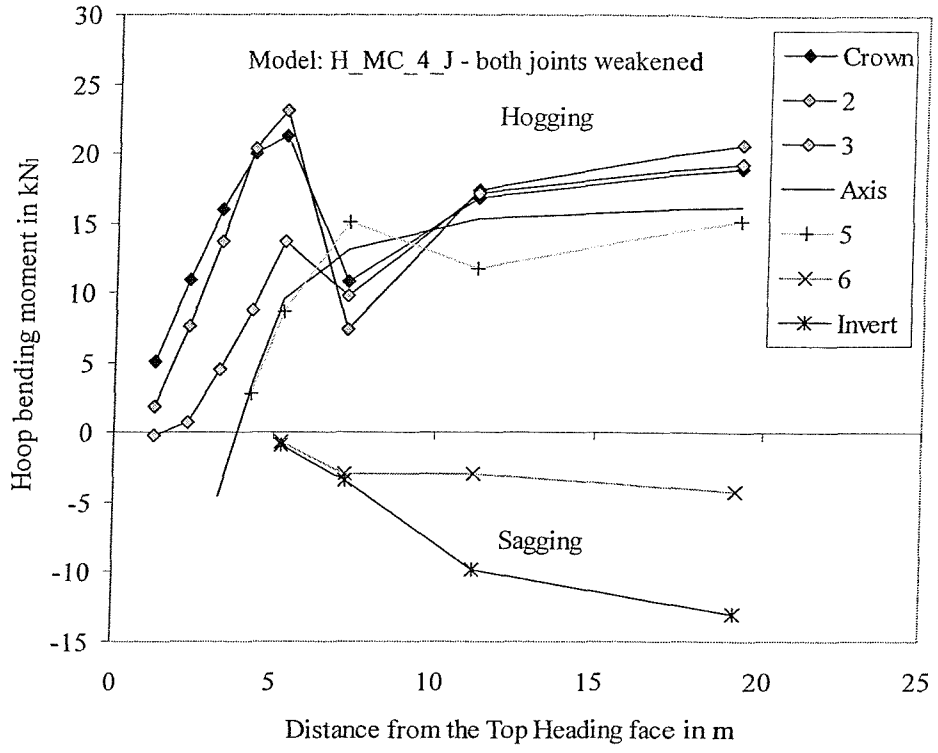

Figure 7.31 Normalized hoop loads vs (RCD/AR) at 9m from the face

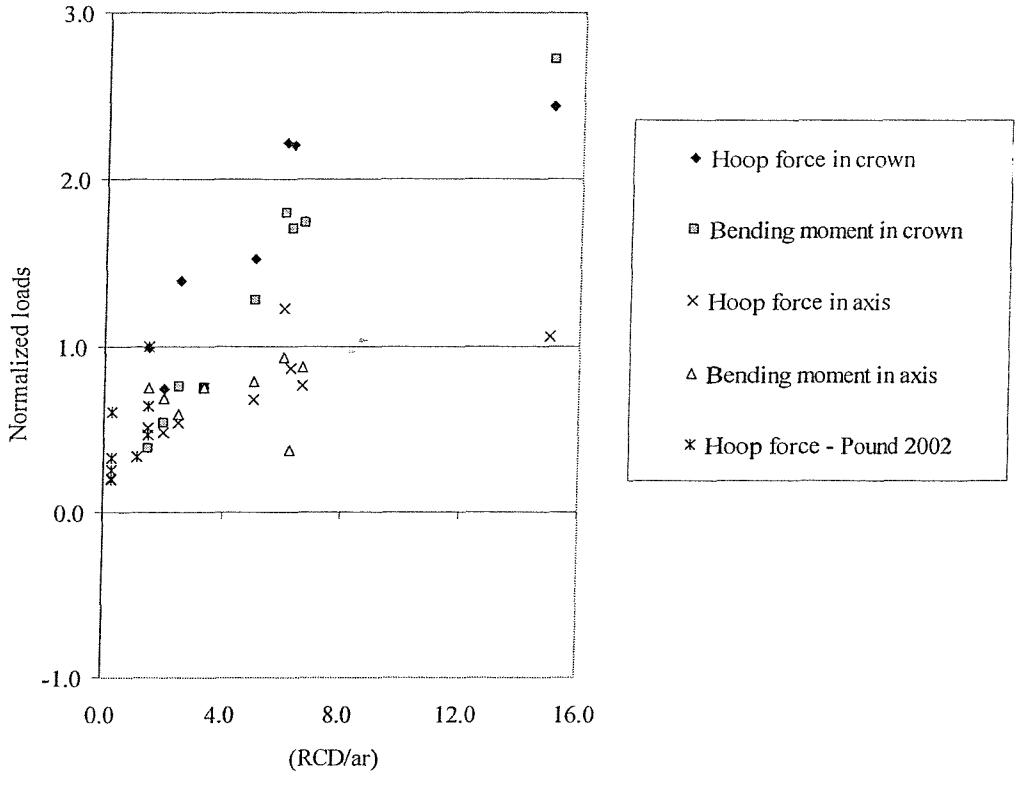

Figure 7.32 Normalized hoop loads vs (AL/R) at 9m from the face

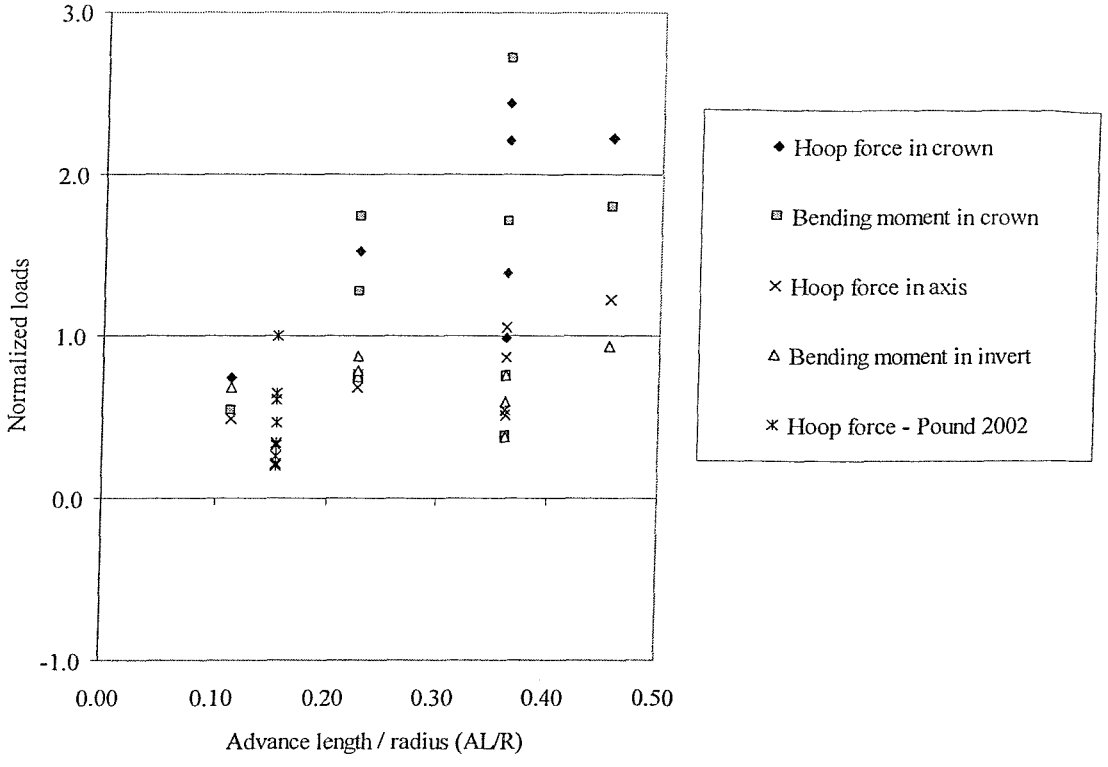

Figure 7.33 Normalized hoop loads vs (E / E_{28}) at 9m from the face

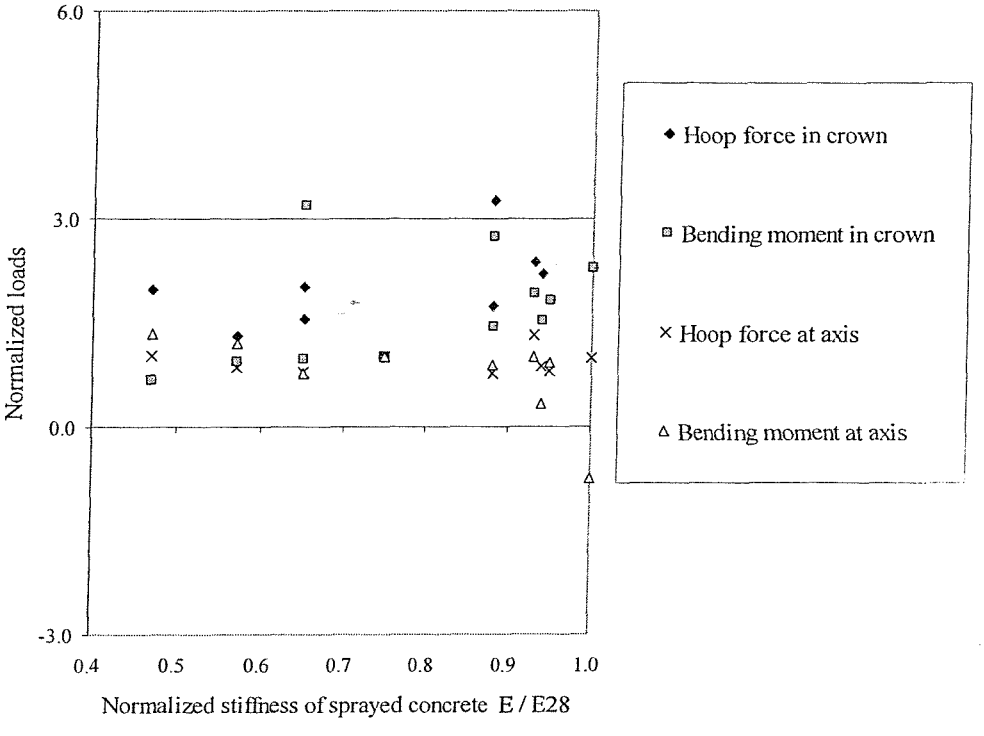

Figure 7.34 Normalized hoop loads vs (RCD/ar)*(al/r) corrected for tunnel radius and stiffness at ring closure at 9m from the face

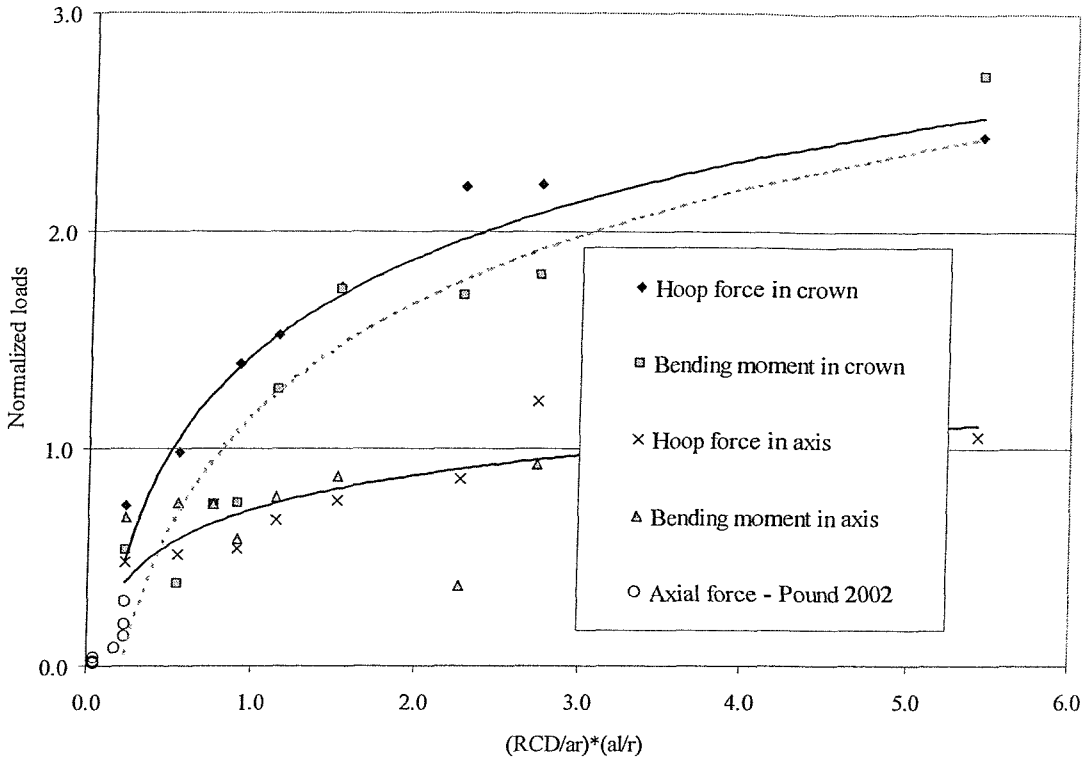

Figure 7.35 Bending moment – axial force interaction diagram

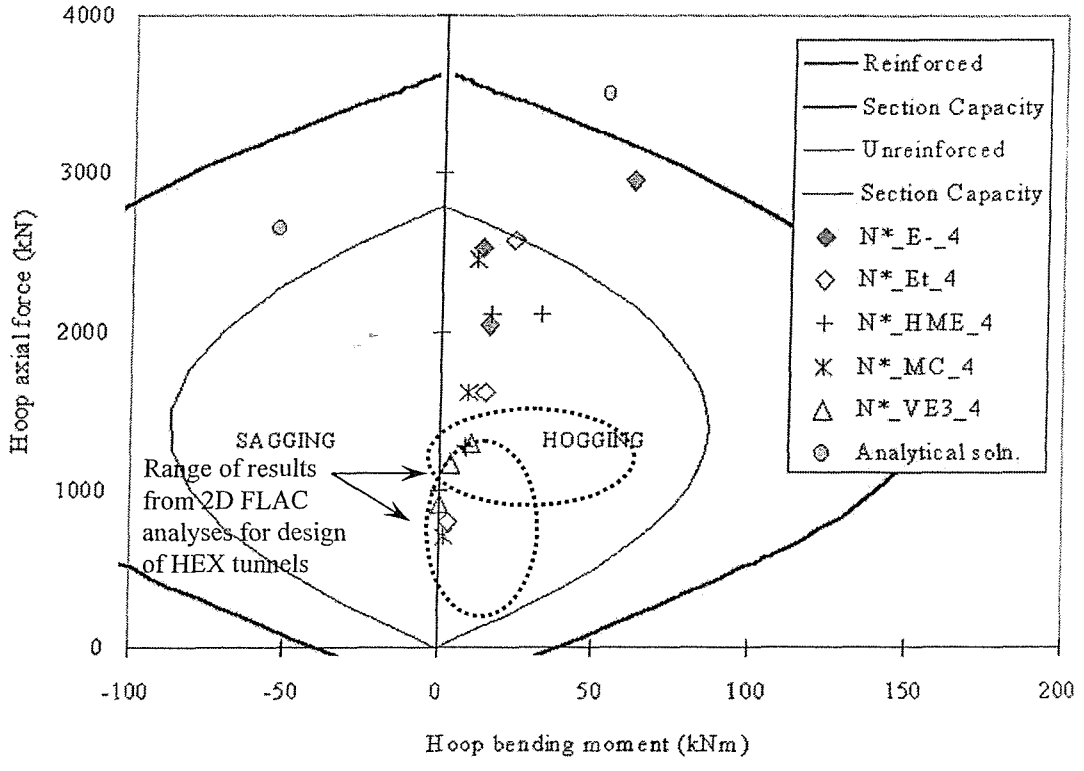

* Analytical solution by Einstein & Schwarz (1979)

8 CONCLUSIONS & RECOMMENDATIONS

As Fourier said, *"nature is oblivious to the difficulties that it poses for mathematicians"*. Similarly, sprayed concrete is blissfully unaware of the headaches it causes tunnel engineers.

8.1 Sprayed concrete – current knowledge

As is clear from the literature in this thesis, sprayed concrete is a complex material. The salient points are summarised below.

- Sprayed concrete consists of 3 phases: solids – both chemically active and inactive components, such as cement and aggregate respectively; a liquid – water, which can move through the solid structure, can shift from between being held within the crystals to being free water and can both leave and enter the material, in response to changes in the environment and the load on the concrete; gases – air trapped within the material and air in contact with it, which can react with components of the material (e.g.: carbonation shrinkage).
- Fortunately, though complex, sprayed concrete is not unique. Its composition is basically the same as conventional concrete. The method of placement of sprayed concrete may lead to a higher variability in the final product, compared to cast insitu concrete. While the material properties may be variable, the material behaviour remains essentially the same. Therefore the body of knowledge about conventional concrete can guide the efforts to understand sprayed concrete.
- Sprayed concrete is vulnerable to poor workmanship. Typically this manifests itself as areas which are too thin or areas of low strength material (e.g.: due to poor surface preparation, poor spraying technique or variations in mix composition). Joints are high-risk areas because they are more difficult to form than the body of the lining.
- Like conventional concrete, sprayed concrete starts life as a fluid mixture. The mechanical properties of the material change considerably as the hydration reaction proceeds and a hardened concrete is formed (i.e. it *ages*). The rate of change of properties is rapid initially, due to the accelerated hydration, and slows with age but may continue for months, even years. The hydration reaction produces heat which causes volume changes.

- In its hardened (and hardening) form sprayed concrete is a nonlinear elastoplastic material when under compression. In tension it is initially a linear elastic material which then fails in a brittle manner. Sprayed concrete exhibits both shrinkage and creep.

The age of the material at loading is the main reason for the difference in behaviour of sprayed concrete and conventional concrete in tunnel linings. An increasing but variable load is applied to the sprayed concrete from the moment that it is sprayed. The loading of sprayed concrete at an early age means that creep may be important and the material may be "overstressed" – i.e. loaded to a high percentage of its strength, leading to pronounced nonlinear behaviour and possibly long-term damage to the microstructure. Since the properties of sprayed concrete change considerably with age during the early life of a SCL tunnel, the response of the tunnel lining to loading varies, depending on when the load is applied.

The early loading and method of placement demand a cocktail of additives, to aid pumping and spraying, and to speed the hydration reaction. Mix design and additive technology are ever changing and these themselves are not precise sciences. Hence sprayed concrete has evolved considerably in its short life as a construction material. It is partly for this reason that a detailed, quantitative picture of the behaviour of sprayed concrete at early ages has yet to be formed. Other contributory factors are that it is difficult to test at early ages and that there has been relatively little research on certain aspects (notably, creep behaviour).

8.2 SCL tunnelling – the state-of-the-art

Having painted a somewhat pessimistic picture of the complexity of sprayed concrete, one must state that SCL tunnels have been successfully built in many different types of ground during the past 50 years. SCL is an increasingly favoured technology because of its versatility. It is particularly cost-effective for tunnel junctions and short tunnels with complex shapes. If simple quality control and quality assurance procedures are implemented sprayed concrete can be produced which is as good as conventionally cast concrete.

Traditionally – as in all branches of tunnelling – relatively simple design methods have been used for SCL tunnels. On one hand there is heavy reliance on precedent practice, supplemented by simple empirical or "closed-form" analytical calculations. A current state-of-the-art design comprises a handful of simple 2D numerical analyses using a rudimentary constitutive model for the tunnel lining – usually, a linear elastic model with a Hypothetical Modulus of Elasticity.

On the other hand, this is often combined with an observational or "semi-observational" approach during construction. All SCL tunnels are monitored to verify that they are performing in line with the design predictions. In what one might term "classic" NATM, the support measures are determined in the tunnel according to the prevailing ground conditions and the results from monitoring of the part of the tunnel that has already been constructed. This approach has been most successfully applied in deep rock tunnels.

Along with the many successful examples of SCL tunnels, there have also been serious collapses. This has given rise to concern over current design and construction practices. The management of SCL construction has already been dealt with in detail elsewhere (e.g.: HSE 1996 & ICE 1996). Arguably less attention has been paid to design methods. The main weaknesses in current design practice are as follows:

- Simple design tools – such as "closed-form" analytical solutions or simplistic 2D numerical models – are incapable of modelling the true complexity of an SCL tunnel. This is a 3-dimensional soil-structure interaction problem, involving complex material behaviour (both for the ground and sprayed concrete). Time is an important factor – in terms of material behaviour (e.g.: ageing and creep) and the placement of support. To compensate for the shortcomings of simple design methods engineering judgement plays a large role in determining the design of SCL tunnels.
- The stress in sprayed concrete linings is difficult to measure. Therefore there is uncertainty over the actual factor of safety in SCL tunnels and it is hard to validate the design predictions fully.

- There has been concern that high levels of loading at early ages may damage the sprayed concrete and compromise the long-term durability of the lining (e.g.: by causing cracks).
- The most commonly used monitoring instruments (e.g.: pressure cells and in-tunnel deformation monitoring) may not provide sufficiently accurate, clear and quick information on the performance of the lining during the critical early period in the construction of shallow soft ground tunnels. The critical period is from the construction of the Top Heading of a tunnel to the closure of the whole ring. Therefore applying the observational approach (as used in deep rock tunnels) carries significant risks in shallow SCL tunnels. There may not be enough time from the identification of adverse behaviour to act to correct it before a collapse.

More realistic numerical modelling offers one way to improve current design practice. If the tunnel can be modelled more realistically, this could reduce the reliance on empirical correction factors and subjective engineering judgement. Explicit modelling of features, such as the construction process, the three dimensional shape of the tunnel heading and nonlinear material behaviour, may provide more insight into the influence of various parameters and how the tunnel lining behaves in general. The benefits of more sophisticated numerical modelling of geomaterials have already been demonstrated in the prediction of ground movements around tunnels.

8.3 Advanced numerical modelling – the method

This study has explored the possibility of improving SCL design by using more sophisticated numerical models. 3D effects, the construction sequence, the complex material behaviour of the sprayed concrete and construction defects have all been considered explicitly. While the power of numerical models lies in their ability to simulate such features, the models are still only approximations of reality (see 1.2.3). For this reason a staged process was followed, starting with the numerical modelling of simple cases (e.g.: uniaxial compression tests), progressing to more complex laboratory tests and culminating in the detailed 3D simulation of the construction of large diameter, shallow SCL tunnel, using a variety of constitutive models (for the ground and lining). The results from all models were compared with data from the original laboratory experiments or construction records. It is worth noting that

careful planning is as important in numerical modelling as it is in laboratory testing or fieldwork, in order to ensure a consistent set of data, that has been designed to test clearly defined hypotheses.

The hypotheses for this study were:

- 3D numerical modelling is a viable design tool.
- The constitutive model of the sprayed concrete has a significant influence on the predicted stress distribution in the lining.
- The predicted stress distribution in the lining depends heavily on the modelling of the ground.
- The construction sequence is an important influence and therefore should be modelled in detail.

As outlined in more detail below all of these hypotheses were proved to be true.

The chosen tool for this study was FLAC, a commercially available 3D finite difference program. Typically the numerical models of the tunnel took 1 to 3 days to complete using a standard PC. The existing FLAC constitutive models were customised with user-defined FISH functions to include ageing, to convert the Maxwell rheological model into a Kelvin model and to implement nonlinear elastic models for the ground and sprayed concrete, which were capable of modelling unloading/reloading cycles.

8.4 Advanced numerical modelling – the results

The principal conclusion of this study is that there is merit in considering the behaviour of SCL tunnels (whether temporary primary linings or permanent works) in detail with due regard to their complexity, since apparently minor changes in design or behaviour may have large impacts on the predicted performance of the tunnel. For example, the advance rate of the tunnel and the distance to closure of the ring are parameters which often vary in real tunnels and both have been show to influence the loads in the lining.

In general the predicted stress distribution in the lining was not uniform. The stress at the Leading Edge of each advance length was found to be greater than at the Trailing Edge. This may have been due to the difference in the concrete stiffness and the higher radial loads at the Leading Edge. Stresses were higher in the first part of the lining that was constructed – i.e. the stresses were higher in the Top Heading than the Invert. The utilization factor in the lining was highest near the face and reduced with distance away from the face.

The choice of constitutive model for the sprayed concrete was found to affect the predicted stress distribution in the lining. This was more pronounced if the utilization factor in the lining exceeded 50%. Assuming that the tunnel face is stable, the loads in the lining and its movements are governed by the relative stiffness of the ground and lining, since this is a soil-structure interaction problem. Hence, introducing "softer" models for the lining (such as a creep model) resulted in lower stresses. Bending moments were more strongly influenced than hoop forces by the constitutive model (both for the sprayed concrete and ground).

The details of the constitutive model may also be significant. For example, the shape of the yield criterion in the deviatoric plane is important for the sprayed concrete because the stress paths in the tunnel lining lie in between triaxial compression and extension. Typically the Lode angle is about 40°. This nuance of modelling may cause purely elastic behaviour or yielding, depending on whether a Drucker-Prager or Mohr-Coulomb yield criterion is used. Similarly, the choice of the parameters for creep models change with age affected strongly the amount of creep deformation.

Considering the ground, the numerical model predicted some movements in the ground reasonably well – notably, the movement ahead of the face and the overall volume loss. The constitutive model for the sprayed concrete did not have a large influence on the far-field behaviour of the ground. As might be expected, the assumed insitu stress state and the constitutive model for the ground both had a considerable influence on the predicted loads on the lining.

A linear elastic perfectly plastic model for the ground was found to be adequate in a firm, overconsolidated clay for the prediction of the radial stresses on the lining. The nonlinearity of the stiffness of this material did not have a large influence on this because this effect was most pronounced at small strains.

The SCL tunnelling method is known to be vulnerable to poor construction quality, e.g.: at joints. This study found that the presence of weak zones at circumferential and radial joints do alter the stress distribution within the tunnel lining.

Considering the construction sequence, three of the main parameters – advance length (AL), advance rate (AR) and distance to ring closure (RCD) – are interrelated since altering one will affect the others. It is proposed that the impact of changes in construction sequence can be examined by combining key parameters into a new factor – the "Sequence Factor".

$$\left(\frac{RCD}{AR}\cdot\frac{Ex}{E_{28}}\cdot\frac{AL}{R}\right)$$

which consists of:

RCD/AR - ring closure distance/advance rate ~ the time taken to close the ring

E_x/E_{28} - the ratio of Young's modulus of the sprayed concrete at ring closure to the 28-day value ~ a measure of how stiff the ring is in compression at closure

AL/R - advance length / tunnel radius (R) ~ a measure of the relative size of the unsupported length during excavation

Results from the numerical modelling in this study suggest that lining loads – both hoop forces and hoop bending moments – in the top part of the tunnel increase with an increase in the Sequence Factor (see 7.4).

8.5 Implications for the design of SCL tunnels in future

As discussed earlier the design of SCL tunnels needs to be improved.

It is recommended that sophisticated numerical models are used more widely in the design of SCL tunnels, in conjunction with empirical and "closed-form" analytical design tools. Simple

design tools do not replicate the complexity of SCL tunnels adequately on their own. 3D numerical modelling is both necessary and viable for the design of tunnels. It avoids the empirical choice of correction factors for stress relief ahead of the face, provides information on the stresses in the lining at all locations and times and can be performed in an acceptably short period of time.

However, numerical modelling is not a panacea for the current weaknesses in design. Sound engineering judgement remains the key to good design. The more simple design tools have a vital role to play as a check on the results from numerical models. No matter how sophisticated the numerical model, it is still only an approximation of reality. Therefore, wherever possible, numerical modelling should be validated by comparing it with high quality field measurements and experimental data.

State of the art SCL designs often employ a relatively crude usage of the Hypothetical Modulus of Elasticity (HME). It is suggested that there is sufficient data to use more realistic constitutive models – e.g.: an ageing linear elastic perfectly plastic model based on site data for strength development with age (and stiffness estimated from the strength) or an ageing linear elastic model with the stiffness reduced to account for creep - a *refined* HME method.

Turning to the case study at the centre of this work – namely the Heathrow Express project - the new, more sophisticated numerical models predicted bending moments that would have been small enough to permit the use of steel fibres instead of wire mesh. Having removed this major durability concern related to bar reinforcement, a "one-pass" permanent sprayed concrete lining might have been a viable option. This would have resulted in an estimated cost saving for the HEX Platform tunnel of 30% [88]. However, one should note that the lining loads are only one of many considerations in lining design.

[88] Based on a crude estimate of the saving in time and materials cost, assuming that no secondary lining would have been required for the steel fibre reinforced sprayed concrete option.

8.6 Further work

Finally, there is the question of what more remains to do in order to utilise the full potential of SCL technology. The use of "one pass" linings – in which all the concrete sprayed forms part of the permanent works – would represent a significant improvement in the cost effectiveness of this technology.

To achieve this, the first requirement is a reliable means of measuring the stress in SCL tunnels (in order to verify the actual factor of safety in the lining). This would remove the uncertainty that still hangs over design predictions and would help to avoid over-conservative designs. Although this study has helped to identify some of the key influences on the behaviour of SCL tunnels, those need to be confirmed by comparison with accurate measurements of the actual stresses in the lining.

Further information on sprayed concrete at early ages is required, specifically on stiffness development, the creep capacity and the nonlinear stress strain behaviour, so that the behaviour can be correlated with mix design. Then design parameters could be determined with confidence at the design stage, on the basis of the mix design, rather than through expensive pre-construction testing.

Since sprayed concrete is a relatively new material, further work should be done to examine the durability of the products of hydration. Ideally this would include accelerated ageing tests.

Once these steps have been taken there will be enough confidence in the safety and durability of sprayed concrete lined tunnels to permit the widespread use of "one pass" linings.

Appendix A The evolution of mechanical properties with time

Property & Author	Equations	Constants	Range of applicability	Age range	Ref.erences
Elastic modulus – Weber	$E_b = E_b^{28}.\ a_e.e^C$ $C = C_e/t^{0.60}$ t = age in days	$a_e = 1.084$ $C_e = -0.596$ $E^{28} = 30$ Gpa; $a_e = 1.132$ $C_e = -0.916$ A = 1.084; $C_e = -0.916$ $E^{28} = 26$ GPa –Yin; $a_e = 1.084$; $C_e = -0.196$ – Huang (Typing error?) $a_e = 1.084$; $C_e = -0.596$ – Schropfer, Pottler	Z35F/45F cement Normal concrete Z25, 35L, 45L(Pottler) Used by Yin, Huang, Pottler & Schropfer		Alkhiami 1995; Yin 1996; Huang 1991, Schropfer 1995; Pottler 1990;
Compressive strength – Weber	$\beta_b = \beta_b^{28}.\ a_\beta .e^C$ $C = C_\beta/t^{0.55}$ t = age in days	$a_\beta = 1.27$ $C_\beta = -1.49$	Z35F/45F cement Normal concrete (Yin)		Alkhiami 1995; Yin 1996
Elastic modulus – Chang	$E = E^{28}.\ a.e^C$ $C = c/t^{0.70}$ t = age in days	a = 1.062 c = -0.446 $E = 3.86\ \sigma_c^{0.60}$	Based on literature review	E - σ_c valid for 0 - 7 days; E valid for 4 hours to 28 days; $\alpha < 0.70$	Chang & Stille 1993; Chang 1994
Compressive strength - Chang	$\sigma_c = \sigma_c^{28}\ .\ a\ .e^C$ $C = c/t^{0.70}$ t = age in days	a = 1.105 c = -0.743 $\sigma_c = 0.105\ E^{1.667}$	Based on literature review	E - σ_c valid for 0 - 7 days; valid for 4 hours to 28 days; $\alpha < 0.70$	Chang & Stille 1993; Chang 1994
Compressive strength – modified Byfors	$f^t_{cc} = 0.01 \times (A_1 t^{B1}/X).f^{28}_{cc}$ in % $X = 1 + (A_1/A_2).t^{(A1-B2)}$	Cylinder str in MPa, t = age in hours, For w/c = 0.4 – 0.5, A1 = 0.300 %; A2 = 29.446 % B1 = 2.676; B2 = 0.188 $f^{28}_{cc} = 29.022$ MPa	Back-calc from cores on panels sprayed in-situ		Kuwajima 1999
Elastic modulus – modified Byfors	$Ec = c_1 f_{cc}^{d1}/X$ in GPa $X = 1 + (c_1/c_2).f_{cc}^{(d1+d2)}$	$C_1 = 1306$ $C_2 = 7194$ $D_1 = 1.920$; $D_2 = 0.363$	Wide scatter for t < 10 hrs		Kuwajima 1999
υ Poisson's ratio	Graph only – no eqn.		Kuwajima 1999, Fig. 4		Kuwajima 1999
Elastic modulus – Golser	$E_t = E_{28}.\ ([a + bt]/t)^{-0.5}$	a = 4.2; b = 0.85; t in days			Yin 1996
Compressive	$\beta_t = \beta_{28}.0.03t$	t =< 8 hours	For prisms;		Aldrian 1991

Property & Author	Equations	Constants	Range of applicability	Age range	Ref.erences
strength – Aldrian	$\beta_t = \beta_{28}.[(t-5)/(45+0.975t)]^{0.5}$	t > 8 hours	$\beta_{cube} = 1.07.\beta_{prism}$ for the sizes used by Aldrian		
Elastic modulus – Aydan	$E_t = A(1 - e^{Bt})$	A = 5000, B = -0.42	Wet mix, loaded at right angles to spraying	Age = 3 hrs to 28 days	Yin 1996; Aydan et al 1992
υ - Poisson's ratio - Sezaki	$\upsilon_t = a + b.e^{ct}$	a = 0.18, b = 0.32, c = -5.6	Wet mix, loaded at right angles to spraying	Age = 3 hrs to 28 days	Yin 1996; Aydan et al 1992
Compressive strength - Meschke	$f_{cu(t)} = f_{cu(1)}[(t+0.12)/24]^{0.72453}$ $f_{cu(t)} = ac\ e^{(-bc/t)}$ ac =1.027.fcu28 bc = 17.80	for t< 24 hours for t > 24 hours, where $\kappa = 0.489 = f_{cu1}/f_{cu28}$; ac & bc are functions of κ	Austrian shotcrete guidelines for t < 24 hours		Meschke 1996 ; Kropik 1994
Elastic modulus - Meschke	$E_t = \beta_{Et}.E_{28}$ $\beta_{Et} = 0.0468t - 0.00211\ t^2$ $\beta_{Et} = (0.9506 + 32.89/[t - 6])^{-0.5}$	t < 8 hours 8 < t < 672 hours	Modified CEB-FIP	Age = 0 to 28 days	Meschke 1996, Kropik 1994
Compressive strength – Pottler	$\beta_t = \beta_1.t^{0.72453}$ or $\beta_t = \beta_1.(1 + 4t)/5$	β_1 = 1 day str	From cube tests.	Age > 1 day	Pottler 1993; Pottler 1990
Compressive strength - Eierle & Schikora	$f_{cc}(\alpha)/ f_{cc,\alpha=1} = [(\alpha - \alpha_0)/(1 - \alpha_0)]^{3/2}$	$f_{cc,\alpha=1}$ = compressive strength at complete hydration; α = degree of hydration α_0 = 1.8 est.	For plain concrete; for tensile strength, $f_{ct}(\alpha)/ f_{ct,\alpha=1} = (\alpha - \alpha_0)/(1 - \alpha_0)$		Eierle & Schikora 1999
Elastic modulus - Eierle & Schikora	$E(\alpha)/ E_{\alpha=1} = [(\alpha - \alpha_0)/(1 - \alpha_0)]^{2/3}$	$E_{\alpha=1}$ = modulus at complete hydration; α = degree of hydration			
Compressive strength - Kusterle	Prisms $Y = 1.8171X^{0.8285}$; Cylinders $Y = 0.0521X^2 + 0.3132X + 0.9213$; Beams $Y = 0.9208X^{0.9729}$	Y = prism, cylinder or beam X = cube str in MPa Cube = 20x20x20 cm; Prism = 4x4x16 cm; Cylinder = 10 cm dia.x10 cm; Beam = 10x10x50 cm	Str range = 1 to 12 MPa		Kusterle 1998

NB: (see Appendix C Part 3 for tensile strength)

Appendix B Rheological models and rate of flow method

Author	Equations	Constants	Range of applicability & notes	Type	References
Rheological models					
Rokahr & Lux	$\Delta\varepsilon_v/\Delta t = [\ (1/2\eta_{k\ \sigma v\ ta}).(1 - \{\varepsilon_v^{v,tr}.3G_{k(\sigma v)}/\sigma_v\}).M.\sigma]$ ta = age of shotcrete $\varepsilon_v^{v,tr}$ = accumulated transient inelastic deformation (eff. strain) – $\varepsilon_v^{v} = (2^{0.5}/3).([\varepsilon_{1v} - \varepsilon_{2v}]^2 + [\varepsilon_{2v} - \varepsilon_{3v}]^2 + [\varepsilon_{3v} - \varepsilon_{1v}]^2)^{0.5}$ σ_v = eff stress = $(3J_2)^{0.5}$ M = condensation matrix ε_v = integral over time of viscous strain rate $\Delta\varepsilon_v/\Delta t$ = viscous strain rate	$3G_k = G^*_k\ .\ e^{k1\sigma v}$ $3\eta_k = \eta^*_k\ .\ t_a^n\ .e^{k2\sigma v}$ At 8 hours age: G^*_k = 8450 MPa, η^*_k = 6900 day.MPa, k1 = -0.459 MPa^{-1}, k2 = -0.642 MPa^{-1}, n = 0.74	8 hours to 10 days (?); stress < 10 MPa; At 24 hours age: G^*_k = 52500 MPa, η^*_k = 17000 day.MPa, k1 = -0.0932 MPa^{-1}, k2 = -0.100 MPa^{-1}, n = 0.73 (Berwanger's parameters)	Visco-elastic Modified Kelvin	Rokahr & Lux 1987; Watson et al 1999
Schropfer	See Rokahr &Lux	At 30 hours age: G^*_k = 1312 MPa (?), η^*_k = 17315 day.MPa, k1 = -0.0309 MPa^{-1}, k2 = -0.2786 MPa^{-1}, n = 0.70	Time = 0 to 30 hours, Assumes const. Volume during creep, Assumes hydrostatic stress has no influence on creep ; B35 shotcrete	Visco-elastic Modified Kelvin	Schropfer 1995
Mertz	(see Schropfer)	Not given	-	Visco-elastic Modified Kelvin	Schropfer 1995
Kuwajima	$\varepsilon_c(t')/\sigma_0 = 1/E_t.(1 - e^{-\lambda t'})$ $\lambda = E_t/\eta$	E = 15 Gpa $1/E_t$ = 0.03 Gpa^{-1} λ = 0.003 min^{-1} NB: average values	Age = 10 to 100 hrs; time = 10 to 100 hrs; Notes that adding time dependency might overcome some inaccuracy due to use of average values.	Visco-elastic Generalised Kelvin unit	Kuwajima 1999
Swoboda	$\varepsilon_c(t')/\sigma = 1/E_{b\ ta}.(1 - e^{-\lambda t'})$ $\lambda = E_{b\ ta}/\eta$	t < 2 days: E_b = 15 GPa, $E_{b\ ta}$ = 6 GPa, η = 6 x 10^8 day kPa t > 2 days: E_b = 25	-	Visco-elastic Generalised Kelvin unit	Swoboda & Wagner

Author	Equations	Constants	Range of applicability & notes	Type	References
	$\varepsilon = \sigma/E_b + \varepsilon_c$	GPa, $E_{b\,ta}$ = 10 GPa, η = 10 x 10^8 day kPa			
Petersen	$\Delta\varepsilon^v_{ij}/\Delta t = [\ (1/3\eta_{k\ \sigma v\,t}).(e^{A\,t}).(3/2).M_2.\sigma_{ij}]$ $A = -3G_{k(\sigma v)}/3\eta_{k(sv,t)}$	$3G_k = G^*_k\ .^{\ ek1\sigma v}$ $3\eta_k = \eta^*_k\ .\ t^{\ n}.e^{k2\sigma v}$ $\Delta\varepsilon_v/\Delta t$ = viscous strain rate	30 hours to 10 days and σ_v < 12MPa, G^*_k = 1312 MPa, η^*_k = 17312 day.MPa, k1 = -0.0309, k2 = -0.2786, n = 0.70	Based on modified Burger's model	Yin 1996; Pottler 1990
Pottler	$\Delta\varepsilon^v_{ij}/\Delta t = [\alpha_t.\sigma_v^{\ 2} + \beta_t.\sigma_v^{\ 3}\ ].(3/2).M_2.\sigma_{ij}$ $\alpha_t = (0.02302 - 0.01803t + 0.00501t^2).10^{-3}$ $\beta_t = (0.03729 - 0.06656t + 0.02396t^2).10^{-3}$	(see Petersen) υ = 0.167;		Polynomial form of Petersen	Yin 1996; Pottler 1990
Yin	$\Delta\varepsilon^v_{ij}/\Delta t = [(a_t.\sigma_v^{(b-1)}).(3/2).M_2.\sigma_{ij}]$ $a_t = A1.e^{(A2/(A3+t))}$ $b_t = B1.e^{(B2/(B3+t))}$ See also el. Vis. pl. rock model with DP and strain softening	υ = 0.2, A1 = 0.20167 x 10^{-5}, A2 = 3.9444, A3 = 0.758, B1 = 1.4791, B2 = 0.15983, B3 = 0.602	Stress up to 20 MPa +, Duration up to 20 days +,	Based on Petersen but with age dependent creep	Yin 1996
Huang	$\Delta\varepsilon_{ij} = \Delta\varepsilon_{ij}^{\ E} + \Delta\varepsilon_{ij}^{\ I} + \Delta\varepsilon_{ij}^{\ II}$ $\Delta\varepsilon_{ij}^{\ E} = E_{ijkl}(t + \Delta t)\Delta\sigma_{kl} + \Delta E^{-1}_{ijkl}.\sigma_{kl}$; $\Delta\varepsilon_{ij}^{\ I}/\Delta t = Sij/\eta_{n(t,\sigma v)}$; $\Delta\varepsilon_{ij}^{\ II} = \Sigma_\mu\Delta\varepsilon_{ij}^{\ \mu}$ $\Delta\varepsilon_{ij}^{\ \mu} = (S_{ijkl}.\sigma_{kl}.(t + \Delta t)/E_\mu) - \varepsilon_{ij}^{\ \mu}(1 - e^{A\Delta t})$, $A = -E_\mu/\eta_\mu$, $\varepsilon_{ij}^{\ \mu}$ = sum of strains to t from t = τ_o, υ = 0.2, τ_o = 0.3 days	Spring, E_{b28} = 34 GPa see also below, Dashpot calculated using Berwanger's values at 8 hrs; Kelvin units 1 & 2 – E_1 = 1.0 x 10^4 MPa, η_1 =1.0 x 10^5 MPa / day, E_2 = 1.4 x 10^4 MPa, η_2 =1.4 x 10^6 MPa / day	As for Rokahr & Lux	Visco-elastic (Spring in series with dashpot and 2 Kelvin units) Time-dep E	Huang 1991

Author	Equations	Constants	Range of applicability & notes	Type	References
Zheng	(see Yin)	(see Yin)	Limited to low stress	Spring in series with dashpot and 2 Kelvin units	Yin 1996
Brite Euram	Strain rate, $\varepsilon'_{ij} = \varepsilon'^{e}_{ij} + \varepsilon'^{vp}_{ij}$ $\varepsilon'_{ij} = -(\upsilon/E)\sigma'_{kk}\delta_{ij} + (1+\upsilon)\sigma'_{ij}/E$ $\varepsilon'^{vp}_{ij} = (F/2\eta)\sigma''_{ij}$ F = yield function = $1-K/(0.5\ \sigma''_{ij}.\sigma''_{ij})^{0.5}$ σ''_{ij} = deviatoric stress = $\sigma_{ij} - (1/3)\sigma_{kk}\delta_{kk}$ $K = A\sigma_h + B$ σ_h = hydrostatic stress	At age = 4 hours, E = 255 MPa η = 2145 MPa/s K = 2.06 MPa (A = -14, B = 0.7 for K = 9.1 MPa)	E, K, η available for age t = 1 to 72 hours; Stress = 0 to 30 MPa ? At age = 72 hours, E = 4865.24 MPa η = 2966.7 MPa/s K = 18.34 MPa	Elastic visco-plastic (in shear) Bingham model	Brite Euram C1 1997,
Power creep law models					
Alkhiami	$\varepsilon = \varepsilon^{el} + \varepsilon^{kr}$ $\varepsilon^{kr} = k.\sigma_{eff}^{\ n}.t^{\ m}$ σ_{eff} is effective stress	m = 0.252 n = 2.574 $k = 1.88 \times 10^{-5}$ (?)	Large exc.; Range of m for stress = 5 to 9 MPa and n for 0.1 to 168 hours Creep law in Abaqus	Straub 1931	Alkhiami 1995
Rathmair	$\Delta\varepsilon/\Delta t = A.\sigma_{eff}^{\ n}.t^{\ m}$ (is this formula correct? – see Alkhiami) - see also Schubert's Rate of Flow Method	m = - 0.252 n = 2.574 $A = 1.88 \times 10^{-5}$	Doesn't handle elastic strain well; transverse strains don't agree well; Creep law in Abaqus		Rathmair 1997; Golser 1999;
Probst	$\varepsilon = A.\sigma_{eff}^{\ n}.t^{\ m}$	m = 0.36 n = 0.75 $A = 1.12 \times 10^{-4}$	Stress range = 2.5 - 10 MPa; age range = 1 to 100 hours		Probst 1999

Author	Equations	Constants	Range of applicability & notes	Type	References
Rate-of-flow					
Aldrian-modified Schubert model	$\varepsilon_2 - \varepsilon_1 = (\sigma_1 - \sigma_2)/(E_{28}.V^*.f) + \sigma_2 \Delta C.(e^{8\alpha-6} + 1) + \Delta\varepsilon_d + \Delta\varepsilon_{sh} + \Delta\varepsilon_t$ $V^* = (1/22.5).[25.(1-\alpha)(t/\{25+1.2t\})^{0.5} + 3\alpha(t/\{100+0.9t\})^{0.5}]$ Viscous deform. $\Delta C = A(t-t_1)^X$, $X = 0.25.\alpha^{0.2}$ (or simply $X = 0.25$); Delayed elastic increment, $\Delta\varepsilon_d = (\sigma_2 C_{d00} - \varepsilon_d)\{1 - e^C\}$, $C = -\Delta C/\theta$; $\varepsilon_{sh} = \varepsilon_{sh,00} . t/(B + t)$; Temp. deform, $\varepsilon_t = 30.[1-\cos(250t^{0.25})]$	ε = in 10^{-6}; t In days, except for ε_t ; V^* = Relative deformation modulus; α = utilisation factor; unload constant, $f = 1.0$; A = constant, where $A = 0.25 \times 10^{-3}$, $t = 0$; $A = 0.04 \times 10^{-3}$, t = 500 hours; C_{d00} = limiting value of rev. creep = 0.0001, $A/\theta = 10$; $\varepsilon_{sh,00}$ = limiting value of shrinkage=1200$\mu\varepsilon$, B = 35 (ACI 1978) to 70 hours (Probst);	Age = 1 to 14+ days; Dry mix; for $0 < \alpha < 1.0$ though behaviour may be different for $\alpha > 0.8$; Aldrian supersedes Schubert model; the temp. deform only applies for $0 < t < 4$ days; Unloading constant may vary between 1.1 and 1.5 (Probst 1999)		Golser et al 1989 Golser 1999; Schubert 1988; Aldrian 1991; Probst 1999
Schubert original model	Plastic deform. $C_t = At^{0.33}.e^{k\sigma}$ for $\alpha > 0.5$; $C_t = At^{0.33}$ for $\alpha < 0.5$		Power law		Schubert 1988;

Appendix C - Plasticity models

Part 1 Plasticity (& non-linear elasticity) models for compressive stress region

Author	2D/ 3D	Elastic region	Yield criterion	Post-yield	Notes	Visco-plasticity	Shrinkage
Meschke, Kropik	3D	Time dependent elastic modulus	Drucker-Prager	Strain hardening, with limit strain dependent on age	Ultimate strength dependent on time; constant yield / ultimate strength ratio; biaxial; isotropic	Yes – Duvant-Lions formulation	?
Hellmich	2D	Hyperelastic	Drucker-Prager	Strain hardening	Potential damage levels assessed; isotropic	No	No
Lackner	2D	?	Drucker-Prager	Strain hardening	Isotropic	No	No
Hafez	3D	Linear elastic ?	3 parameter Chen-Chen model	Strain hardening	Post peak strain softening could be included; multiple SCL layers; isotropic	No	No
Haugeneder	3D	Time dependent elastic modulus	Buyukozturk model	?	Reinforcement smeared across elements but assumed isotropic ?	No	No
Moussa, Aydan	2D	Non-linear elastic model (implicitly) with time dependent elastic modulus	Strain history model	Strain hardening	Damage effects included; post peak strain softening could be included; isotropic; reinforcement incorporated using effective areas	No	No
Hellmich et al	2D	Thermo-chemo-mechanical coupling to account for ageing	Drucker-Prager	Strain hardening?	Associated flow rule	No	Yes – but autogeneous shrinkage only
Watson et al	2D ?	Linear elastic E=7.5 GPa for t<10 days, then E = 15 GPa	?	Perfectly plastic	Yield stress = 5 MPa for t<10 days, then yield stress = fcu/1.5; ultimate strain calculated using Rokahr & Lux's Kelvin rheological model	No	No

Appendix C Part 2 Plasticity (& non-linear elastic) models for tensile stress region

Author	2D/ 3D	Yield criterion	Post-yield	Type of crack model	Notes
Meschke, Kropik	3D	Rankine	Linear softening	Rotating crack	Exponential softening also possible
Lackner	2D	Rankine	Linear softening, exponential or both	Fixed and rotating crack models investigated	Anisotropic; damage model
Hafez	3D	Chen-Chen	Strain hardening, brittle failure	-	Extensive of compression model
Haugeneder	3D	Composite	Curve fitted to match tension stiffening effect of reinforcement	?	Reinforcement smeared across elements; isotropic ?
Moussa	2D	Extended compression model	Linear softening	Smeared crack	Non-linear elastic model
Hellmich et al	2D	Tension cut-off	-	-	Drucker-Prager surface up to cut-off

Appendix C Part 3 Parameters for plasticity models

Author	Age	Compressive yield/ ultimate strength	Comp. yield strain %	Comp. ultimate strain %	Tensile ultimate strength	Tensile yield strain %	Tensile ultimate strain %
Meschke / Kropik (1. see below)	t < 8 hours 8 < t < 16 t > 16 hours	-	-	6 – 0.25 0.25 - 0.17 0.17 - 0.20	$0.0067.fcu^{1.09}$ (fcu in kN/cm^2)	-	-
Meschke (ACI)	28 days	0.1 - 0.25	-	-	$0.32.fcu^{0.5}$	-	Softening gradient, Dt = Et/100
Lackner	?	0.4	-	-	$0.3.fcu^{0.67}$	-	-
Hafez	28 days	0.3	-	-	0.1.fcu	Linear up to 0.6 ftu	-
Moussa / Swoboda	28 days ?	0.3	Strain @ peak stress, ε_1 0.3 – 0.5 – 1.0	0.5 – 1.0	$0.21 - 0.3.fcu^{0.67}$	$\varepsilon_{cr} = \varepsilon_1[1-v(1-(f_t/f_c))]$	0.03
Aydan et al	12 hours	-	-	3	-	-	-
BS 8110 Part 1 1997	?	-	$0.24 (fcu)^{0.5}$ (@ peak)	0.35	-	-	-

1.Formulae for strain at compressive failure, $t < 8$ hours, $\varepsilon = 0.06 - [0.0575.t/8]$; $8 < t < 16$, $\varepsilon = 0.0025 - [0.0008.(t-8)/8]$; $t > 16$ hours, $\varepsilon = 0.0017 + [0.003.(t-16)/634]$

Appendix D Nonlinear models for London clay

1 Logarithmic law – Puzrin & Burland 1996

$$\frac{E_{\tan}}{E_{\max}} = 1 - \alpha.[\ln(1+x)]^R - \frac{\alpha.Rx}{(1+x))}[\ln(1+x))]^{R-1}$$

with $$\alpha = \frac{x_L - 1}{x_L[\ln(1+x_L)]^R}$$

and $$R = \frac{(1+x_L).\ln(1+x_L)}{x\ (x_L - 1)}$$

where x is strain and x_L is the ultimate strain . E_{max} = 620 MPa and x_L = 39 for an undrained ultimate deviatoric stress of 372 kPa (see original paper for further details).

2 Power law – Dasari 1996

$$G_{tan} = B.p'^{\,n2}.OCR^{m2}.\varepsilon_q^{\,b2}$$

where , above ε_q= 0.00125%, G_{tan} is the tangent shear modulus, p' is the effective mean stress, OCR is the overconsolidation ratioand ε_q is the deviatoric shear strain with B = 0.828, n2 = 1.0, m2 = 0.2 and b2 = -0.501. Below ε_q= 0.00125%, the value of G_{tan} is the same as at this limiting value.

3 Curve-fitted relationship for a strain-softening plasticity model – Pound 1999

$$cohesion = Cu.\left(1 - \frac{\tau_{mob}}{\left(1+\left(190\varepsilon_{pl}\right)^2 + \left(145\varepsilon_{pl}\right)^{0.56}\right)}\right)$$

where *cohesion* is the value of cohesion in the FLAC strain-softening plasticity Tresca model, *Cu* is the (peak) undrained shear strength and ε_{pl} is the plastic shear strain with τ_{mob} = 0.99.((1-Cu'/*Cu*) and Cu' = the mobilised shear strength, given by the initial insitu stresses.

Appendix E Nonlinear elastic model for sprayed concrete

Part 1

$$G_{\tan} = \frac{G_0}{(1 + (C.d.(\frac{\tau_0}{f_{cyl}})^{d-1}))} \quad (1)$$

$$K_{\tan} = \frac{K_0}{\left(1 + \left(A.b.\left(\frac{\sigma_0}{f_{cyl}}\right)^{b-1}\right) - \left(k.l.m.e\left(\frac{\tau_o}{f_{cyl}}\right)^{n}\right)\right)} \quad (2)$$

where

$$e = \frac{\left(\frac{\sigma_0}{f_{cyl}}\right)^{m-1}}{\left(1 + \left(l.\left(\frac{\sigma_0}{f_{cyl}}\right)^{m}\right)\right)^2} \quad \text{if } \sigma_0 > 0.0, \text{ otherwise e} = 1.0 \quad (3)$$

and

fcyl = the uniaxial compressive cylinder strength in MPa
Gtan = the tangent shear stiffness in MPa
Go = the initial shear stiffness in MPa
Ktan = the tangent bulk stiffness in MPa
Ko = the initial bulk stiffness in MPa
σ_0 = octohedral mean stress in MPa = $(\sigma_1 + \sigma_2 + \sigma_3)/3$
τ_0 = octohedral shear stress in MPa = $\{\sqrt{((\sigma_1-\sigma_2)^2+(\sigma_2-\sigma_3)^2+(\sigma_3-\sigma_1)^2)}\}/3$

If fcyl $\leq$ 31.7 MPa, A = 0.516

Otherwise, $A = \frac{0.516}{\left[1 + 0.0027 \cdot (fcyl - 31.7)^{2.397}\right]}$

b = 2.0 + ($1.81e^{-08}$.($fcyl^{4.461}$))

If fcyl $\leq$ 31.7 MPa, C = 3.573

Otherwise, $C = \frac{3.573}{\left[1 + 0.0134 \cdot (fcyl - 31.7)^{1.414}\right]}$

If fcyl $\leq$ 31.7 MPa, d = 2.12 + (0.0183*fcyl)
Otherwise, d = 2.70

If fcyl $\geq$ 15.0 MPa, $k = \dfrac{4.000}{\left[1+1.087\cdot\left(fcyl-15.0\right)^{0.23}\right]}$

Otherwise k = 4.000

$l = 0.22 + (0.01086*fcyl) - (0.000122*fcyl^2)$

If fcyl $\leq$ 31.7 MPa, m = -2.415
Otherwise, m = -3.531 + (0.0352*fcyl)

If fcyl $\leq$ 31.7 MPa, n = 1.0
Otherwise, n = 0.3124 + (0.0217*fcyl)

Other notes: Kotsovos & Newman's model is formulated in terms of octahedral stresses, normalized by division by the uniaxial cylinder strength of the concrete. For height to diameter ratios of 2.0 to 2.5, the uniaxial cylinder strength is approximately equal to the uniaxial cube strength (Neville 1995); the relationships provided by Kotsovos & Newman for predicting the initial bulk and shear moduli have not been used, since they are valid for mature concrete. The model has also been extended to apply to concrete at strengths of less than 15 MPa.

The model above has been encoded into FISH functions for use in FLAC3D as outlined in Appendix E Parts 2 and 3 – a flowchart showing how the function works and the FISH code respectively.

Appendix E Part 2 FLAC3D FISH routine for nonlinear elastic model for sprayed concrete after Kotsovos & Newman 1978

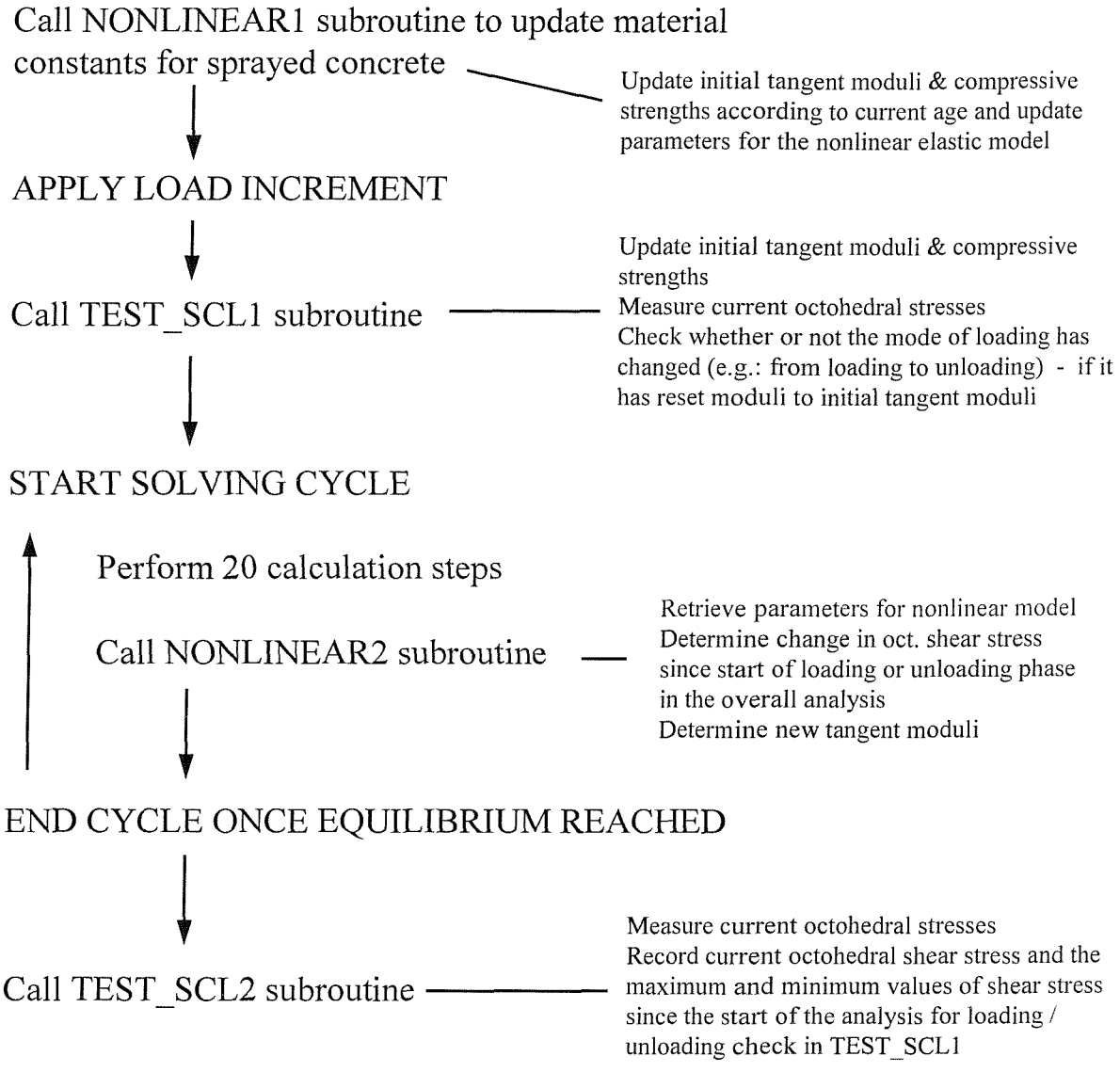

Each subroutine acts on every sprayed concrete zone in turn; all parameters and other variables are stored as zone_extra variables.

Appendix E Part 3 FLAC3D FISH function to model a uniaxial compression test

```
;SECTION 0 - INTRODUCTION
;PROJECT - test for non-linear elastic SCL models

;RUN - SCL AHT model
; 1 zone model, units are m, kN, kPa
; Parameters for Tunnel analyses
; Kotsovos & Newman model as described in BE subtask C2
; no loading/unloading check

; Uniaxial test at age 28 days
; sigma2 = sigma3 = 0.0 kPa
; fcyl = 31.5 MPa
; NB Kotsovos & Newman use fcyl = uni cyl str

new

title 'SCL_NLE_u1'

config zextra 20


def solving
                flimit = 1.0e-4
; NB FLAC does not recalculate elastic constants at every step but
; only at start of cycling
                loop while unbal >= flimit
command
                step 20
endcommand
                nonlinear2      ; to update stiffness values
                endloop

end

;SECTION 1 - MESH GENERATION

;SECTION 1.1 - MESH PART A  100 mm cube
gen zone brick &
                size 1 1 1 &
                p0 0 0 0 p1 0.1 0 0 p2 0 0.1 0 &
                p3 0 0 0.1
```

```
;SECTION 2 - MODEL PROPERTIES
;SECTION 2.0

def moduli_0

                y_mod0 = 18.8e+06
                                ;Eo
                p_ratio_SCL = 0.2
                                ;vo
                s_mod0 = y_mod0  / (2.0 * (1.0 + p_ratio_SCL))
                ;Go
                b_mod0 = y_mod0  / (3.0 * (1.0 - 2.0 * p_ratio_SCL))        ;Ko

if mmt003 = 1
z_extra(pnt,20) = 2             ; for first step - include when new scl zones added
endif
end

def fcyl_str

                fcyl = 31.5
                mmt064 = 1000*fcyl                              ; peak compressive
strength in kPa @ 28 days
end

def oct_stresses

                mmt051 = (z_sig1(pnt) - z_sig2(pnt))^2
                mmt052 = (z_sig2(pnt) - z_sig3(pnt))^2
                mmt053 = (z_sig3(pnt) - z_sig1(pnt))^2

                mmt061 = (sqrt(mmt051 + mmt052 + mmt053))/3
                ; oct shear stress in kPa
                mmt062 = -(z_sig1(pnt) + z_sig2(pnt) + z_sig3(pnt))/3        ; oct
hydrostatic stress in kPa, comp = +ve
                fcyl_str
end
```

```
def test_SCL1

  pnt = zone_head
  loop while pnt # null

                if abs(mmt063) > 0                                        ; for
change in moduli near peak
                        if mmt061 < (0.85*mmt063)  ; value of 0.85
chosen by trial & error
                        z_extra(pnt,19) = 0
                        else
                        z_extra(pnt,19) = 100
                        endif
                endif

                moduli_0
                oct_stresses

                mmt019 = (mmt061-z_extra(pnt,2))              ; current shear stress -
stress at end of last step

                if mmt019 > -0.025*mmt064                     ; if change more than
                z_extra(pnt,20) = 2             ; 2 = Loading

                        if z_extra(pnt,1) < 0                             ; i.e.
if Unloading
                z_prop(pnt, 'shear') = s_mod0                 ; to start first unload
stiffly
                z_prop(pnt, 'bulk') = b_mod0
                        endif

                else

                z_extra(pnt,20) = -2            ; -2 = Unloading

                        if z_extra(pnt,1) > 0                             ; i.e.
if Loading
                z_prop(pnt, 'shear') = s_mod0                 ; to start first unload
stiffly
                z_prop(pnt, 'bulk') = b_mod0
                        endif
                endif

  pnt = z_next(pnt)
 endloop

end
```

```
def test_SCL2
  pnt = zone_head
  loop while pnt # null

                    oct_stresses

                    if z_extra(pnt,20) > 0
                    mmt016 = max(mmt061,z_extra(pnt,4))
                    z_extra(pnt,3) = mmt016                    ;set 3 to max norm. shear
stress during loading
                    else

                              if z_extra(pnt,20) < 0
                    mmt017 = min(mmt061, z_extra(pnt,3))
                    z_extra(pnt,4) = mmt017                    ;set 4 to lowest norm.
shear stress during unload
                              endif

                    endif
                    z_extra(pnt,2) = mmt061                    ;record shear stress at
end of last step
                    mmt068 = z_extra(pnt,20)
                    z_extra(pnt,1) = mmt068                    ;to record change in
loading
    pnt = z_next(pnt)
  endloop
end

def nonlinear1

;constants for K & N model, str in MPa

pnt = zone_head
  loop while pnt # null

                    moduli_0
                    fcyl_str

                    if fcyl > 31.7

                    KN_Aa = 1 + 0.0027*((fcyl - 31.7)^2.397)
                    z_extra(pnt,11) = 0.516 / KN_Aa

                    z_extra(pnt,12) = 2.0 + (1.81e-08*(fcyl^4.461))

                    KN_Ca = 1 + 0.0134*((fcyl - 31.7)^1.414)
                    z_extra(pnt,13) = 3.573 / KN_Ca

                    z_extra(pnt,14) = 2.7

                    KN_ka = 1 + (1.087*(fcyl - 15.0)^0.23)
                    z_extra(pnt,15) = 4.0 / KN_ka
```

```
                z_extra(pnt,16) = 0.22 + (0.01086*fcyl) - (0.000122*fcyl*fcyl)
                z_extra(pnt,17) = -3.531 + (0.0352*fcyl)
                z_extra(pnt,18) = 0.3124 + (0.0217*fcyl)

                else

                z_extra(pnt,11) = 0.516
                z_extra(pnt,12) = 2.0 + (1.81e-08*(fcyl^4.461))
                z_extra(pnt,13) = 3.573
                z_extra(pnt,14) = 2.12 + (0.0183*fcyl)
                                  if fcyl < 15.0
                                  z_extra(pnt,15) = 4.0
                                  else
                                  KN_ka = 1 + (1.087*(fcyl - 15.0)^0.23)
                                  z_extra(pnt,15) = 4.0 / KN_ka
                                  endif
               z_extra(pnt,16) = 0.22 + (0.01086*fcyl) - (0.000122*fcyl*fcyl)
               z_extra(pnt,17) = -2.415
               z_extra(pnt,18) = 1.0

               endif

               pnt = z_next(pnt)
 endloop

end

def nonlinear2

pnt = zone_head
 loop while pnt # null

               KN_A = z_extra(pnt,11)
               KN_b = z_extra(pnt,12)
               KN_C = z_extra(pnt,13)
               KN_d = z_extra(pnt,14)
               KN_k = z_extra(pnt,15)
               KN_l = z_extra(pnt,16)
               KN_m = z_extra(pnt,17)
               KN_n = z_extra(pnt,18)

               moduli_0
               oct_stresses

               if mmt062 < -0.05*mmt064
               mmt062 = -0.05*mmt064
               endif
```

```
KN_Toc = 0.944*(((mmt062/mmt064) + 0.05)^0.724) + 0.001     ; falls to 0.1 % fcyl at
Soct = 0.05 fcyl
KN_Toe = 0.633*(((mmt062/mmt064) + 0.05)^0.857) + 0.001     ; in order to avoid zero
KN_cos0 = -(z_sig1(pnt) + z_sig2(pnt) - 2*z_sig3(pnt))/(3*(sqrt(2))*mmt061)     ; comp =
+ve
mmt054 = 2*KN_Toc*((KN_Toc)^2 - (KN_Toe)^2)*KN_cos0
mmt055 = 4*((KN_Toc)^2 - (KN_Toe)^2)*((KN_cos0)^2) + 5*((KN_Toe)^2) -
4*KN_Toc*KN_Toe
mmt056 = 4*((KN_Toc)^2 - (KN_Toe)^2)*((KN_cos0)^2) + ((KN_Toc - 2*KN_Toe)^2)
mmt063 = mmt064*(mmt054 + (KN_Toc*(2*KN_Toe -
KN_Toc))*sqrt(mmt055))/mmt056                    ; peak oct shear stress
mmt065 = mmt061/mmt063


            if z_extra(pnt,20) > 0                                  ; Masing rule, applied to
shear stress only
            aa = aa + 1                                             ; hydrostatic loading /
unloading ignored
            mmt066 = ((mmt061-z_extra(pnt,4))/mmt064)

            else
                        if z_extra(pnt,20) < 0                                  ;
Unloading
                        bb = bb + 1
                        mmt066 = ((z_extra(pnt,3)-mmt061)/mmt064)
                        endif
            endif


            if z_extra(pnt,19) < 10
                        KN_Gta = (1 + (KN_C*KN_d*((mmt066)^(KN_d - 1))))
                        s_mod = s_mod0 / KN_Gta                         ; Gtan
                        if mmt062 > 0.0
                        KN_Bta = KN_A*KN_b*((mmt062/mmt064)^(KN_b -
1))
                        KN_Btb =
KN_k*((mmt066)^KN_n)*KN_l*KN_m*((mmt062/mmt064)^(KN_m-1))
                        KN_Btc = (1 + (KN_l*((mmt062/mmt064)^KN_m)))^2
                        b_mod = b_mod0 / (1 + KN_Bta - (KN_Btb/KN_Btc))
                        else
                        b_mod = b_mod0*(1+0.67*(mmt062/(0.05*mmt064)))
                        endif
            else
                        if mmt065 < 1.10                                ; to
avoid sudden drop in Gtan
                        mmt067 = 0.5*(cos(4*pi*(mmt065-0.85))+1.2)/2
                        else
                        mmt067 = 0.05
                        endif
```

```
                    s_mod = mmt067*s_mod0 / KN_Gta
; Gtan
                    b_mod = 0.33*b_mod0          ;*(1-0.67*mmt065)
; Gerstle 1981
endif


z_prop(pnt,'shear') = s_mod
z_prop(pnt,'bulk') = b_mod

pnt = z_next(pnt)
endloop

end



;SECTION 2.1 - SPRAYED CONCRETE
;model must be assigned initially , later revised see mmf002 - section 4.1
;must set initial parameters to non-zero arbitrary values

nonlinear1
model elastic
prop bulk = b_mod0 shear = s_mod0



;SECTION 3 - INITIAL CONDITIONS

;SECTION 3.0 - SET-UP

set grav 0 -10 0

;SECTION 3.1 - BOUNDARY FIXITIES
;Frictionless platens
fix z range z -0.001 0.001

;SECTION 4 - ANALYSIS

;SECTION 4.0 - SET-UP
ini xd=0 yd=0 zd=0
ini xv=0 yv=0 zv=0
```

```
;Histories

his unbal                                   ;No.1
pl create unbal
pl current unbal
pl add his 1
pl show unbal

his nstep 10
his gp zd 0.0 0.0 0.1                       ;No.3
his gp yd 0.0 0.0 0.1
his gp xd 0.0 0.0 0.1
his zone szz 0.05 0.05 0.05                 ;No.4

tab 1 name 'Sigma1 vs e1'
tab 2 name 'Sigma1 vs e2'
tab 3 name 'Gtan/Go vs To/fcyl'
tab 4 name 'Ktan/Ko vs So/fcyl'
tab 5 name 'So vs e_vol'
tab 1 era
tab 2 era
tab 3 era
tab 4 era
tab 5 era

;SECTION 4.1 - Loading1

def mmf001      ;loading sequence for series 5
                array loading1(9,2)
                loading1(1,1) = 1
                loading1(1,2) = -5e3
                loading1(2,1) = 2
                loading1(2,2) = -10e3
                loading1(3,1) = 3
                loading1(3,2) = -15e3
                loading1(4,1) = 4
                loading1(4,2) = -20e3
                loading1(5,1) = 5
                loading1(5,2) = -25e3
                loading1(6,1) = 6
                loading1(6,2) = -30e3
                loading1(7,1) = 7
                loading1(7,2) = -31.5e3
                loading1(8,1) = 8
                loading1(8,2) = -30.5e3
                loading1(9,1) = 9
                loading1(9,2) = -31.5e3

end
```

```
def mmf002
                mmt063 = 0      ; initially
                loop mmt003(1,7)
                mmt004 = loading1(mmt003,2)
                nonlinear1                                      ; run at start of every
load step to update constants

command
apply szz = mmt004 range z 0.099 0.101

step 10

test_SCL1       ; to determine Gtan, Ktan
solving
test_SCL2

endcommand

pnt = gp_near(0,0,0.1)
mmt0051 = -gp_zdisp(pnt)*100/0.1            ; in %
izone = z_near(0.05,0.05,0.05)
mmt0061 = -z_szz(izone)                                         ; in kPa
xtable(1,mmt003) = mmt0051
ytable(1,mmt003) = mmt0061

pnt2 = gp_near(0,0.1,0)
mmt0081 = -gp_ydisp(pnt2)*100/0.1           ; in %
xtable(2,mmt003) = mmt0081
ytable(2,mmt003) = mmt0061

xtable(3,mmt003) = mmt061/mmt064
ytable(3,mmt003) = s_mod/s_mod0
xtable(4,mmt003) = mmt062/mmt064
ytable(4,mmt003) = b_mod/b_mod0
xtable(5,mmt003) = z_vsi(izone)
ytable(5,mmt003) = mmt062

                if mmt003 = 7
command
sav SCL_NLE_u1.sav
endcommand
                endif
                endloop
end


mmf001
mmf002
```

```
;
;SECTION 5 - OUTPUTS
;see mmf002 - file saved at penultimate load step
;see section 4.0 - histories write to file creep1.his
;write histories to file

;his write 1 2 3 4 &
;                    begin 1 skip 50 file SCL_NLE_u1.his

pl add tab 1 red both xmin 0.0 ymin 0.0 xmax 0.25
pl add tab 2 green both
;pl add tab 2 green both
pr tab 1 tab 2 aa bb


ret
```

Appendix F Geotechnical models

Model 0 Linear elastic isotropic model

Cu=0.67*(50+(8*depth below surface)) in kPa
(the 0.67 factor is to convert values from laboratory tests to a mass property)
E = 600*Cu in kPa
Equivalent to the stiffness at a deviatoric strain of 0.1 %
ν = 0.49
K = 100*G for undrained case

Sources: Mott MacDonald 1990

Model 1 Linear elastic perfectly plastic isotropic model

Cu, E, ν, K – as per Model 0, for undrained case
Mohr Coulomb (Tresca) yield criterion
Tension limit, dilation and friction for plastic model all set to zero.

Model 2 Linear elastic transversely anisotropic model

Cu – as per Model 0, for undrained case

E_{vu} = 600*Cu (vertical stiffness) in kPa
E_{hu} = 1.6*E_{vu} (stiffness in horizontal plane) in kPa
G_{vh} = 0.433*E_{vu} in kPa

ν_{hh} = 0.20
ν_{vh} = 0.48 (as per Lee & Rowe 1989 for undrained case)

Sources: Van der Berg 2000, Lee & Rowe 1989

Model 3 Nonlinear elastic tranversely anisotropic model

Cu, E_{hu}/E_{vu}, G_{vh}/E_{vu}, ν_{hh}, ν_{vh} – as per Model 2 for undrained case
The overconsolidation ratio, OCR, varies with depth.

If $\varepsilon_{dev} < 1.0e\text{-}05$,
$G_{vh} = 0.828.(OCR)^{0.2}.p'.(0.00001^{-0.501})$ in kPa
If $0.01 > \varepsilon_{dev} > 1.0e\text{-}05$,
$G_{vh} = 0.828.(OCR)^{0.2}.p'.(\varepsilon_{dev}^{-0.501})$ in kPa
If $0.01 < \varepsilon_{dev}$,
G_{vh} = (G_{vh} max)/ 25 in kPa

Masing rules applied for loading, unloading and reloading (see Figure 2.33).
Sources: Dasari 1996

Model 4 Strain-hardening plastic isotropic model

Cu, ν, K as per Model 0 for undrained case

$E = 1500*Cu$ in kPa
Cohesion $= 0.01*Cu$ in kPa
Which initially is increased to $(\sigma_v-\sigma_h)/2$ since $K_0 \neq 1.0$

Cohesion $= Cu*(1.0 - A/B)$ for strain-hardening relationship in kPa
$A = 0.99*(1.0 - ((\sigma_v-\sigma_h)/2)/Cu)$
$B = 1.0 + (190.0* \varepsilon_{dev})^2 + (145.0*\varepsilon_{dev})^{0.56}$

The plasticity model is applied to a region from the surface to 22 m below tunnel axis level, within 22 m of the centreline in the X direction and for 64 m in the Y direction from the start of the tunnel (see Figure 6.3). Outside this area, the model is linear elastic, with a stiffness, $E = 1500*Cu$ in kPa.

Sources: Pound 1999

Model 5 Linear elastic perfectly plastic isotropic model
(high stiffness)

As per Model 4, except that in the plastic region, the yield criterion is based on Cu and the pre-yield behaviour is linear elastic, with $E = 1500*Cu$.

Appendix G Numerical model runs for tunnel excavation

Run	Key feature – see also Chapters 4 & 6
H series	*Exact geometry of HEX Platform tunnels*
H_Et_4	*BASE CASE* – Linear elastic, age-dependent stiffess for lining; ground model 4 = strain-hardening plasticity
H_E-_4	Linear elastic, age-independent stiffness
H_HME_4	Hypothetical Modulus of Elasticity
H_MCSS_4	Strain-hardening plasticity model (Mohr Coulomb)
H_NLE_4	Nonlinear elastic model after Kotsovos & Newman (1978)
H_VE1_4	Visco-elastic "Kelvin" creep model - stress independent
H_VE2_4	Visco-elastic "Kelvin" creep model - stress dependent
H_MC_4_JR	MCSS model but strength reduced by 50% on radial joints
H_MC_4_JL	MCSS model but strength reduced by 50% on longitudinal joints
H_MC_4_J	MCSS model but strength reduced by 50% on radial & long. Joints
H_Et_4_A_0.5	Base case with advance length = 0.5m
H_Et_4_A_2.0	Base case with advance length = 2.0m
H_MC_4_A_2.0	H_MC_4 with advance length = 2.0m
H_Et_4_X_6.0	Base case with average ring closure distance of 6.0m
H_Et_4_X_8.0	Base case with average ring closure distance of 8.0m
H_Et_0	Ground model 0 = linear elastic
H_Et_1	Ground model 1 = linear elastic perfectly plastic – spft
H_Et_2	Ground model 2 = anisotropic linear elastic
H_Et_3	Ground model 3 = nonlinear anisotropic elastic
H_HME_3	As per H_Et_3 with HME lining model
H_Et_5	Ground model 5 = linear elastic perfectly plastic – stiff
H_Et_4_K_1.5	Constant K_0 = 1.50
H_Et_5_K_1.5	Constant K_0 = 1.50
N series	*Circular tunnel with face area equivalent to HEX Platform tunnel*
N_Et_4	Base case – see H_Et_4
N_E-_4	Linear elastic, age-independent stiffness
N_HME_4	Hypothetical Modulus of Elasticity
N_MCSS_4	Strain-hardening plasticity model (Mohr Coulomb)
N_VE2_4	Visco-elastic "Kelvin" creep model - stress dependent
N series*	*Circular tunnel with face area equivalent to HEX Concourse tunnel* *NB: K0, advance rate, advance length & ring closure distance differ from H_Et_4*
N*_Et_4	Base case – see H_Et_4
N*_E-_4	Linear elastic, age-independent stiffness
N*_HME_4	Hypothetical Modulus of Elasticity
N*_MCSS_4	Strain-hardening plasticity model (Mohr Coulomb)
N*_VE1_4	Visco-elastic "Kelvin" creep model - stress independent
N*_VE3_4	Visco-elastic "Kelvin" creep model – after Yin (1996)

N*_Et_4_S_1.2	Base case with advance rate of 1.2 m /day
N*_Et_4_S_0.5	Base case with advance rate of 0.5 m /day
N*_Et_4_X_4.5	Base case with average ring closure distance of 4.5m
N*_Et_0	Ground model 0 = linear elastic
N*_Et_1	Ground model 1 = linear elastic perfectly plastic – spft
N*_Et_2	Ground model 2 = anisotropic linear elastic
N*_Et_3	Ground model 3 = nonlinear anisotropic elastic
N*_Et_5	Ground model 5 = linear elastic perfectly plastic – stiff
N*_Et_4_K	K_0 profile varies with depth

References:

ACI 209R (1992) "Prediction of Creep, Shrinkage and Temperature Effects in Concrete Structures", American Concrete Institute.

ACI 506R-90 (1990) "Guide to Shotcrete", American Concrete Institute.

ACI 506.2 (1995) "Specification for Shotcrete", American Concrete Institute.

Abler, P. (1992) "Einflusse auf das Verformungsverhalten von jungem Spritzbeton im Tunnelbau", Diplomarbeit, University of Innsbruck.

Abu-Krisha (1998) "Numerical modelling of TBM tunnelling in consolidated clay", PhD Thesis, University of Innsbruck.

Addenbrooke, T.I. (1996) "Numerical analysis of tunnelling in stiff clay", PhD Thesis, Imperial College, London.

Aggoun & Torrenti (1996) "Effect of heat on the mechanical behaviour of concrete linings for tunnel", Concrete for Infrastructure and Utilities, Dhir & Henderson (ed.s), pp 161 – 170.

Aldrian, W. (1991) "Beitrag zum Materialverhalten von fruh belastetem Spritzbeton", Diplomarbeit Montanuniversitat Leoben.

Aldrian, W. & Kattinger, A. (1997) "Monitoring of performance of primary support of NATM station at Heathrow Terminal 4", Tunnels for People, (eds) Hinkel, Golser & Schubert, pp 71 – 77.

Alkhiami, H. (1995) "Ein Naherungsverfahren zur Abschatzung der Belastung einer Spritzbetonkalottenschale auf der Grundlage von in-situ-Messungen", PhD Thesis, Hannover University.

Annett, M., Earnshaw, G. & Leggett, M. (1997) "Permanent sprayed concrete tunnel linings at Heathrow Airport", Tunnelling '97, IMM, pp 517 – 534.

Arnold, J. and Neumann, C. (1995) "Umsetzung eines innovativen NOT-Konzeptes im Zuge eines "Know-how-Transfers"", Felsbau Vol. 13 No. 6, pp 459 - 463.

Atkinson, J.H. (2000) "Non-linear soil stiffness in routine design", Geotechnique, Vol. 50 No. 5, pp 487 – 508.

Atzwanger, R. (1999) " Die Sulfatbestandigkeit alkalifrei beschleunigter Spritzbetone", Diplomarbeit, University Of Innsbruck.

Audsley, R.C., Favaloro, G. & Powell, D.B. (1999) "Design and implementation of the Heathrow Express Headshunt", Tunnel Construction & Piling '99, IMM, pp 382 – 398.

Austin, S.A. & Robins, P.J. (1995) "Sprayed concrete: Properties, design and application", Whittles Publishing, Latheronwheel.

Austin, S.A., Robins P.J. & Peaston C.H. (1998) "Effects of silica fume on dry-process sprayed concrete", Magazine of Concrete Research, Vol. 58, March No. 1, pp 25 - 36.

Austin, S.A., Robins, P.J. & Goodier, C.I. (2000) "Construction and repair with wet-process sprayed concrete and mortar", The Concrete Society Technical Report 56 (Draft).

Aydan, O., Sezaki, M. & Kawamoto, T. (1992a) "Mechanical and numerical modelling of shotcrete", Numerical models in geomechanics (ed.s Pande Pietruszczak), pp 757 – 764.

Aydan, O., Sezaki, M., Kawata, T., Swoboda G. & Moussa, A. (1992b) "Numerical modelling for the representation of shotcrete hardening and face advance of tunnels excavated by bench excavation method", Numerical models in geomechanics (ed.s Pande Pietruszczak), pp 707 – 716.

BS8110 Part 1 (1997) "Structural use of concrete – Code of practice for design and construction", British Standards Institution, London.

BS8110 Part 2 (1985) "Structural use of concrete – Code of practice for special circumstances", British Standards Institution, London.

Barratt, D.A., O'Reilly, M.P. & Temporal, J. (1994) "Long-term measurements of loads on tunnel linings in overconsolidated clay", Tunnelling '94, IMM, pp 469 – 481.

Barrett, S.V.L. & McCreath, D.R. (1995) "Shotcrete support design in blocky ground: towards a deterministic approach", Tunnelling and Underground Space Technology, Vol. 10, No. 1, pp 79 - 89.

Barton, N., Lien, R. & Lunde J. (1975) "Estimation of support requirements for underground excavations", ASCE Proc. of 16th Symposium on Rock Mechanics, pp 163 - 177.

Bernard, E.S. & Clements, M.J.K. (2001) "The influence of curing on the performance of fibre reinforced shotcrete panels", Engineering Developments in Shotcrete, pp 59 – 63.

Berwanger, W. (1986) "Dreidimensionale Berechnung von tiefliegenden Felstunneln unter Berucksichtigung des rheologischen Verhaltens von Spritzbeton und des Bauverfahrens", Forschungsergebnisse aus dem Tunnel- und Kavernenbau, University of Hannover, Vol. 10.

Bieniawski, Z.T. (1984) "Rockmechanics Design in Mining and Tunneling", Balkema, Rotterdam.

Blasen, A. (1998) "Bestimmung von Porositätskennwerten am Spritzbeton und deren Einfluss auf betontechnologische Parameter", Diplomarbeit, University of Innsbruck.

Bolton, A. (1999) "Mont Blanc: The Aftermath", New Civil Engineer, 15 April 1999, pp 18 – 20.

Bolton, A. & Jones, M. (1999) "Second road tunnel tragedy heightens safety fears", New Civil Engineer, 3 June 1999, pp 3.

Bolton, M.D., Dasari, G.R. & Rawlings, C.G. (1996) "Numerical modelling of a NATM tunnel construction in London Clay", Geotechnical Aspects of Underground Construction in Soft Ground (ed.s Mair & Taylor), pp 491 - 496.

Bonapace, P. (1997) "Evaluation of stress measurements in NATM tunnels at the Jubilee Line Extension Project", Tunnels for People, eds Hinkel, Golser & Schubert, pp 325 - 330.

Bond, A.J. & MacLeod, 1. A. (2001) "A strategy for computer modelling in geotechnical design", Proc Instn Civ Eng Geotech Engng, Vol. 149, No. 2, pp 95 – 102.

Bowers, K.H, Hiller, D.M. & New, B.M. (1996) "Ground movement over 3 years at the Heathrow Express Trial Tunnel", Geotechnical Aspects of Underground Construction in Soft Ground (ed.s Mair & Taylor), pp 647 - 652.

Bowers, K.H. & Redgers, J.D. (1996) "Discussion: Observations of lining load in a London clay tunnel", Geotechnical Aspects of Underground Construction in Soft Ground (ed.s Mair & Taylor), pp 335.

Blasen, A. (1998) "Bestimmung von Porositatskennwerten am Spritzbeton und deren Einfluss auf betontechnologische Parameter", Diplomarbeit, University Of Innsbruck.

Brite Euram B6 (1997) "Evaluation of mechanical and physical properties", BRE-CT92-0231, Imperial College, London & Institute of Mechanics of Materials and Geostructures.

Brite Euram C1 (1997) "Sub Task C1: Development of time-dependent mathematical model", BRE-CT92-0231, Institute of Mechanics of Materials and Geostructures.

Brite Euram C2 (1997) "Sub Task C2: Collapse limit-state model", BRE-CT92-0231, Imperial College, London.

Brite Euram D1 (1997) "Sub-Task D1: Structural Design Guidelines", BRE-CT92-0231 (MM ref: 06460/D01/A), Mott MacDonald Ltd.

Brite Euram (1998) "New materials, Design and Construction Techniques for Underground Structures in Soft Rock and Clay Media", BRE-CT92-0231 Final Technical Report, Mott MacDonald Ltd.

Brooks, J. (1999) "Shotcrete for ground support as used in the Asia Pacific region", RETC Proceedings, pp 473 - 524, 1999.

Brown, E.T. (1981) "Putting the NATM into perspective", Tunnels & Tunnelling, November 1981, pp 13 - 17.

BTS (2003) "UK EPBM collapse comparisons", British Tunnelling Society in Tunnels & Tunnelling International, March 2003, pp 25 – 26.

BTS (2004) "Tunnel lining design guide", British Tunnelling Society, Thomas Telford, in print.

BTS/ABI (2002) "Insuring an industry", British Tunnelling Society in Tunnels & Tunnelling International, October 2002, pp 44 – 47.

Burd, H.J. Houlsby, G.T., Augarde, C.E. & Liu, G. (2000) "Modelling tunnelling-induced settlement of masonry buildings", Proc. Instn. Civ. Engng. Vol. 143, January, pp 17 – 29.

Burland, J.B., Simpson, B. & St John, H.D. (1979) "Movements around excavations in London Clay", Design Parameters in geotechnical engineering, British Geotechnical Society, London, Vol. 1, pp 13 – 29.

Byfors, J. (1980) "Plain concrete at early ages", Research Report, Swedish Cement & Concrete Research Institute, Dept. of Building, Royal Institute of Technology Stockholm.

Celestino, T.B., Bortolucci, A.A., Re, G. & Ferreira, A.A.(1999) "Diametral compression tests for the determination of shotcrete anisotropic elastic constants", Shotcrete for Underground VIII, Sao Paulo.

Cervera, M., Oliver, J. & Prato, T. (1999a) "Thermo-Chemo-Mechanical Model for Concrete. I: Hydration and Aging", Journal of Engineering Mechanics ASCE, Sept., pp 1018 – 1027.

Cervera, M., Oliver, J. & Prato, T. (1999b) "Thermo-Chemo-Mechanical Model for Concrete. II: Damage and Creep", Journal of Engineering Mechanics ASCE, Sept., pp 1028 – 1039.

Chan, A., Sharpe, L., Chapman, D., Cooper, M. & Rogers, C. (2000) "Numerical modelling of volume loss for tunnel excavation", Conf. Of Assoc. for Computational Mechanics in Engineering, Cross (ed), pp 190 – 193.

Chang, Y. (1994) "Tunnel support with shotcrete in weak rock - a rock mechanics study", PhD Thesis, Royal Inst. Of Tech. Stockholm.

Chang, Y. & Stille, H. (1993) "Influence of early-age properties of shotcrete on tunnel construction sequences", Shotcrete for Underground Support VI, pp 110 – 117.

Chen, W.F. (1982) "Plasticity in reinforced concrete", McGraw-Hill, Inc., New York.

Choi, S., Thienel, K.-C. & Shah, S.P. (1996) "Strain softening of concrete in compression under different end conditions", Magazine of Concrete Research, Vol. 48, Issue 175, pp 103 – 115.

Clayton, C.R.I., Hope, V.S., Heyman, G., van der Berg, J.P., & Bica, A.V.D. (2000) "Instrumentation for monitoring sprayed concrete lined soft ground tunnels", Proc Instn Civ Eng Geotech Engng, Vol. 143, July, pp 119 – 130.

Clayton, C.R.I. & Heyman, G. (2001) "Stiffness of geomaterials at very small strains", Geotechnique 51, No. 3, pp 245 - 255.

Clayton, C.R.I., van der Berg, J.P., Heyman, G., Bica, A.V.D. & Hope, V.S. (2002) "The performance of pressure cells for sprayed concrete tunnel linings", Geotechnique 52, No. 2, pp 107 - 115.

Coetzee, M.J., Hart, R.D., Varona, P.M. & Cundall, P.A. (1998) "FLAC Basics", Itasca Consulting Group, Minnesota.

Concrete Society (1988) "Permeability testing of site concrete: a review of methods and experience", Technical Report 31, The Concrete Society.

Concrete Society (2001) "Construction and repair with wet-process sprayed concrete and mortar", Austin, Robins & Goodier (eds), Technical Report 56, The Concrete Society (draft).

Cooper, M.L. & Chapman, D.N. (1998) "Movement of the Piccadilly Line Tunnels caused by the new Heathrow Express Tunnels", Tunnels and Metropolises (Negro Jr & Ferreira ed.s), pp 249 – 254.

Cornejo-Malm G. (1995) "Schwinden von Spritzbeton", Internal Report, ETH Zurich.

Cosciotti L., Lembo-Fazio A., Boldini D., Graziani A. (2001) "Simplified Behavior Models of Tunnel Faces Supported by Shotcrete and Bolts", Proc. of the International Conference on Modern Tunneling Science and Technology (IS-Kyoto 2001), Adachi et al. eds, Kyoto, vol.1, 407-412.

Curtis, D.J. (1976) "Discussions on Muir-Wood, The circular tunnel in elastic ground", Geotechnique, Vol. 26, No. 1, pp 231 - 237.

DBV (1992) " Design basis for steel fibre reinforced concrete in tunnel construction", Code of Practice, Deutscher Beton Verein.

DIN 1045 (1988) "Structural use of concrete. Design and construction." Deutsches Institut für Normung, e.V..

DIN 18551 (1992) "Sprayed concrete: Production and inspection", Deutsches Institut für Normung, e.V..

D'Aloia & Clement (1999) "Meeting compressive strength requirements at early age by using numerical tools - determination of apparent activation energy of concrete", Modern Concrete Materials: Binders, Additions and Admixtures (ed.s Dhir & Dyer), pp 637 – 652.

Darby, A. & Leggett, M. (1997) "Use of shotcrete as the permanent lining of tunnels in soft ground", Mott MacDonald Milne Award submission (unpublished).

Dasari, G.R. (1996) "Modelling the variation of soil stiffness during sequential construction", PhD Thesis, University of Cambridge.

Dawes, A., Grose, B., Eddie, C. & Willows, K. (1997) "Heathrow transfer baggage system - Phase 2", Tunnels & Tunnelling International, July 1997, pp 40 – 41.

Davik, K. & Markey, I. (1997) "Durability of sprayed concrete in Norwegian road tunnels", Tunnelling '97, IMM pp 251 - 261.

Deane, A.P. & Bassett, R.H. (1995) "The Heathrow Express Trial Tunnel", Proceedings Institution of Civil Engineers, Geotechnical Engineering, Vol. 113, pp 144 - 156.

Deane, A.P. (1997) - personal communication.

Ding, Y. (1998) "Technologische Eigenschaften von jungem Stahlfaserbeton und Stahlfaserspritzbeton", PhD Thesis, University of Innsbruck.

Douglas, T.H., Richards, L.R. & Arthur, L.J. (1979) "Dinorwic Power Station Rock support of the underground caverns", Proc. 4th Congress Int. Society for Rock Mechanics, Vol. 1, pp 361 – 369.

Douglas, T.H. & Keeble, S. (1990) "Design and construction of a new service tunnel at Edinburgh Castle", Tunnel Construction '90, IMM, pp 9 - 13.

Duddeck, H. & Erdmann, J. (1985) "On structural design models for tunnels in soft soil", Underground Space, Vol. 9, pp 246 - 259.

EFNARC (1996) "European Specification for Sprayed Concrete", European Federation of Producers and Applicators of Specialist Products for Structures.

Eberhardsteiner, J., Meschke G. & Mang H.A. (1987) "Comparison of constitutive models for triaxially loaded concrete", Computational mechanics of concrete structures - advances and applications, colloquium in Delft, pp 197 – 208.

Eierle, B. & Schikora, K. (1999) "Computational Modelling of Concrete at Early Ages", Diana World 2/99.

Einstein, H. H. & Schwartz, C. W. (1979) "Simplified Analysis for Tunnel Supports", Journal of Geotechnical Engineers Division, ASCE 105 GT4, pp 499 - 518.

Eisenstein, Z., Kuwajima, F.M. & Heinz H.K. (1991) "Behaviour of shotcrete tunnel linings", RETC Proceedings, pp 47 – 57.

England, G.L. & Illston, J.M. (1965) "Methods of Computing Stress in Concrete from a History of Measured Strain Parts 1, 2 & 3", Civil Engineering and Public Works Review, Issues April (pp 513 – 517), May (pp 692 - 694) & June (pp 846 – 847).

Feenstra P H & de Borst (1993) "Aspects of robust computational models for plain and reinforced concrete", Heron Vol. 48, Issue 4, pp 5 – 73.

Fischnaller, G. (1992) "Untersuchungen zum Verformungsverhalten von jungem Sprtizbeton im Tunnelbau: Grundlagen und Versuche", Diplomarbeit, University Of Innsbruck.

Gerstle, K.H. (1981) "Simple formulation of biaxial concrete behaviour", American Concrete Institute Journal, Vol. 78 , No. 1, pp 62 – 68.

Golser, H. (1999) "Application of numerical simulation methods on site", Felsbau, 17 Nr 1, pp 21 – 25.

Golser, J. (1999) "Behaviour of early-age shotcrete", Shotcrete for Underground VIII, Sao Paulo.

Golser, J. & Kienberger, G. (1997) "Permanente Tunnelauskleidung in Spritzbeton - Beanspruchung und Sicherheitsfragen", Felsbau, Issue 6, pp 416 – 421.

Golser, J., Schubert, P. & Rabensteiner, K. (1989) "A new concept for evaluation of loading in shotcrete linings", Proc. Int. Congress on Progress and Innovation in Tunnelling, pp 79 – 85.

Gourvenec, S.M., Bolton, M.D., Soga, K., Gui, M.W., Mair, R.J., Edmonds, H., Chudleigh, I.J.L. & Bulter, A.P. (1999) "Field investigations of long term ground loading on an old tunnel in London Clay", Geotechnical Aspects of Underground Construction in Soft Ground (ed.s Kusakabe, Fujita & Miyazaki), pp 219 - 224.

Grose, W.J. & Eddie, C.M. (1996) "Geotechnical aspects of the construction of the Heathrow Transfer Baggage System tunnel", Geotechnical Aspects of Underground Construction in Soft Ground (ed.s Mair & Taylor), pp 269 – 276.

Groves, P.N. & Morgan, S.R. (1997) "Engineering consequences of ground conditions on NATM works at London Bridge Station, Jubilee Line Extension", Tunnelling '97, pp 677 – 692.

Guilloux, A., le Bissonnais, H., Robert, J. & Bernardet, A. (1998) "Influence of the K_0 coefficient on the design of tunnels in hard soils", Tunnels and Metropolises (Negro Jr & Ferreira ed.s), pp 387 – 392.

Gunn, M.J. (1993) "The prediction of surface settlement profiles due to tunnelling", Predictive Soil Mechanics, Thomas Telford, London.

HSE (1996) "Safety of New Austrian Tunnelling Method (NATM) Tunnels", Health & Safety Executive, HMSO, Norwich.

HSE (2000) "The collapse of NATM tunnels at Heathrow Airport", HSE Books, HMSO, Norwich.

Hafez, N. M. (1995) "Post-failure modelling of three-dimensional shotcrete lining for tunnelling", PhD thesis, University of Innsbruck.

Han, N. (1995) "Creep of high strength concrete", Progress in Concrete Research, Vol. 4, pp 107-118.

Hannant, D.J., Branch, J. & Mulheron, M. (1999) "Equipment for tensile testing of fresh concrete", Magazine of Concrete Research, 51, 4 August, pp 263 – 267.

Harris, D.I., Pooley, A.J., Menkiti, C.O. & Stephenson, J.A. (1996) "Construction of low-level tunnels below Waterloo Station with compensation grouting for the Jubilee Line Extension", Geotechnical Aspects of Underground Construction in Soft Ground (ed.s Mair & Taylor).

Harrison, E. (1995) "An assessment of the design procedure for the Jubilee Line Extension shotcrete tunnels at London Bridge", MSc Dissertation, Imperial College, London.

Haugeneder, E., Mang, H., Chen, Z.S., Heinrich, R., Hofstetter, G., Li, Z.K., Mehl, M. & Torzicky, P., (1990) "3D Berechnungen von Tunnelschalen aus Stahlbeton", Strassenforschung Heft 382, Vienna.

Hefti, R. (1988) "Einfluss der Nachbehandlung auf die Spritzbetonqualität", Research report from ETH Zurich.

Hellmich, C., Mang, H.A., Schon, E. & Friedle, R. (1999a) "Materialmodellierung von Spritzbeton - vom Experiment zum konstitutiven Gesetz", report of internal seminar, TU Wien.

Hellmich, C., Ulm, F-J. & Mang, H.A. (1999b) "Multisurface Chemoplasticity. I: Material Model for Shotcrete", ASCE Journal of Engineering Mechanics, June, pp 692 – 701.

Hellmich, C., Ulm, F-J. & Mang, H.A. (1999c) "Multisurface Chemoplasticity. II: Numerical Studies on NATM Tunneling", ASCE Journal of Engineering Mechanics, June, pp 702 – 713.

Hellmich, C. & Mang H. A. (1999) "Influence of the Dilatation of Soil and Shotcrete on the Load Bearing Behaviour of NATM-Tunnels, Felsbau Vol. 17 Nr 1, pp 35 – 43.

Hellmich, C., Sercombe, J., Ulm, F-J. & Mang H. (2000) "Modeling of early-age creep of shotcrete. II: Application to Tunneling", Journal of Engineering Mechanics, Vol. 126 Issue 3, pp 292 – 299.

Hirschbock U. (1997) "2D FE Untersuchungen zur Neuen Österreichischen Tunnelbaumethode", Diplomarbeit, TU Wien.

Hobson, D.A. & Gilchrist, D.C. (1994) "Shotcrete in the construction of Pen-Y-Clip tunnel, North Wales", Tunnelling ' 94, IMM, pp 513 - 529.

Hoek, E., Kaiser, P.K. & Bawden, W.F. (1998) "Support of Underground Excavations in Hard Rock", Rotterdam, Balkema.

Hofstetter, G., Oettl, G. & Stark, R (1999) "Development of a Three-Phase Soil Model for the Simulation of Tunnelling under Compressed Air", Felsbau, Vol. 17, No. 1, pp 26 – 31.

Hrstka, O., Cerny, R. & Rovnanikova, P. (1999), "Hygrothermal stress induced problems in large scale sprayed concrete structures", Specialist techniques & materials for concrete construction, pp 103 – 109.

Huang, Z. (1991) "Beanspruchungen des Tunnelbaus bei zeitabhangigem Materialverhalten von Beton und Gebirge", Inst. Für Statik Report No. 91 - 68, TU Braunschweig.

Huber, H. G. (1991) "Untersuchungen zum Verformungsverhalten von jungem Spritzbeton im Tunnelbau", Diplomarbeit, University of Innsbruck.

Hughes, T.G. (1996) " Flat Jack Investigation of Heathrow Terminal 4 Concourse Tunnel", Report for the University of Surrey by University of Wales, Cardiff.

ICE (1996) "Sprayed Concrete Linings (NATM) for tunnels in soft ground", Institution of Civil Engineers design and practice guides, Thomas Telford, London.

Itasca (1997) "FLAC 3D User's Manual", Itasca Consulting Group, Minnesota.

Itasca (1998) "FLAC User's Manual", Itasca Consulting Group, Minnesota.

Jaeger, J. C. & Cook, N. G. W. (1979) "Fundamentals of rock mechanics", Chapman and Hall, London.

Jardine, R.J., Potts, D.M., Fourie, A.B. & Burland, J.B. (1986) "Studies of the influence of non-linear stress-strain characteristics in soil-structure interaction", Geotechnique 36, No. 3, pp 377 – 396.

John, M. & Crighton, G.S. (1990) "Monitoring and interpreting of results of geotechnical measurements for NATM linings design for the Channel Tunnel", Geotechnical instrumentation in practice, Thomas Telford, pp 517 – 534.

Kambo, G. S. (1997) "An investigation into the pore pressure changes due to tunnelling and grouting in stiff clay", MSc Dissertation, Imperial College, London.

Kammerer, G. & Semprich, S. (1999) "The prediction of the air loss in tunnelling under compressed air", Felsbau 17, No. 1, pp 32 – 35.

Kimmance, J.P. & Allen, R. (1996) "NATM and compensation grouting trial at Redcross Way", Geotechnical Aspects of Underground Construction in Soft Ground (ed.s Mair & Taylor).

Kompen, R. (1990) "Wet process steel fibre reinforced shotcrete for rock support and fire protection, Norwegian practice and experiences", Spritzbeton Technologie '90, pp 87 - 92.

Kotsovos, M.D. & Newman, J.B. (1978) "Generalized stress-strain relations for concrete", Journal of Engineering Mechanics Division, ASCE, Vol. 104, EM4, pp 845 – 856.

Kovari, K. (1994) "On the existence of the NATM: erroneous concepts behind the New Austrian Tunnelling Method", Tunnels & Tunnelling, November, pp 38 - 42.

Krenn, F. (1999) "Small strain stiffness and its influence on the pattern of ground behaviour around a tunnel", Diplomarbeit, TU Graz.

Kritischke, A. (1987) "Pneumatically places shotcrete used for the construction of the Munich Underground", Spritzbeton Technologie ' 87, pp 17 – 25.

Kropik, C. (1994) "Three-Dimensional Elasto-Viscoplastic Finite Element Analysis of Deformations and Stresses Resulting from the Excavation of Shallow Tunnels", PhD Thesis, TU Wien.

Kullaa J. (1997) "Finite element modelling fibre-reinforced brittle materials", Heron, Vol. 42, No. 2, pp 75 – 95.

Kusterle, W. (1992) "Qualitatsverbesserungen beim Spritzbeton durch technologische Massnahmen, durch den Einsatz neuer Materialien und auf Grund der Erfassung von Spritzbetoneigenschaften", Habilationsschrift, Vol. 1 & 2, University of Innsbruck

Kuwajima, F.M. (1999) "Early age properties of the shotcrete", Shotcrete for Underground VIII, Sao Paulo.

Laabmayr, F, (1976) "Soft ground tunnel for the Munich metro", Shotcrete for Ground Support, ASCE, pp 352 – 372.

Lackner, R. (1995) "Ein anisotropes Werkstoffmodell fur Beton auf der Grundlage der Plastitatstheorie und der Schadigungstheorie", Diplomarbeit, TU Wien.

Lake, L. (1990) "Tunnelling in chalk", Tunnel Construction '90, IMM, pp 53 – 61.

Leca, E. (1996) "Modelling and prediction for bored tunnels", Geotechnical Aspects of Underground Construction in Soft Ground (ed.s Mair & Taylor), pp 27 - 41.

Lee, G.T.K. & Ng, C.W.W. (2002) "Three-dimensional analysis of ground settlements due to tunnelling: Role of K_0 and stiffness anisotropy", Geotechnical Aspects of Underground Construction in Soft Ground, 3rd International Symposium, ISSMGE, 6th Session, pp 19 - 24.

Lee, K. M. & Rowe, R. K. (1989) "Deformations caused by surface loading and tunnelling: the role of elastic anisotropy", Geotechnique, Vol. 39, Issue 1, pp 125 - 140.

Lukas, W., Huber, H., Kusterle, W., Pichler, W., Testor, M. & Saxer, A. (1998) "Bewertung von neuentwickelten Spritzbetonverfahrenstechniken", Strassenforschung Heft 474, Vienna.

Macklin, S.R. (1999) "The prediction of volume loss due to tunnelling in overconsolidated clay based on heading geometry and stability number", Ground engineering, April, pp 30 – 34.

Mair, R.J. (1998) "Geotechnical aspects of design criteria for bored tunnelling in soft ground", Tunnels & Metropolises, Negro (Jr) & Ferreira (eds), pp 183 - 199.

Mair, R.J. & Taylor, R.N. (1993) "Prediction of clay behaviour around tunnels using plasticity solutions", Predictive Soil Mechanics, Thomas Telford, London, pp 449 – 463.

Malmberg, B. (1993) " Shotcrete for Rock Support: a Summary Report on the State of the Art in 15 Countries", ITA report, Tunnelling and Underground Space Technology, Vol. 8, No. 4, pp 441 - 270.

Martin, C.J.H. & Pakes, G. (1994) "Tunnelling on the Penzance and St Ives sewerage scheme, Cornwall, England", Tunnelling '94, IMM, pp 147 - 160.

Mayne, P.W. & Kulhawy, F.H. (1982) "K0-OCR relationships in soil", ASCE GT6, 108, June, pp 851 – 872.

Melbye, T. A. (1994) "Shotcrete for rock support", MBT, Treviso.

Meschke, G. (1994) "A multisurface viscoplastic model for shotcrete. Algorithmic aspects and finite element analyses of tunnel linings", Proc. Int. Conf. On Computational Modelling of Concrete Structures, H. Mang, R .de Borst & N. Bicanic (eds), pp 243 - 253.

Meschke, G. (1996) "Elasto-viskoplastische Stoffmodelle fur numerische Simulationen mittels der Methode der Finiten Elemente", Habilitationsschrift, TU Wien.

Michelis, P. (1987) "True triaxial cyclic behaviour of concrete and rock in compression", International Journal of Plasticity, Vol. 3, pp 249 – 270.

Minh, N.A. (1999) "The investigation of geotechnical behaviour near excavated tunnel face by means of three-dimensional stress-flow coupled analysis", MEng Dissertation, Asian Institute of Technology, Bangkok.

Mott MacDonald (1990) "Heathrow Express Rail Link – Geotechnical Design Parameter Report", MMC/01/23/R/1508, December 1990.

Mott MacDonald (1998) Compilation of internal reports on field measurements from HEX project, A.H. Thomas (ed.), (unpublished).

Mott MacDonald (2002) "Investigation of the Lasershell Method", T5-RY-CR-C1-29X-RX-00003 version 1.1, Heathrow Terminal 5 Project report, (unpublished).

Moussa, A. M. (1993) "Finite Element Modelling Of Shotcrete In Tunnelling", PhD thesis, University of Innsbruck

Mosser, A. (1993) "Numerische Implementierung eines zeitabhangigen Materialgesetzes fur jungen Spritzbeton in Abaqus", Diplomarbeit Montanuniversitat Leoben.

Muir Wood, A.M. (1975) "The circular tunnel in elastic ground", Geotechnique, Vol. 25, No. 1, pp 115 – 127.

NAFEMS (1993) "Quality System Supplement to ISO 9001 Relating to Finite Element Analysis in the Design and Validation of Engineering Products", NAFEMS, Issue 1.3, 1993.

NCA (1993) "Sprayed concrete for rock support", Publication No. 7, Norwegian Concrete Association.

Negro, A., Kochen, R., Goncalves, G.G., Martins, R.M. & Pinto, G.M.P. (1998) "Prediction and measurement of stresses in sprayed concrete lining (Brasilia South Wing tunnels)", Tunnels and Metropolises, Negro Jr & Ferreira (eds), pp 405 – 410.

Neville, A. M. (1995) "Properties of concrete", Addison Wesley Longman Ltd, Harlow.

Neville, A. M., Dilger, W. H. & Brooks, J. J. (1983) "Creep of plain & structural concrete", Construction Press (Longman), Harlow.

New, B. M. & Bowers, K.H. (1994) "Ground movement model validation at the Heathrow Express trial tunnel", Tunnelling '94, IMM, pp 301 – 329.

Nordstrom, E. (2001) "Durability of steel fibre reinforced shotcrete with regard to corrosion", Shotcrete: Engineering Developments, Bernard (ed), pp 213 - 217.

Norris, P. (1999) "Setting the ground rules for wet-mix sprayed concrete", Concrete, May 1999, pp 16 – 20.

Norris, P. & Powell, D. (1999) "Towards quantification of the engineering properties of steel fibre reinforced sprayed concrete", 3rd Int. Symp. on Sprayed Concrete, Gol, Norway.

ÖBV (1990) "Guideline on Shotcrete Part 1 - Application", Österreichischer Beton Verein.

Oberdörfer, W. (1996) "Auswirkung von unterschiedlichen Betonnachbehandlungs-massnahmen auf die Qualitat des Nassspritzbetons", Diplomarbeit, University of Innsbruck.

Oettl G. (1997) "Vergeleiche von ausgewählten elasto-plastischen Materialmodellen auf der Grundlage zweidimensionaler Tunnelberechnungen mit der FEM", Diplomarbeit, University of Innsbruck.

Oettl, G., Stark, R.F. & Hofstetter, G. (1998) "A comparison of elastic-plastic soil models for 2D FE analyses of tunnelling", Computers and Geomechanics, Vol. 23, pp 19 - 38.

Owen, D.J.R. & Hinton, E. (1980) "Finite Elements in Plasticity: theory and practice", Pineridge Press Ltd, Swansea.

Palermo, G. & Helene, P.R.d.L. (1998) "Shotcrete as a final lining for tunnels", Tunnels and Metropolises, Negro Jr & Ferreira (ed.s), pp 349 - 354.

Panet, M. (1979) "Time-dependent deformations in underground works", Proc. 4th ISRM Congress, Montreux, Vol. 3, pp 279 – 289.

Panet, M. & Guenot, A. (1982) "Analysis of convergence behind the face of a tunnel", Tunnelling '82, IMM, pp 197 - 204.

Peck, R. B., Hendron, A. J., & Mohraz, B. (1972) "State of the art in soft ground tunnelling". Proceedings of the Rapid Excavation and Tunneling Conference, American Institute of Mining, Metallurgical, and Petroleum Engineers, New York, pp 259-286.

Peila, D., Pelizza, S. & Oreste, D.D. (1998) "Time factor in shotcrete lining design", Tunnels and Metropolises, Negro Jr & Ferreira (ed.s), pp 343 – 348.

Penny, C., Stewart, J., Jobling, P.W. & John, M. (1990) "Castle Hill NATM tunnels: design and construction", Tunnelling '92, IMM, pp 285 - 297.

Pichler, P. (1994) "Untersuchungen zum Materialverhalten und Uberprufungen vom Rechenmodellen fur die Simulation des Spritzbetons in Finite-Elemente-Berechnungen", Diplomarbeit Montanuniversitat Leoben.

Podjadtke, R. (1998) "Bearing capacity and sprayed-in-behaviour of the star profile compared to other lining profiles", Tunnel, Vol. 2, 1998, pp 46 – 51.

Pöttler, R. (1985) "Evaluating the stresses acting on the shotcrete in rock cavity constructions with the Hypothetical Modulus of Elasticity", Felsbau, Vol. 3, No. 3, pp 136 - 139.

Pöttler, R. (1990) "Green shotcrete in tunnelling: stiffness - strength - deformation", Shotcrete for Underground Support VI, pp 83 - 91.

Pöttler, R. (1993) "To the limits of shotcrete linings", Spritzbeton Technologie 3rd International Conference, pp 117 - 128.

Potts, D. M. & Zdravkovic, L. (1999) "Finite element analysis in geotechnical engineering: Theory", Thomas Telford, London.

Pound, C. (1999) - personal communication.

Pound, C. & Beveridge, J.P. (2001) "Prediction of ground movements due to NATM tunnelling", FLAC and Numerical Modeling in Geomechanics, Billaux et al. (eds), Swets & Zeitlinger, pp 391 –398.

Powell, D.B., Sigl, O. & Beveridge, J.P. (1997) "Heathrow Express - design and performance of platform tunnels at Terminal 4", Tunnelling '97, IMM, pp 565 –593.

Powers, T .C. (1959) "Causes and Control of Volume Change", Journal of the PCA Research & Development Laboratories, January, pp 30 – 39.

Probst, B. (1999) "Entwicklung einer Langzeitdruckversuchsanlage fur den Baustellenbetrieb zur Bestimmung des Materialverhaltens von jungenm Spritzbeton", Diplomarbeit, Montanuniversitat Leoben.

Puzrin, A.M. & Burland, J.B. (1998) "Nonlinear model of small strain behaviour of soils", Geotechnique, Vol. 46, No. 1, pp 157 – 164.

Purrer, W. (1990) "Spritzbeton in den NOT-Abschnitten des Kanaltunnels", Spritzbeton Technologie '90, IMM, pp 67 – 78.

Rabcewicz, L. v. (1969) "Stability of tunnels under rock load Part 2", Water Power, July, pp 266 – 273.

Rathmair, F. (1997) "Numerische Simulation des Langzeitverhaltens von Spritzbeton und Salzgestein mit der im FE Program Abaqus implementierten Routine", Diplomarbeit Montanuniversitat Leoben.

Rokahr, R.B. & Lux, K.H. (1987) "Einfluss des rheologischen Verhaltens des Spritzbetons auf den Ausbauwiderstand", Felsbau, Vol. 5 Nr 1, pp 11 - 18.

Rokahr, R.B. & Zachow, R. (1997) "Ein neues Verfahren zur taglichen Kontrolle der Auslastung einer Spritzbetonschale", Felsbau, Vol. 15 Nr 6, pp 430 – 434.

Röthlisberger, B. (1996) "Practical experience with the single-shell shotcrete method using wet-mix shotcrete during the construction of the Vereina Tunnel", Spritzbeton Technologie ' 96, pp 49 – 56.

Rose, D. (1999) "Steel-fiber-reinforced-shotcrete for tunnels: an international update", RETC Proceedings, pp 525 – 536.

Rowe, R. K. and Lee, M. K. (1992) "An evaluation of simplified techniques for estimating three-dimensional undrained ground movements due to tunnelling in soft soils", Canadian Geotechnical Journal, Vol. 29, pp 31 - 59.

Ruffert, G. (1995) "Rehabilitation of concrete structures by use of shotcrete", Shotcrete for Underground Support VII, ASCE, pp 53 – 57.

Sandter, A.K. (1990) "Channel Tunnel - excavation of the Castle Hill section by use of roadheaders", Tunnel Construction '90, IMM, pp 125 – 135.

Schiesser, K. (1997) "Untersuchung des Langzeitverhaltens permanenter Spritzbetonauskleidung im Tunnelbau mittels numerischer Simulation", Diplomarbeit Montanuniversitat Leoben.

Schmidt, A., Bracher, G & Bachli, R. (1987) "Erfahrungen mit Nasspritzbeton", Schweizer Baublatt, 59/60, pp 54 – 60.

Schubert, P. (1988) "Beitrag zum rheologischen Verhalten von Spritzbeton", Felsbau, Vol. 6, Issue 3, pp 150 - 153.

Scholey, J., Jones, R.A. & Irvine, S.J. (1990) "New Studley tunnel - excavation and support by observational method", Tunnel Construction '90, IMM, pp 137 – 145.

Schröpfer, T. (1995) "Numerischer Analyse des Tragverhaltens von Gebirgsstrecken mit Spritzbetonausbau im Ruhrkarbon", PhD Thesis, TU Clausthal

Schweiger, H. & Beer G.E. (1996) "Numerical Simulation in Tunnelling", Felsbau 14, pp 87 - 92.

Seith, O. (1995) "Spritzbeton bei hohen Temperaturen", Internal Report, ETH Zurich.

Sercombe, J., Hellmich, C., Ulm, F-J. & Mang H. (2000) "Modeling of early-age creep of shotcrete. I: Model and Model Parameters", Journal of Engineering Mechanics, Vol. 126, No. 3, 284 – 291.

Sharma, J.S., Zhao, J. & Hefny, A.M. (2000) "NATM – Effect of shotcrete setting time and excavation sequence on surface settlements", Tunnels and Underground Structures, Zhao, Shirlaw & Krishnan (eds), pp 535 – 540.

Shin, J.H. (2000) "NATM Tunnelling in decomposed granite soil", PhD Thesis, Imperial College, London.

Soliman, E., Duddeck, H. & Ahrens, H. (1993) "Two- and Three-dimensional Analysis of Closely Spaced Double-tube Tunnels", Tunnelling and Underground Space Technology, Vol. 8, No. 1, pp 13 - 18.

Soliman, E., Duddeck, H. & Ahrens, H. (1994) "Effects of development of stiffness on stresses and displacements of single and double tunnels", Tunnelling and Ground Conditions, Abdel Salam (ed) pp 549 - 556.

Springenschmid, R., Schmiedmayer, R. & Schöggler, G. (1998) "Comparative examination of shotcrete with gravel or chippings as aggregate", Tunnel, Vol. 2, 1998, pp 38 – 45.

Stallebrass, S.E., Jovicic, V. & Taylor, R.N. (1994) "The influence of recent stress history on ground movements around tunnels", Pre-failure Deformation of Geomaterials, Shibuya, Mitachi & Miura (eds), pp 615 – 620.

Standing J.R., Farina M. & Potts D.M. (1998)"The prediction of tunnelling induced building settlements – A case study", Tunnels and Metropolises, Negro Jr & Ferreira (eds), pp 1053 – 1058.

Steindorfer, A.F. (1997) "Short-term Prediction of Rock Mass Behaviour in Tunnelling by Advanced Analysis of Displacement Monitoring Data", PhD Thesis, TU Graz.

Strobl, B. (1991) "Die NATM im Boden in Kombination mit Druckluft", Diplomarbeit, Universität für Boden Kultur (BOKU), Vienna.

Strubreiter, A. (1998) "Wirtschaftlichkeitsvergleich von verschiedenen Spritzbeton-verfahren im Tunnelbau", Diplomarbeit, University Of Innsbruck.

Sturmath, R. (1993) "The analysis of closed circular ring components", Mechanical Engineering Publications, London, (pp 21 – 24).

Swoboda, G. & Hafez, N.M. "Structural analysis of shotcrete in tunnelling", Shotcrete for Underground Support VII, pp 170 - 179.

Swoboda, G. & Wagner, H. (1993) "Design based on numerical modelling. A requirement for an economical tunnel construction", RETC Proceedings, pp 367 - 379.

Swoboda, G. & Moussa, A. M. (1992) "Numerical modeling of shotcrete in tunnelling", Numerical models in geomechanics (ed.s Pande Pietruszczak), pp 717 - 727.

Swoboda, G. & Moussa, A. M. (1994) "Numerical modeling of shotcrete and concrete tunnel linings", Tunnelling and Ground Conditions, Abdel Salam (ed), pp 427 - 436.

Swoboda, G., Moussa, A. M., Lukas, W. & Kusterle, W. (1995) "On constitutive modelling of shotcrete", Sprayed shotcrete Proc ?? Norway.

Tang, D.K.W., Lee, K.M. & Ng, C.W.W. (2000) "Stress paths around a 3-D numerically simulated NATM tunnel in stiff clay", Geotechnical Aspects of Underground Construction in Soft Ground (Kusakabe, Fujita & Miyazaki (eds)), pp 443 – 449.

Tatnall, P.C. & Brooks, J. (2001) "Developments and applications of high performance polymer fibres in shotcrete", Shotcrete: Engineering Developments, Bernard (ed), pp 231 – 235.

Testor, M. (1997) "Alkaliarme Spritzbetontechnologie - Verfahrenstechnik; Druckfestigkeits-, Ruckprall- und Staubuntersuchungen", PhD Thesis, University of Innsbruck.

Testor, M. & Pfeuffer,M. (1999) "Staub- und Rückprallreduktion beim Auftrag von Trockenspritzbeton", Spritzbeton-Technologie '99, Innsbruck-Igls, pp 137 – 149.

Thomas, A.H. (1999) "Notes on FLAC3D runs investigating face stability", internal Mott MacDonald memo.

Thomas, A.H., Powell, D.B. & Savill, M. (1998) " Controlling deformations during the construction of NATM tunnels in urban areas", Underground Construction in Modern Infrastructure, Franzen, Bergdahl & Nordmark (eds), pp 207 – 212.

TRL (1992) "Heathrow Express Trial Tunnel: Surface-installed instrumentation and mesaurements. Factual report", GE/TP/183/92

Ulm, J. & Coussy, O. (1995) "Modeling of thermochemomechanical couplings of concrete at early ages", Journal of Engineering Mechanics, July 1995, pp 785 – 794.

Ulm, J. & Coussy, O. (1996) "Strength growth as chemo-plastic hardening in early-age concrete", Journal of Engineering Mechanics, December 1996, pp 1123 – 1133.

Van der Berg, J.P. (1999) " Measurement and prediction of ground movements around three NATM tunnels", PhD Thesis, University of Surrey.

Van der Berg, J.P. & Clayton C.R.I. (2000) "Monitoring ground deformation around a heading in London clay", Geotechnical Aspects of Underground Construction in Soft Ground, Kusababe, Fujita & Miyazaki (eds), pp 173 - 178.

Vandewalle, M. (1996) "Dramix Tunnelling the world", Bekaert S.A.

Vandewalle, M., Rock, T., Earnshaw, G. & Eddie, C. (1998) "Concrete reinforcement with steel fibres", Tunnels & Tunnelling International, April, pp 39 – 41.

Varley N. & Both C. (1999) "Fire protection of concrete linings in tunnels", Concrete, May, pp 27 – 30.

Ward, W.H. & Thomas, H.S.H. (1965) "The development of earth loading and deformation in tunnel linings in London Clay", Soil Mechanics and Foundation Engineering: Proceedings of the Sixth International Conference, Montreal, Vol. 2 , pp 432 – 436.

Ward, W.H., Tedd, P. & Berry N.S.M. (1983) "The Kielder experimental tunnel: final results", Geotechnique 33 No. 3.

Watson, P.C. (1997) "NATM design for soft ground", World Tunnelling, November, pp 394 - 400.

Watson, P.C., Warren, C.D., Eddie, C. & Jager, J. (1999) " CTRL North Downs Tunnel", Tunnel Construction & Piling '99, IMM, pp 301 – 323.

Weber, J.W. (1979) "Empirische Formeln zur Beschreibung der Festigkeitsentwicklung und der Entwicklung des E-Moduls von Beton", Betonwerk- & Fertigteiltechnik 12 pp 753 – 756.

Wong, R. C. K. & Kaiser, P. F. (1986) "Ground behaviour near soft ground tunnels", Large underground openings, Proc. Int. Congress, Firenze, Vol. 1, pp 942 - 951.

Woods, R.I. & Clayton C.R.I. (1993) "The application of the CRISP finite element program to practical retaining wall problems", Retaining structures. Thomas Telford, London, pp 102 – 111.

Yin, J. (1996) "Untersuchungen zum zeitabhangigen Tragverhalten von tiefliegenden Hohlraumen im Fels mit Spritzbetonausbau", PhD thesis, TU Clausthal.

Zangerle, D. (1998)"The use of wet mix sprayed concrete", Tunnels and Metropolises, Negro Jr & Ferreira (ed.s), pp 861 - 867.

Zeidler, K., Groves, P., Sharrocks, D. & Allen, R. (1997) "Surface settlement due to the construction of the London Bridge Station tunnels by NATM", Tunnels for People, eds Hinkel, Golser & Schubert, pp 429 – 434.